Programm Nukleare Sicherheitsforschung

Jahresbericht 2001
Teil 2

B. Mühl (Hrsg.)

Programm Nukleare Sicherheitsforschung

FORSCHUNGSZENTRUM KARLSRUHE

in der Helmholtz-Gemeinschaft

Wissenschaftliche Berichte

FZKA 6742

Programm Nukleare Sicherheitsforschung

Jahresbericht 2001

Teil 2

Herausgegeben von B. Mühl

Programm Nukleare Sicherheitsforschung

Forschungszentrum Karlsruhe GmbH, Karlsruhe

2002

Summary

The R&D work of Forschungszentrum Karlsruhe (FZK) related to reactor safety and the safety of nuclear waste disposal is concentrated in the Nuclear Safety Research Programme (NUKLEAR). In the reporting period 2001, the programme NUKLEAR covered five main topics of work:

Light Water Reactor safety

Innovative systems

Studies related to the transmutation of actinides

Safety research related to final waste storage

Immobilisation of HAW

Numerous institutes of the research centre contribute to the work programme, as well as several external partners. The tasks are coordinated in agreement with internal and external working groups.

The contributions to this report, which are either written in German or in English, correspond to the status of early 2002.

Zusammenfassung

Die F+E-Arbeiten des Forschungszentrums Karlsruhe (FZK) zur Reaktorsicherheit und zur Sicherheit der nuklearen Entsorgung sind im Programm Nukleare Sicherheitsforschung (NUKLEAR) zusammengefasst. Das Programm NUKLEAR umfasste im Berichtsjahr 2001 die folgenden fünf Arbeitsthemen:

Leichtwasserreaktorsicherheit

Innovative Systeme

Studien zur Actinidenumwandlung

Sicherheitsforschung zur Endlagerung

Immobilisierung von hochradioaktivem Abfall

Die konkreten Forschungsvorhaben innerhalb dieser Arbeitsthemen werden laufend mit internen und externen Fachgremien abgestimmt.

An den beschriebenen Arbeiten sind im wesentlichen die folgenden Institute und Abteilungen des FZK beteiligt:

Institut für Hochleistungsimpuls- und Mikrowellentechnik	IHM
Institut für Kern- und Energietechnik	IKET
Institut für Materialforschung	IMF I, II, III
Institut für Nukleare Entsorgung	INE
Institut für Reaktorsicherheit	IRS
Institut für Technische Chemie	ITC

sowie vom FZK beauftragte externe Institutionen.

Die einzelnen Beiträge stellen den Stand der Arbeiten im Frühjahr 2002 dar und sind entsprechend dem F+E-Programm 2001 nummeriert.

Inhalt

Contents

IV

Teil 2 (FZKA 6742)

32.25   SICHERHEITSFORSCHUNG ZUR ENDLAGERUNG

32.25.01   Szenarienentwicklung und Vergleich von Endlagerkonzepten

I.   Thermomechanical analysis of backfilled drifts in a radioactive waste repository

(A. Pudewills, INE)

Abstract

In the framework of the European project "BAckfill and Material Behaviour in Underground Salt Repositories" (BAMBUS) the validation of the numerical models and the constitutive equations available for rock salt and backfill material was demonstrated by comparison of calculated results and measured data from a large-scale in situ test. On the basis of these results, the thermomechanical analyses of a backfill disposal drift in a planned waste repository were carried out to examine the long–term sealing behavior of the crushed salt. To perform this task, finite element codes containing a set of time- and temperature-dependent constitutive models have been used. The results of the modeling show that under expected repository conditions the volume closure and the compaction of the backfill are mainly determined by the temperature increase and the lithostatic pressure. Finally, the implications for the post-closure safety evolution are discussed.

Zusammenfassung

Im Rahmen des EU-Projektes BAMBUS II (Backfill and Material Behaviour in Underground Salt Repositories) wurde die Bewertung der vorhandenen Rechenmodelle und Stoffgesetze für Steinsalz und Versatzmaterial durch Vergleich der Rechenergebnisse mit den Messungen aus in situ Experimenten durchgeführt.

Im Hinblick auf des Langzeitverhalten einer verfüllten BE-Lagerstrecke wurden die Entwicklung der Porosität sowie der Aufbau des Kompaktierungsdruckes im Versatzmaterial ermittelt. Die Rechnungen wurden mit Finite Elemente Programmen durchgeführt, die speziell für die Untersuchung der Endlagerstruktur entwickelt wurden, unter Berücksichtigung des zeit- und temperaturabhängigen Stoffverhalten von Steinsalz und Versatzmaterial. Die Rechenergebnisse zeigen, dass die Wärmeentwicklung und der lithostatische Primärspannungszustand einen maßgeblichen

Einfluss auf die Konvergenz der Lagerstrecke als auch auf das Kompaktierungs-verhalten der Versatzmaterials haben.

1. Introduction

Repository concepts for disposal of high-level radioactive waste from reprocessing and spent-fuel elements are based on multiple barriers for protection of the environment against the radioactive nuclides. According to these concepts, the containers with heat generating radioactive waste will be placed in vertical boreholes or long parallel drifts at a depth of about 800 to 1000 m below the surface in a rock salt formation [1]. The remaining space between the containers and host rock will be filled with dry crushed salt. It is expected that in response to the thermally induced creep closure of the excavations the backfill material will compact sufficiently to serve as an efficient seal for the radioactive waste. The performance assessment of such nuclear waste repositories in rock salt requires laboratory tests, field experiments, and the use of adequate numerical models to predict the long-term thermomechanical effects in the near and far fields of the repository. The numerical reliability of the calculations and the predictive capabilities were demonstrated in international benchmark activities and also by comparison with results of the *in situ* heater test , "Thermal Simulation of Drift Emplacement" – TSDE [2].

The objective of this paper is to give an overview of the actual repository concepts focusing on long-term thermomechanical effects related to the drift emplacement of heat-generating waste. This includes numerical modelling of the temperature fields, thermally induced closure of the openings followed by the compaction of the backfill material and the resulting stresses in the surrounding salt. With regard to the behaviour of crushed salt as backfill, the reduction of the porosity and the increase of the compaction pressure on the waste containers were estimated.

The FAST-BEST code, based on the coarse mesh method [3], [4] and specifically developed for studying the drift disposal, was used to predict the temperatures. This program includes temperature-dependent material models for rock salt and crushed salt. The material model for crushed salt takes into account a compaction-dependent thermal conductivity. For the thermomechanical analyses, two finite element codes have been used. One is the general-purpose code ADINA [5] which was extended to investigate the creep compaction of a loose backfill material [6], and the other one is

the special-purpose code MAUS [7] which also includes suitable material models for rock salt and crushed salt.

2. Repository Concepts

During the last decade the research and development program on direct disposal was focused on a "dual-purpose" repository accommodating both high-level radioactive waste from reprocessing and spent-fuel assemblies [1]. Concerning the disposal concepts, two emplacement techniques were investigated, namely the borehole emplacement and drift emplacement. This paper deals with the drift emplacement concept only.

In a repository designed for drift emplacement, the waste is disposed of in large self-shielded containers (POLLUX casks) which will be placed horizontally on the floor of drifts. Immediately after emplacement, the drifts are backfilled with dry crushed salt. The emplacement panels are bordered by two parallel access drifts as illustrated in Figure 1. At the time of emplacement, the heat generated in a cask will be approximately 7.5 kW, depending on the interim storage period. The cask is 5.5 m long, has a diameter of 1.5 m and weighs ~65 tons in its loaded state. The emplacement drifts are 3.5 m wide, 4.0 m high, and about 200 m long and will be excavated into the emplacement panels at a distance of 17 m from each other.
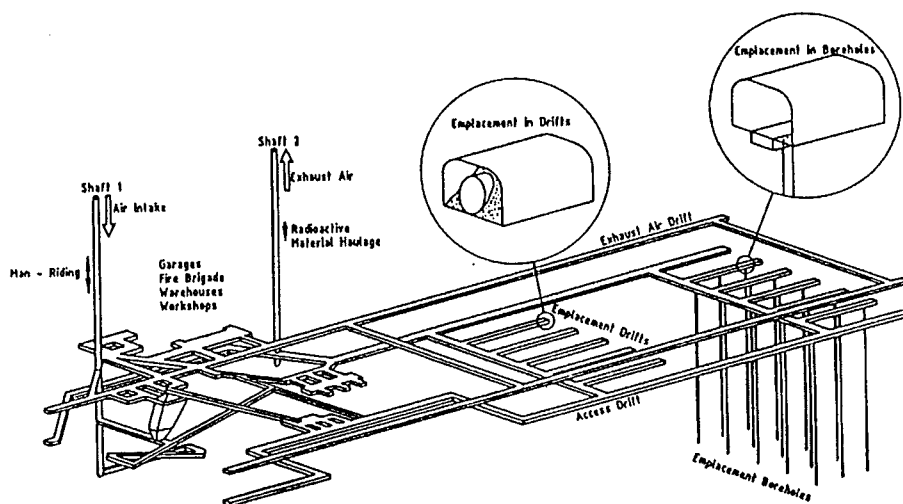
Fig. 1: Sketch of Repository Concepts, Ref. [1]

459

3. Numerical analysis of a disposal drift

Taking into account the periodic pattern and symmetry of the disposal field, it was also assumed that all disposal drifts in the emplacement panel were excavated at time zero and filled with POLLUX casks and crushed salt instantaneously after 0.7 years. A three-dimensional model of a representative portion of the disposal drift was defined for the thermal analysis. In further two-dimensional thermomechanical calculations the temperatures are interpolated from a vertical section passing through the center of the model geometry. A plane strain finite element model was used for this investigation. The vertical section right through the center of a POLLUX cask represents only one half of the disposal drift and of the pillar between adjacent drifts (Fig. 2). Symmetry conditions are assumed on the left and the right border. The upper boundary of the model was loaded with18 MPa (i.e. the lithostatic pressure at the depth of the emplacement level).

The numerical simulation started with the calculation of the isothermal drift closure and the stress distribution around the disposal drift prior to the emplacement of the POLLUX casks. After about 0.7 years, the temperature development and the of backfill material in the drift were taken into account. The thermomechanical analyses were continued over a period of 50 years. After emplacement of the casks and backfill in the disposal drift, the volume closure and, hence, the compaction of the backfill material are mainly determined by the temperature development and the thermomechanical behavior of the crushed salt.

Fig. 2: Geometry and boundary conditions
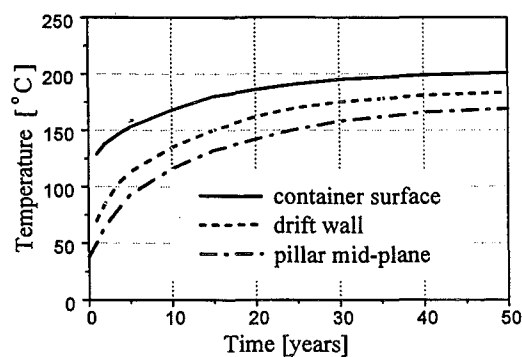
Fig. 3: Calculated temperature histories at different positions

The histories of the calculated temperatures at three characteristic points are presented in Fig. 3. The development of the decrease of the backfill porosity at two positions in the drift and the stresses in the backfill material are shown in Figs. 4 and 5. These results show that in a repository at a depth of about 870 m the creep rates of rock salt and closure rates will be significantly higher than in the TSDE test drifts [8] and that the backfill will be compacted to a porosity of about 1% after about 20 years of heating. The region in the pillar next to the drift shows highest shear stress during the operational phase. Over time, the compaction pressure in the crushed salt increases and becomes large enough to support substantially the rock salt around the drift and a relaxation and redistribution of the stresses in the pillar takes place during the first 10 years after the emplacement of the casks. Figure 6 shows the distribution of the "Safety Factor" (ratio between the calculated shear stress and the assumed fracture criterion) in the pillar at different times. It should be pointed out that the safety factor at the drift wall decreases relatively fast from values of about 0.55 at the start of heating to the values less than 0.1 after 10 years. Due to this fact there are no cracks to be expected according to the failure criterion applied.
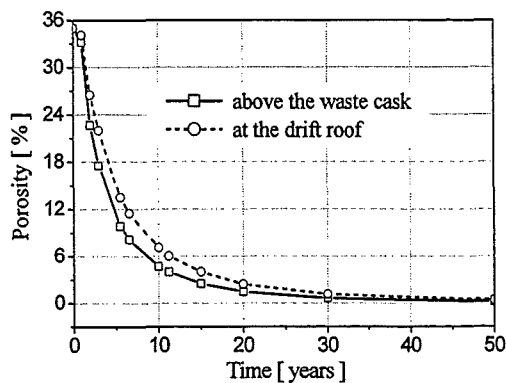
Fig. 4: Development of the backfill porosity
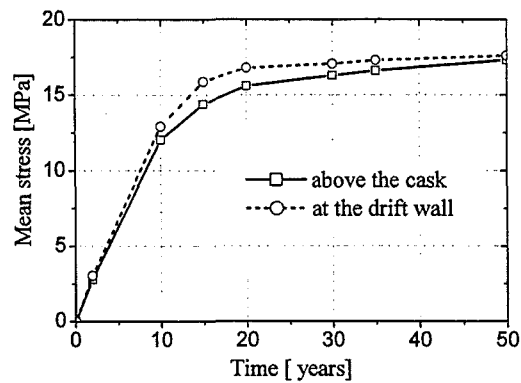
Fig. 5: Development of stresses into the backfill
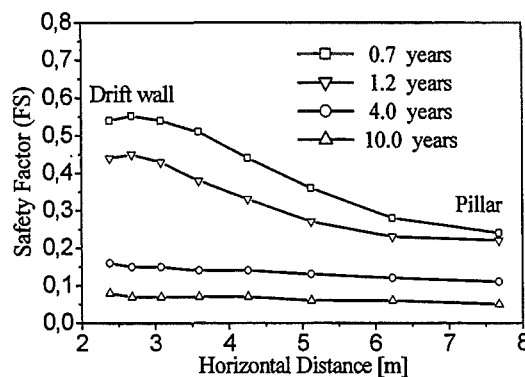
Fig. 6: Distribution of the "Safety Factor" in the pillar
at different times after drift excavation

4. Conclusions

From the results, the following conclusions are drawn:

- At the repository depth of about 870 m the creep rates of rock salt and closure rates will be significantly higher than in the TSDE- test drifts and the backfill will be compacted to a porosity of about 1% after 20 years of heating.

- With time, the compaction pressure in the backfill increases and therefore supports the rock salt around the drift. A relevant relaxation and redistribution of the stresses in the pillar takes place.

- During the operational phase high shear stresses have been calculated in the vicinity of the drift. However, the ratio of the actual shear stress to the assumed failure criterion (the safety factor) remains less than unity, i.e. no cracks in the pillar are expected.

- Furthermore, the simulation results together with *in situ* observations demonstrate that the behaviour of the crushed salt is a key factor in the long-term stability of the emplacement drifts in a repository in rock salt.

References

1. Bechthold, W., Closs, K.D., Knapp, U., Papp, R., "System analysis for a dual-purpose repository", Final Report, EUR 14595 EN,Brussels, 1993.

2. Bechthold, W., Rothfuchs, T., Poley, A., Ghoreychi, M., Heusermann, S., Gens, A., Olivella, S., "Backfill and Material Behaviour in Underground Repositories for Radioactive Waste in Salt (BAMBUS Project)", Final Report, EUR-19124 EN, Brussels, 1999.

3. Ploumen, P., Strickmann, G., Winske, P., "Untersuchungen zur Temperaturent-wicklung bei der Endlagerung hochradioaktiver Abfälle", Teil I: Berechnung der zeit- und ortsabhängigen Temperaturfelder, ATW, No.2, pp. 85-91, Feb.1979.

4. Korthaus, E., "Abschließende Verbesserung der vorliegenden Rechenpro-gramme zur Bestimmung der Temperaturentwicklung", Abschlußbericht 1980-1982, Vertrag Nr.266-80-7-WASD, EUR 8667 DE, 1983.

5. ADINA, Automatic Dynamic Incremental Nonlinear Analysis, Watertown, MA, ADINA R&D, 2000.

6. Pudewills, A., Krauss, M., "Implementation of a viscoplastic model for crushed salt in the ADINA program", Computers and Structures, vol. 72, pp. 293-99, 1999.

7. Albers, G., (1983), "MAUS - A Computer Code for Modelling Thermomechanical Stresses in Rock Salt," Computer Modelling of Stresses in Rock, Proc. Tech. Session, EUR9355 EN, Brussels.

8. Pudewills, A., Rothfuchs, T.,"Thermomechanical Analyses for the TSS-Experi-ment and Comparison with In Situ Measurements". The Mech. Behavior of Salt : Proc. of the 5th Conf., Bucharest, Ro., August 9-14, 1999, (in print).

II. Code Development for Modelling of Coupled Effects at Corrosion of Carbon Steel Containers under Repository Conditions

(E. Korthaus, INE)

Abstract

The corrosion and hence the lifetime of carbon steel containers under repository conditions is depending on electrochemical, chemical and transport processes at the metal surface and in the near vicinity. A 1-dimensional coupled code is being developed and tested for numerical modelling of these effects in the context of general corrosion of high-level nuclear waste and spent fuel containers or overpacks.

Introduction

The general corrosion of steel containers and the development of the pore-fluid chemistry in the adjacent backfill material are a result of several coupled processes:

- Electrochemical corrosion processes of the container surface
- Reactive transport of dissolved chemical species in the pore-fluid
- Changes of backfill porosity due to precipitation of corrosion products or other precipitation/dissolution effects
- Growth of (more or less) protective layers on the container surface
- Generation and build-up of hydrogen at the container surface

The main objectives of model calculations on these processes are the support of the interpretation of corrosion tests and a prediction of long-term corrosion rates and near-field chemistry under repository conditions.

Code Development

The 1-dimensional code TRANSAL is being developed as a numerical modelling approach to these effects. The current version of TRANSAL consists of several iteratively coupled programme parts for the calculation of

- Saturated porous flow for porosities under the influence of precipitation/dissolution effects and of thermomechanic convergence/consolidation
- Diffusive and advective mass transport (with linear sorption)

- Thermodynamic equilibrium and precipitation/dissolution at high ionic strength and elevated temperatures (Pitzer's formalism for calculation of activity coefficients).

Parts of the THCC code [1] were used to develop this module.

- Kinetic effects in complexation and precipitation/dissolution with the aid of variable equilibrium constants

- Electrochemical corrosion rate and potential as a function of the composition and transport characteristics of the adjacent pore-fluid

Test Calculations

Calculations were performed in order to test and to improve the numerical procedures. Most of them were focused on the reactive transport in the pore-fluid and used a fixed corrosion rate (assuming a constant source of Fe^{++}, OH^-) as a boundary condition. A considerable numerical effort was introduced when the oxidation kinetics of Fe^{++} by dissolved oxygen were taken into account under aerobic initial conditions. Some exemplary results, the development of pH and Eh distributions, are shown in figures 1 – 2. A column of 0.1mol NaCl of 0.5m length at 25°C was considered in this test case. The aquatic species Na^+, Fe^{++}, Fe^{3+}, H^+, Cl^-, OH^-, $Fe(OH)_2(aq)$, $Fe(OH)_3(aq)$, $Fe(OH)_2^+$ and $O_2(aq)$ and the solids $Fe(OH)_2$, $FeOOH$, Fe_2O_3 and Fe_3O_4 were taken into account in the model.
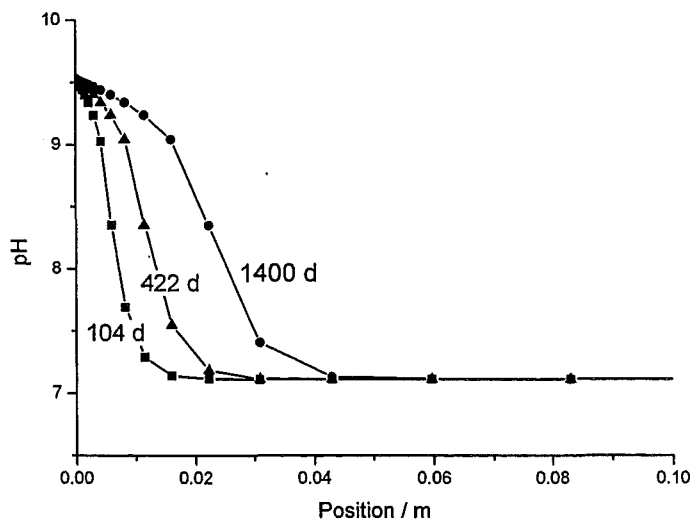
Fig. 1: Development of pH near the 'corrosion plane'
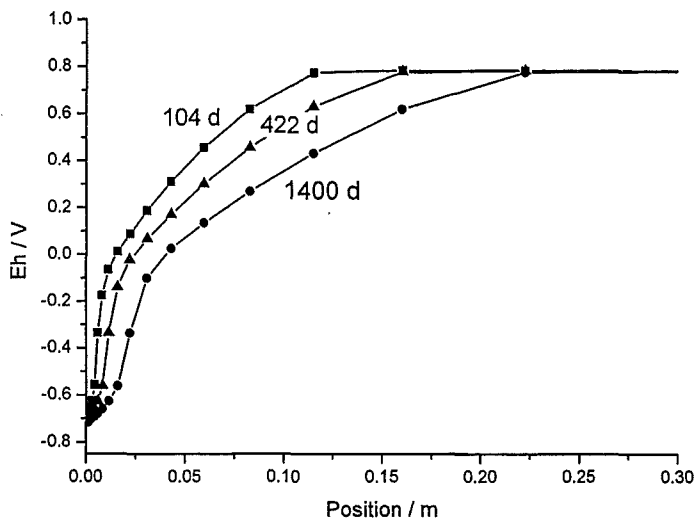
Fig. 2: Development of redox potential (from Fe^{3+}/Fe^{++} ratio)

When the calculation of the electrochemical corrosion rate (based on kinetic data from [2]) is introduced in this test case instead of using a fixed source term, it is found that the reduction of O_2 is the dominating cathodic reaction for a very short time only, because the supply of O_2 is limited by diffusion. In parallel, while the electrode potential is slightly decreasing, the water reduction reaction is rising to a small value remaining constant hereafter (Fig. 3). It is the dominating cathodic reaction because of the alkaline conditions prevailing near the corrosion plane in this test case. The situation would be quite different under acidic conditions as found in magnesium rich brines at elevated temperatures. The reduction of H^+ then will be the dominating cathodic reaction, giving rise to a more pronounced coupling between corrosion rate and pore-fluid chemistry.

Outlook

Apart from the obvious need of additional data for an adequate modelling of the pore-fluid chemistry, it is well known that a more realistic prediction of long-term corrosion rates will not be possible without taking into account of the effects of protective layers. The search for a method to handle this problem will be started in the near future.
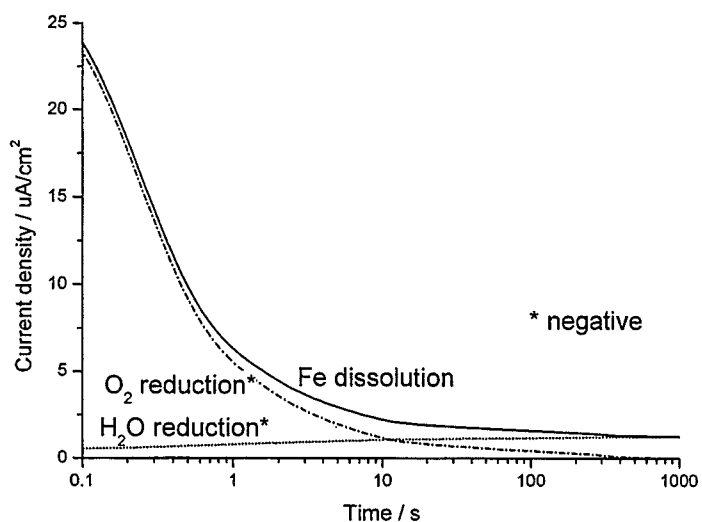
Fig. 3: Anodic and cathodic current densities of Fe corrosion in NaCl solution

References

1.   Carnahan, C.L., 1987. Simulation of Uranium Transport with Variable
      Temperature and Oxidation Potential: The Computer Program THCC.
      Mat. Res. Soc. Symp. Proc., 84 : 713-721.

2.   Marsh, G.P., 1988. Progress in the Assessment of the Corrosion of Low and
      Intermediate Level Waste Containers under Repository Conditions.
      Harwell Laboratory, UKAEA, Report NSS/R126.

32.25.02 Radionuklidrückhaltung durch technische und geotechnische Barrieren

I. Radionuclide retention by secondary alteration products of HLW glass

(B. Luckscheiter, M. Nesovic, P. Zimmer, INE)

Abstract

Two fundamental controls of glass dissolution rates in water and brines are (1) initial water diffusion and ion exchange, and (2) subsequent hydrolysis and dissolution of the network forming elements. The accumulation of dissolved Si leads to a significant decrease in the dissolution rate. The release of less soluble fission products and actinides may be controlled by the solubility of secondary alteration products and /or by sorption onto the alteration layer of the glass surface. To get information about the incorporation of radionuclides into newly formed secondary phases, the surface layers on simulated HLW glass corroded over 7 years at 150°C in $MgCl_2$-rich and NaCl-rich solutions were investigated. The identified mineral phases mainly consist of Ca-Mg-silicates, Ba-sulfates, Ba-molybdates and, in NaCl brine, of $CaMoO_4$. In $MgCl_2$ brine high amounts of REE and Sr were found in some phases. In NaCl brine only Sr was accumulated in the sulfates and molybdates.

In order to quantify the sorption effect on the retention of metal ions, sorption tests were performed in dependence on pH with Eu, Th, U(VI) and Am at 80°C in water using precorroded, simulated HLW glass GP WAK1 as substrate. The results of these sorption tests show clearly that the alteration layer on the glass surface has a strong effect on the retention of the four elements above pH 3.

1. Incorporation of radionuclides in secondary alteration products of HLW glass

1.1 Introduction

During the corrosion of high level waste (HLW) glasses in aqueous solutions many different secondary phases could be formed (e.g. silicates, sulphates). These newly formed mineral phases could serve as host minerals for radionuclides. Static corrosion experiments in two different concentrated salt solutions ($MgCl_2$-rich (solution 1) and NaCl-rich (solution 3)) were carried out at 190°C over 7 years at surface-to-volume ratios (S/V) of 1000 m^{-1} and 10000 m^{-1} in tantalum-lined autoclaves. The incorporation of REE, as chemical analogue to the actinides, and

other fission products in the formed secondary phases was studied by scanning electron microscopy (SEM) and an energy dispersive x-ray detector (EDX).

1.2 Results from SEM/EDX measurements

After 7.5 years corrosion time in both salt solutions, silicates, sulphates and molybdates were identified as the major secondary phases on the glass surfaces.

Silicates

Solution 3 (MgCl$_2$-rich): At both S/V-ratios, the glass surfaces were covered with hydrous Mg-silicate phases including small amounts of Zr. Cs, Zr and Gd were enriched in the underlying gel-layers.

Solution 3 (NaCl-rich): The corroded glass surfaces with S/V = 1,000 m^{-1} showed hydrous Ca-Mg-silicate layers. Additionally, a few isolated hydrous silicate spheres comprising REE with up to 20 wt.-% were observed. On the glass sample surfaces with initial S/V = 10,000 m^{-1} three hydrous silicate phases with different morphology were identified: (1) numerous platy Ca-Mg-silicate phases (ø = 1 - 5 µm), (2) several fibrous, hydrous silicate-aggregates and (3) clusters of hydrous silicates in form of spheres. The silicates show similar chemical composition, but they differ in their REE content which varies between 5 and 35 wt.

Sulphates

Solution 1 (MgCl$_2$-rich): At both S/V-ratios the formed egg-shaped barite crystals (BaSO$_4$) contain up to 15 wt.-% of Sr. At the higher S/V ratio of 10000 m^{-1} also hexagonal REE-sulphates (La,Ce,Nd,Gd)$_2$(SO4)$_3$ were observed. The REE concentration in REE-sulphates varies between 3 - 5 wt.-% for La, 4 - 9 wt.-% for Ce, 7 - 14 wt.-% for Nd and 3 - 5 wt.-% for Gd.

Solution 3 (NaCl-rich): The barite crystals show typical orthorhombic morphology and include Sr between 5 - 15 wt.-%. Additionally, Ce concentration up to 5 wt.-% were detected in some crystals.

Molybdates

Solution 1 (MgCl$_2$-rich): The identified REE containing Ba-molybdates at S/V = 1000 m^{-1} and the REE-molybdates at S/V = 10000 m^{-1} showed indications of dissolution

(etch pits) attributed to the low final pH-values in the corrosion medium (pH = 3.5 at S/V = 1000 m^{-1} and pH = 2.9 at S/V = 10000 m^{-1}) after the long corrosion time.

Solution 3 (NaCl-rich): Well-crystallized, tetragonal powellite crystals (CaMoO$_4$) were found on the glass surfaces at both S/V-ratios. As verified by 34 replicate EDX measurements in different regions of 13 powellite crystals, they contain no detectable amount of REE in contrast to the powellites formed in solution 1. The SEM images (Fig. 1) show the elemental mapping of powellite crystals, surrounding silicates and barites observed on corroded glass surfaces in solution 3. It indicates an enrichment of REE in the silicates and an incorporation of Ce in the barites, but no significant REE concentrations in the powellite.

low   high
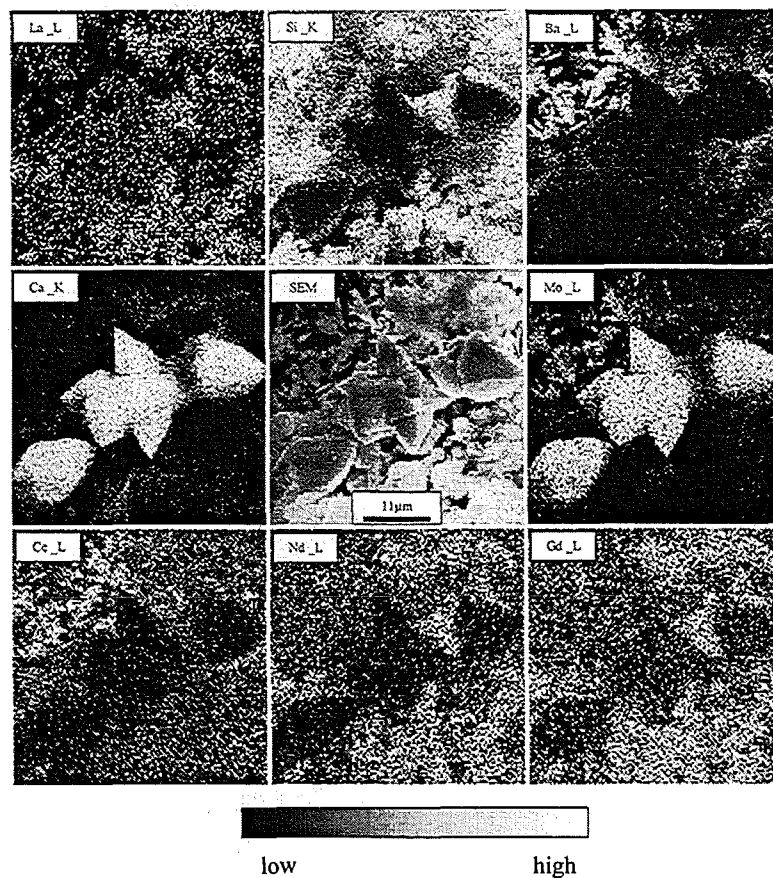
Fig. 1: Elemental mapping of powellite, silicates and barite observed on glass chip surface after 7.5 years corrosion in solution 3 (NaCl-rich).

2. Sorption behaviour of Eu, Th, U and Am on precorroded HLW glass

2.1 Introduction

Contact of glass by an aqueous solution results in the diffusion of water into the glass surface and ion exchange of the alkali metal ions against H_3O^+. The dissolution of the glass occurs by hydrolysis of the silicate network. The hydrated silicate network subsequently dissolves and in a closed system the solution becomes saturated with repect to $Si(OH)_4$. When silica approches its solubility limits, condensation reactions of the silanol groups take place forming a largely amorphous alteration layer (gel layer). The initial high dissolution rate (forward rate) of the glass decreases by several orders of magnitude [1 - 3]. Less soluble elements like Al, Zr, REE and actinides are assumed to be retained in the alteration layer of the glass by sorption with increasing pH and/or by formation of secondary alteration products controlling the solution concentrations. In order to quantify the sorption effect on the retention of metal ions, sorption tests were performed with Eu, Th, U(VI) and Am at 80°C in water using precorroded, simulated HLW glass GP WAK1 as substrate.

2.2 Experimental

For preparing precorroded glass, several samples of 2.5 g glass powder (grain size 200-280 μm) were exposed to 50 ml water (S/V = 1000 m^{-1}). After 40 days, aliquots were taken from the leachates and analysed for various elements. After sampling, the pH of the solutions was adjusted to different fixed values between pH 2 and 10 by addition of either HNO_3 or NaOH. Sorption studies were performed at 10^{-6} up to 5×10^{-4} mol/l of the elements Eu, Th and U(VI) by adding stock solutions to the leachates. For ^{241}Am starting concentrations of 10^{-9} to 10^{-7} mol/l were used. The concentrations of these cations in the leachates were analysed 10 days after stock solutions addition. For solution analyses, aliquots were taken and filtered (0.45 μm filter) and the filtrates were also passed through a ultrafiltration membrane (1.8 nm).

2.3 Results and discussion

Results of the sorption experiments are given in the figures in terms of R_s (L/kg) values as a function of pH ($R_s = C_{sorb}/C_{sol} \times$ V/m; C_{sorb} = amount of cation sorbed, C_{sol} = concentration of cation in the solution, V= solution volume, m = mass of alteration layer).

Fig. 2 shows the sorption behaviour of Eu, Th and U(VI) in dependence on pH for a starting concentration of 10^{-4} mol/l. The distribution ratios (R_s) reflect the different

charge of the three cations. The R_s values are highest for Th(IV), followed by the R_s values of Eu(III), which are lower by about a factor 10 and finally those of U(VI) which are the lowest. Above pH 8, the R_s values decrease again. This effect can be attributed to the formation of anionic carbonate complexes as the solutions are in contact with air. The results of these sorption tests show clearly that the alteration layer on the glass surface has a strong effect on the retention of the three elements.
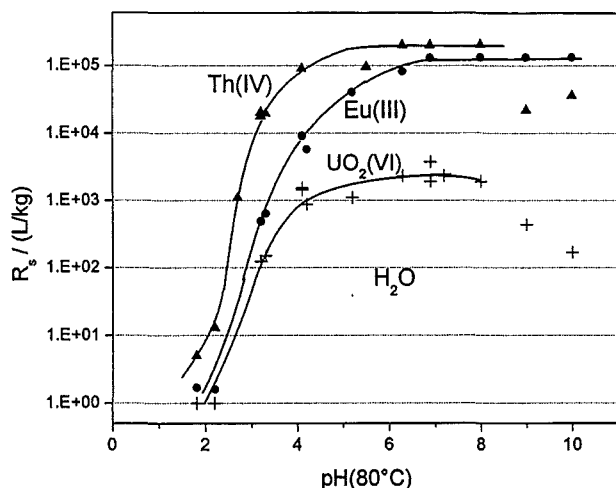
Fig. 2: Distribution ratios R_s of Eu, Th and U on precorroded HLW glass in water

To demonstrate that the sorption behaviour of Eu is representative for homologue trivalent actinides, additional sorption tests were performed with ^{241}Am. Distribution ratios (R_s) of Am at 80°C for three starting concentration of 10^{-9}, 10^{-8} and 7×10^{-8} mol/L as a function of the pH after 10 days contacting time are shown in Fig. 3. The sorption edges are shifted slightly to higher pH values with increasing starting concentration. This is an effect of the non-constant pH in the solutions, especially during the first sorption test at the lowest starting concentration. In the last test, the changes in pH were much lower than in the previous tests. Therefore, the R_s values determined at the highest Am concentration are more reliable. At pH values above 5, Am-bearing colloidal particles were detected in all sorption tests. The respective R_s values (calculated from unfiltered and filtered solution samples) are included in Fig. 3 to illustrate the colloidal effect. The Am-bearing colloids mainly contain silica. Therefore, the colloids may consist of detached fine gel-layer particles containing sorbed Am.
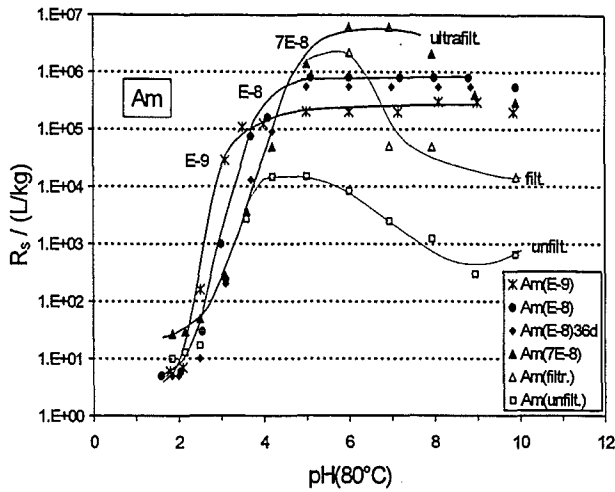
Fig. 3: Distribution ratios R_s of Am on precorroded HLW glass in water

Fig. 4 shows a comparison of the distribution ratios of Am with those of Eu at various starting concentrations. Despite the relatively large scattering of the data points, it is quite evident that the sorption behaviour of Am is nearly identical with the behaviour of Eu. As shown by the previous sorption tests with Eu, at constant pH the sorbed concentration is about proportional to the solution concentration. Therefore, the sorption behaviour of Eu and Am can be described by a Nernst/Langmuir isotherm [4]. The strong dependence of the R_s values of Eu And Am on the pH can be explained by a surface complexation reaction of Me(III) ions with the alteration layer. As shown by modelling calculations, the sorption data obtained from Eu and Am can best be described by the formation of a bidentate surface complex:

$$2 \equiv SiOH + Me^{3+} \Longleftrightarrow (\equiv SiO)_2Me^+ + 2H^+$$
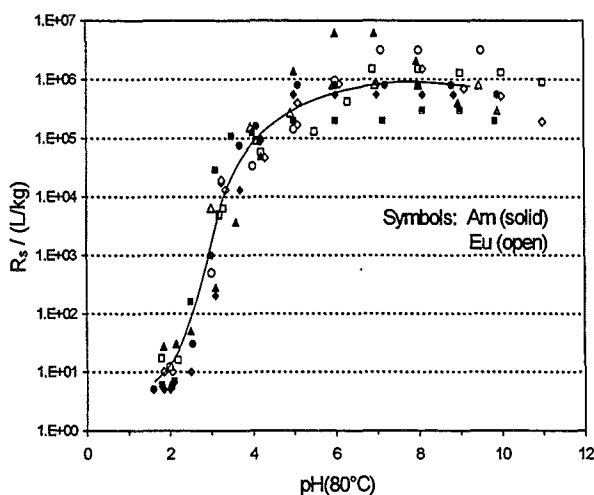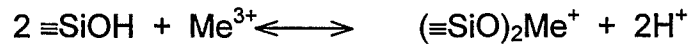
Fig. 4: Comparison of the distribution ratios R_s of Eu and Am in water at 80°C

472

References

1. Ebert, L.: The Effects of the Glass Surface Area/Solution Volume Ratio on Glass Corrosion: A Critical Review. Argonne Nat. Lab. Report ANL-94/34 (1995).

2. Grambow, B.: Nuclear Waste Glass Dissolution: Mechanism, Model and Application, Technical Report, JSS Project Phase IV 87-02, edited by SKB, Stockholm, Sweden (1987)

3. Vernaz, E. Y., Dussossoy, J. L.: Current state of knowledge of nuclear waste glass corrosion mechanisms: the case of R7T7 glass. Appl. Geochem. 1, 13 (1992).

4. Luckscheiter, B., Kienzler, B.: Determination of sorption isotherms for EU, Th, U and Am on the gel layer of corroded HLW glass. J. Nucl. Mater. 298, 155 (2001).

II.   Radiolysis and corrosion of ^{238}Pu doped UO$_2$ pellets in chloride brine
(M. Kelm, E. Bohnert, INE)

Abstract

Deaerated 5 M NaCl solution was irradiated in the presence of UO$_2$ pellets with α-radiation from ^{238}Pu. Some experiments were conducted with ^{238}Pu doped pellets, while others were conducted with ^{238}Pu dissolved in the brine. The radiolysis products as well as the yield of mobilized U and Pu from the oxidative dissolution of UO$_2$ were determined. The same results for radiolysis products and for the oxidation/dissolution of the pellets were found in the case of homogeneous distribution of the Pu in the brine and in the case of doped pellets, where the radiation chemical processes occur only in the liquid layer of some 10 µm thickness adjacent to the pellet. The yield of radiolysis products was comparable to earlier results, that of mobilized U from the pellets summed up to only < 1% of the total amount of oxidized species. Thus, the radiation chemical yield (G-value) for mobilized hexavalent U was only < 0.01 ions/100eV. In spite of the low radiation yield for the corrosion the rate of UO$_2$ dissolution is still higher than expected from the concentrations of long-lived oxidizing radiolysis compounds.

Zusammenfassung

5 M NaCl Lösung wurde in Gegenwart von UO$_2$-Pellets mit α-Strahlen aus ^{238}Pu unter Luftausschluss bestrahlt. Dabei wurden zum einen ^{238}Pu dotierte Pellets verwendet, zum anderen wurde ^{238}Pu in der Lauge gelöst. Die gebildeten Radiolyseprodukte sowie die durch oxidative Auflösung des UO$_2$ mobilisierten Mengen U und Pu wurden bestimmt. Es zeigte sich, dass es bei gleicher Dosis sowohl für die Radiolyseprodukte als auch für die Oxidation/Auflösung der Pellets unerheblich ist, ob der α-Strahler praktisch homogen in der Lösung verteilt ist, oder ob die strahlen-chemischen Prozesse nur in einer wenige 10 µm dicken Flüssigkeitsschicht nahe der Pellets ablaufen. Die Ausbeute an Radiolyseprodukten war mit der in früheren Arbeiten gefundenen vergleichbar. Die Ausbeute an oxidativ mobilisiertem U aus den Pellets betrug nur < 1 % der insgesamt gebildeten oxidierenden Spezies. Der G-Wert für mobilisiertes 6-wertiges Uran betrug dementsprechend nur < 0,01 Moleküle / 100 eV. Trotz der niedrigen strahlen-chemischen Ausbeute bei der Korrosion ist die

Auflöserate des UO_2 immer noch höher, als sie von der Konzentration der langlebigen oxidierenden Radiolyseprodukte erwartet werden kann.

Introduction

In the past the α- and γ- radiolysis of concentrated chloride brines was investigated with respect to the final disposal of spent nuclear fuel in a rock salt formation [1- 4]. The radiation chemical processes in the solution could be simulated by means of a reaction kinetic model [5, 2, 4].

The first step of the mobilization of radionuclides from spent fuel is the oxidative dissolution of the fuel matrix [6 - 8]. As in a final disposal in the deep underground the only source of oxidizing species is radiolysis it is important to know the radiation chemical yield of the fuel oxidation. In a final disposal the spent fuel is protected from contact with water for at least 500 years by a thick-walled or corrosion resistant container. After that period of time the α-dose rate from the actinides is dominant over the γ-radiation. Therefore, UO_2 pellets doped with a short-lived α-emitter are suitable to be used in experiments to simulate the corrosion processes of 'old' spent fuel. [238]Pu doped UO_2 pellets were frequently used in the past [9 - 11] for experiments in diluted or aerated solutions. This work describes corrosion experiments with [238]Pu doped UO_2 pellets in deaerated 5 M NaCl solution and compares them with experiments using undoped UO_2 pellets in deaerated 5 M NaCl solution containing dissolved [238]Pu. The different contents of doping material in the pellets correspond to an α-dose rate which is 2.5 and 250 times higher than the dose rate of 500 years old fuel.

Experiments

All experiments were conducted in glove boxes in an Ar atmosphere. The pellets had a diameter or edge length, respectively of about 6 mm and a mass of 0.3 to 0.8 g. After cutting, polishing and cleaning they were annealed for several hours at 1400 °C and then cooled down in an Ar/H2 stream to re-establish a stoichiometric composition at the surface according to UO_2. The annealing procedure was tested by XPS analysis of an undoped pellet. The U 5f peak in the valence band spectrum (Fig. 1) indicates that 92 % of the pellet's surface had a composition according to UO_2 which equals a mean surface composition of $UO_{2.08}$. The nominal pellet composition and the activity concentration in the brine is given in Table 1. The isotopic compositions of the 'plutonium' used for doping the pellets and which was dissolved in the

No.	UO₂-pellet: ²³⁸PuO₂ nom. wt.%	5 M NaCl sol.: act. conc. GBq/L	pH at start
1	10	0	12
2	10	0	8
3	0.1	0	8
4	0	8.41	12
5	0	8.41	8
6	0	841	8
7	0	0	8

Table 1: Composition of the pellets and activity concentration of the solutions.

brine were slightly different. In both cases the main components were about 65 % ^{238}Pu, 16 % ^{239}Pu and 15 % ^{234}U.

After annealing the cold pellets were placed on a glass support in a glass vessel and 20 ml of deaerated solution (Table 1) was added. An evacuated gas sampling vessel was mounted and the valve to the sampling vessel was then opened to establish a reduced pressure in the whole apparatus. The solution with the pellet was kept at room temperature and stirred from time to time over such a period of time that reduced pressure persisted in spite of the radiolysis gas evolution. For sampling the gas sampling vessel was removed from the apparatus after closing its valve. The gas composition was determined by mass spectroscopy, the total amount from its pressure. An aliquot of the solution was used to determine the radiolysis products HClO, ClO_2^- and ClO_3^- as well as pH and the redox potential [1]. The gas space above the remaining solu-
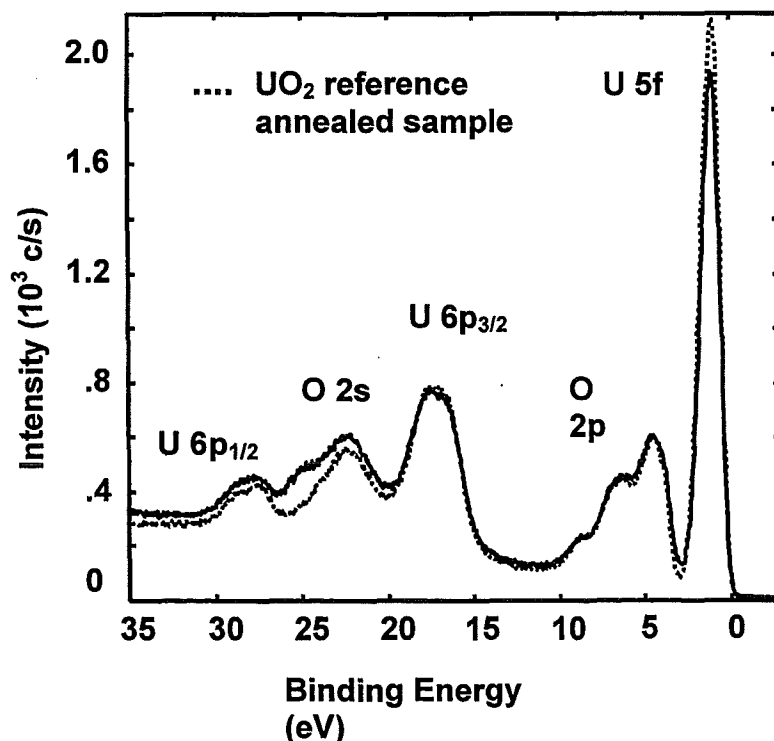
Fig. 1: XPS spectrum of a UO₂ sample annealed at 1400 °C in Ar/H₂ compared to a reference sample which was broken in the ultra high vacuum

tion was flushed with Ar and a new gas sampling vessel was attached to continue with the experiment. In the first part of the experiment (about 3 samples within 9 months) an aliquot of each liquid sample was filtrated through 450 and 1.8 nm filters. In the filtrates U and Pu were determined by ICP-MS using suitable isotopes in the mass range 234 to 242. Additionally, Pu was determined from the α-activity. This procedure allowed the determination of truly dissolved U and Pu and gave information about the particle size of the material mobilized from the pellets. In the second part of the experiment the aliquot of each sample was not filtrated but acidified with nitric acid to determine the total amount of mobilized U and Pu. In the future the sampling regime will be changed one more time: It is planned to exchange the solution completely after each sampling interval to reduce effects from oversaturation and precipitation of secondary phases.

Results

Most of the results are expressed as concentrations depending on the applied α-dose. For the radiolysis gases the amount of gas per kg solvent is given. To calculate the applied dose on the solution it is assumed that 18.8 % of the radiation energy released within a pellet's surface layer of 11.8 μm thickness (which is the range of 5.5 MeV α-particles in UO_2) is homogeneously dissipated in the solution even though the maximum range of the α-radiation in the brine is only about 45 μm. This percentage M (eq. 1) considers only the geometric effect of α-radiation emerging from the surface but not the linear energy transfer which varies with the particle energy.

$$M = \frac{\int_0^r \frac{1}{3} \cdot \pi \cdot (r-x)^2 \cdot (2 \cdot r + x) \cdot dx}{\frac{4}{3} \cdot \pi \cdot r^4} = 0.118 \qquad \text{(eq. 1)}$$

r = range of α-radiation in the solid

A derivation for CANDU fuel [12] gives even a smaller percentage of radiation energy which is effective in the adjacent solution.

For pellet 1 and 2 (Table 1) the calculated mean dose rate increases from 10 to 35 Gy/h because sampling reduces the amount of solution. For pellet 3 the dose rate increases from 0.1 to 0.17 Gy/h. The local dose rate in the actually irradiated solution layer is more than 3 orders of magnitude higher. For the experiments with pellet 4, 5

and 6 (Table 1) it is assumed that the total decay energy is homogeneously dissipated in the solution which equals a dose rate of 22.5 Gy/h or 2250 Gy/h (pellet 6), respectively. The experiment with pellet 7 serves as a reference as the radiation level is negligible.

Fig. 2 and 3 show the generation of radiolysis gases. Hydrogen and oxygen are formed proportional to the dose. The gas formation does not depend on the pH and the distribution of the α-emitter in the solution. Based on the same mean dose the solutions with doped pellets where the primary products are formed in a volume of only 4 mm^3 give the same results as the solutions with Pu homogeneously distributed in 20 ml. Additional to the gases hypochlorite (Fig. 4), chlorite and chlorate Fig. 5) are formed. While the chlorite concentration always remains at some 10^{-5} Mol/kg the yield of hypochlorite increases with increasing pH and its concentration reaches a plateau value. The chlorate concentration increases practically with the dose but the yield was somewhat smaller than found in earlier experiments [4].

Fig. 6 and 7 show the results with respect to mobilized U and Pu from the pellets. At the beginning of the experiments when the samples were filtrated through 450 and 1.8 nm filters prior to analysis the mobilization of both U and Pu from pellets with
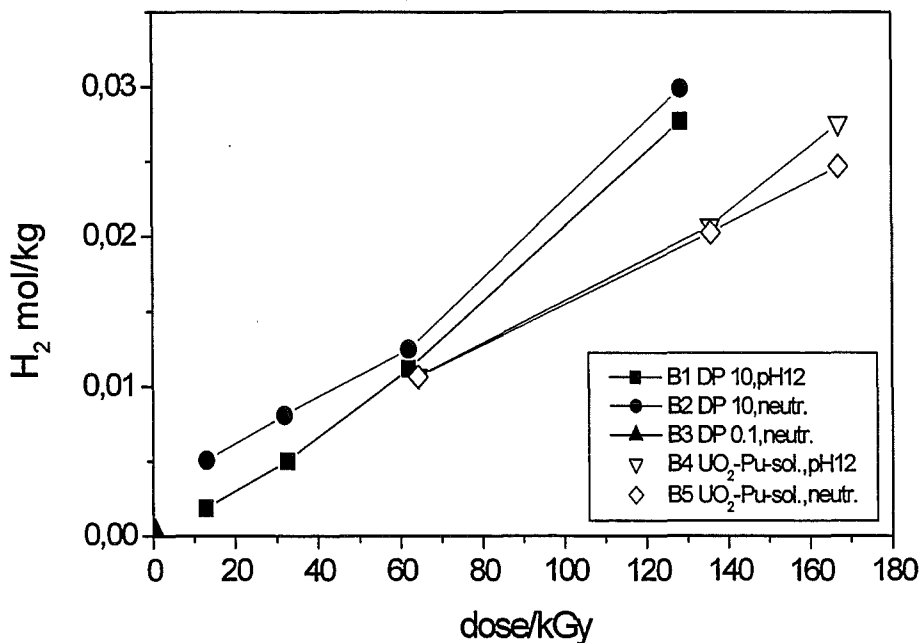
Fig. 2: : H$_2$ formation in 5 M NaCl solution in contact with Pu-doped pellets (B1, B2, B3) in comparison to solutions containing an UO$_2$ pellet and dissolved Pu (B4, B5).
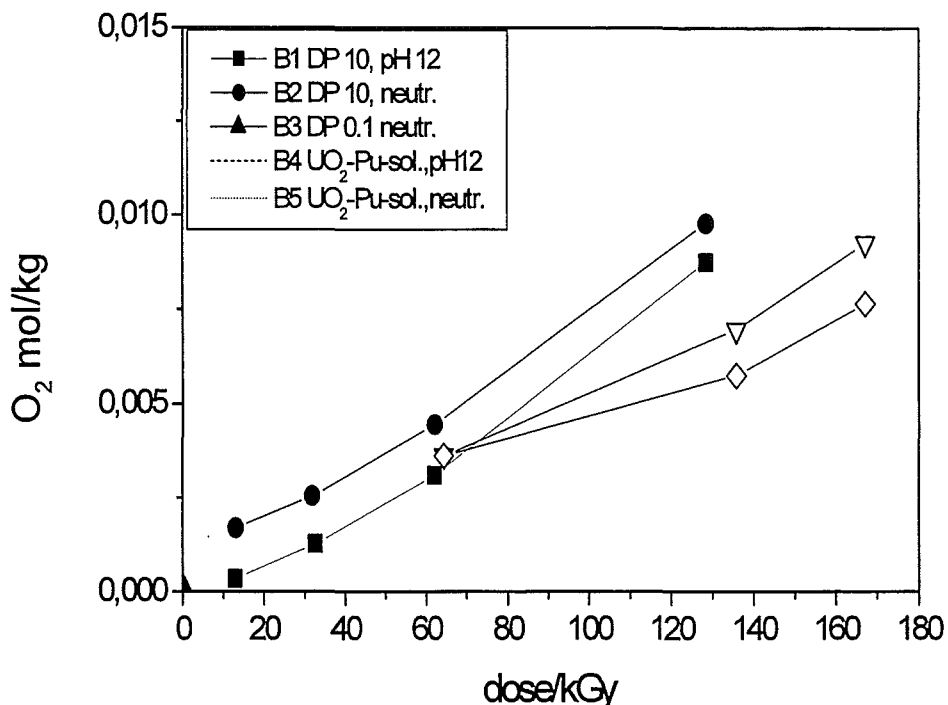
Fig. 3: O₂ formation in 5 M NaCl solution in contact with Pu-doped pellets (B1, B2, B3) in comparison to solutions containing a UO₂ pellet and dissolved Pu (B4, B5).
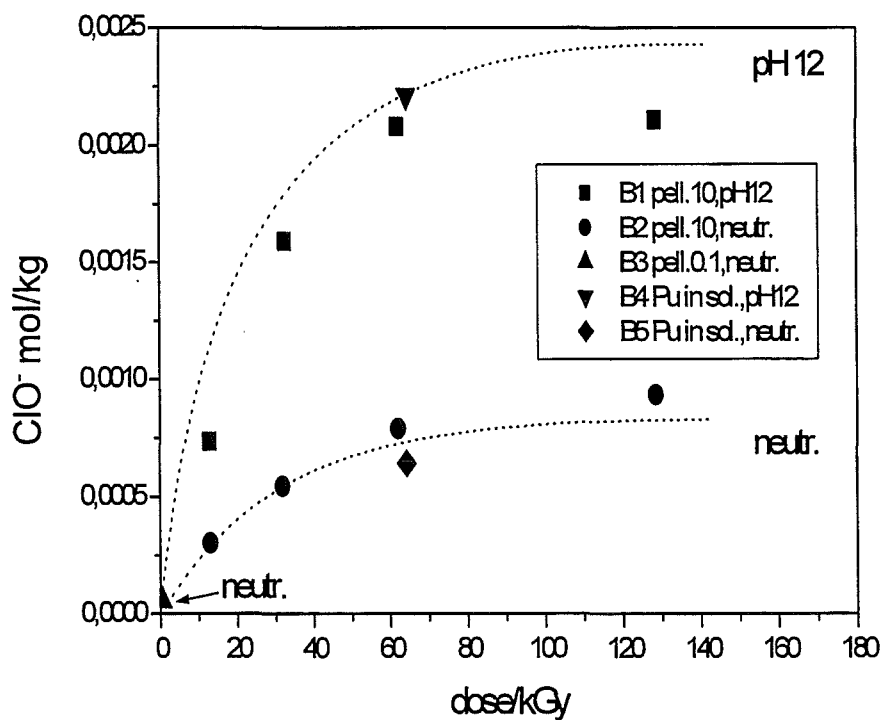
Fig. 4: Formation of hypochlorite in 5 M NaCl solution in contact with Pu-doped pellets (B1, B2, B3) in comparison to solutions containing a UO₂ pellet and dissolved Pu (B4, B5).
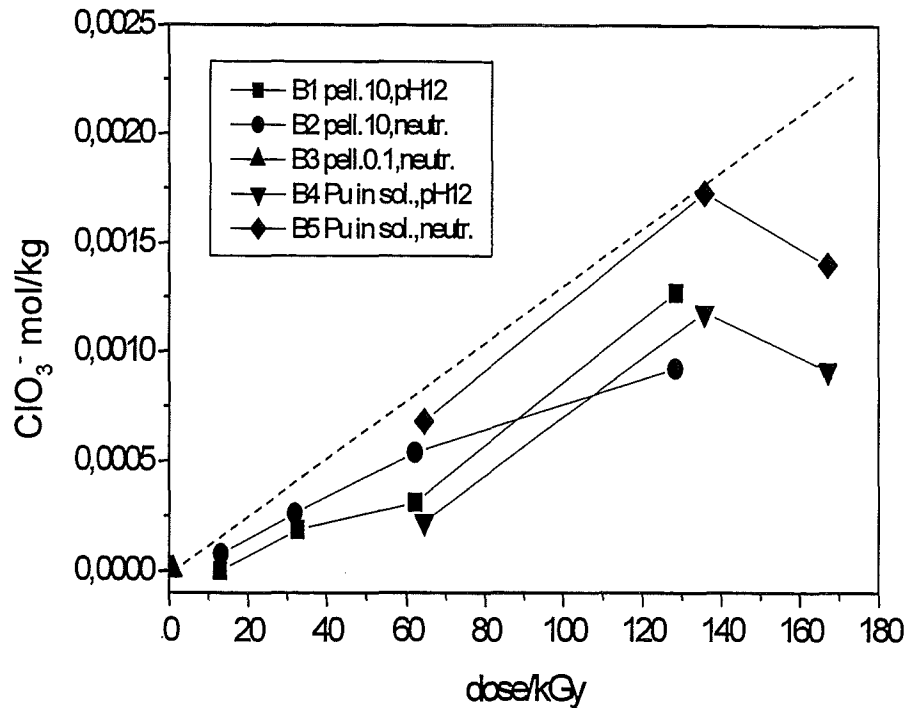
Fig. 5 : Formation of chlorate in 5 M NaCl solution in contact with Pu-doped pellets (B1, B2, B3) in comparison to solutions containing a UO₂ pellet and dissolved Pu (B4, B5). The dashed line corresponds to earlier results [4].

10 % Pu is higher at neutral pH compared to pH 12. With increasing time the differences between the two filtrates become negligible which means that both elements form precipitates which are coarse enough to be removed from both filters. Finally, in the alkaline solution the U concentration is 3 and the Pu concentration 2 orders of magnitude smaller than in neutral solution. The difference in U concentration on grounds of different pH is less pronounced in the experiments with undoped pellets (samples 4 and 5 in table 1). After the application of about 150 kGy the solutions which were acidified straight after sampling show a U concentration of some 10^{-5} Mol/kg and a Pu concentration of a few 10^{-6} Mol/kg independent from pH and from the distribution of the α-source (doped pellet and Pu containing brine, respectively).

Practically no radiolysis products were found in the solutions with pellet 3 and 7 because of the low radiation level. Within the first 9 months of the experiments the U concentration in the solution with pellet 7 ranged between 10^{-8} and 10^{-9} Mol/kg , that in the solution with pellet 3 ranged around 10^{-6} Mol/kg. The Pu concentration in the latter solution was about 10^{-8} Mol/kg.
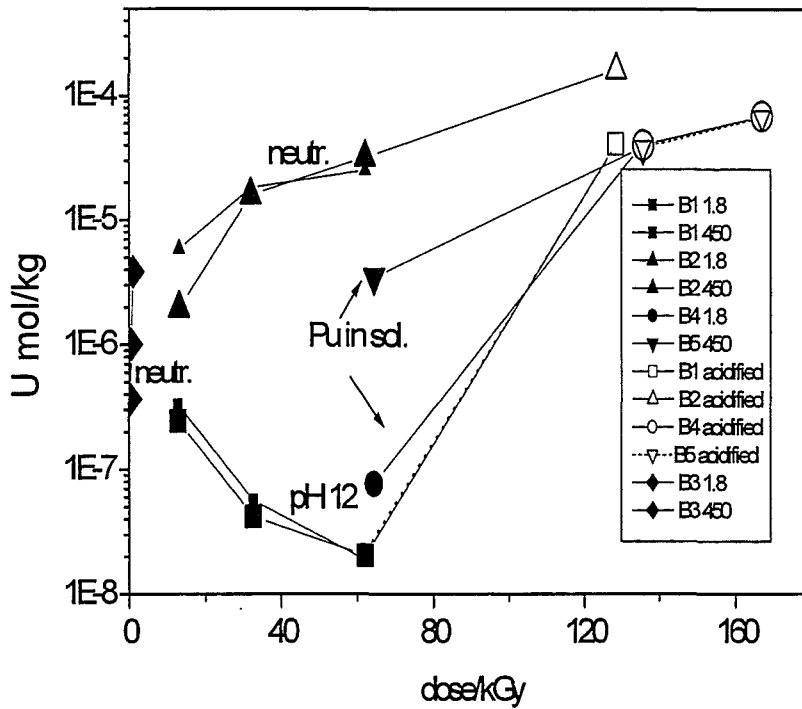
Fig. 6: Mobilized Uranium from UO_2 pellets in 5 M NaCl solution. (Pu-doped pellets: B1, B2, B3; UO_2 pellets and Pu in solution: B4, B5). Closed symbols: Concentration in filtrated (1.8 or 450 nm) samples. Open symbols: Concentrations in acidified samples.
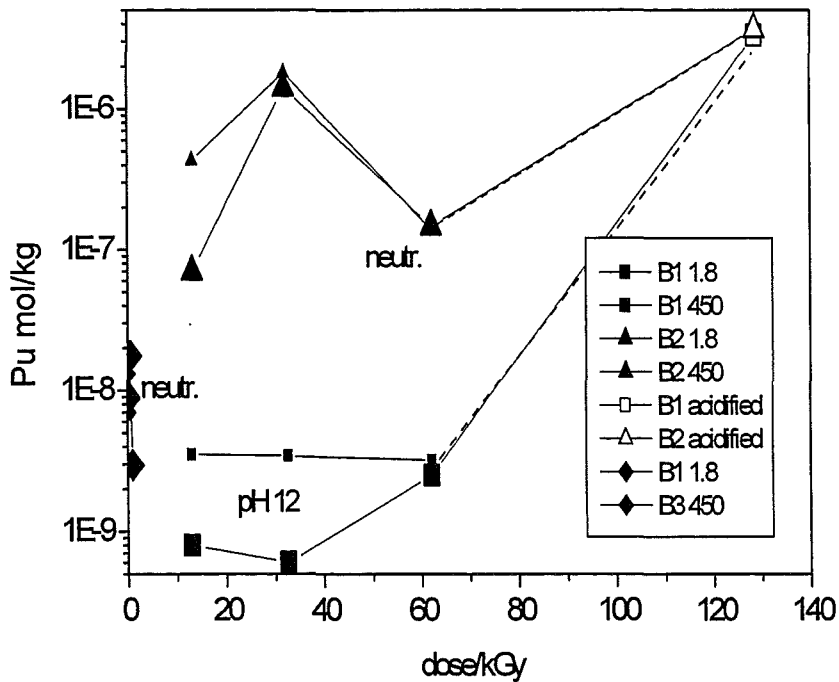
Fig. 7: Mobilized Plutonium from doped UO_2 pellets in 5 M NaCl solution. Closed symbols: Concentration in filtrated (1.8 or 450 nm) samples. Open symbols: Concentrations in acidified samples.

The pH of the solutions with the pellets 1, 2, 4, 5 and 6 (table 1) did not vary with the dose. The redox potential in the alkaline solutions 1 and 4 was about +650 mV, that in the neutral solutions 2 and 5 above +950 mV. The solution with pellet 6 showed more than 1000 mV. The pH of the solutions with pellet 3 and 7 (table 1) which were neutral at the start of the experiment shifted slightly to acidic (down to pH 5.5 and 6.5, respectively) but the pH of solution 3 started to recover after several months. The redox potential of solution 3 reached about +650 mV, that of solution 7 about 530 mV.

The experiment with pellet 6 (table 1) was finished after 4800 hours which equaled the application of 10.8 MGy. The pellet was rinsed with water, dried and then investigated by scanning electron microscopy. Fig. 8 shows the surface of the pellet after the test compared to an uncorroded surface. The surface roughness has increased during the experiment but it is unclear if it is a result of corrosion or/and of secondary phase precipitation.
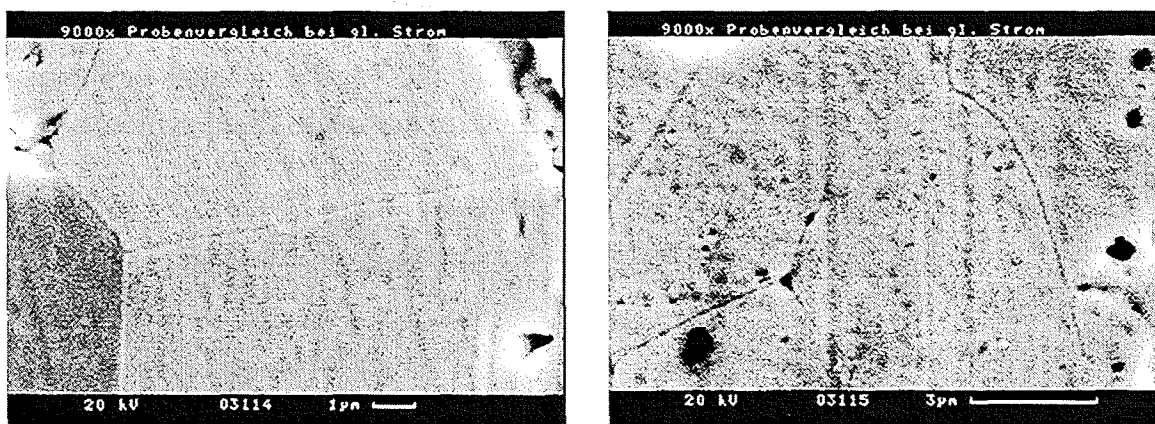
Fig. 8 : SEM picture of a UO_2 pellet before (left) and after (right) corrosion in a Pu-containing 5 M NaCl solution (4800 h, 10.8 MGy).

Discussion

The results with respect to radiolysis gas formation correspond well to earlier experiments [4]. The presence of UO_2 pellets and the irradiation solely from doped pellets has no impact on the radiolytic decomposition of the brine. The yields of $HClO$, ClO_2^- and ClO_3^- can be qualitatively described by the reaction model already published [2], [4]. According to the model chlorate is formed in three ways: Very fast by short-lived radiolysis species, by the slower reaction between chlorite and an excess of hypochlorite and very slowly by the spontaneous decay of hypochlorite.

This mechanism explains the permanently low concentration of chlorite and the limitation of the hypochlorite concentration to a plateau value which depends on the dose rate. In the lower dose range the chlorate formation does not reach the level measured for high dose [1] because of the build-up of hypochlorite. Only at high dose and/or long time the amount of hypochlorite which has not yet been converted to chlorate becomes negligible. The yields of water soluble products do not depend on the distribution of the α-source in the solution (doped pellets or homogeneously dispersed Pu).

Pu and/or U are mobilized from the pellets by oxidative corrosion. The U concentration in the filtrate of the alkaline solution of about 10^{-8} Mol/kg and of some 10^{-5} Mol/kg in the neutral solution of pellet 1, 2, 4 and 5, respectively (fig. 6) correspond to the published solubility data of the orange coloured sodium uranate [13]. The U concentration in the solution 3 of about 10^{-6} Mol/kg seems not to be solubility controlled.

The mobilized Pu from the doped pellets behaves similar to U (fig. 7). The Pu concentrations in solution 1 is probably controlled by the hydrolysis of Pu(VI), while that in solution 2 is about 2 orders of magnitude higher due to complexation by Cl$^-$ and ClO$^-$ [14]. The Pu concentration in solution 3 seems not to be solubility controlled.

From the concentrations of U and Pu in the solutions 1, 2 and 3 one can estimate that the pellets are dissolved congruently and proportional to the α-dose, provided that the analyzed concentrations in the acidified solutions represent the total amounts of mobilized material from the pellets (no precipitation of secondary phases on the walls of the vessel and on the pellets themselves). The U concentration in solution 7 of 10^{-8} – 10^{-9} Mol/kg is within the order of magnitude which is observed for the solubility of 4-valent U [15].

The radiation chemical yield for the oxidation of U and Pu based on the concentrations found in the acidified solutions is less than 1% of the total yield of oxidizing species. Thus, the G-value for U is only <0.01 molecules U^{6+}/100 eV. Even a somewhat lower yield for corrosion is found in experiments in 0.1 M perchlorate solution with an external α-source [17].

The mean corrosion rate for the pellets 1, 2, 4 and 5 after 7400 h which equals a dose of 150 kGy was calculated to be 1.7 μg/(cm^2·d). This UO$_2$ corrosion rate is high

when it is compared to observed rates due to the presence of oxidizing compounds [6], [16] as after 7400 h the solutions contained roughly 10^{-3} Mol/kg ClO^-, 10^{-3} Mol/kg ClO_3^- (fig. 4 and 5) and $3 \cdot 10^{-6}$ Mol/kg dissolved O_2 as potentially oxidizing agents. According to the published data for chemical corrosion a UO_2 dissolution rate of 1.7 $\mu g/(cm^2 \cdot d)$ would require a concentration of about 0.1 Mol/kg of H_2O_2 or O_2 [6] or ClO^- [16]. From that fact one can conclude for the time/dose range under investigation that the UO_2 corrosion under irradiation conditions is much more effective than that caused by the oxidizing long-lived radiolysis species.

The mean corrosion rate for solution7 (table 1) after 7500 h was $2.7 \cdot 10^{-4}$ $\mu g/(cm^2 \cdot d)$ which is close to the published rate $(2 \cdot 0^{-4}$ $\mu g/(cm^2 \cdot d))$ for diluted aqueous solutions [6].

Acknowledgement

References

1. Kelm, M. and Bohnert, E.: Radiation chemical effects in the near field of final disposal site. Part 1: Radiolytical products formed in concentrated NaCl solutions, Nucl. Technol., 129, 119-122 (2000)

2. Kelm, M. and Bohnert, E.: Radiation chemical effects in the near field of final disposal site. Part 2: Simulation of the radiolytic processes in concentrated NaCl solutions, Nucl. Technol., 129, 123-130, (2000)

3. Kelm, M., Pashalidis, I. and Kim, J., I.,: Spectroscopic investigation on the formation of hypochlorite by alpha radiolysis in concentrated NaCl solutions. Appl.Radiat.Isot. 51, 637-642 (1999)

4. Kelm, M., Bohnert, E., Pashalidis, I.; Products formed from alpha radiolysis of chloride brines, Res.Chem.Intermed., 27, No 4,5, 503 - 507 (2001)

5. Carver, M.B., Hanly, D.V., Chaplin, K.R.,1986/87. MACKSIMA-CHEMIST, Mass Action Chemical Kinetics Simulation; Automatic Chemical Equation Manipulation and Integration using stiff, sparse Techniques.1978/79. Revised by Paquette, J. .Atomic Energy of Canada Ltd., AECL 6413

6. Shoesmith, D., W., Sunder, S., The prediction of nuclear fuel (UO_2) dissolution rates under waste disposal conditions, J.Nucl.Mater. 190, 20-35 (1992)

7.   Sunder, S, Shoesmith, D., W., Chemistry of UO_2 fuel dissolution in relation to the disposal of used nuclear fuel. AECL - 10395 (1991)

8.   Shoesmith, D., W., Fuel corrosion processes under waste disposal conditions, J.Nucl.Mater. 282 (2000) 1-31

9.   Rondinella, V.,V., Matzke, Hj., Cobos, J., Wiss, T., α-Radiolysis and α-radiation damage effects on UO_2 dissolution under spent fuel storage conditions, Mat.Res.Soc.Symp.Proc. 556 (1999) 447-454

10.   Rondinella, V.,V., Matzke, Hj., Cobos, J., Wiss, T., Leaching behaviour of UO_2 containing α-emitting actinides, Radiochim.Acta, 88, 527-531 (2000)

11.   Gray, W., J., Comparison of Uranium release from spent fuel and unirradiated UO_2 in salt brine, Mat. Res.Soc.Symp.Proc. 84 (1987) 141-152

12.   Garisto, F., The energy spectrum of α-particles emitted from used CANDU™ fuel, Ann.Nucl.Energy 16 No1, 33-38 (1989)

13.   Diaz Arocas, P., Grambow, B., Solid-liquid phase equilibria of U(VI) in NaCl solutions, Geochim.Cosmochim.Acta, 62, No2, 245-263 (1998)

14.   Pashalidis, I., Kim, J., I.,Untersuchung der Übertragbarkeit von Labordaten auf natürliche Verhältnisse. Chemisches Verhalten des sechswertigen Plutoniums in konzentrierten NaCl- Lösungen unter dem Einfluß der eigenen Alpha-Strahlung. RCM 01092 (1992)

15.   Ollila, K., Dissolution of unirradiated UO_2 fuel in synthetic groundwater - Final report (1996 - 1998), Posiva 99-24 (May 1999)

16.   Grambow, B., Loida, A., Dressler, P., Geckeis, H., Gago, J., Casas, I., de Pablo, J., Giminez, J., Torrero, M.E., Chemical Reaction of Fabricated and High Burnup Spent UO_2 Fuel with Saline Brines, FZKA 5702 (1996)

17.   Sunder, S:, Shoesmith, D., W., Miller, N., H., Oxidation and dissolution of nuclear fuel (UO_2) by the products of the alpha radiolysis of water, J.Nucl.Mater. 244(1997) 66-74

III.   Assessment of the Barrier Disposal Container: Contact corrosion between Ti99.8 and carbon steel

(E. Smailos, B. Fiehn, R. Weiler, INE)

Abstract

Present designs for long-lived HLW/spent fuel disposal containers in a rock salt repository consider the use of a thick-walled container made of the corrosion allowance material carbon steel that is surrounded by an outer thin-walled container made of the corrosion resistant alloy Ti99.8-Pd. In this study, it was investigated whether by pitting corrosion of the outer container material and intrusion of brine in the space between the containers, a contact corrosion can occur on this material pair resulting to an acceleration of the corrosion rate of the less noble carbon steel or to a change of the corrosion mechanism. For this, long-term immersion experiments were performed on coupled specimens of Ti99.8-Pd and the preselected carbon steel TStE355 in a disposal relevant NaCl-rich brine (25.9 wt% NaCl) at 150°C with and without a gamma radiation field (10 Gy/h). The results indicate that no contact corrosion occurs between Ti99.8-Pd and carbon steel in the NaCl-rich brine. The coupled specimens of both materials are resistant to pitting corrosion and their general corrosion rates are not accelerated compared to the values of uncoupled specimens obtained in previous work.

Introduction

The aim of the project is the determination of materials for long-lived HLW/Spent Fuel disposal containers, and the quantification of the effectiveness of such containers (overpacks) as a barrier against a mobilization of radionuclides from the waste forms by attack of brines. This requires detailed knowledge of the long-term corrosion behaviour of the container materials under realistic disposal conditions and of the retention of leached radionuclides on container corrosion products.

An important aspect of the corrosion studies is the investigation of the influence of the container design on the long-term corrosion behaviour of the container materials under relevant disposal conditions in a rock salt repository. A potential packaging design for vitrified HLW and spent fuel is the use of a double-walled container (overpack) surrounding the canisters. This consists of an inner thick-walled carbon steel container as mechanical support against the rock pressure which is corrosion

486

protected by a thin-walled container made of the alloy Ti99.8-Pd. By use of a such metal combination and penetration of the outer steel container (e.g. by pitting corrosion) with resulting intrution of brine in the space between the containers, a contact corrosion can be established between the container materials. In this case, an increase in the corrosion rate of the less noble carbon steel and a decrease in the corrosion rate of the more noble Ti99.8-Pd is expected. However, due to the formation of aggressive Fe^{3+} from the corrosion of the steel, an acceleration of the pitting corrosion of Ti99.8-Pd could occur. Under this aspect it is investigated in this study whether under realistic disposal conditions (salt brines, high temperature) a contact corrosion occurs on the metal pair Ti99.8-Pd and TStE355 carbon steel (0.17 wt.% C).

Experimental

The materials TStE355 carbon steel and Ti99.8-Pd were investigated in the hot-rolled and annealed condition and had the following composition in wt.%:

TStE355 steel: 0.17 % C; 0.44 % Si; 1.49 % Mn; bal. Fe.

Ti99.8: 0.18 % Pd; 0.05 % Fe; 0.01 % C; 0.04 % O_2; bal. Ti.

Contact assemblies were formed by bolting one flat coupon of Ti99.8-Pd (40mm x 20mm x 4mm) with one flat coupon of carbon steel (40mm x 20mm x 4mm). The two coupons were provided with bores in both ends and were fastened with titanium-screws. The bores were isolated by PTFE. The experiments were performed in autoclaves and the specimens were totally immersed in a NaCl-rich brine (25.9 wt.% NaCl, pH (25°C) = 6.5). The test temperature was 150°C and the maximum test duration about 18 months. Experiments were performed both with and without gamma radiation of 10 Gy/h. This dose rate corresponds to the value on the surface of the thick-walled container discussed.

The experimenal setups used for the experiments are described in previous work [1]. Briefly, for the experiments without irradiation, stainless steel pressure vessels provided with corrosion resistant insert vessels made of PTFE were used to avoid evaporation of the brine (boiling point: about 115°C). The experiments under gamma irradiation were performed in the spent fuel storage pool of KFA Jülich. For these experiments, autoclaves made of Ti99.8-Pd were used. Every autoclave contained 160 ml brine and two coupled specimens of 80 cm^2 total surface. This gave a brine volume-to-specimen surface ratio of 2 ml/cm^2. With these experimental equipments,

the initial test conditions were oxidizing. The total amount of oxygen available in the systems was about 15 mg, corresponding to 0.19 mg O_2/cm^2 specimen. This oxygen amount was consumed very fast by reactions with Fe so that after a few days reducing conditions were established.

Evaluation of the specimens regarding general and local corrosion was carried out by gravimetry, measurements of pit depth, surface profilometry and metallography. Both the contact area and the free specimen area were investigated for local attacks. The integral corrosion rate of the specimens was calculated from the experimental determined weight losses and the material density.

Results

The thickness reduction (general corrosion) of the coupled specimens of Ti99.8-Pd and TStE355 carbon steel specimens in NaCl-rich brine at 150°C with and without gamma radiation is plotted in Figures 1 and 2. In both cases with and without gamma radiation the thickness reduction of the passive corroded alloy Ti99.8-Pd is negligible low (0.1 μm at the maximum). The thickness reduction of the carbon steel in the brine with and without gamma radiation increases linearly with the exposure time (Figure 1 and 2). The calculated linear corrosion rates of the coupled specimens of Ti99.8-Pd and carbon steel in the NaCl-rich brine (T = 150°C) are given in Table 1. For comparison the values of uncoupled (single) specimens of these materials determined in previous investigations [1,2] are also given. For Ti99.8-Pd, the corrosion rates of the coupled specimens are negligible low (0.07 μm/a - 0.1 μm/a) and very close to the values of the uncoupled specimens (0.02 μm/a - 0.05 μm/a). In the case of the carbon steel the corrosion rates of the coupled specimens in NaCl-rich brine without radiation (14.2 μm/a) correspond very well to the values of the uncoupled specimens (15.3 μm/a). In the presence of a gamma radiation field of 10 Gy/h, the corrosion rate of the contact steel specimens in the brine is clearly lower (5.4 μm/a) than without irradiation. The lower corrosion rate under irradiation could be explained by the formation of a very dense protective oxide layer (Fe_3O_4) on the steel specimens in the contact area between steel and Ti99.8-Pd, which was observed in the metallographic examinations.
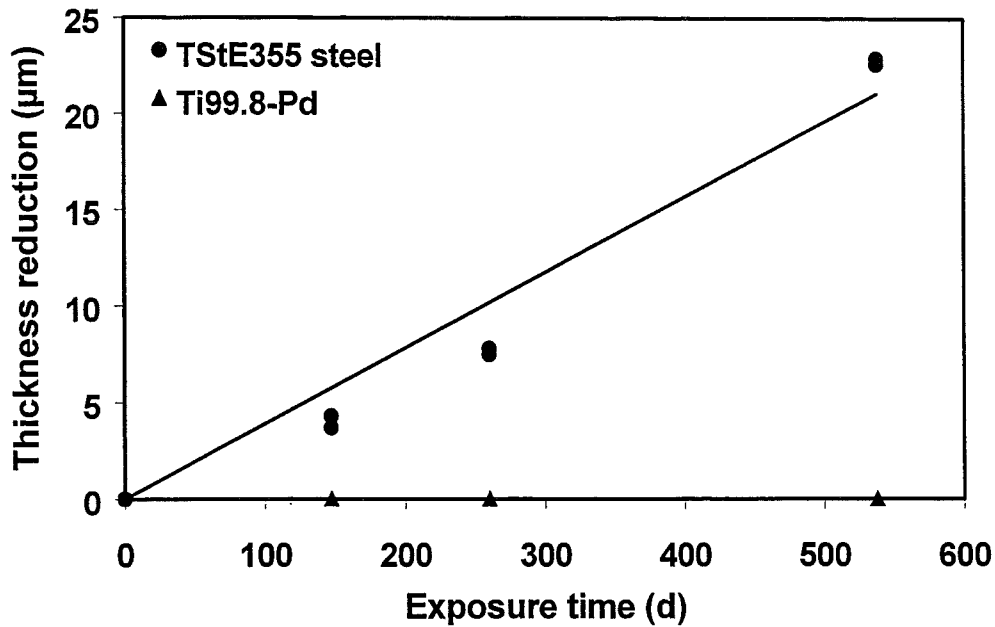
Fig. 1: General corrosion of coupled specimens of Ti99.8-Pd and TStE355 carbon steel in NaCl-rich brine at 150°C
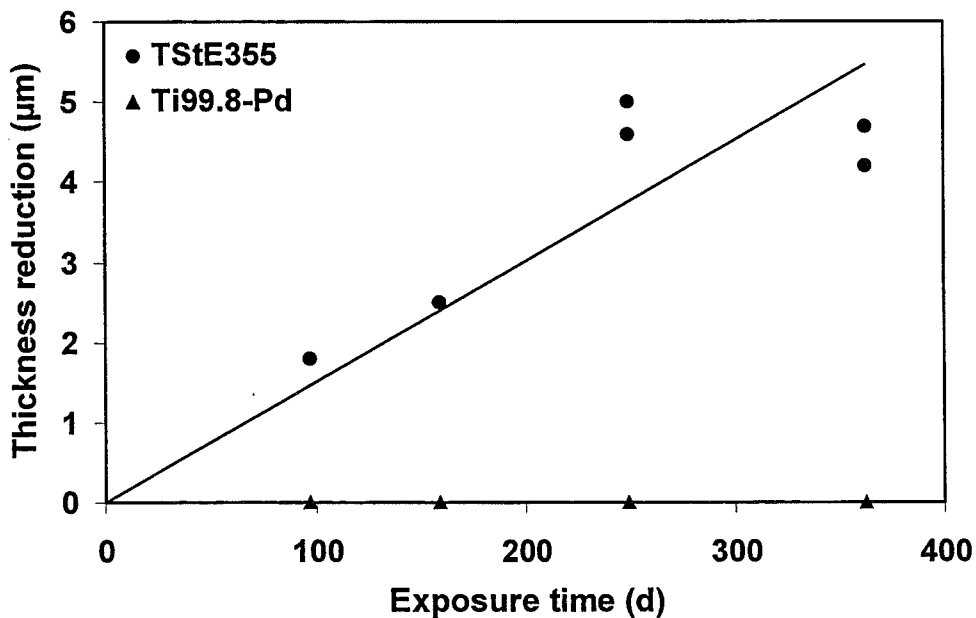
Fig. 2: General corrosion of coupled specimens of Ti99.8-Pd and TStE355 steel in NaCl-rich brine at 150°C and 10 Gy/h

The metallographic examinations of coupled Ti99.8-Pd specimens do not show any signs of corrosion neither in the contact area to steel nor in the free specimen area. For the steel specimens, a slight non-uniform corrosion (20 - 30 μm after one year

immersion) was observed in the contact area to Ti99.8-Pd and in the free area of the specimens. In general, it can be stated that in the contact area of the coupled specimens no preferential corrosion attack was observed, compared to the free specimen area.

The results obtained indicate that the coupling of Ti99.8-Pd and TStE355 carbon steel does not accelerate the corrosion rate of the individual materials in NaCl-rich brine. This means that in this brine no serious contact corrosion between Ti99.8-Pd and TStE355 carbon steel is expected. Contact corrosion studies in MgCl$_2$-rich brine are in progress.

Table 1: Comparison of the corrosion of coupled and uncoupled specimens of Ti99.8-Pd and TStE355 steel in NaCl-rich brine at 150°C

Material	Corrosion conditions	Corrosion rate (µm/a)	
		coupled specimens	uncoupled specimens
Ti99.8-Pd	NaCl-brine	0.07 ± 0.01	0.02 ± 0.01
	NaCl-brine/10 Gy/h	0.10 ± 0.05	0.05 ± 0.02
TStE355 steel	NaCl-brine	14.2 ± 1.6	15.3 ± 1.0
	NaCl-brine/10 Gy/h	5.4 ± 0.5	13.5 ± 1.8

References

1.   E. Smailos, A. Martínez-Esparza, B. Kursten, G. Marx, I. Azkarate, "Corrosion Evaluation of Metallic Materials for Long-Lived HLW/Spent Fuel Disposal Containers," EUR-Report 19112 (1999).

2.   E. Smailos, J.A. Gago, I. Azkarate, B. Fiehn, "Corrosion Studies on Selected Packaging Materials for Disposal of Heat-Generating Radioactive Wastes in Rock-Salt Formations," FZKA-Report 5587 (1995).

IV.   Chemie und Stabilität der Versatzmaterialien
(H. Hofmann, A. Bauer, T. Schäfer, Th. Rabung, INE; F. Claret, E. Ferrage, B. Lanson, Environmental Geochemistry Group, University Grenoble)

Einleitung

Ein Teil unserer aktuellen Arbeiten steht im Zusammenhang mit einem möglichen Endlager im Salz. Aufgrund von Arbeiten für das Forschungsbergwerk Asse und das ehemalige Endlager Morsleben werden verschiedene Materialen auf Ihre mögliche Eignung als Versatzmaterial im Salz untersucht. Hierbei steht neben ihrer mineralogischen Stabilität auch die durch sie beeinflusste Entwicklung der Lösungschemie und somit der Einfluss auf die Löslichkeit von Radinukliden im Vordergrund. Als potenzielle Wirtsgesteine für Endlager kommen sowohl Salz als auch andere Gesteinsformationen wie Granit und Ton in Betracht.

Unsere Forschungsarbeiten auf dem Gebiet der Tone sind vielfältig. Untersucht werden aufgereinigte Tone, Bentonite, aber auch Proben aus Tonformationen, welche für die Endlagerung vorgesehen sind (z. B. Opalinus Ton und Tone aus dem zukünftigen französischen Forschungslabor in Bure).

Einen Schwerpunkt der Arbeiten bildet die Untersuchung der Wechselwirkungen der verschieden Barrieren untereinander. Untersucht werden hierbei z. B. die Wechselwirkungen von Bentonit aber auch Wirtsgesteinen aus Tonformationen mit Fe^0 (Kanistermaterial) oder Zement. Ein weiterer aktueller Forschungsschwerpunkt dreht sich um die thermische Stabilität der Tonmineralien in Bure. Diese Arbeiten finden in Kooperation mit der Universität in Grenoble und der ANDRA (Agence nationale pour la gestion des déchets radioactifs) statt.

Bei Voruntersuchen zur chemischen Stabilität der Tonmineralien aus Bure wurde im alkalischen Milieu die Freisetzung von humin- und fulvinartiger Substanz beobachtet [1]. Der Einfluss dieser Organik auf die chemische Stabilität und das Sorptionsverhalten von Tonen ist ein weiterer Gegenstand aktueller Forschungsarbeiten.

Untersuchungen zur Sorption von Radionukliden an aufgereinigten Tonen werden zusammen mit dem FZ Rossendorf mit dem Ziel durchgeführt, das hier gewonnene Prozessverständnis auf komplexe Wirtsgesteinformationen zu übertragen.

Im folgenden werden ausgewählte Beispiele der Arbeiten vorgestellt.

1. Stabilität von Ton in salinaren Lösungen

Im Forschungsbergwerk Asse werden seit über 30 Jahren unter realistischen Bedingungen Forschungs- und Entwicklungsarbeiten für die sichere Endlagerung radioaktiver Abfälle durchgeführt. So kam es in den Jahren 1967 bis 1978 zur Versuchseinlagerung von 125.000 Behältern schwach- und 1300 Fässern mittelradioaktiver Abfälle. Seit August 1995 werden zur Stabilisierung des Grubengebäudes die im jüngeren Steinsalz noch offen stehenden Abbaue in der Südflanke mit Rückstandssalz des ehemaligen Kalibergwerkes Ronnenberg verfüllt. Da eine weitere Verwendung des Bergwerkes nicht beabsichtigt ist, wird die Schließung der Anlage vorbereitet.

Das übergeordnete Ziel aller Maßnahmen zur Schließung der Schachtanlage Asse ist ein gefahrloser Abschluss der eingelagerten radioaktiven Abfälle von der Biosphäre. Es ist deshalb ein Konzept zu entwickeln, das den Abschluss mit ausreichender Rückhaltung realisiert und den wesentlichen Prozessen und Abläufen in den einzelnen Grubenbereichen in der Nachbetriebsphase Rechnung trägt.

Im Rahmen der Schließung der Schachtanlage Asse hat der im Grubengebäude aufgeschlossene Carnallitit im Zusammenhang mit dem Lösungszutritt eine besondere Bedeutung. Wegen der Löslichkeit der im Carnallitit enthaltenen Minerale in diesen Lösungen ist bei einem NaCl - Salzlösungszutritt in der Nachbetriebsphase mit Umlöseprozessen im Carnallitit zu rechnen.

Als Beispiel für die aktuellen Arbeiten sei die Stabilität von Smectit näher erläutert. Der Hauptbestandteil von Bentoniten, Smectit, kann mit Salzlösungen zu Illit/Smectit Wechsellagerungen reagieren. Dies führt zum Verlust der quellfähigen Schichten und – damit verbunden – der Plastizität aber auch zu einer deutlichen Verringerung der Kationen-Austausch-Kapazität. Zu Klärung der Stabilitätsfrage unter Asse-spezifischen Bedingungen wurden zwei handelsübliche Smectite (Ibeco „Seal 80" und „Tixoton TE") mit Mg- reichen Lösungen zur Reaktion gebracht. Die Versuche wurden bei 25°C in einer Argon-Handschuhbox unter CO_2 Ausschluss durchgeführt.

Asse System Ibeco Seal 80
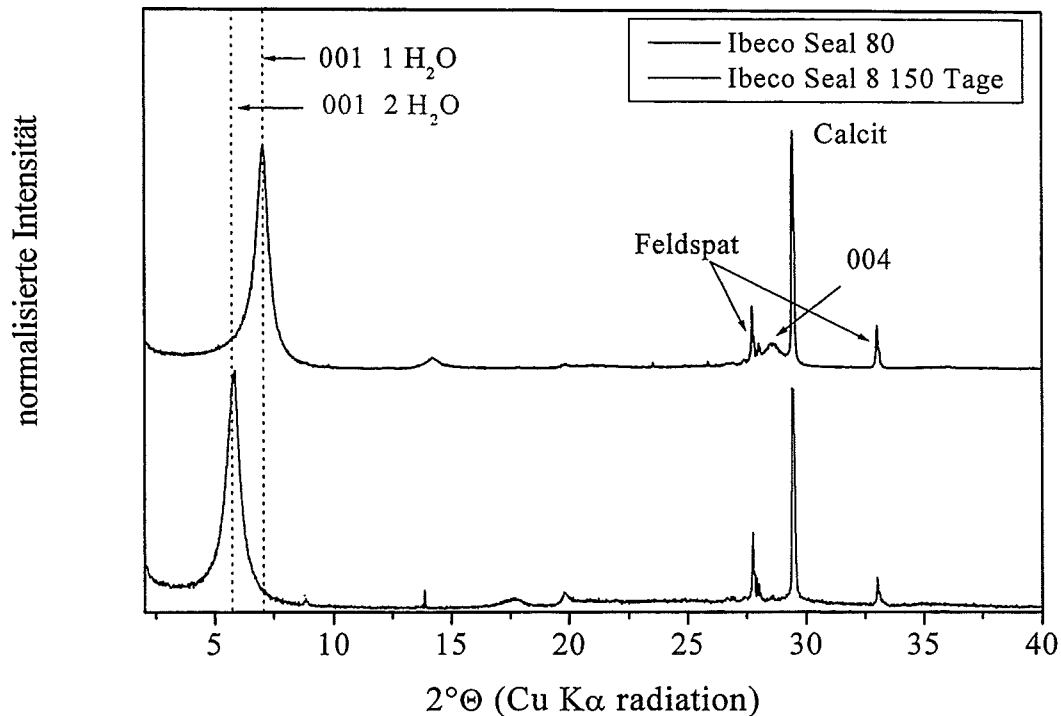
Abb. 1: Die Tone zeigen nur den Austausch von Natrium gegen Magnesium. Ansonsten ist keinerlei Veränderung der Röntgendiffraktogramme zu erkennen.

Zur Beantwortung der Frage, ob sich verschiedene Materialen für den Versatz bei der Schließung des Forschungsbergwerks Asse eignen, werden von Seiten des INE zahlreiche Arbeiten durchgeführt. Im Vordergrund der Untersuchungen steht neben der Stabilität der Materialen in magnesiumreichen Laugen auch der Einfluss, den diese Materialien auf die Lösungschemie und damit die Radionuklidlöslichkeit haben.

Schon innerhalb der ersten 3 Tage ist bei den orientierten Proben der Austausch von Natrium aus den Schichtzwischenräumen gegen das Magnesium aus der Lösung zu erkennen. Dadurch kommt es zu einer Quellung, da Magnesium mit seinen zwei Hydratwasser in den Schichtzwischenräumen Natrium mit nur einem Hydratwasser verdrängt (Abb. 1). Ansonsten ist über die gesamte Versuchsdauer keinerlei Veränderung des Systems zu erkennen. Weder die Lage der 001-Reflexe der Proben noch ihre Form bzw. Halbwertsbreite änderte sich merklich.

493

Schichtladungsverteilung IBECO Seal 80 bulk

$\xi = 0{,}326$

Häufigkeit [%]

Schichtladung [eq/(Si, Al)$_4$O$_{10}$]

Schichtladungsverteilung IBECO 3 Tage

$\xi = 0{,}310$

Häufigkeit [%]

Schichtladung [eq/(Si, Al)$_4$O$_{10}$]

Schichtladungsverteilung IBECO 80 Tage

$\xi = 0{,}308$

Häufigkeit [%]

Schichtladung [eq/(Si, Al)$_4$O$_{10}$]

Schichtladungsverteilung IBECO 150 Tage

$\xi = 0{,}321$

Häufigkeit [%]

Schichtladung [eq/(Si, Al)$_4$O$_{10}$]
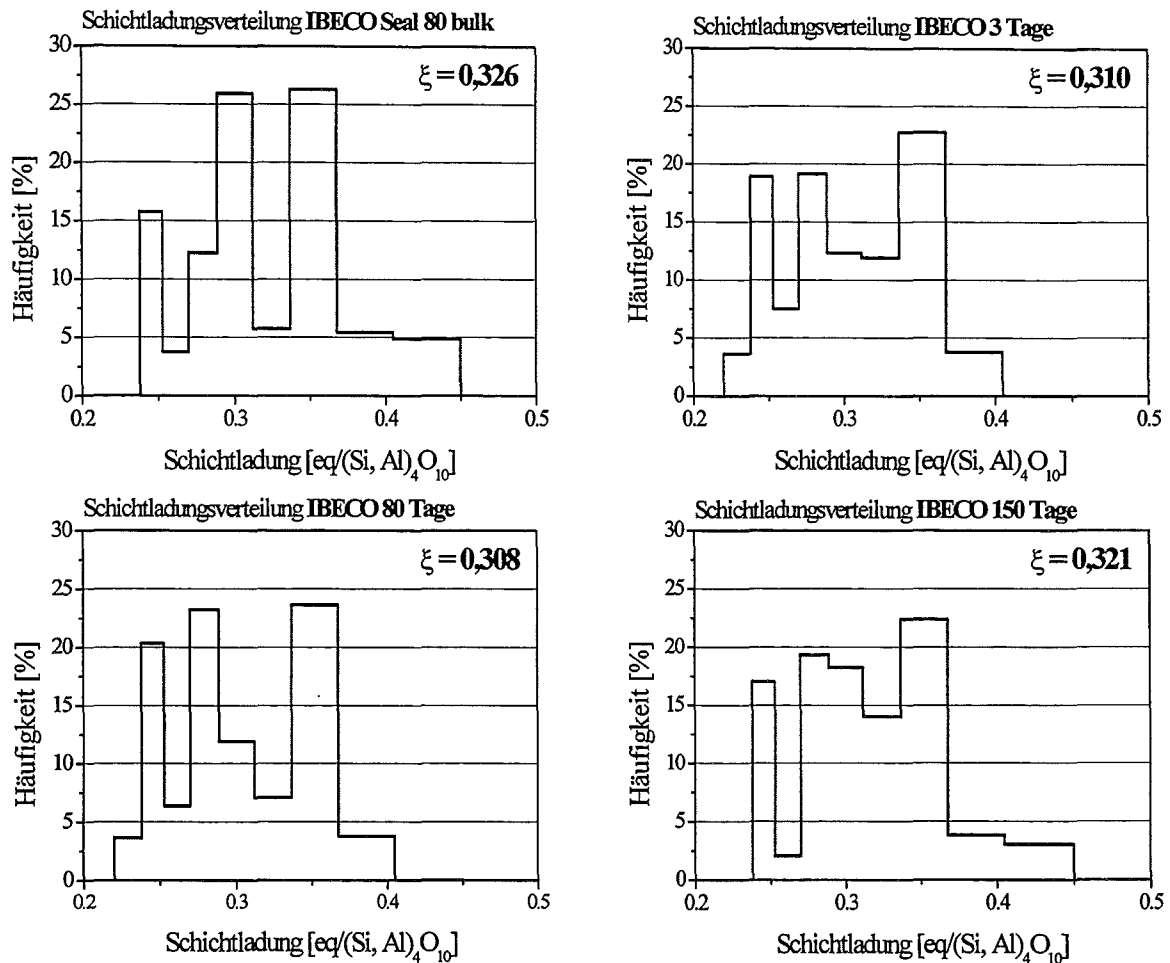
Abb. 2: Entwicklung der Schichtladung von Ibeco Seal 80 in Mg-reicher Lauge mit zunehmender Reaktionsdauer

Im Versuchsverlauf schwankte die Kationen-Austausch-Kapazität (KAK) bei Ibeco Seal 80 nach Salzzugabe innerhalb des Messfehlers. Bei Tixoton TE reduzierte sich die KAK innerhalb der ersten 3 Versuchstage von 72 auf 66 meq/100g. Abgesehen von diesem Rückgang konnte nach den ersten 3 Versuchstagen für Tixton TE keine nennenswerte Änderung der KAK beobachtet werden.

Die permanente Schichtladung des Ausgangsmaterials Ibeco Seal 80 liegt geringfügig höher (ca. 0,02 eq/(Si,Al)$_4$O$_{10}$) als die des Ausgangsmaterials Tixoton TE. Bei beiden Materialien ist die Ladungsdichte während des Versuchszeitraumes von bis zu 150 Tagen sehr geringen Schwankungen unterworfen, wobei jedoch keine tendenzielle Änderung festzustellen ist (Abb. 2). Auch bei Betrachtung der Ladungsverteilung der beiden Ausgangsstoffe ist in Abhängigkeit der Versuchsdauer keine

Änderung in der Charakteristik der Verteilungskurven festzustellen. In Anbetracht dessen ist davon auszugehen, dass die Salzlösungen keine mikrostrukturellen Änderungen innerhalb der Kristallstruktur der Minerale verursacht haben, welche zu einer Änderung der permanenten Schichtladung hätten führen können.

Die durchgeführten Versuche zeigen, dass Smectit sich als Versatzmaterial unter denen für das Forschungsbergwerk Asse definierten Bedingungen eignet.

Wechselwirkung von Tonen aus dem zukünftigen französischen Felslabor in Bure und alkalischen Lösungen

Einen zentralen Arbeitsschwerpunkt bildet das zukünftige französische Felslabor in Bure. Durch die Anordnung vom dritten August 1999 autorisierte die französische Regierung die ANDRA mit dem Bau eines wissenschaftlichen Forschungslabors in Bure.

Das zukünftige Forschungslabor befindet sich im Osten Frankreichs im Departement Haute Marne. Geplant ist das Labor in einer Tiefe von 490 Metern. Es nimmt damit Platz in den Schichten des Oberen Jura. Diese marinen Sedimente haben eine Mächtigkeit von 130 Metern und wurden an der Grenze des mittleren und oberen Jura (~ 160 Mio. Jahren) abgelagert. Sie bestehen im wesentlichen aus Ton mit Calcit und Pyrit als Nebengemengteil. Die Organik variiert zwischen 1-2 Gewichtsprozent im Sediment. Messungen der Vitrinit-Reflexion und Untersuchungen an Fluideinschlüssen ergaben, dass die maximale im Sediment erreichte Temperatur 50°C nicht überstieg [2 – 4].

Im Rahmen einer Doktorarbeit wurde zusammen mit Universität in Grenoble zunächst die Charakterisierung der Tonmineralogie durchgeführt. Die abgetrennte Tonfraktion (< 2μm) besteht hauptsächlich aus einer Wechsellagerung, welche sich wiederum aus einer ungeordneten Illit/Smectit/Vermiculit Wechsellagerung, Illit und Smectit zusammensetzt (Abb. 3). Mit zunehmender Teufe nehmen die relativen Anteile von Kaolinit und Chlorit zu. Die Modellierung der Röntgenspektren zeigte, dass bei der ungeordneten Illit/Smectit/Vermiculit Wechsellagerung der Vermiculit-
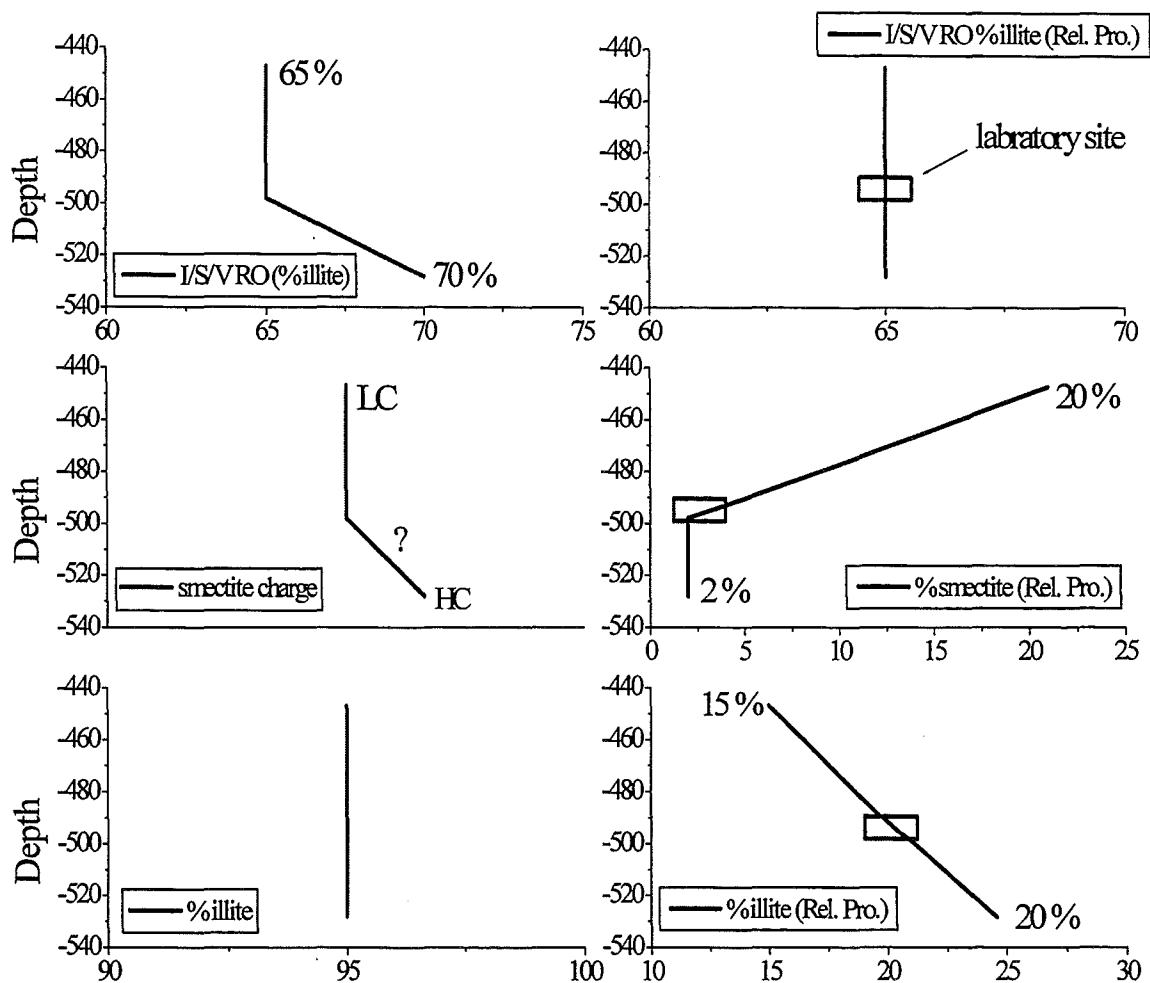
Abb. 3: Entwicklung der Tonmineralogie als Funktion der Tiefe im zukünftigen französischen Forschungslabor in Bure [1].

Anteil mit zunehmender Teufe abnimmt, die relativen Anteile an der Wechsellagerung aber konstant bleiben. Der Smectit scheint mit zunehmender Teufe seine Schichtladung zu erhöhen, während die relativen Anteile mit der Tiefe hin abnehmen. Etwa auf dem Niveau des zukünftigen Felslabors (~ 490 m) erreicht der Smectit-Gehalt seinen niedrigsten Wert, bleibt aber dann konstant. Die rein illitische Phase setzt sich aus Illit mit keinerlei oder kaum quellfähigen Anteilen zusammen, welcher mit zunehmender Teufe von 15 auf etwa 20 Prozent an relativen Anteilen zunimmt.

Einen Arbeitsschwerpunkt stellen Untersuchungen zur Wechselwirkung von alkalischen Lösungen, welche typisch für die Alteration von Zement sind, und den Sedimenten potentieller Endlagerformationen dar. Ausgangsmaterialien für die

Untersuchungen sind neben Sedimenten aus dem französischen Felslabor in Bure der Opalinus-Ton.

Sample 447, L/S 80 EG
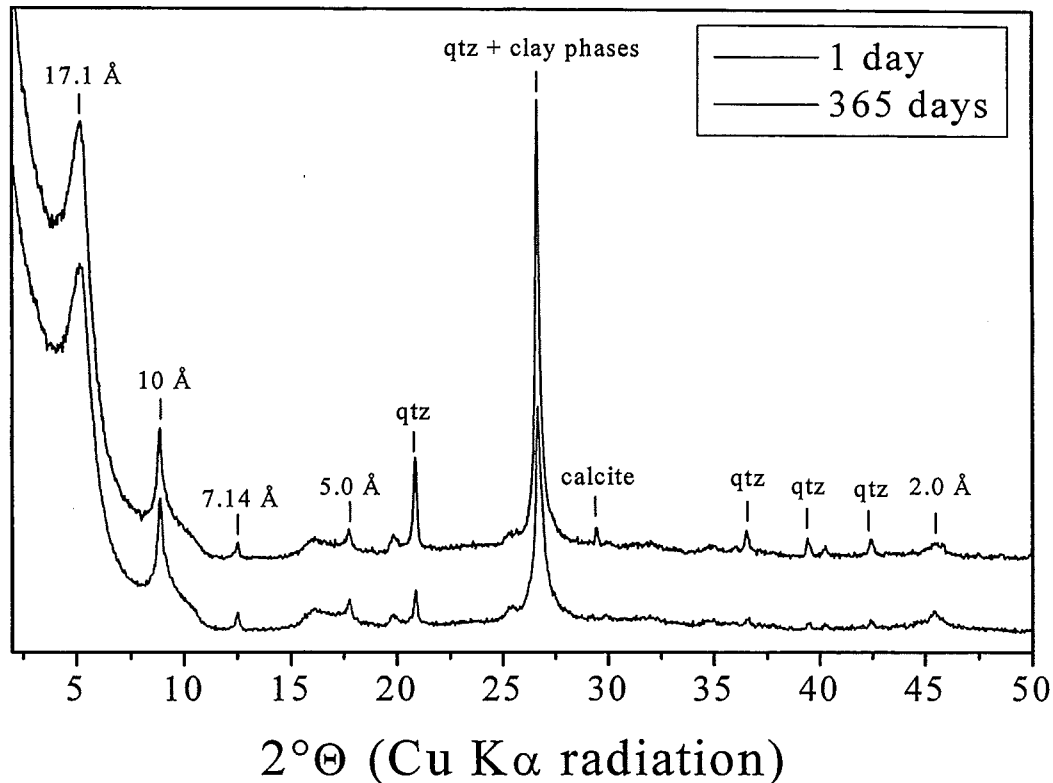
Abb. 4: Tonproben aus Bure (hier aus einer Teufe von 447 m) zeigen in alkalischen Lösungen (pH 13.2) über die Versuchsdauer von einem Jahr keine Reaktion [5].

Unsere Arbeiten konnten zeigen, dass die Tone aus Bure mit alkalischen Lösungen nur wenig reagieren (Abb. 4). Während aufgereinigte Tone wie Kaolinit oder Smektit in äquivalenten Lösungen Transformationen nach Illit zeigten, schien das Probenmaterial aus Bure wenig anfällig. Messungen der Lösungszusammensetzung ergaben mit Fortlauf der Experimente eine Zunahme der $C_{org.}$ Gehalte (bis 270mg C/l). Die Messung der Größenverteilung mittels Ultrafiltration zeigte eine stete Abnahme der Größe der organischen Partikel. UV/VIS und IR Untersuchungen ergaben, dass es sich bei der Organik um humin- und fulvinartige Substanz handelt. Es kam nun die Frage auf, welchen Einfluss die Organik auf die Reaktion der Tonminerale hat.

Um die Wechselwirkung zwischen Tonmineralien und der Organik zu untersuchen, wurden STXM Untersuchungen am Brookhaven National Lab. (BNL) in New York durchgeführt. Es konnte gezeigt werden, dass im Ausgangsmaterial die organische Substanz dispers in den Proben auf Flächen und Kanten der Tonminerale verteilt ist. Mit Fortlauf der Reaktion wurde beobachtet, dass sich die Organik von den Flächen löste, aber die Kanten selbst nach einem Jahr Versuchsdauer noch blockiert waren. Die Blockade der reaktiven Kanten der Tonmineralien durch organisches Material ist also für die Inhibierung der Tonmineralreaktion verantwortlich. Weitere Untersuchungen sind unter Einbeziehung des Opalinus- Tones unter Ausschluss von Sauerstoff geplant.

Literatur

1. Claret F., Bauer A., Schäfer Th., Griffault L. and Lanson B. Experimental Investigation of the Interaction of Clays with High pH Solutions: A Case Study from the Callovo-Oxfordian Formation, Meuse - Haute Marne Underground Laboratory (France). Submitted to Clays and Clay Minerals.

2. Cathelineau, M., M. Ayt Ougougdal, M. Elie and R. Ruck (1997). "Mise en evidence d'une diagénèse de basse température dans les series mésozoiques du site Est : une étude des inclusions fluides des argiles et de la metière organique." Journées scientifiques, Bar-le-Duc, ANDRA, CNRS: 28.

3. Elie, M. and P. Landais (1999a). "Cinétique de transformation des biomarqueurs pour la détermination d'un paléoenfouissement maximun du Callovo-Oxfordien." Journées scientifiques, Bar-le-Duc, ANDRA, CNRS: 76-77.

4. Elie, M. and P. Landais (1999b). "Utilisation de la géochimie organique pour la détermination du paléoenvironnement et de la paléothermicité dans le Callovo-Oxfordien du site de l'Est de la France. Etude du bassin Parisien." Actes des journées scientifiques CNRS/ANDRA, Bar-le-Duc, 20 et 21 Octobre 1997: 35-61.

5. Claret, F.: Caractérisation structurale des transitions minéralogiques dans les formations argileuse: Contrôles et implications géochimiques des processus d'illitisation. Cas particulier d'une perturbation alacaline dans le Callovo-Oxfordien Laboratoire souterrain Meuse-Haute-Marne. Dissertation, Université Grenoble, 2001

V.   Solid and surface analysis: Nanoscopic observation of U(IV)-oxide surface dissolution and remineralization by electrochemical AFM

(M. Plaschke, J. Römer, INE)

Abstract

Surface chemical processes of UO_2 are investigated on a nanoscopic scale by electrochemical atomic force microscopy (ECAFM) using a home-developed electrochemical cell. Dissolution reactions of the solid surface and subsequent remineralization are observed at the solid-water interface under different redox conditions and carbonate concentrations.

The local dissolution rates vary between different grain faces, grain boundaries and etch pits. A correlation between dissolution rates and the grain orientations relative to the specimen is found by electron backscatter diffraction (EBSD). Remineralization under oxidizing conditions occurs mainly at grain faces with higher dissolution rates. The remineralized products are particles of 200-900 nm in diameter and exhibit a tabular morphology. Locally different dissolution and remineralization processes on a nano-scale may lead to large uncertainties in the interpretation of macroscopic dissolution rates.

Zusammenfassung

Mit einem elektrochemischen Kraftmikroskop (AFM) wurden die chemischen Prozesse auf einer UO_2-Oberfläche in einer selbstkonstruierten elektrochemischen Zelle untersucht. Bei unterschiedlichen Redoxbedingungen und Karbonatkonzentrationen wurden Auflösereaktionen und nachfolgende Remineralisierungen an der fest-flüssig Phasengrenze beobachtet.

Die lokalen Auflöseraten variierten dabei stark zwischen unterschiedlichen Kornflächen und Korngrenzen. Es konnte eine Korrelation zwischen der Auflöserate und der Kornorientierung relativ zur Oberfläche mit Hilfe der Elektronenrückstreubrechung (Kikuchipattern) aufgezeigt werden. Unter oxidierenden Bedingungen traten die Remineralisierungen bevorzugt auf Kornoberflächen mit hoher Auflöserate auf. Die entstandenen Partikel zeigten eine tafelartige Struktur mit einem Durchmesser von 200 – 900 nm. Diese lokalen, unterschiedlichen Auflöse- und Remineralisierungsprozesse im mikroskopischen können zu großen Unsicherheiten in der Interpretation von makroskopischen Auflöseraten führen.

Introduction

For a safety assessment of a nuclear waste repository, the release of radionuclides from spent fuel after an assumed contact with groundwater has to be considered. The major part of radionuclides, i.e. actinides, is retained in the grains of sintered UO_2 pellets and will not be mobilized before the solid matrix dissolves. The UO_2 dissolution depends on physio-chemical parameters, such as pH, redox potential, carbonate concentration and the availability of oxidative radiolysis products [1]. Increasing dissolution rate is observed under oxidizing conditions because of the higher solubility of U(VI) compared to U(IV). In addition, dissolved carbonate enhances the dissolution rate due to the complexation with the uranyl ion. Even though in a nuclear waste repository generally reducing conditions can be expected, the UO_2 surfaces can exhibit over a distinct period of time an oxidizing environment due to the alpha radiolysis of water. While gamma radiolysis decreases markedly after about 500 years, alpha and beta radiolysis will remain over periods of about 10^5 years. This period is beyond the life time of canister materials [2,3].

Electrochemical methods allow the adjustment of redox potentials which are considered to be relevant for surface chemical processes of the fuel matrix under waste disposal conditions [4,5]. By a combination with atomic force microscopy (AFM) (so-called Electrochemical AFM (ECAFM)) local dissolution rates can be quantified at the solid-liquid interface under the (electro-)chemical conditions of interest. In previous works ECAFM was mainly applied for the investigation of corrosion processes of metals, such as steel, copper or titanium [6-9]. The atomic structure of UO_{2+x} in the presence of oxygen was studied by scanning tunneling microscopy in ultra high vacuum and at elevated temperature [10]. In situ corrosion studies of the UO_2 surface applying ECAFM have not been published so far.

Electron backscatter diffraction (EBSD) introduced by S. Kikuchi is a technique for the determination of crystal orientations and phase identification in composite materials. High-energy electrons are scattered by the atomic planes of a crystalline sample. The diffraction pattern, the so-called Kikuchi or electron backscatter pattern, results from the interaction of elastically scattered electrons (acting as a point source) and the crystal planes. When electron waves originating from a point source constructively interfere with the grating of the crystal planes according to the Bragg's law, a pattern is obtained with dimensions directly related to the grating. Considering

the Bragg equation the interplanar spacings and angles of the most prominent lattice planes can be indexed and the crystal orientation can be calculated. Details of generation and processing of Kikuchi patterns and their application in texture analysis of metals and other materials are described in the literature [11,12].

As corrosion generally begins and proceeds at the fuel surface being in contact with the aqueous environment, the dissolution process has to be understood from a surface chemical point of view. Using ECAFM the composition of the aqueous environment and the redox potential can be varied accordingly to the waste disposal conditions. Their influence on surface chemical processes is studied in-situ with a nanometer resolution. By combination with EBSD performed in an environmental scanning electron microscope (ESEM) the role of crystal orientation on matrix dissolution can be examined.

Experimental

A sintered pellet of uranium dioxide (Joint research Centre, Central Bureau for Nuclear Measurements (CBNM), Geel, Belgium) is used as sample which is characterized as a certified nuclear reference material (CBNM Reference Material No. 106). The uranium has an isotopic composition obtained by mass spectrometry of ^{238}U : 99.2787, ^{235}U : 0.7158, ^{234}U : 0.0055 weight percent. A commercial AFM (Topometrix, TMX 2000, Explorer) with a home-developed electrochemical cell is used (Fig.1). The UO_2 sample is embedded in an epoxy resin using a holder of stainless steel and electrically contacted (working electrode). Additionally, flexible silicon tubes are embedded and used for the liquid exchange and salt bridge. This liquid cell enables the preparation of a plane and fresh sample surface for several times by polishing. The counter electrode is a platinum coated ring of titanium which is sealed towards the sample holder and forms the wall of the liquid cell. The Ag/AgCl reference electrode (1 M KCl) is connected with an embedded tube and sealed with a ceramic diaphragma against the cell. At room temperature the reference electrode has a potential of +236 mV against SHE [13]. NaHCO$_3$ solutions (3% or 0.3%) are adjusted to pH 8.7 and filled in the liquid cell. The potential is adjusted by a bipotentiostat (type MP81, Bank Elektronik, Clausthal-Zellerfeld, Germany) to values ranging from −1.0 V (reducing) to +1.0 V (oxidizing). A series of AFM images are
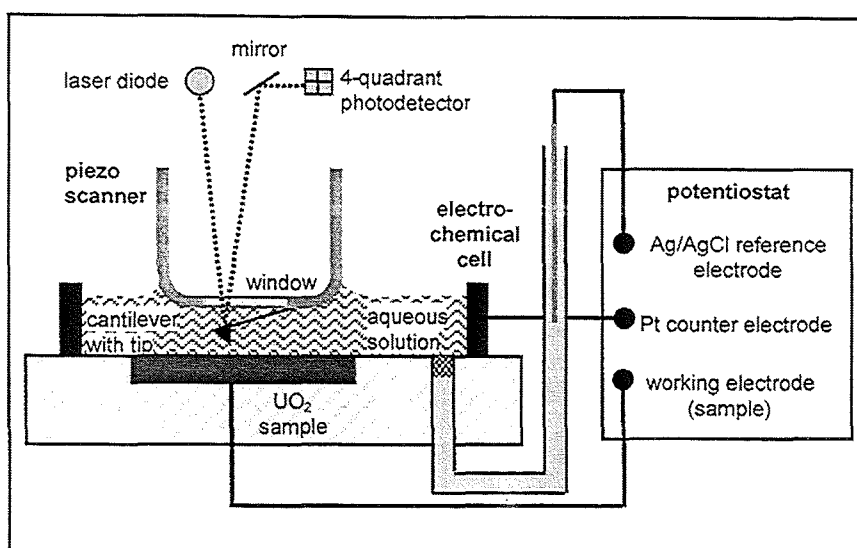
Fig. 1: Experimental setup of ECAFM (see Experimental section)

recorded in the contact-mode using triangular cantilevers with silicon nitride tips (tip radius < 50 nm). The crystal lattice structure of a pulverized UO_2 sample is analyzed by X-ray diffraction (Seifert XRD 3000, Ahrensburg, Germany). Electron backscatter diffraction (EBSD) of the altered UO_2 surface is performed in an environmental scanning electron microscope (Philips ESEM XL 30 FEG) equipped with a backscatter electron detector for imaging and a phosphorous screen/SIT camera to monitor Kikuchi patterns. As UO_2 is a semi-conducting sample, it can be analyzed by ESEM without a conducting surface coating which may impair backscatter diffraction bands. For the analysis of Kikuchi patterns the experimental arrangement is calibrated with respect to the working distance using a Ni standard. The calibration yields the position of the pattern centre on the screen, the specimen-to-screen distance and the specimen tilt. The grain orientations are obtained by comparison of the measured EBSD pattern with pattern calculated by the instrument software for the known crystal lattice. The general procedure of EBSD and orientation analysis is described in the literature [14,15].

Results

Dissolution process

Surface alterations can be imaged by electrochemical AFM under potentiostatic conditions at the surface nearly in real time. An overview of the UO_2 surface corroded by anodic oxidation is given in Fig. 2. Significantly different dissolution progress is

observed at different grain faces, grain boundaries and etch pits, while simultaneously particulate deposits are formed.
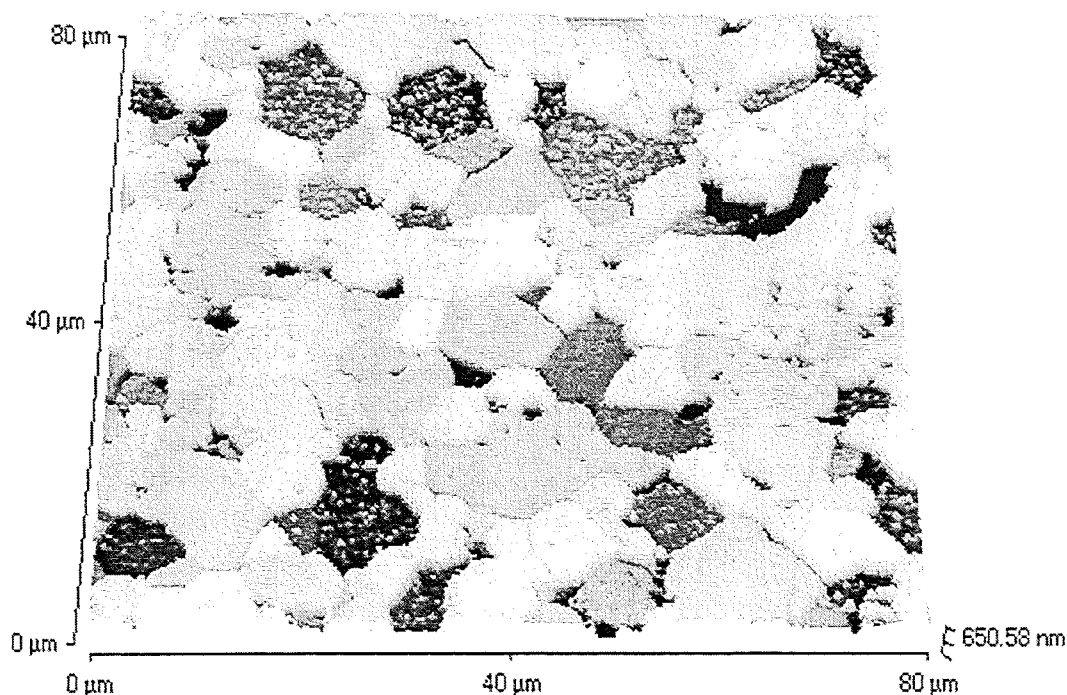
Fig. 2: AFM overview of an UO_2 surface after corrosion under oxidizing condition (reaction time 160 min; potential + 1.0 V vs. Ag/AgCl; 3% sodium bicarbonate; pH 8.7; see text)

For the determination of dissolution rates at the respective potentials, a series of images is recorded with a time interval of about 5 min. The dissolution process is investigated under reducing and oxidizing conditions. Under strongly reducing condition (potential –1000 mV) no surface dissolution can be observed over a period of several hours which is the time frame of an in situ AFM experiment. In contrast, under strong oxidizing condition (+1000 mV) intense surface change is monitored over a period of nearly 3 hours (Fig. 3). Surface alterations, i.e. height differences between a series of AFM images, are quantified with reference to an area where the observed surface changes are small compared with the rest of the surface (the reference area is indicated with R in Fig. 3). This procedure represents a relative or semi-quantitative analysis of the dissolution progress, because absolute surface changes can only be obtained in the presence of unalterable reference points [16,17]. As an example, Fig. 3 shows a selected surface area of 11 x 11 μm^2 before and after a dissolution period of 103 minutes in 3% bicarbonate solutions ($NaHCO_3$).
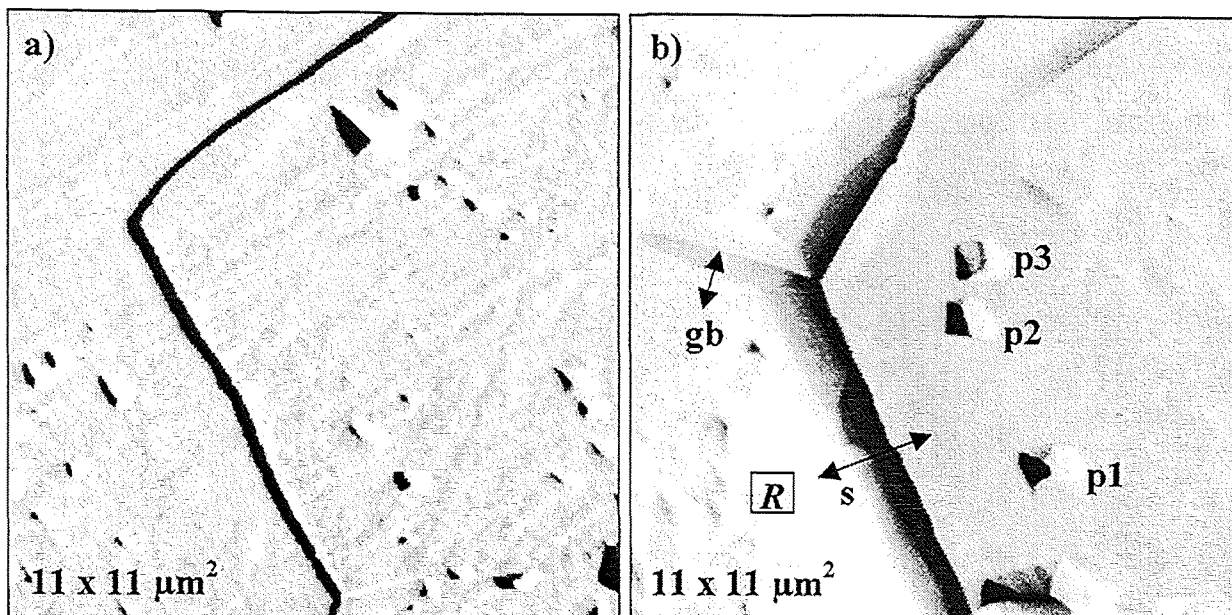
Fig. 3: UO_2 surface area before a) and after b) corrosion under oxidizing condition (reaction time 103 min; potential + 1.0 V vs. Ag/AgCl; 3% sodium bicarbonate; pH 8.7; symbols: grain boundary (gb), step (s), etch pits (p1, p2, p3), reference area (R); see text)
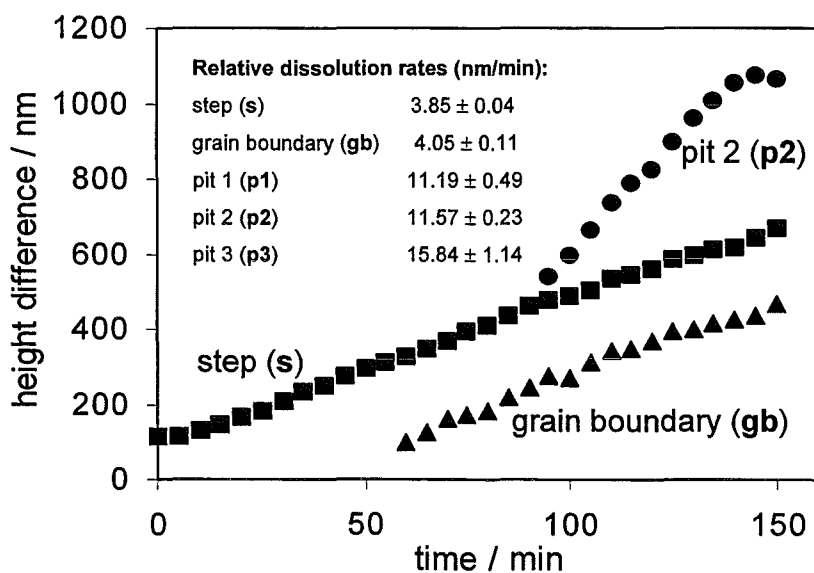
Fig. 4: Dissolution process at different sample sites as indicated in Fig. 3 (potential + 1.0 V vs. Ag/AgCl; 3% sodium bicarbonate; pH 8.7; see text)

Surface alterations at a step between two grains (s), a grain boundary (gb) and at etch pits (p1, p2 and p3) are analyzed (see symbols in Fig.3). The dissolution progress, i.e. height difference as a function of time, at these sample sites is described in Fig. 4. The dissolution rates can be calculated from the respective curve slopes (see table in fig. 4). Dissolution rates found at the step (s) between two grains and at the grain boundary (gb) provide similar values of 3.85 and 4.05 nm/min, respectively. At the etch pits (p1, p2, p3) three-fold higher dissolution rates in the range of 11.1 and 15.8 nm/min are observed.

Influence of redox potential and carbonate concentration

The dependency of the applied potential on the dissolution rate is investigated at two different concentrations of $NaHCO_3$ solution, 3% and 0.3%. A series of images is recorded for a period of about 30 min at a respective constant potential which is increased in steps of 100 mV from +100 to +600 mV (vs Ag/AgCl). It is typical for AFM that images recorded over a longer period of time show a marked lateral drift, probably due to temperature fluctuations. This drift is corrected using a mathematical procedure described elsewhere [16,17].

In Fig. 5 dissolution rates (in nm/min) at high carbonate concentrations (3 %) are plotted against the applied potentials. Three grains are selected in this plot with the highest rate observed, an intermediate and a low dissolution rate. For all selected grains a linear relationship between the applied potentials and the relative dissolution rates is found, which is representative for other grain faces. From the curve fits a mean value of 0.03 ±0.02 V can be calculated for the straight lines cutting the x-axis. This value can be regarded as a threshold for dissolution, because below this potential no dissolution is observed within the time frame of the experiment.

Similar investigations are performed in solutions with intermediate carbonate concentrations (0.3%) which is typical for natural aquatic systems. In Fig. 6 the results for 0.3 and 3% carbonate concentrations are compared for a respective grain face with a high dissolution rate. As in the 3% carbonate solution a linear relationship between the dissolution rates and the potentials can be found in 0.3% carbonate solution. From the curve fit a value of 0.16 ±0.03 V can be calculated as a threshold for dissolution. Beyond this potential dissolution of UO_2 can be observed at rates which are 5 to 10 times smaller than in the 3% carbonate solutions. As described for

the experiments in 3% carbonate, very different dissolution rates are found on different grain faces in 0.3% carbonate solution.
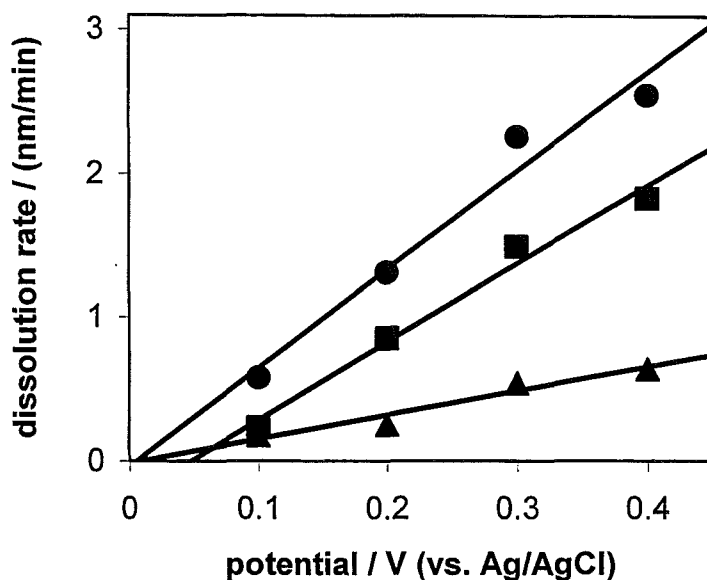
Fig. 5: Dissolution rates vs. redox potentials at three different grains with high (λ), intermediate (v) and low (σ) dissolution rates (3% sodium bicarbonate; see text)
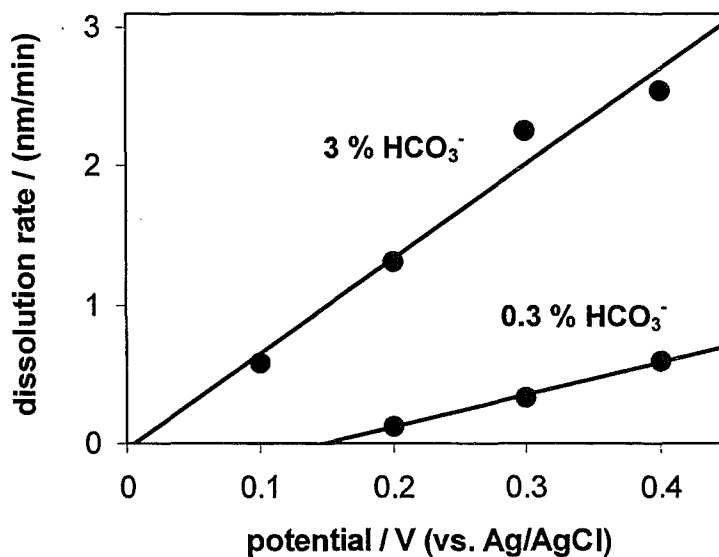
Fig. 6: Dissolution rates vs. redox potentials at grain faces with high dissolution rates (3% and 0.3% sodium bicarbonate; see text)

Remineralization

In addition to the electrochemical surface dissolution, particulate species are observed on grain faces with high dissolution rates, which can be seen in the overview of Fig. 2. These particles shown in Fig. 7a exhibit shapes of stacked platelets with irregular, partly angular contours, diameters and heights in the range of 200-900 and 10-150 nm, respectively. From AFM analysis alone one can not decide whether these particles are crystalline or amorphous. However, EBSD results indicate a crystalline structure (see next paragraph). Interestingly, the nucleation of these crystallites is not observed in the ECAFM dissolution experiments where the surface is continuously scanned by the AFM tip (see marked square in Fig. 7b). In this case, formation of small crystallites is probably disturbed by the movement of the AFM tip. On neighbouring surface areas, which are not continously scanned, a large number of platelet-shaped particles is found (outlying the square of Fig. 7b).

These observations indicate that remineralization proceeds simultaneously at surface areas with high dissolution rates probably due to a local oversaturation of the solution with uranyl carbonato ions and subsequent nucleation (see discussion). The remineralized particles show a tabular morphology [18].

X-Ray Diffraction (XRD) and Electron backscatter diffraction (EBSD)

The crystal lattice structure of the UO_2 matrix is analyzed by X-ray diffraction (not shown). From a powder diffractogram a face centered cubic structure (fcc) can be derived which is in agreement with the known fluorite structure of UO_2.

Different grains are investigated in an ESEM using a standard EBSD geometry. For a comparison of the measured Kikuchi pattern with the data base, the pattern centre, camera length and specimen tilt have to be calibrated as mentioned in the experimental section. In Fig. 8 an ESEM image of the UO_2 surface with grains showing different dissolution progress and the related Kikuchi patterns are depicted. Different grains with different dissolution progress exhibit different Kikuchi pattern and, as expected, different sites on the same grain form the same Kikuchi pattern (see numbers in Fig. 8). Therefore, different grains as fundamental building units of the material show different crystal orientations, whereas one grain apparently exhibits one predominant crystal orientation. Surprisingly, no difference in the Kikuchi pattern could be detected between the grain face and remineralized particles formed on top of it (see Fig. 8 and discussion).
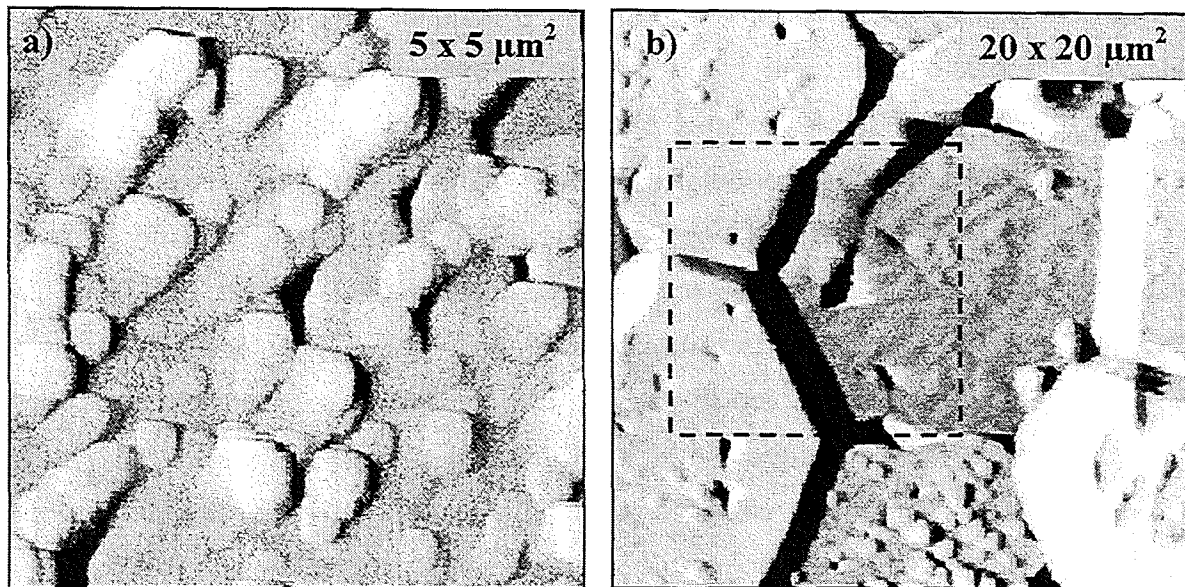
Fig. 7: a) Remineralized particles formed on UO_2 surface after corrosion under oxidizing condition; the marked square in b) is the continuously scanned area of Fig. 3 (see text)
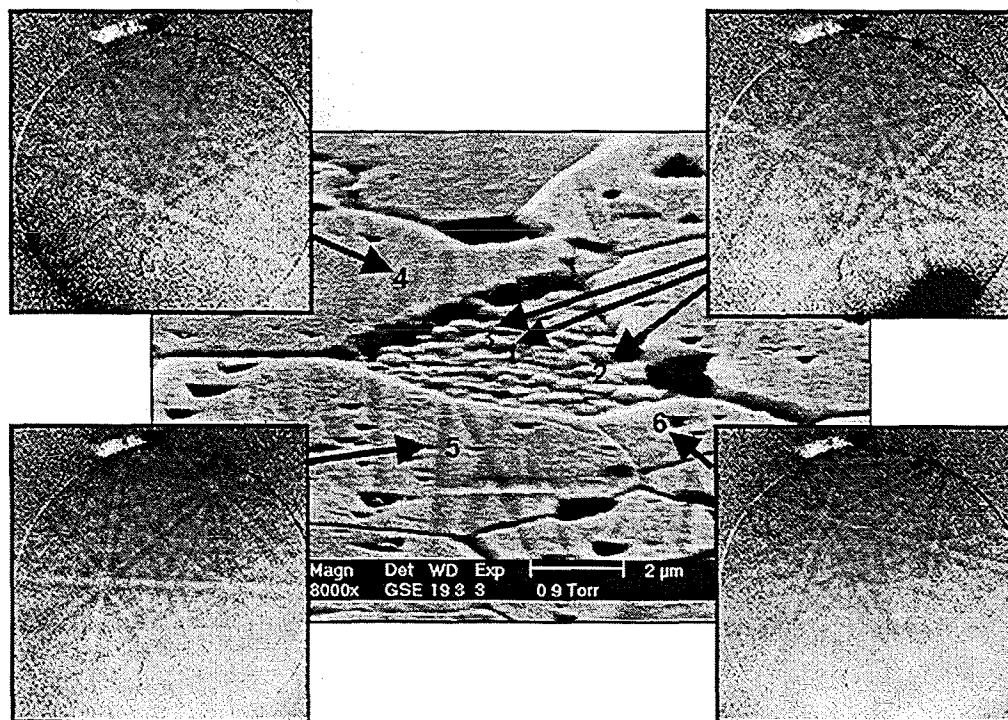
Fig. 8: ESEM image of a corroded UO_2 surface showing grains with different dissolution progress and the related Kikuchi patterns (see text)

With the known fcc crystal lattice structure from XRD the number of possible and plausible pattern is strongly restricted. The software performs a Hough transformation, which extracts the dominant Kikuchi bands from the image. The width of the bands and their relative angles can be calculated. The orientation of the crystal atomic planes can be determined by comparison of the measured pattern with simulated or known pattern from a database. After this analysis, grains with the highest dissolution rates have a grain orientation with the (001) crystal plane parallel to the specimen surface. Grains with lower dissolution rates are characterized by *hkl* crystal planes of higher order parallel to the sample surface. Therefore, the grain orientation seems to play a major role for inhomogeneous dissolution of sintered UO_2 pellets.

Discussion

The release of radionuclides, i.e. actinides and fission products, from spent nuclear fuel in a repository after an assumed contact with groundwater will be controlled by the dissolution rate of the UO_2 matrix. The availability of oxidizing reagents, either oxygen or radiolysis products, seems to be a major factor influencing UO_2 dissolution.

In this study the UO_2 surface alterations are directly investigated under oxidizing condition at the solid-water interface. Dissolution rates increase with increasing oxidizing potentials and with carbonate concentration which is in general agreement with results from previous studies [1]. The reasons for this behaviour are the increased solubility of U(VI) compared to U(IV) and the carbonate complexation of UO_2^{2+} ions. An appropriate mechanism including uranyl carbonate intermediates is described [1].

From a microscopic point of view, different dissolution rates are found on different grain faces leading to a very inhomogeneous surface morphology. It can be demonstrated that the dissolution rate strongly depends on the grain orientation. The grain orientation with the (001) crystal plane exhibits the highest dissolution rate. Furthermore, increased dissolution is observed at some grain boundaries, where dissolution rates are found to resemble those on grain faces with the highest rates. However, grain boundaries do not generally dissolve faster than the neighboring grain faces. In the overview of Fig. 2 one can find as well grain boundaries showing the same dissolution rate as the grain faces. One may conclude from this observation

that these grain boundaries terminate with grain orientations with favouring accelerated dissolution. Therefore, the inhomogeneous dissolution process of UO_2 pellet surfaces seems to be strongly influenced by the grain orientations.

After a corrosion time of several hours particulate species are found predominantly on grain faces with high dissolution rates. Furthermore, particulate structures are not observed when the nucleation is disturbed by a continuously scanning AFM tip. These particulate morphologies are probably generated by a remineralization process due to a local oversaturation with uranyl carbonato ions. Moreover, the nucleation of crystallites is facilitated on edges as reactive sites which are formed in consequence of dissolution.

The electron beam in an ESEM penetrates several tenth to hundreds of nanometers into a sample bulk, depending on parameters like the accelerating voltage and material properties (i.e. densities). In the EBSD experiment the information depth of backscattered electrons can be estimated to values <20 nm (see [19] for the definition and estimation of the information depth). This is the range of the measured heights (AFM) of remineralized particles on the corroded surface. Therefore, backscatter Kikuchi bands apparently measured in a deposited particle probably reflect the crystalline structure of the particle and not of the underlying crystal face. The deposited particles seem to crystallize in the same type of crystal structure (fcc) and orientation as the underlying grain face, which can be gathered from the accompanying Kikuchi patterns. This does not automatically mean that the remineralized particles and the crystal face consist of the same phases because the Kikuchi patterns characterized by the relative angles of the backscatter bands primarily reflect the type of crystal structure and the orientation. More detailed information about the structure of a secondary phase may be extracted from the band width which could not be analyzed here.

References

1.   D.W. Shoesmith, J. Nucl. Mat. 282 (2000) 1-31.

2.   D.W. Shoesmith, S. Sunder, Svensk Kärnbränslehantering AB, Swedish Nuclear Fuel and WasteManagment Co., SKB Technical Report 91-63 (1991).

3.   E. Smailos, Nucl Technol. 104 (1993) 343.

4.   D.W. Shoesmith, W.H. Hocking, B.M. Ikeda, F. King, J.J. Noel, S. Sunder, Can. J. Chem. 75 (1997) 1566.

5.   Electrochemical Techniques Applied to Natural UO_2 Corrosion in Aqueous Solutions; in: Institut for Transuraniumelements, Annual Report 1992 EUR 15154 EN, p. 93.

6.   U. Kamachi Mudali, Y Katada, Electrochim. Acta 46 (2001) 3735.

7.   R.E. Williford, C.F. Windisch Jr., R.H. Jones, Mater. Sci. Eng. A288 (2000) 54.

8.   G. Bertrand, E. Rocca, C. Savall, C. Rapin, J.-C. Labrune, P. Steinmetz, J. Electroanal. Chem. 489 (2000) 38.

9.   J.P. Bearinger, C.A. Orme, J.L. Gilbert, Surface Science 491 (2001) 370.

10.   C. Muggelberg, M.R. Castell, G.A.D. Briggs, D.T. Goddard, Surf. Sci. 402-404 (1998) 673.

11.   R.A. Schwarzer, Micron 28 (1997) 249-265.

12.   A.J. Schwartz, M. Kumar, B.L. Adams (Eds.), in: Electron backscatter diffraction in material science, Kluwer Academic/Plenum Publishers, New York 2000.

13.   R. Holze; Leitfaden der Elektrochemie, B.G. Teubner, Stuttgart, Leipzig 1998.

14.   A.J. Wilkinson, P.B. Hirsch, Micron 28 (1997) 279.

15.   B.L. Adams, S.I. Wright, K. Kunze, Metallurgical Trans. A 24A (1993) 819.

16.   M. Plaschke, J. Römer, J. I. Kim, Ultramicroscopy 75 (1998) 77.

17.   J. Römer, M. Plaschke, J.I. Kim, Ultramicroscopy, 85 (2000) 99.

18.   M.E. Torrero, I. Casas, J. de Pablo, M.C.A. Sandino, B. Grambow, Radiochim. acta 66/67 (1994) 29.

19.   M.P. Seah, W.A. Dench, Surf. Interf. Anal. 1 (1979) 2.

VI.   <u>Solid and surface analysis: Untersuchung der Oberfläche von Chlorit mit</u>
        <u>ADXPS</u>

        (D. Schild, F. Brandt, INE)

Abstract

The surface of nature chlorite particles were analyzed by angle dependent XPS (ADXPS). The results are fitted by a combination of calculated ADXPS profiles of a homogenous solid, corresponding to statistically oriented chlorite particles, and of a TOT layer sequence at the surface. Compared to reference layer composition the concentrations of Mg, Al and Fe are diminished at the outermost surface layers.

Zusammenfassung

Die Oberfläche natürlicher Chloritpartikel wurde mit winkelabhängiger XPS (ADXPS) untersucht. Die Messergebnisse können mit einer Kombination aus dem homogenen Fall, entsprechend statistisch orientierter Chloritpartikel, und dem berechneten Profil einer TOT Schichtabfolge an der Oberfläche beschrieben werden. Im Vergleich zur idealen Schichtzusammensetzung weisen die obersten Schichten geringere Konzentrationen von Mg, Al und Fe auf.

Einleitung

Für ein Endlager radioaktiver Abfälle in Hartgestein stellen die Klüfte mögliche Wegsamkeiten für die Migration freigesetzter Radionuklide (RN) dar. RN Migration und chemische Eigenschaften des Grundwassers werden durch die Wechselwirkung mit den Oberflächen der in den Klüften enthaltenen Minerale und Verwitterungsprodukten des Wirtsgesteins bestimmt [1, 2]. Eines der Verwitterungsprodukte des Granits ist Chlorit mit der Summenformel $(Mg,Al,Fe)_{12}(Si,Al)_8O_{20}(OH)_{16}$. Chlorit besteht aus vier sich wiederholenden Schichten: $(Si,Al)_4O_{10}$ (<u>T</u>etraeder) | $(Mg,Fe)_6(OH)_4$ (<u>O</u>ktaeder) | $(Si,Al)_4O_{10}$ (<u>T</u>etraeder) | $(Mg,Fe,Al)_6(OH)_{12}$ (<u>B</u>rucit-ähnliche Schicht) mit unterschiedlicher Koordination der Kationen (Abb. 1). Bei Alteration des Chlorits kann Eisen freigesetzt und Ferrihydrit gebildet werden. Einbau von RN in Ferrihydrit kann diese immobilisieren, falls Ferrihydrit auf Gesteinsoberflächen sorbiert ist, oder mobilisieren, falls Ferrihydritkolloide vorliegen. Zusätzlich kann sich die RN-Migration durch pH-Wert Änderung bei Auflösung des Chlorits ändern. Als Beitrag zur Beschreibung der RN-Migration in Granitklüften werden die Prozesse bei Auflösung des Chlorits mit verschiedenen analytischen Methoden untersucht.

T ← $(Si_{2.665}Al_{1.335})O_{10}$ 3 Å

O ← $(Mg_{3.38}Fe_{2.62})(OH)_4$ 4 Å

T ← $(Si_{2.665}Al_{1.335})O_{10}$ 3 Å

B ← $(Mg_{2.18}Fe_{1.34}Al_{2.48})(OH)_{12}$ 4 Å

○ = O
◉ = OH
• = Si,Al
● = Al,Mg,Fe
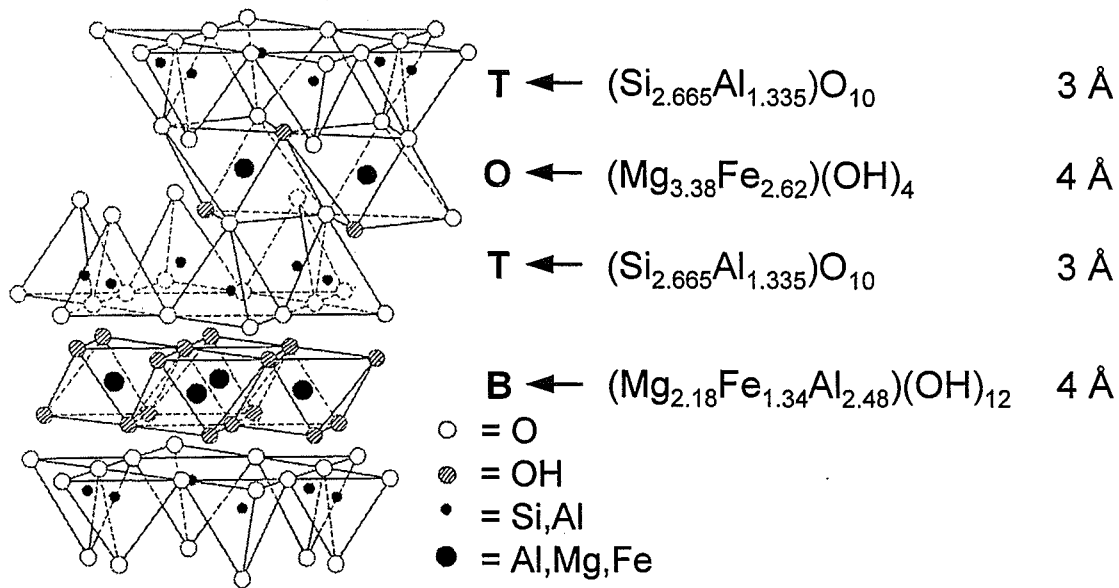
Abb. 1: Die periodische Schichtstruktur von Chlorit mit TOT und Brucit Schicht (B). Schichtdicken und -Zusammensetzungen der untersuchten Probe sind angegeben.

Winkelabhängige XPS und Modellsystem

Mit winkelabhängiger XPS (ADXPS, Angle-Dependent X-ray Photoelectron Spectroscopy) können Element- und Speziationsprofile der Oberfläche innerhalb der Informationstiefe der XPS (wenige nm) gemessen werden. Durch Variation des Winkels θ zwischen Probennormalen und Analysatorachse werden Photoelektronen mit unterschiedlicher Austrittstiefe detektiert. Beim Durchgang von Elektronen mit bestimmter Intensität und Energie durch Materie mit der Dicke z kommt es zur Intensitätsabschwächung, die näherungsweise mit dem Gesetz von Lambert-Beer-Bouguer der linearen Absorption beschrieben werden kann: $I = I_0 \cdot \exp(-z / \lambda)$, mit Absorptionskoeffizient $1/\lambda$, Primärintensität I_0 und Intensität I nach Durchlauf der Schichtdicke z. Nach Durchgang von Elektronen unter einem Winkel θ zur Oberflächennormalen durch Materie mit der Dicke z ist

$$I = I_0 \exp\left(\frac{-z}{\lambda \cos\Theta}\right). \tag{1}$$

Integration liefert für eine Schicht mit Dicke z und relativer Dichte d_i emittierender Atome eine relative Intensität I_z

$$I_z \propto d_i \lambda \cos\Theta \cdot \left[1 - \exp\left(\frac{-z}{\lambda \cos\Theta}\right)\right]. \tag{2}$$

Aus der Austrittstiefe $d_a := \lambda \cos\theta$ stammt 63 % des gemessenen Photoelektronen-signals, aus der Informationstiefe $d_{inf} := 3\,d_a$ entsprechend 95 % des Signals. Für $z \to \infty$ ist $I \propto d_i\,\lambda\cos\theta$. Die Abschwächungslänge λ ist für Elektronen energie- und matrixabhängig und kann aus Dichte und Stöchiometrie mit folgender Beziehung, die auch elastische Streuung berücksichtigt, berechnet werden [3]:

$$\lambda = 0{,}316\,a^{3/2}\left\{\frac{E_{kin}}{Z^{0,45}\left[\ln(E_{kin}/27)+3\right]}+4\right\}\quad [nm] \tag{3}$$

$$\text{mit } a = 10^7\left(\frac{A}{\rho\,n\,N_L}\right)^{1/3}\quad [nm]$$

a [nm]: Mittlere Atomgröße (Monolagendicke), A [g Mol^{-1}]: Mittleres Atomgewicht,

ρ [g cm^{-3}]: Dichte, n: Anzahl der Atome im Molekül, N_L: Avogadro-Konstante

Z: Kernladung, E_{kin}: Kinetische Energie der Photoelektronen einer Elementlinie.

Die so erhaltene Abschwächungslänge λ ist kleiner als die mittlere inelastische freie Weglänge (IMFP) der Elektronen [4]. Für einen homogenen Festkörper mit der Zusammensetzung von Chlorit ergeben sich die in Tabelle 1 zusammengestellten Werte der Austrittstiefen bei verschiedenen Winkeln θ und die maximale Austrittstiefe d_a ($\theta = 0°$) = λ der Elektronen von Elementlinien.

Die Modellierung eines Schichtmodells allein aus Messergebnissen durch Entfaltung führt zu keiner mathematisch eindeutigen Lösung [5]. Umgekehrt können ADXPS Profile aus Schichtstrukturen berechnet und mit gemessenen Profilen verglichen

Element-linie	E_{kin} [eV]	λ [nm]	d_a (40°) [nm]	d_a (70°)	d_a (80°)
Fe 2p$_{3/2}$	776	1,55	1,19	0,53	0,27
O 1s	956	1,83	1,40	0,63	0,32
C 1s	1202	2,20	1,68	0,75	0,38
Si 2p	1385	2,47	1,89	0,84	0,43
Mg 2s	1399	2,49	1,90	0,85	0,43
Al 2p	1413	2,51	1,92	0,86	0,44

Tab. 1: Kinetische Energien E_{kin} der Elektronen von Elementlinien bei Anregung mit Al K$_\alpha$ (hν = 1486,6 eV), Austrittstiefen $d_a(\theta)$ bei verschiedenen Winkeln, Abschwächungslängen λ der Elementlinien.

werden. Bei Chlorit ist z.B. eine Frage, ob die TOT Schicht oder die Brucit Schicht die Oberfläche bildet. Um die Messergebnisse für Chlorit zu interpretieren wurden ADXPS Profile für verschiedene Schichtfolgen an der Oberfläche berechnet. Um die Beiträge zu den Intensitäten der Elementlinien bis zur maximalen Informationstiefe ($\theta = 0°$) zu erfassen, wurden 8 TOTB Schichten entsprechend $n = 32$ Einzelschichten mit den jeweiligen Elementkonzentrationen berechnet. Für die Rechnung wird angenommen, dass sich die Elektronen auf geraden Bahnen bewegen (Straight Line Approximation), elastische Streuung wird durch die Abschwächungslängen aus Gl. (3) berücksichtigt. Für n homogene Schichten mit verschiedenen d_i, λ_i und Dicken z_i folgt aus Gl. (1) und (2) für die unter dem Winkel θ zur Oberflächennormalen detektierten relativen Intensität I_x der Elektronen einer Elementlinie des Elements x:

$$I_x \propto \sum_{i=1}^{n} d_i \, \lambda_{i,x} \cos\Theta \cdot \left\{ 1 - \exp\left(\frac{-z_i}{\lambda_{i,x} \cos\Theta} \right) \right\} \cdot \prod_{j=1}^{n-1} \exp\left(\frac{-z_j}{\lambda_{j,x} \cos\Theta} \right) \tag{4}$$

mit Indizes der einzelnen Schichten von der Oberfläche her beginnend. Die relative Atomkonzentration in % für Element x ist

$$c_x = \frac{I_x \, \lambda_x^{-1}}{\sum_m I_m \, \lambda_m^{-1}} \cdot 100 \tag{5}$$

mit λ_x, λ_m eines homogenen Festkörpers mit der Stöchiometrie von Chlorit.

Experimentelles

Eine Suspension aus natürlichen Chloritpartikeln ($< 63 \, \mu m$) und Isopropanol wurde auf Graphitfolie getropft und getrocknet. Ein Teil der Chloritpartikel liegt wie für ADXPS erforderlich mit der Oberfläche parallel zur Substratoberfläche, von den übrigen Partikeln wird angenommen, dass sie statistisch orientiert sind und einen Beitrag entsprechend dem eines homogenen Festkörper zum Messsignal liefern. ADXPS Messungen erfolgten bei Austrittswinkeln von $\theta = 80°$, 75°, 70°, 60°, 40° und 10°. Für jeden Austrittswinkel werden aus den Intensitäten der Elementlinien unter Berücksichtigung der Transmissionsfunktion des Analysators relative Atomkonzentrationen berechnet und als ADXPS Profil dargestellt. Der Akzeptanzwinkel des Analysators beträgt $\pm 2°$, die Analysenfläche ist $3 \times 10 \, mm^2$ bei $\theta = 0°$, Röntgenquelle und Analysatorachse schließen einen Winkel von 54,7° ein.

Ergebnisse

Zur Prüfung des Schichtmodells (Gl. 4) wurde das ADXPS Profil für den Fall homogener Elementverteilung, entsprechend gleicher Einzelschichten, mit der Stöchiometrie des Chlorits berechnet. Es ergeben sich wie erwartet konstante Atomkonzentrationen (ohne H, in at-%: O (64,3), Mg (9,9), Si (9,5), Al (9,2), Fe (7,1)) der vorgegebenen Stöchiometrie für verschiedene Austrittswinkel θ.

Das C 1s Spektrum der Chloritproben wurde nicht ausgewertet, da der Bedeckungsgrad der aufgetropften Chloritpartikel auf dem Kohlenstoffsubstrat nicht überall gleich ist, die Größe der analysierten Fläche sich aber mit dem Winkel θ ändert. Bei Rechnungen kann eine C_xH_y Kontaminationsschicht auf der Oberfläche des Probenmaterials berücksichtigt werden, da diese die Intensitäten der Elementlinien energieabhängig schwächt und die ADXPS Profile ändert.

Mit Gl. (4) wurden für verschiedene Schichtabfolgen auf der Oberfläche des Chlorits ADXPS Profile unter Berücksichtigung einer C_xH_y Kontaminationsschicht berechnet und mit den Messergebnissen verglichen (Abb. 2). Anhand der Verläufe der berechneten Profile können OTB , TB und B Oberflächen ausgeschlossen werden. Die
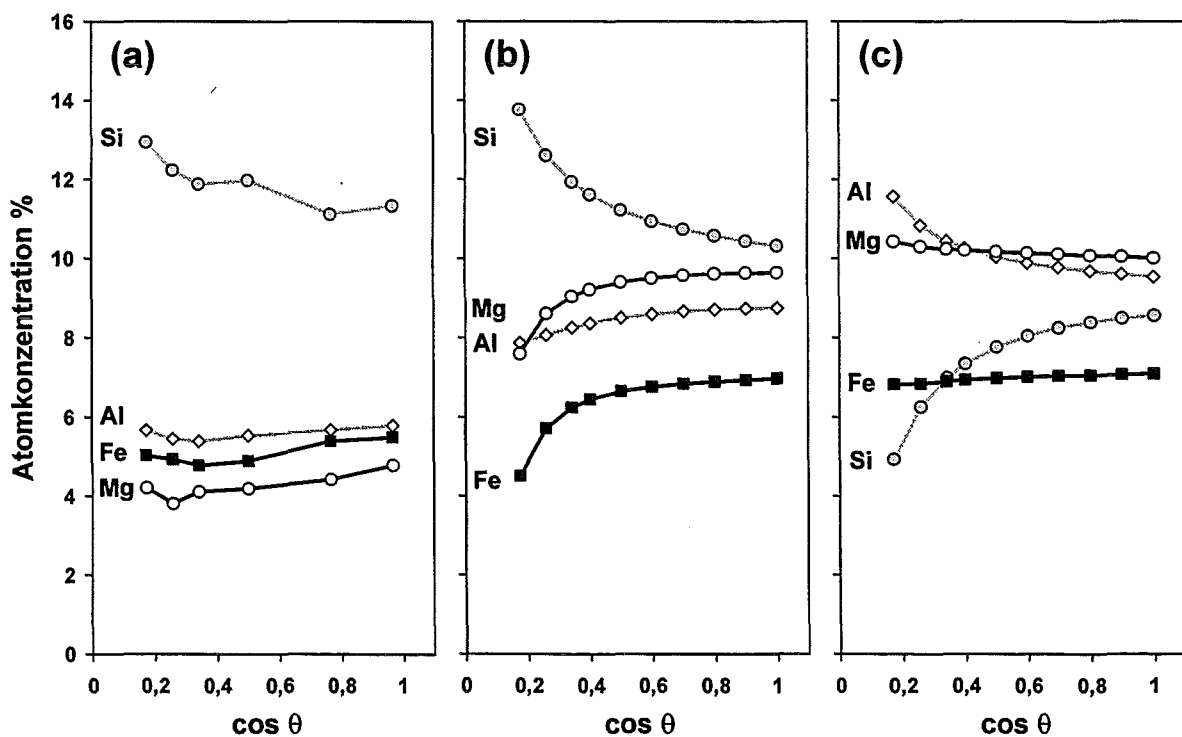
Abb. 2: Gemessenes (a) und berechnete ADXPS Profile: (b) TOT Schicht auf der Oberfläche, (c) Brucit Schicht auf der Oberfläche. Berechnete Profile ohne zusätzliche Kontaminationsschicht. Elementlinien: Fe $2p_{3/2}$, O 1s, Si 2p, Mg 2s, Al 2p.

Messergebnisse entsprechen einer Kombination aus dem berechneten Profil für den homogenen Fall, entsprechend statistisch orientierter Chloritpartikel, und aus dem berechneten Profil für eine TOT Oberfläche. Das gemessene ADXPS Profil zeigt, dass in den obersten Schichten im Vergleich zur ungestörten Schichtung die Konzentrationen von Mg die Hälfte, von Al ein Drittel und von Fe ein Fünftel niedriger sind. Aus der Anpassung berechneter an gemessene ADXPS Profile können Aussagen über die Zusammensetzung der äußeren Schichten von Chlorit oder anderer Schichtsilikate zu erhalten werden, z.B. über deren Alteration durch Auslaugung bzw. Kationenaustausch in verschiedenen Lösungen.

Referenzen

1. Th. Arnold, T. Zorn, H. Zänker, G. Bernhard, H. Nitsche: Sorption behavior of U(VI) on phyllite: experiments and modeling. J. Contaminant Hydrology 47 (2001) 219-231.

2. P.J. Cumpson, M.P. Seah: Elastic Scattering Corrections in AES and XPS.II.Estimating Attenuation Lengths and Conditions Required for their Valid Use in Overlayer/Substrate Experiments. Surf. Interface Anal. 25 (1997) 430-446.

3. P.J. Cumpson: Angle-resolved XPS depth-profiling strategies. Appl. Surf. Sci. 144-145 (1999) 16-20.

4. M.P. Seah, W.A. Dench: Quantitative Electron Spectroscopy of Surfaces: A Standard Data Base for Electron Inelastic Mean Free Paths in Solids. Surf. Interface Anal. 1 (1979) 2-11.

5. K.V. Ticknor: Actinide Sorption by Fracture-Infilling Minerals. Radiochim. Acta 60 (1993) 33-42.

32.25.03 Radionuklidrückhaltung in der geologischen Barriere

I. Colloid-Detection in Trace Concentrations by LIBD

(C. Walther, C. Bitea, F.J. Scherbaum, INE)

Abstract

Colloids play an important role in the transport of pollutants in the environment. Harmful substances can undergo transport over large distances if bound to colloids in aqueous surrounding. One example is the migration of the normally insoluble Pu(IV) at unexpected rates over several miles at the Nevada test site. For long term safety assessments of waste disposal sites, it is crucial to know about the amounts, size distributions and chemical composition of colloids in the ground water. Standard methods as light scattering (PCS) can be applied for high concentrations and large sizes of particles. However, colloids smaller than 50 nm in size are detected with very low efficiency. The laser induced breakdown detection (LIBD) can fill this gap. Particles as small as 5 nm are detected down to concentrations below 1 ppt. Developed for the in situ control of process waters in the semi-conductor production, the method was used in a rather phenomenological manner. For the more advanced requirements defined above a deeper understanding of the underlying physical processes is essential.

Zusammenfassung

Kolloide spielen eine wichtige Rolle beim Schadstofftransport in der Umwelt. Die Migrationsgeschwindigkeit toxischer Substanzen im Grundwasser kann durch Kolloid-gebundenen Transport stark erhöht werden, wie dies für den Fall schwer löslichen Pu(IV) in der Nähe eines Bombentestgeländes in Nevada demonstriert wurde. Im Rahmen der Langzeitsicherheits-Analyse von Endlagerstätten muss daher die Speziation des Grundwassers hinsichtlich Kolloidgehalt und -zusammensetzung einen integralen Bestandteil bilden. Standard Methoden wie die Laser-Lichtstreuung (PCS) können auf Wässer hoher Gehalte großer Partikel (>50nm) angewandt werden. Für natürliche Wässer ist jedoch die Empfindlichkeit häufig nicht ausreichend. Die Laser induzierte Breakdown Detektion ergänzt diese Methoden und erlaubt den Nachweis kleiner Partikel (>5nm) in Spurenmengen (1ppt). Diese Technik wurde ursprünglich zur Kontrolle von Prozesswässern in der Halbleiter-

Industrie entwickelt und wurde eher phänomenologisch interpretiert. Um den komplexen Vorgängen in natürlichen Systemen Rechnung zu tragen, ist ein genaueres physikalisches Verständnis der Vorgänge und eine darauf basierende Verfeinerung der Methode notwendig.

Introduction

For the safety assessment of nuclear waste repositories, the risk of radionuclide migration into the environment has to be evaluated on time scales of the order of 100.000 years. Container materials cannot be expected to withstand corrosion for these time periods and finally, radionuclide retention in the surrounding geological formation becomes an integral component of a multibarrier safety system. However, in recent years plutonium was found to migrate fast over km-distances in the aquifer near a Nevada nuclear detonation site [1] and this unexpected effect was attributed to colloid mediated transport. Aquatic colloids of organic or inorganic composition originating from mobilization of preformed colloid-sized materials or in situ precipitation of supersaturated mineral phases are omnipresent in natural ground-waters [2]. Obeying Pareto's power law, particle number density increases strongly as the size decreases (αD^{-5}) and natural ground waters may contain up to 10^{15} particles per liter below 50nm. They may form pseudocolloids by uptake of actinide ions and due to their large number may act as a very efficient carrier in the groundwater [3]. But even a groundwater poor in natural colloids does not circumvent this problem entirely, because the tetravalent actinides are known to form stable eigencolloids by aggregation of the hydrolyzed species [4]. Destabilizing conditions lead to the formation of large aggregates and finally to immobile precipitates. If, however, only very small (<100nm) colloids are formed, they remain suspended and migration is strongly enhanced [5]. Detailed knowledge on formation mechanisms and stability of the colloidal phase is hence of cardinal importance and the investigation of long term stability as a function of colloid concentration and geochemical parameters is a prerequisite for the assessment of actinide migration.

The Method

Conventional detection methods, e.g., photon correlation spectroscopy (PCS), are not capable of characterizing size distribution and number density for small species (<50nm). Other methods, like scanning (SEM) or tunneling (TEM) electron microscopy or field flow fractionation (FFF), perturb the initial state of aquatic colloids

in the characterization procedure. Atomic force microscopy (AFM) is a non-discomposing method but requires a relatively concentrated colloid suspension, which means that a condensation of sample is necessary for the colloid characterization.

For this means, the laser induced breakdown detection (LIBD) was developed, tailored to the in-situ detection of very small colloids (> 5nm) down to very low concentrations ($10^5 cm^{-3}$) [6, 7]: A pulsed laser is focused tightly into a quartz cell containing the sample (Fig.1). In the focal region, free charge carriers are created due to multi photon ionization and inverse bremsstrahlung - a dielectric breakdown occurs. Further heating leads to the formation of a hot expanding plasma which is detected via its (acoustic) shock wave [8] or optical emission [9]. The pulse energy density (threshold) necessary to induce a breakdown event is lower for solid matter as compared to pure water. By a suitable choice of pulse energy, breakdown events can be selectively initiated by particles in the focal volume and from the characteristic photon-flux dependence (s-curves), particle size distributions·and concentrations are deduced.
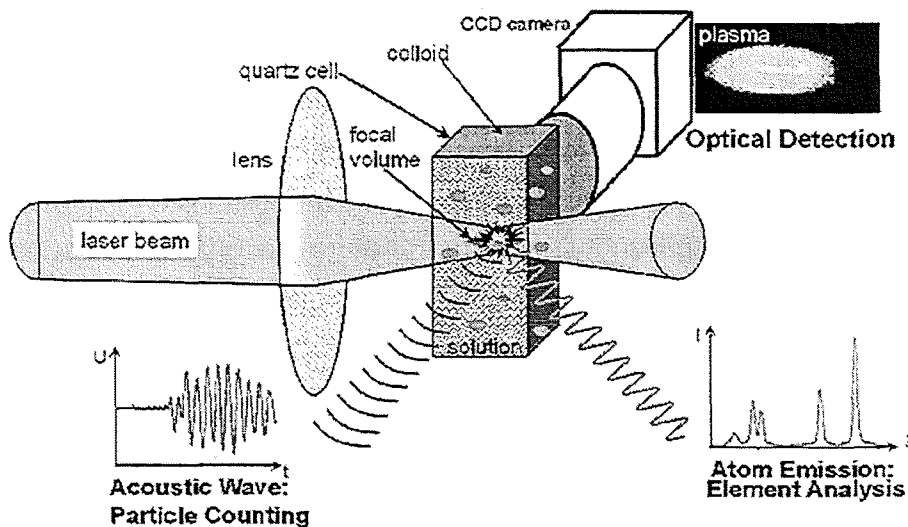
Fig.1:   LIBD detection setup. Details see text.

Status

For the detection of simple systems such as monodisperse spherical colloids of well defined chemical composition, the LIBD can be used straightforward, i.e. on a merely phenomenological basis. If, however, the sample is of more complex nature, e.g. in the aquifer, a closer look at the underlying physical processes is necessary for a meaningful interpretation of data:

Plasma creation is initiated by generation of a first, 'lucky', electron via multiphoton-ionisation (MPI, Fig.2). The corresponding formation rate depends on the product of photon flux density, laser pulse duration and MPI-cross-section of the colloid. This 'lucky' electron, once generated, is multiplied rapidly by inverse bremsstrahlung in the further course of the laser pulse and a plasma is formed. However, there are loss processes such as recombination and diffusion out of the particle which counteract plasma formation, and in order to obtain a realistic model of the breakdown process, a multitude of parameters has to be known and taken into account:

Comparatively easy to obtain and control are the laser-parameters: Pulse energy, temporal and spatial profile (beam waist in the focus), which are used to determine the photon flux density in the focal region. The photon energy is given by the fixed wavelength (usually 532 nm).

Colloid related parameters represent a more difficult problem: Radius, number density and molar mass of a monomer unit of the particle can be determined at least for model substances. The specific density is harder to obtain, because colloids might form different phases as known from bulk matter. The same holds for the order of the process n, i.e. the number of photons necessary to ionize one atom or molecule of the particle. Approximate values can be calculated from bulk and gas phase molecular data. Even more difficult is the determination of the MPI cross-
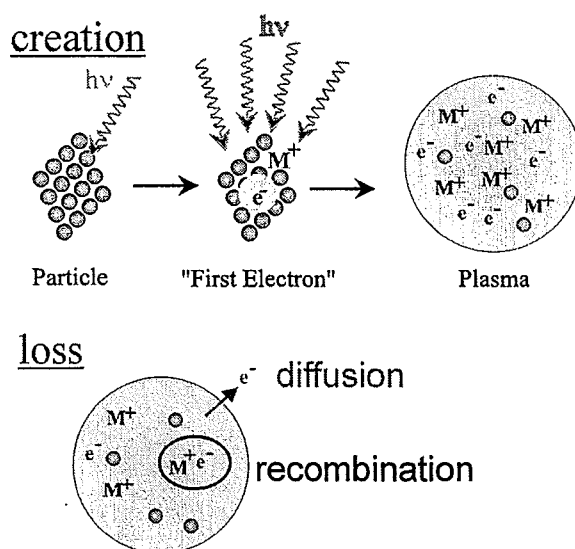
Fig. 2: Generation of free charge carriers by multiphoton ionisation (top) and loss due to recombination or diffusion (bottom)

section, which, due to the high non-linearity of the process (typically n=4-5), is of cardinal importance. First order approximations are accessible by the Keldysh theory [10, 11] or direct measurements in the gas phase, as performed on the phenyl ring, the monomer of polystyrene particles [12].

Electron loss due to recombination or diffusion is measured by pump-probe experiments, where the plasma, created by a 10ns Nd:YAG pulse, is probed by a delayed ps-pulse of a Ti:Sa laser [13] gaining information on the temporal evolution of plasma temperature and electron density.

Finally the sensitivity of the detection device is to be taken into account. For optical detection a minimum luminosity of the plasma plume is necessary, for acoustic detection the energy (loudness) of the shockwave has to overcome the piezo detector threshold of approximately 10nJ. A plasma formed late during the laserpulse might not contain sufficient energy to overcome the threshold and hence is not counted.

The breakdown process for a single colloid is modeled by a four step procedure:

- The probability to create at least one "lucky" electron at time t is evaluated taking into account the electron density $n^*(t)$ and the ionization rate k_{MPI}

- Electrons lost by diffusion k_{loss} and recombination k_{recomb} are subtracted

- It is checked, whether the irradiance F at time t still suffices to multiply electrons, and their total number $N(t)$ is calculated

- The critical time t_{crit} to deposit enough energy in the plasma to overcome the detection threshold is evaluated.

Mathematically the above processes are described by three coupled differential equations, which have to be solved partly numerically. The algorithm is implemented in a FORTRAN code and allows to work with arbitrary temporal and spatial beam profiles. While simpler models, not taking into account electron loss, could only describe either small (10-50nm) or large (100-1000nm) particles satisfactory with one set of parameters, good agreement with measurements of high statistics applying a gaussian shape TEM00 laser beam has been achieved recently. Future work includes modeling of multimodal size distributions as well as detailed investigations on various colloidal material.

Applications

Applications of LIBD are of great variety and are reported on in different contributions to this report: groundwaters are characterized with respect to colloid content in-situ in underground laboratories in Grimsel (CH) and Äspö (S) (see 32.25.03 VI) [14]. In order to understand formation and growth processes of actinide colloids, aggregation is observed as a function of time for model colloids ZrO_2 [15] as well as for Pu(IV) species. Trace detection of colloids in oversaturated solutions can be used to very precisely determine thermodynamic solubility data (see 32.25.04 I) [16].

Outlook

Recently a dye-laser is employed in order to tune the excitation wavelength in a REMPI (resonance enhanced MPI) like manner, allowing to probe element-composition and valence state of the colloids. Optionally, the laser beam can be guided into an inert gas glovebox suited for the investigation of radioactive colloids (e.g. Pu(IV)). An additional instrumentation is built, where the plasma plume is observed by two cameras perpendicular to each other, allowing to image in three dimensions. In contrast to the 2-dimensional imaging by a single camera, the exact spatial position of the plasma within the laser focus and hence the exact photon flux density is accessible, which is necessary to gain information on the colloid size distribution.

References

B. D. Honeyman, Nature **397,** 23-24 (1999).
J. N. Ryan, Colloids Surf. A. **107,** 1 (1996).
J. I. Kim, MRS Bulletin **19,** 47-53 (1994).
R. E. Wildung, T. R. Garland, and D.A.Cataldo, IAEA Viena **2,** 319 (1979).
P. Zhao and S. A. Steward, LLNL Report **126039,** 2-13 (1997).
T. Kitamori, K. Yokose, K. Suzuki, T. Sawada, and Y. Goshi, Japanese Journal of
        Applied Physics **27,** L983-L985 (1988).
F. J. Scherbaum, R. Knopp, and J. I. Kim, Appl. Phys. B **63,** 299-306 (1996).
C. Walther, C.Bitea, J. I. Kim, and F. J. Scherbaum,
        Nucl.Instr. Meth. ,submitted (2002).
T. Bundschuh, R. Knopp, and J. I. Kim, Colloids and Surfaces A **177,** 47-55 (2001).
C. J. G. J. Uiterwaal, C. R. Gebhardt, H. Schröder, and K.-L. Kompa, Phys. Rev. Lett
        in print, (2002).
L. V. Keldysh, Sov. Phys. JETP **20,** 1307-1314 (1965).
C. Walther, A. Herlert, J. I. Kim, F. J. Scherbaum, L. Schweikhard, and M. Vogel,
        Chem. Phys. **265,** 243-250 (2001).
C. Walther, T. Fanghänel, G. Geipel, and J. I. Kim, in preparation (2002).

W. Hauser, H. Geckeis, J. I. Kim, and T. Fierz, Coll. Surf. A in print (2002).

C. Bitea, J. I. Kim, and C. Walther, submitted (2002).

V. Neck, J. I. Kim, B. S. Seidel, C. M. Marquardt, K. Dardenne, M. P. Jensen, and W. Hauser, Radiochim. Acta **89,** 1-8 (2001).

II.   Characterization of aquatic colloids by a combination of LIBD and ICP-MS
following the size fractionation

(H. Geckeis, M. Bouby, Th. Ngo Manh, F. Scherbaum, INE)

Abstract

The colloid size fractionation of a natural groundwater from Gorleben is made by two
different methods: flow field flow fractionation (FFFF) and size exclusion chromato-
graphy (SEC), followed by analysis of chemical composition using UV spectroscopy
for organic components and ICP-MS for inorganic components. Relative number
density of humic colloids following the size fractionation is determined by laser-
induced breakdown detection (LIBD). Humic colloids are interacted with radioactive
tracers, ^{155}Eu(III) and ^{228}Th(IV), to appreciate their sorption behaviour onto different
colloid size fractions and thus to compare with natural humic colloid-borne elements
of M(III) and M(IV). For the appraisal of colloid size change upon metal ion com-
plexation, purified Aldrich humic acid is loaded with the Eu^{3+} ion on increasing the
concentration and the size change is then determined by LIBD. The results of the
present experiment indicate that the natural humic colloid-borne heavy metal ions ap-
pear in different chemical states as compared to the same but laboratory traced
metal ions.

Zusammenfassung

Die Charakterisierung von Huminkolloiden in einem natürlichen Grundwasser aus
dem Gorleben Aquifer erfolgte mit der Fluss-Feld-Fluss Fraktionierung (FFFF) und
der Größenausschlusschromatographie (SEC) und anschließender Detektion des
Eluats mittels Spektrophotometrie und ICP-MS. Als zusätzlicher Detektor für Kolloide
diente die Laser-induzierten Breakdowndetektion (LIBD). Das Grundwasser wurde
mit den Radiotracern ^{155}Eu(III) and ^{228}Th(IV) gespiked, um deren Wechselwirkung mit
unterschiedlich großen Kolloiden zu untersuchen. Der Einfluss der Metallbeladung
auf die Kolloidgrößenverteilung wurde mit der LIBD quantifiziert, indem Eu(III) zu
einer Aldrich-Huminsäurelösung zuaddiert wurde. Die experimentellen Ergebnisse
zeigen, dass U, Th und SEE in den natürlichen Kolloiden in einer anderen chemi-
schen Umgebung vorliegen als dies für im Labor zugegebene Tracerionen beob-
achtet wird.

Introduction

Humic colloids in natural water are composed of humic or fulvic acid loaded with inorganic elements either by complexation or by peptizing of small inorganic composite particles [1, 2]. Once actinides are dissolved in groundwater containing humic colloids, they may undergo interaction with ion exchange functional groups of humic component [3] and/or with inorganic component [4]. Speciation of such interactions over long time periods is not yet well appraised. The heterogeneous reactions of actinide ions with different components of humic colloids in ground water lead most likely to diverse kinetic processes, as observed in the migration experiment of humic colloid-borne actinides [5]. The role of humic colloids as a carrier for the actinide migration can only be ascertained, if their interaction processes are well comprehended. One important question is how the actinide ions shall be incorporated into humic colloids under geochemical conditions of groundwater. The irreversible reaction may facilitate the migration of humic colloid-borne actinides at considerable space and time in a given aquifer system, whereas, the reversible reaction leads to a limitation of humic colloids as an actinide carrier. As the formation of humic colloids in groundwater has been undergone for a long period of reaction time, a simulation of such reactions in laboratory is not easily practicable. The present investigation deals, therefore, with the distribution of polyvalent metal ions originally present in humic colloids of different size. Groundwater containing humic colloids is taken from the Gorleben aquifer system in northern Germany (lower Sachsonia). Humic colloids are characterized for their average size by laser-induced breakdown detection (LIBD) and for their size distribution by flow field-flow fractionation (FFFF) and size exclusion chromatography (SEC). For the first time the size fractions of natural aquatic colloids are monitored by both LIBD and UV spectroscopy in parallel and then analysed for the inorganic element distribution by inductively coupled plasma mass spectrometry (ICP-MS).

Results

The coagulation of purified humic acid by complexation with polyvalent metal ions is well known. As the metal ion loading onto humic acid changes its size and structure, a coagulation experiment is made with purified Aldrich humic acid by adding the Eu^{3+} ion to ascertain under what condition the coagulation becomes significant. A relative estimation of the coagulation size change is made according to a calibration using

latex spheres. The size for humic colloids in the Gohy-2227 groundwater and Aldrich humic acid as determined by LIBD is found to be smaller than the smallest particles used for calibration (polystyrene spheres with a diameter of 32 nm). Extrapolation of the calibration line leads to an average colloid size of (12 ± 7) nm. Since the material difference between polystyrene particles and humic colloids is not taken into account and the the size is obtained by extrapolation of the calibration line, the humic colloid size from LIBD has to be considered as an apparent value that reflects approximately the size range of humic colloids for the moment. The actual loading of Eu^{3+} onto the proton exchange groups of humic acid is calculated based on the available complexation study [3]. A gradual occupancy of humic acid functional sites by Eu^{3+} up to 50 % does not cause a measurable size change as observed by LIBD. The proton exchanging carboxylate groups as determined by titration are considered as the functional groups and one Eu(III) is assumed to interact with three of these functional groups. Once the functional groups are occupied about 60 %, the size increase can be monitored. Further to 63 % results in a significant coagulation, increasing the size to about 200 nm at the beginning and then nearly to 900 nm after 52 days. At this stage Eu-borne humic acid becomes flocculated, same as the case of Am(III) loading [3]. The present experiment leads to a loading capacity of purified Aldrich humic acid for Eu(III) about 60 %, which closely corresponds to the value determined for Am(III). The results suggest that humic colloids in groundwater at the low concentration of 260 µg/l used in this experiment can probably be loaded with metal ions up to 50 % of functional sites to remain stable in water and, if over loaded, humic colloids become unstable and undergo flocculation or precipitation. At higher humic acid concentrations flocculation is already observed at much lower metal ion loading [3].

Fig. 1 illustrates the results of the polyvalent element distribution in natural groundwater humic colloids of different size as fractionated by asymFFF and detected by ICP-MS and LIBD. The polyvalent metal ions, like Th(IV), and Ce(III) etc., appear at least partially in colloids of larger size (30-40 nm). Size calibration is made by calibration with reference polystyrene sulfonate colloids. The major part of humic/fulvic acid component, as detected by UV spectroscopy, is located at a size of 3 nm. The LIBD results indicate the particle size distribution from 10 nm to 25 nm followed by a background tailing. The number density of colloids given in the upper part of Fig. 1 is converted to a relative mass- weighted size distribution, as shown in
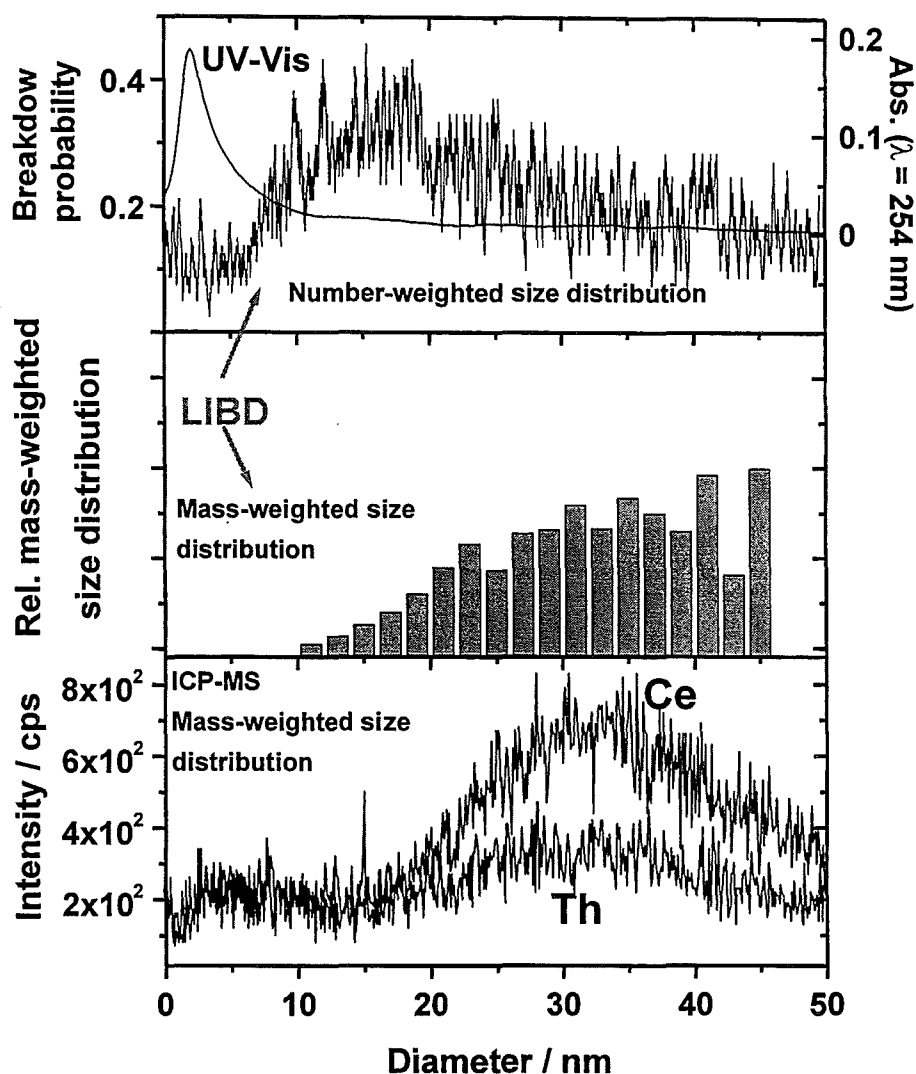
Fig. 1: FFFF fractograms of Gohy 2227 humic colloids detected by UV/VIS
absorbance ICP-MS and LIBD; The relative mass-weighted size distribution
is calculated from the fractogram detected by LIBD (see explanations in the
text).

the middle part of figure. The conversion is made at 2 nm size intervals from the relative number and size of colloids to their relative mass ratios, compensating the same mass density. From Fig. 1 one can conclude that the humic/fulvic acid component loosely structured and hydrated requires higher laser irradiance for breakdown and thus is more or less invisible. The LIBD relative mass-weighted distribution of colloids appears closely comparable to the elution profile of Th and Ce present originally in humic colloids. The larger colloids visible by LIBD are assumed to consist of inorganic nanoparticles with higher density hosting the naturally abundant actinides and REE. The LIBD results of the fractionated colloid sizes in Fig.

1 are found somewhat larger than the estimated "average" size evaluated for humic colloids in the Gohy 2227 groundwater.

SEC analysis corroborates the FFFF results even though the size fractionation principle is different (Fig.2). In the SEC study, the radiotracers, [228]Th and [155]Eu, added to the groundwater are observed in the size group of the major humic/fulvic acid component, differently from the originally present Th, La and Ce in colloids. This fact infers dissimilar chemical states between the laboratory sorbed polyvalent elements and those originally associated. No exchange between the metal ions is observed even after an equilibration period of 200 d. The different elution profiles lead us to assume that the added tracers, [228]Th and [155]Eu, undergo complexation
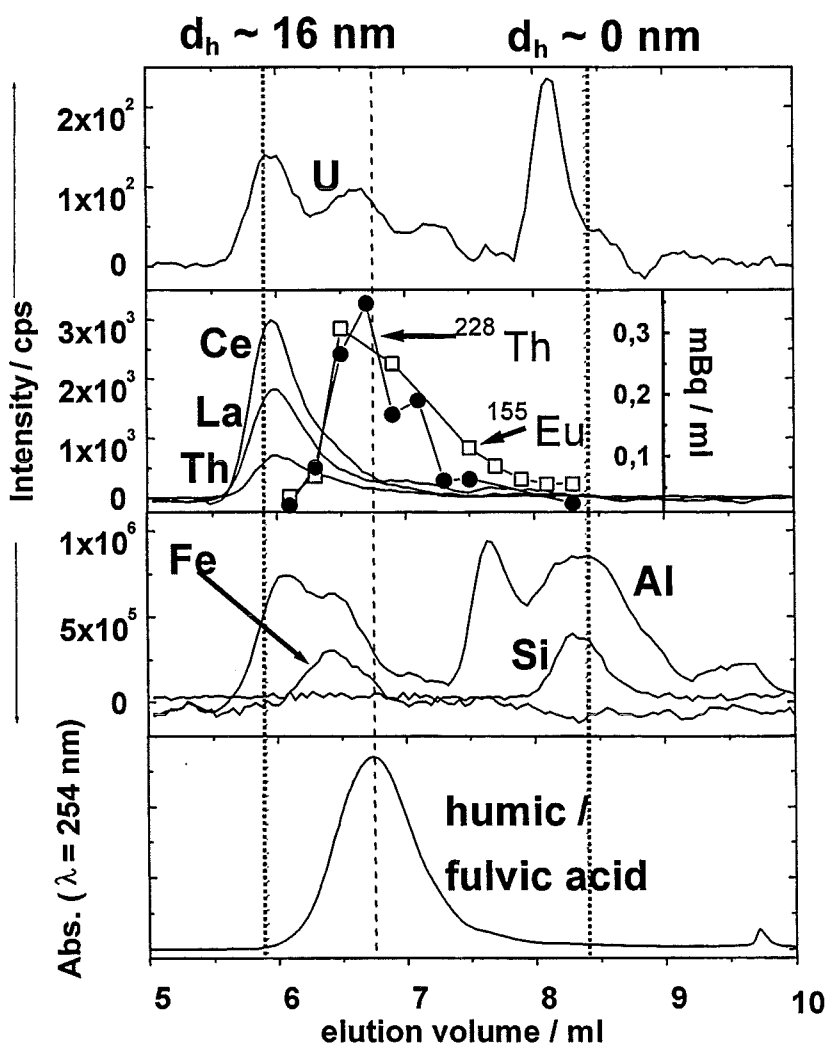
Fig. 2:   Size exclusion chromatograms of Gohy 2227 as recorded by an UV/VIS detector and ICP-MS; the working range of the column and the corresponding hydrodynamic diameters are indicated by the dotted lines. Th-228 and Eu-155 are analysed by α- and γ-spectrometry.

with functional moieties of humic/fulvic acid components, while Th, La and Ce originally present in colloids are composed as inorganic composite particles that are dispersed by humic/fulvic acids.

Conclusions

The possible generation of irreversibly colloid bound actinides under natural conditions can be deduced from experimental evidence. As such processes belong to the key uncertainties of nuclear waste disposal safety assessement, further studies are required to quantify the relevance of such processes for the actinide behaviour under real repository conditions.

References

Kim, J.I., The Chemical Behavior of Transuranium Elements and Barrier Functions in Natural Aquifer Systems, Mat.Res.Soc.Symp.Proc., 294, 3-21, (1993)

K.J. Wilkinson, J.C. Negre, J. Buffle, Coagulation of colloidal material in surface waters: the role of natural organic matter, J.Contam. Hydrol. 26, 229-243, (1997)

Kim, J. I., Czerwinski, K. R., Complexation of metal ions with humic acid : metal ion charge neutralization model, Radiochim. Acta 73, 5, (1996)

Geckeis, H., Rabung, Th., Ngo Manh, T., Kim, J.I., Beck H.P., Humic Colloid-Borne Natural Polyvalent Metal Ions: Dissociation Experiment, submitted to Env.Sci.Tech. (2002)

Artinger, R., Kienzler, B., Schüßler, W., Kim, J.I., Effects of humic substances on the [241]Am migration in asandy aquifer: Column experiments with Gorleben Groundwater/Sediment systems, J.Cont.Hydrol. 35, 261-275, (1998)

III. Fulvate Complexation of tetravalent Neptunium

(C.M. Marquardt, A. Seibert, J.I. Kim, INE; V. Pirlet, SCK-CEN, Mol)

Abstract

Results are presented on the complexation of the tetravalent actinide element Neptunium (Np(IV)) with fulvic acid. Two fulvic acids have been studied, the Gohy-573(FA) from the Gorleben groundwater 573 (Germany) and BoomClay(FA) from a Boom Clay pore water (Belgium). The Np(IV) interaction with the two fulvic acids was studied at pC_H 1 and 1.5. Fulvic acid was used because it remains in solution, contrary to humic acid generating a flocculate in this low pH range. Despite the low pC_H, the Np(IV) ion is present as different hydrolysis species, dominated by the di-hydroxo neptunyl ion, and the complex formed is $Np(OH)_2FA$. NIR absorption spectroscopy is used for quantification of species involved, i.e. free and fulvate complexed Np(IV). The overall complexation constant for the $Np(IV)(OH)_2FA$ complex is evaluated to be $\log\beta=32.6 \pm 0.4$, with a stepwise complexation constant for the $Np(OH)_2^{2+}$ ion with fulvic acid of $\log\beta_{exp} =5.7_5 \pm 0.3$. The results lay the ground for future extension of the studies of humic substances complexation of tetravalent actinides into the pH-neutral range.

Zusammenfassung

Es werden Resultate zur Komplexierungsreaktion des vierwertigen Actiniden-elements Neptunium mit Fulvinsäure vorgestellt. Zwei Fulvinsäuren wurden hierbei untersucht, GoHy-573(FA) aus dem Gorleben-Grundwasser 573 und BoomClay(FA) aus einem BoomClay-Porenwasser (Belgien). Die Wechselwirkung von Np(IV) mit beiden Fulvinsäuren wurde bei pC_H 1 und 1.5 untersucht. Die Fulvinsäure wurden als Komplexbildner ausgesucht, da sie im Gegensatz zu den Huminsäuren bei niedrigen pH-Werten in Lösung bleiben und nicht wie jene ausfallen. Trotz der hohen Säurekonzentration liegt Np(IV) bereits als hydrolysierte Spezies vor, hauptsächlich als Di-hydroxo-neptunylion, wobei bei der Fulvatkomplexierung ein gemischter Np(IV)-hydroxo-fulvatkomplex $Np(OH)_2FA(II)$ gebildet wird. Zur Quantifizierung des unkomplexierten und fulvatkomplexierten Anteils an Np(IV) wurde NIR-Absorptions-spektroskopie eingesetzt. Die Komplexierungskonstante wurde zu $\log\beta = 32.6 \pm 0.3$ berechnet, unter Berücksichtigung der Stufenkomplexierungskonstante logK der Reaktion von $Np(OH)_2^{2+}$ mit Fulvinsäure ($\log\beta_{exp} = 5.8 \pm 0.3$). Die hier präsentierten

Resultate bilden die Grundlage für weiterführende Studien zur Huminstoff-komplexierung von tetravalenten Actiniden im pH-neutralen Bereich.

Introduction

The goal of the present work is to elucidate the complexation (mechanism and strength) of tetravalent neptunium by humic colloids. One of the biggest problem investigating tetravalent actinide ions is their high tendency for hydrolysis, the reaction with water molecules resulting in different hydrolysis species ($Np(OH)^{3+}$, $Np(OH)_2^{2+}$, $Np(OH)_3^{+}$, $Np(OH)_4$). In order to impede such reactions and to facilitate calculations and interpretations, the experiments were started at low pH in the slighty-hydrolysed range of pH $\leq$ 1.5. In this acidic pH range the fulvic acid fraction (FA) of the humic colloids can be only used as soluble fraction in contrast to non-soluble humic acid fraction. In the present work the reaction between Np(IV) and two natural fulvic acids (BoomClay and GoHy-573) has been examined at H^{+}-concentrations $[H^{+}]$ = $10^{-1.0}$ and $10^{-1.5}$ M. For the work purpose, NIR absorption spectroscopy was chosen, as it provides a direct quantification of species involved in the reaction and the accessibility to the ratio of the free Np(IV) on the complexed Np(IV).

Experimental

Two natural fulvic acids (FA) were used. One FA (BC-FA) was extracted, from the Boom Clay interstitial water sampled in a underground research facility (Mol, Belgium) and the second FA from a Gorleben groundwater (GoHy-573-FA, Gorleben site, North-Germany). The proton exchange capacities (PEC) of the purified FA´s are 3 mmol/g for BC-FA and 5.7 mmol/g for GoHy-573-FA.

The fulvate complexation reaction was studied at $[H^{+}]$ = $10^{-1.0}$ and $10^{-1.5}$ M at ionic strength of 0.1 M HCl-$NaCl$ or $HClO_4$-$NaClO_4$ and at room temperatures. The concentration range of the total Np(IV) ($[Np(IV)]_t$) was varied between $3.5 \cdot 10^{-6}$ and $1.23 \cdot 10^{-4}$ M and the FA concentration range was between $1.5 \cdot 10^{-4}$ and $8.48 \cdot 10^{-3}$ mol/L referring to exchangeable H^{+}.

Results and discussion

NIR absorption spectroscopy

In the absorption spectra of Np(IV) in fulvic acid solution (Fig. 1) two absorption bands are observed, at 960 and 968 nm. The well known absorption band at 960 nm
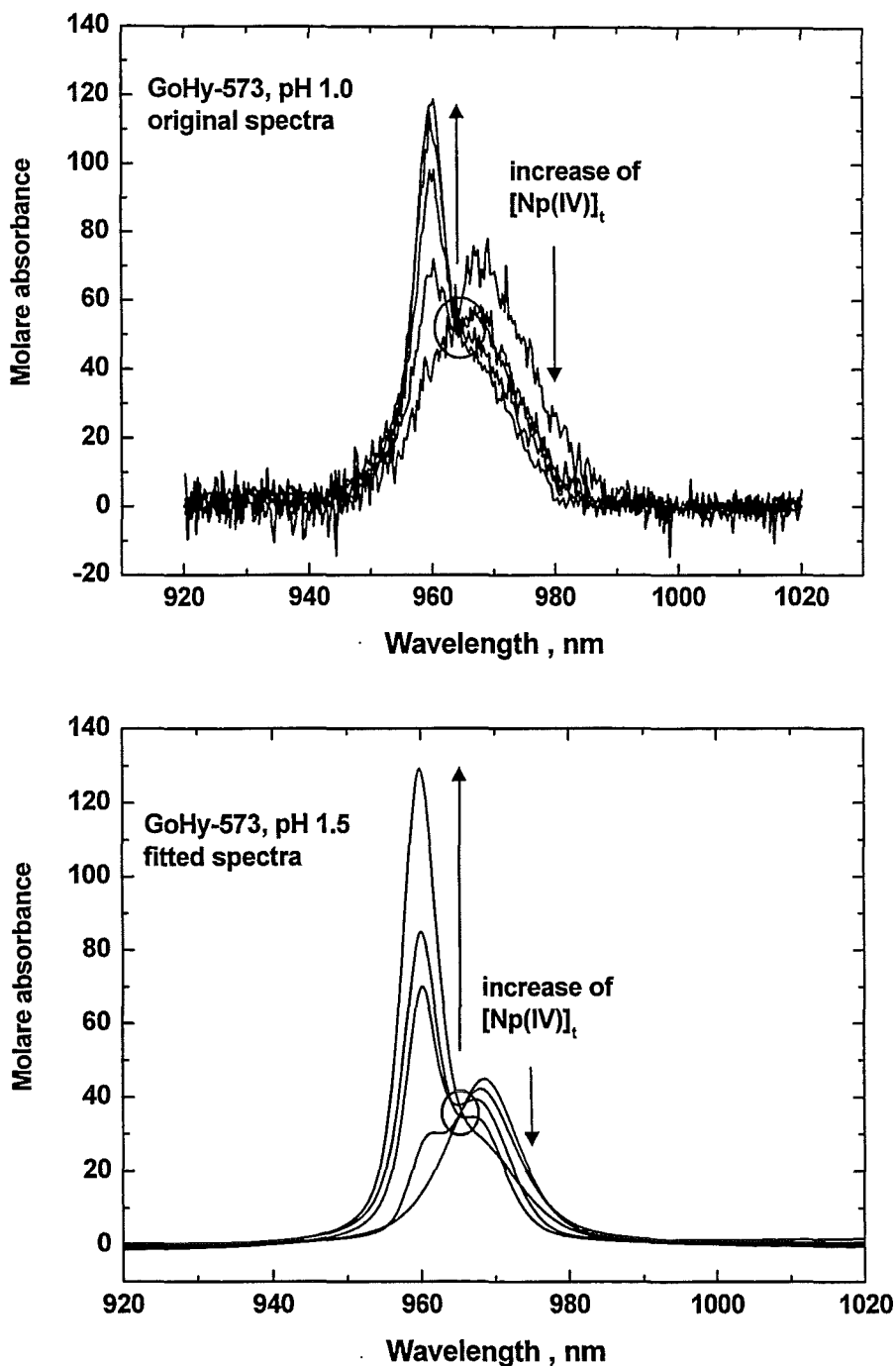
Fig. 1: Molar absorption spectra of Np(IV) in a FA-solution at $-\log[H^+] = 1$ (upper part) and $-\log[H^+] = 1.5$ (lower part). Each figure show one titration series of a FA-solution by adding Np(IV).

$[Np(IV)]_t$: $1.8 \cdot 10^{-5}$ - $1.0 \cdot 10^{-4}$ M for $-\log[H^+] = 1.0$;

$\qquad$ $3.2 \cdot 10^{-5}$ - $1.1 \cdot 10^{-4}$ M for $-\log[H^+] = 1.5$;

$[FA]_t$ (normalised to PEC) varies due to dilution between $7.96 \cdot 10^{-4}$- $7.80 \ 10^{-4}$ mol/L for $-\log[H^+] = 1.0$ and $4.95 \cdot 10^{-4}$ - $4.86 \cdot 10^{-4}$ mol/L for $-\log[H^+] = 1.5$.

comes from the uncomplexed, free Np(IV) ion and the absorption band at 968 nm is attributed to the fulvate complexed Np(IV). In the molare absorption spectra one isobestic point is observed which indicates that only one main fulvate complex exist in solution under the given experimental conditions. By these spectra the concentrations of free Np(IV) and complexed neptunium are determined according to the lambert-beer law.

Calculation of the loading capacity LC

The complexation of metal ion with humic substances is interpreted as a neutralisation reaction of the metal ion with proton exchanging sites of the macro-molecular fulvic acid [1]. In case of the tetravalent Np^{4+} ion four available anionic sites should be necessary for the neutralisation reaction. At such acidic conditions it seems to be hard for the Np^{4+} to find four sites within the compact, folded structure of humic substances. Another problem with the tetravalent neptunium arises, because of its strong tendency in forming hydrolysis species even at acidic conditions. Calculations of the hydrolysis reaction of Np(IV) with hydrolysis constants from Refs. [2,3,4] shows that $Np(OH)_2^{2+}$ is the main species beside a small amount of $NpOH^{3+}$ in solution at $pC_H = 1$ and 1.5 at ionic strengths of 0.1 M $HClO_4$-$NaClO_4$. Earlier studies have shown for the trivalent actinides that such hydrolysis species can also be complexed by humic substances [5,6] at conditions the hydrolysis reaction competes with the humate/fulvate complexation. It is self-evident to express the complexation of Np(IV) with fulvic acid in a first approach by the following reaction:

$$Np(OH)_2^{2+} + FA(II) \quad Np(OH)_2FA(II) \tag{1}$$

and according to the charge neutralisation model described in a earlier publication [1]. XAFS measurements on the neptunium fulvates at same conditions corroborates the existence of a OH⁻ group in the complex [7] under formation of a mixed complex.

$Np(OH)_2^{2+}$ represents the uncomplexed tetravalent neptunium ion, FA(II) the free fulvic acid with equivalent negative charge (two binding sites with charge -1 of FA neutralise one $Np(OH)_2^{2+}$-ion). $Np(OH)_2FA(II)$ denotes the neptunium fulvate complex. According to Eq. (1) the law of mass action is defined at constant ionic strength by:

$$\beta_{exp} = \frac{[Np(OH)_2FA(II)]}{[Np(OH)_2^{2+}][FA(II)]_f} \tag{2}$$

534

Because this is only the first approach the stability constant is denoted as the experimental complexation constant β_{exp}. $[FA(II)]_f$ denotes the effective free fulvic acid concentration and is given by

$$[FA(II)]_f \quad = \quad [FA(II)]_t \cdot LC - [Np(OH)_2FA(II)] \tag{3}$$

and was calculated by the difference of total FA and Np(IV)-fulvate concentration $([FA(II)]_t - [Np(OH)_2FA(II)]_t)$. The loading capacity (LC) describes the behaviour of the fulvic acid as an weak ion exchanger, which can be loaded only by a limited amount of a given metal ion. Such a loading capacity is given by

$$LC = (+2) \cdot [Np(OH)_2{}^{2+}]_{max}/PEC \tag{4}$$

with the metal ion charge +2, the maximum concentration of neptunium bound on the FA, and the proton exchange capacity. A combination of (2) and (3) gives the following relation:

$$\beta_{exp} = \frac{[Np(OH)_2FA(II)]}{[Np(OH)_2^{2+}]([FA(II)]_f \cdot LC - [Np(OH)_2FA(II)])} \tag{5}$$

The LC can be determined from experimental data by the relationship between $[Np(OH)_2FA(II)]/[FA(II)]_t$ and $[Np(IV)]_t/[FA(II)]_t$ according to many studies on other metal ions (Am(III), Cm(III), $NpO_2{}^+$, $UO_2{}^{2+}$) [8-11]. For this purpose Eq. (5) is converted to

$$\frac{[Np(OH)_2FA(II)]}{[FA(II)]_t} = 0.5 \cdot \left\{ \left(A \cdot \frac{[Np(IV)]_t}{[FA(II)]_t} + LC \right) - \sqrt{\left(A \cdot \frac{[Np(IV)]_t}{[FA(II)]_t} + LC \right)^2 - 4LC \cdot \frac{[Np(IV)]_t}{[FA(II)]_t}} \right\}$$

$$\tag{6}$$

with $A = 1+1/(\beta_{exp} \cdot [Np(IV)]_t)$. This relation illustrates a gradual increase of the relative amount of Np(IV)-fulvate as a function of the ratio $[Np(IV)]_t/[FA(II)]_t$, reaching a plateau when the fulvic acid is saturated with the metal ion. The height of the plateau corresponds to the loading capacity, which is illustrated in Fig. 2 for the experimental data. The loading capacities (LC) are calculated by Eq. (6) based on the experimental data at $pC_H = 1.0$ and 1.5 at ionic strength of 0.1 M $H^+/NaClO_4$.
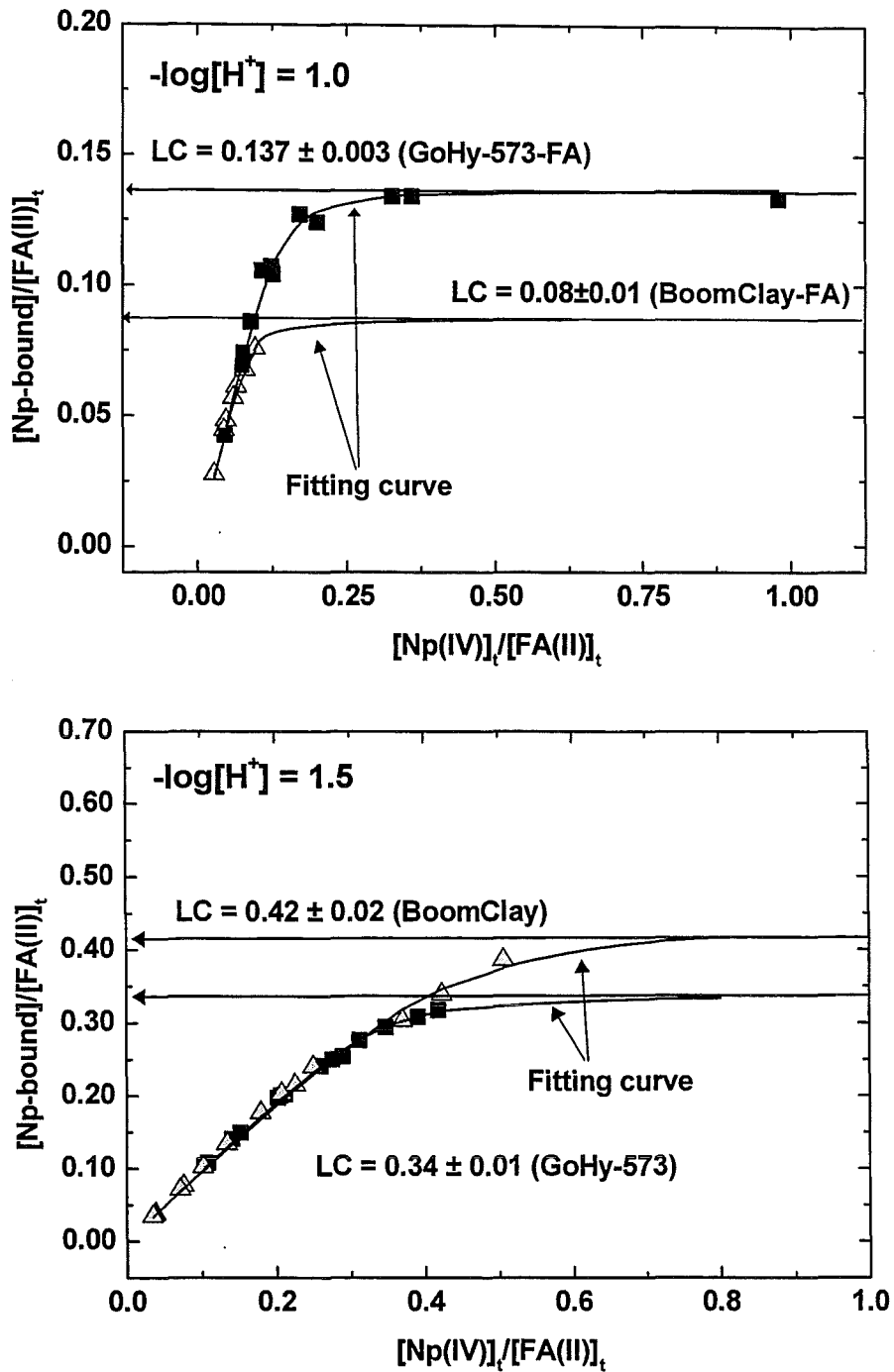
Fig. 2: Determination of the loading capacity (LC) of BoomClay and GoHy-573 fulvic acid with tetravalent neptunium (Np(IV)) at $pC_H = 1$ (upper part) and $pC_H = 1.5$ (lower part). Fulvic acid concentration was normalised according the charge neutralisation model to charge +2 corresponding to the main hydrolysis species $Np(OH)_2^{2+}$ expected at given pH-values. The lines are fitted curves according to Eq. (6).

Calculation of the complexation constant

With the loading capacities and Eq.(5) the experimental complexation constant $\log\beta_{exp}$ is evaluated for each data point and the average value for each FA at each $[H^+]$ concentration is listed together with the LC in Table 1. The $\log\beta_{exp}$ of the GoHy-573-FA and BoomClay are the same within the error bars, even at $pC_H= 1$ a slight lower value is obtain than at $pC_H = 1.5$. Nevertheless, a grand average value of $\log\beta_{exp} = 5.7_5 \pm 0.3$ is obtained between $pC_H = 1.0$ and 1.5.

Table 1: Loading capacities (LC) ,experimental complexation constants ($\log\beta_{exp}$), and overall complexation constant ($\log\beta_{121}$) for the reaction between Np(IV) and fulvic acid at $pC_H = 1.0$ and 1.5.

$Np(OH)_2^{2+}$ + FA(II) $Np(OH)_2FA(II)$		
	GoHy-573-FA	BoomClay-FA
$-\log[H^+] = 1.0$		
LC	0.14 ± 0.01	0.08 ± 0.01
$\log \beta_{exp}$	5.7 ± 0.3	5.6 ± 0.4
$-\log[H^+] = 1.5$		
LC	0.34 ± 0.01	0.42 ± 0.02
$\log \beta_{exp}$	5.8 ± 0.2	5.8 ± 0.2
grand average $\log\beta_{exp}$	**$5.7_5 \pm 0.3$**	

Np^{4+} + 2 OH$^-$ $Np(OH)_2^{2+}$	$\log \beta_{h2}° = 28.3 \pm 0.3$ (I = 0, [4]
	26.8 ± 0.3 (SIT corrected for I = 0.1)
Np^{4+} + 2 OH$^-$ + FA(II) $Np(OH)_2FA(II)$	
overall complexation constant $\log\beta_{121}$	**32.6 ± 0.4**

Due to the invariance of $\log\beta_{exp}$ to the $[H^+]$ it is assumed, that only the reaction (1) plays a role at the experimental conditions. Furthermore, within the XAFS study, no evidences were found for the formation of colloidal Np(IV) [7].

However, a reaction can be defined starting with the Np^{4+} ion in the following way

$$Np^{4+} + 2OH^- + FA(II) \rightleftharpoons Np(OH)_2FA(II) \tag{7}$$

with the corresponding overall complexation constant

$$\beta_{121} = \frac{[Np(OH)_2FA(II)]}{[Np^{4+}][OH^-]^2[FA(II)]_f} = \frac{[Np(OH)_2^{2+}]}{[Np^{4+}][OH^-]^2} \cdot \frac{[Np(OH)_2FA(II)]}{[Np(OH)_2^{2+}][FA(II)]_f} = \beta_{h2} \cdot \beta_{exp}. \tag{8}$$

β_{h2} is the second overall hydrolysis constant of Np^{4+} of the following hydrolysis reaction with the corresponding hydrolysis constant $\log\beta_{h2} = 26.8$ at 0.1 M $NaClO_4$. With this value and the correlation (8)

$$\log\beta_{121} = \log\beta_{h2} + \log\beta_{exp} = 26.8 + 5.75 = 32.6 \pm 0.4$$

a value of 32.6 ± 0.4 is obtained for the overall complexation constant $\log\beta_{121}$.

Conclusions

This work reveals a strong interaction of tetravalent neptunium with fulvic acid at pCH = 1 and 1.5. Hydrolysis of the Np4+ ion occurs in the used pH range and two main hydrolysed species, Np(OH)3+ and Np(OH)22+, are proposed by thermodynamic calculations. As a consequence, mixed complexes have to be considered. But from absorption spectra, the exact concentrations of each possible free Np(IV) species as well as the fulvate bound neptunium species cannot be calculated. Only one signal for unbound and bound Np(IV) are found. Nevertheless, by assuming that the main neptunium species is the Np(OH)22+ ion, a constant complexation constant of 5.75±0.3 is obtained for formation of a Np(IV)-dihydroxo-fulvate complex at pCH = 1.0 and 1.5. XAFS studies [7] corroborate such a mixed complex Np(OH)xFA(IV-x) as the main species in solution without clarifying the value of x. This result is confirmed by a comparison with complexation data of different actinides obtained with carbonate, oxalate and fulvate/humate which anticipates higher logβexp in case of a binary Np4+-fulvate complex. However, due to the pH independent complexation constant, the formation of only Np(OH)2FA(II) as the main species in solution seems justifiable. The stabilisation of such ternary complex is expedited by the rigid, compact, and folded structure of the FA at such low pH-values. By increasing the pH to more nature relevant values, this structure becomes unfolded and more flexible, but the Np(IV) simultaneously is more hydrolysed unless even colloidal. Which type of complex the Np(IV) forms at neutral pH values cannot be predicted up to now,

although it is important for safety aspects of radioactive waste disposal. That the binary Np4+-FA/HA-complexes will not play a role in natural groundwaters seems to be sure. To elucidate the behaviour of tetravalent actinides in the neutral pH range a lot of studies are necessary in the future.

References

Kim, J. I. and Czerwinski, K. R.: Complexation of Metal Ions With Humic Acid: Metal Ion Charge Neutralization Model, Radiochim.Acta, **73**, 5 (1996).

Duplessis, J. and Guillaumont, R.: Hydrolyse Du Neptunium Tetravalent, Radiochem.Radioanal.Letters, **31**, 293 (1977).

Neck, V. and Kim, J. I.: Solubility and Hydrolysis of Tetravalent Actinides, Radiochim.Acta, **89**, 1 (2001).

Neck, V. and Kim, J. I.: Solubility and Hydrolysis of Tetravalent Actinides, Scientific Report FZKA 6350, Karlsruhe, 1999.

Morgenstern, A., Klenze, R., and Kim, J. I.: The Formation of Mixed-Hydroxo Complexes of Cm(III) and Am(III) With Humic Acid in the Neutral PH Range, Radiochim.Acta, **88**, 7 (2000).

Panak, P., Klenze, R., and Kim, J. I.: A Study of Ternary Complexes of Cm(III) With Humic Acid and Hydroxide or Carbonate in Neutral PH Range by Time-Resolved Laser Fluorescence Spectroscopy, Radiochim.Acta, **74**, 141 (1996).

Denecke, M. A., Marquardt, C. M., Rothe, J., Dardenne, K., and Jensen, M. P.: XAFS Study of Actinide Coordination Structure in Np(IV)-Fulvates, submitted to J.Nucl Sci.Techn., (2002).

Marquardt, C. and Kim, J. I.: Complexation of Np(V) With Humic Acid: Intercomparison of Results From Different Laboratories, Radiochim.Acta, **80**, 129 (1998).

Kim, J. I., Rhee, D. S., Buckau, G., and Morgenstern, A.: Americium(III)-Humate Interaction in Natural Groundwater: Influence of Purification on Complexation Properties, Radiochim.Acta, **79**, 173 (1997).

Czerwinski, K. R., Kim, J. I., Rhee, D. S., and Buckau, G.: Complexation of Trivalent Actinide Ions (Am^{3+}, Cm^{3+}) With Humic Acid: The Effect of Ionic Strength, Radiochim.Acta, **72**, 179 (1996).

Czerwinski, K. R., Buckau, G., Scherbaum, F. J., and Kim, J. I.: Complexation of the Uranyl Ion With Aquatic Humic Acid, Radiochim.Acta, **65**, 111 (1994).

IV.   Iron Oxide/-Hydroxide Colloid Facilitated Americium Migration in Gorleben
        Groundwater

(T. Schäfer, R. Artinger, K. Dardenne, A. Bauer, INE)

Abstract

The relevance of colloidal transport to enhance the actinide mobility in the natural environment depends, among others on the reversibility of metal ion colloid binding. In this paper, the influence of the metastable, low crystalline precursor phase 2-line ferrihydrite (2LFh) and the possible structural entrapment of Am(III) in transformation products (thermal treatment at 70°C over 7d) on the colloidal mobility of Am was investigated in batch and column migration experiments. Laser light scattering analysis (PCS) demonstrated a fast 2LFh aggregation (1.8-5.6 mg2LFh/L) in Gorleben groundwater of low humic content (1-7 mgC/L), which can be attributed to surface charge neutralization detected via zeta potential measurements. The column experiments showed in groundwater with low humic content no significant enhancement of humic colloid bond Am recovery (R = 0.5 %). Contrary to this, in humic rich groundwater (30-90 mgC/L) the 2LFh colloids remained stable and showed an almost fivefold increase of the unretarded Am mobility in the case of transformed 2LFh (mainly hematite). Iron oxide/hydroxide selective extractions indicated a strengthening of Am from salt exchangeable in 2LFh to NH_4-oxalate-oxalic acid extractable in transformed 2LFh. Batch experiments revealed no equilibrium state for 2LFh colloid and ^{241}Am sorption onto Gorleben sand after 165 days, therefore indicating that metal colloid association/dissociation and colloid sediment attachment kinetics are a key issue for the actinide mobility.

Introduction

In natural aquifers, aquatic colloids are ubiquitous and take part in geochemical solid-water-interface reactions [1, 2]. Colloidal transport of inorganic nanophases is strongly correlated to the presence of humic substances, either for colloidal stabilization via surface charge reversal [3] or by initiating dissolution of sediment grain coatings (iron oxyhydroxides) and mobilization of clay colloids [4]. The metastable, low crystalline iron oxyhydroxide 2-line ferrihydrite (2LFh) is frequently found as the dominant inorganic Fe-colloid species in aquatic systems including the Gorleben system, but appears also as sediment grain surface coatings determining therefore

the sorption properties of the sediment. Sorption experiments reveal that actinides such as Np(V) are reversibly bound onto 2LFh [5], whereas [239]Pu (V/VI) shows a very slow desorption rate from iron oxide surfaces [6]. Coprecipitation studies from Grigoriev et al. [7] have demonstrated, that Pu(IV) and Np(IV) produce mixed hydroxides with Fe(III). Due to the metastable nature of 2LFh, a possible structural entrapment of actinides in colloidal stable secondary phases (goethite/hematite) might lead to an irreversible actinide binding. Np(V) binding changes with 2LFh alteration have been observed by Sakamoto et al. [8] and Nagano et al. [9] showed by Rietveld refinement analysis a substitution of structural Fe by the Am homologue Nd in the hematite structure.

The aim of this study is to discuss the influence of 2LFh and its thermal transformation product (i. e. hematite) on the mobility of Am(III) by colloid stability, batch and column migration experiments.

Materials and Methods

For the preparation of ^{59}Fe spiked 2-line-ferrihydrite (2LFh), the synthesis described in [10] was modified using an irradiated 99.99+ % pure iron foil (GoodFellow, Germany). 2LFh/Am coprecipitates (later referred to as 2LFh/Am) were synthesised by adding 2ml of the ^{59}Fe stock solution (pH < 1) to a 3 ml aliquot of [241]Am(III) stock solution and adjusting the suspension to pH 6 with 1 M KOH. Washing up to five times with Milli-Q water was performed to purify the synthesized 2LFh/Am precipitates. Tempering 2LFh/Am over a period of 7d at 70°C in an oven generated the transformation products (later referred as Hae/Am). The pH value was set to 6 and adjusted once a day. X-ray diffraction analysis of the transformations products indicate hematite as major mineral component. Photon Correlation Spectroscopy (PCS) analysis showed an intensity weighted mean colloid size of 259 ± 127 nm for the 2LFh/Am sample and a slightly lower colloid size of 180 ± 80 nm for Hae/Am. To determine the fraction of exchangeable, poorly crystalline (bioavailable) and total [241]Am in the colloidal phases an operational three-step extraction scheme selective for iron oxides was used [11]. The influence of humic substance concentration on the coagulation kinetics of 2LFh was investigated with PCS by adding 2LFh colloids to the untreated Gorleben groundwater with a dissolved organic carbon (DOC) range from 0.9 to 81.6 mgC/dm^3. The 2LFh colloid concentration was adjusted to 1.8 mg/L or 5.6 mg/L.

Column experiments were performed under inert gas atmosphere (Ar + 1 % CO_2) in a glove box. For the flow-through column experiments the Pleistocene quartz sand [12] was equilibrated in separate columns with Gorleben groundwater and circulated for a period of 3 months. Continuous injection of approximately one pore volume of Am/2LFh spiked groundwater was initiated. The contact time of Am with colloids (2LFh/humics) is varied in a single column experiment by continuous injection of approximately one pore volume Am spiked groundwater into the column. In the case of the quantitative tritiated water (HTO) elution, dispersion effects in the column could be neglected and the Am recovery was directly detectable from the breakthrough curve. Isotopes under investigation ([241]Am, [243]Am, ^{59}Fe and HTO) were detected by γ-spectrometry and/or liquid scintillation counting.

Results and Discussion

The PCS measurements on the coagulation kinetics of 2LFh in the different Gorleben groundwater revealed a strong dependence of aggregation on the DOC concentration (Fig. 1). Fast coagulation of 2LFh colloids could be observed for the groundwater of low (0.9-5.0 mgC/L) DOC concentration (GoHy-182, -412), whereas the colloids were stabilized in groundwater of higher DOC content (GoHy-532,-2227) with 22.6-81.6 mgC/L. Zetapotential (ζ) measurements of the purified 2LFh revealed,
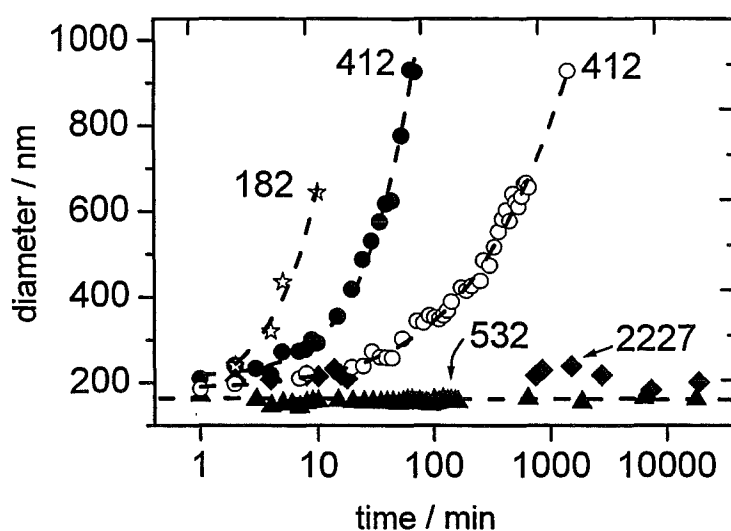
Fig. 1: Time dependent 2LFh colloid hydrodynamic diameter (d_H) change by dynamic light scattering (PCS) analysis in Gorleben groundwater (☆ GoHy-182: 0.9 mg/L DOC; ●,○ GoHy-412: 5.0 mg/L DOC; ▲ GoHy-532: 22.6 mg/L DOC; ◆ GoHy-2227: 81.6 mg/L). 2LFh colloid concentration adjusted to 5.6 mg/L (filled symbols) or 1.85 mg/L (open symbols).

that the isoelectrical point is at pH_{IEP} 8.7 and a positive ζ-potential of +22 mV was found at pH 6.5 (GoHy-182) and +16 mV at pH 7.5 (GoHy-532), respectively. The 2LFh-humic associations showed a decrease of the positively charged 2LFh surface to more negative values with increasing DOC content from -5 mV in GoHy-182 to -30 mV in GoHy-2227. Similar results were obtained from fatty acid and Suwannee humic/fulvic acid sorption experiments on hematite colloids [13]. The results revealed that the negatively charged humics sorbed onto the 2LFh surface force, via charge neutralization, a 2LFh colloid destabilization in Gorleben groundwater of low DOC concentration, whereas higher DOC concentrations were sufficient to exceed the critical coagulation concentration (CCC) and stabilize 2LFh colloids in the mg/L range.

The results of the migration experiments including the Am and 2LFh recoveries are shown in Fig. 2. ^{59}Fe was used as an indicator for iron colloids in the migration experiments. HTO breakthrough is quantitative and in the range of quantitative HTO elution the $[Am]/[Am]_0$ ratio corresponds directly to the recovery of colloid-borne Am. The migration velocity for the iron colloids is 13 % higher (retardation factor R_f = 0.87) than that of HTO in GoHy-532 due to their larger colloid size (Fig. 2) and therefore, a pronounced pore size exclusion effect. The breakthrough of 2LFh/Am colloids in
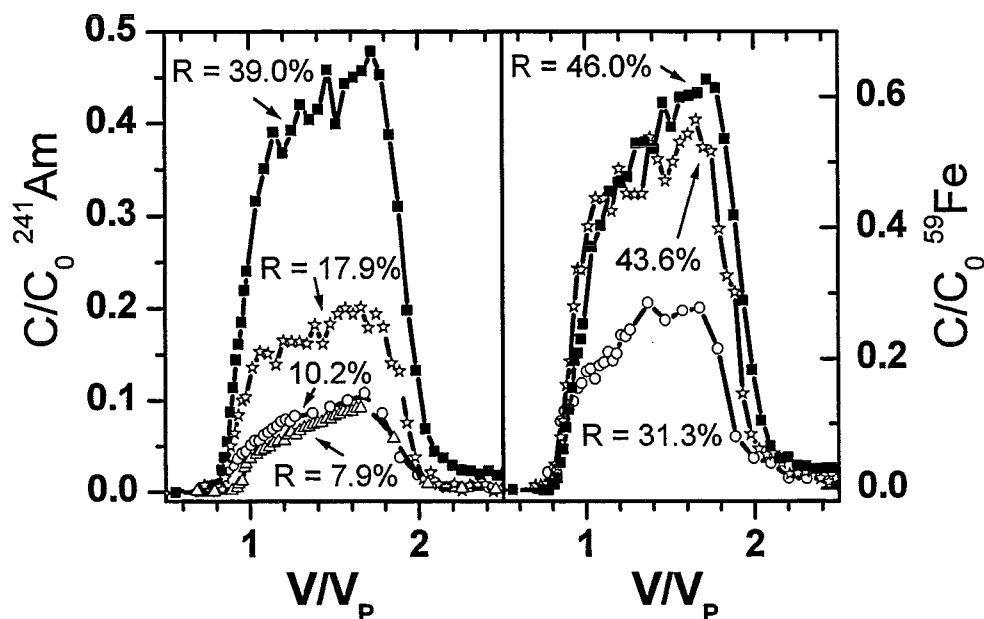
Fig. 2:   Breakthrough curves of ^{241}Am (left side), ^{59}Fe (right side) and recoveries R as a function of colloid type ($\triangle$: humic bond Am, O: Am sorbed on 2LFh, ☆: 2LFh/Am, ■: Hae/Am). Here, C/C_0 is the ratio of the outlet to inlet concentration of ^{241}Am and ^{59}Fe, respectively.

groundwater GoHy-182 (0.9 mgC/L) could not be determined due to the low concentration of ^{241}Am and ^{59}Fe in the column outlet fractions, but the total ^{241}Am recovery of 0.5% showed no enhancement of Am mobility by 2LFh addition. The unretarded Am mobility in GoHy-532 groundwater changed from 7.9 % total recovery for humic colloid-borne migration to 10.2 % Am recovery after addition of 2LFh with a 2LFh recovery of 31.3 %. In all conducted experiments using GoHy-532 groundwater ^{59}Fe was detectable in the column outlet fraction showing that initially positively charged 2LFh colloids are partly mobile in near neutral pH of Gorleben groundwater rich in humic substances. However, the Am mobility is not significantly enhanced compared to humic colloid borne migration. This can be explained by the total ^{241}Am/^{59}Fe recovery ratio of 0.33 (Fig. 3). This ratio shows that a large fraction of the 2LFh bound Am (67 %) dissociates from the iron colloid surface and afterwards adsorbs to the column sediment. The experiments with 2LFh/Am colloids revealed higher recoveries for ^{241}Am and ^{59}Fe, but the total Am/Fe recovery ratio increased only from 0.33 to 0.41. These results show that also a major part of the Am on 2LFh/Am colloids is reversibly bond. The Hae/Am colloids show a completely different effect on Am mobility, with an increase of ^{241}Am recovery to 39.0 % and a ^{59}Fe recovery of 46.0 %. The Am/Fe total recovery ratio thus increased to 0.85 indicating a reduced exchangeable Am fraction of ~ 15 %. Contrary to the unaltered 2LFh experiments, the Am/Fe ratio in the column outlet fractions decreased from almost 1 to a plateau value of 0.8, which could be attributed to a kinetically controlled Am desorption from 2LFh onto humics during the initial stage of the experiment.

The selective extraction procedures on the iron oxide/hydroxide colloids prior to injection validate the changes in Am binding.

Fig. 3: The recovery ratio variation of ^{241}Am / ^{59}Fe as a function of equilibrium time. Equilibrium time is the calculated contact time prior to column injection of the spiked groundwater.

The NH_4-oxalate-oxalic acid extractable $Fe_{(O)}$ changes from 99 % for 2LFh over 77 % in the 2LFh/Am sample to 33 % in the Hae/Am sample, therefore documenting the change in iron colloid mineralogy.

The parallel measured release of ^{241}Am via selective iron phase dissolution showed that 90 % of the 2LFh sorbed Am is salt exchangeable ($Am_{(E)}$), with a slight decrease to 78 % $Am_{(E)}$ in the 2LFh/Am sample and a strong decrease to 19 % in the Hae/Am sample. However, the results also revealed, that the Am in the Hae/Am sample is mostly $Fe_{(O)}$ extractable (76%) whereas the major fraction of iron is citrate-dithionite-bicarbonate ($Fe_{(T)}$) extractable. The extraction results suggest a preferential binding of Am in the 33% $Fe_{(O)}$ of lower crystallinity and demonstrate that 2LFh recrystallization and secondary mineral formation (i.e. hematite) changes drastically the Am/mineral interaction kinetics. This point is of crucial importance for the Am mobility, either for sediment fixation via crystal entrapment or as shown in this work via colloidal mobilization enhancing the Am mobility in a near natural system.

References

Kim, J.I. In Handbook on the Physics and Chemistry of the Actinides, A.J. Freeman; C. Keller, Eds.; Elsevier Science Publication, 1986; Chap. 8.

McCarthy, J.F.; Zachara, J.M. Environ. Sci. Technol. 1989, 23 (5), 497.

Kretzschmar, R.; Sticher, H. Environ. Sci. Technol. 1997, 31 , 3497.

Swartz, C.H.; Gschwend, P.M. Environ. Sci. Technol. 1998, 32 , 1779.

Girvin, D.C.; Ames, L.L.; Schwab, A.; McGarrah, J.E. J. Colloid Interface Sci. 1991, 141(1), 67.

Lu, N.; Triay, I.R.; Cotter, C.R.; Kitten, H.D.; Bentley, J. Reversibility of sorption of Plutonium-239 onto colloids of hematite, goethite, smectite, and silica; Report LA-UR-98-3057; Los Alamos National Laboratory: Los Alamos, 1998.

Grigoriev, M.S.; Fedoseev, A.M.; Gelis, A.V.; Budantseva, N.A.; Shilov, V.P.; Perminov, V.P.; Nikonov, M.V.; Krot, N.N. Radiochim. Acta 2001, 89 , 95.

Sakamoto, Y.; Ohnuki, T.; Senoo, M. Radiochim. Acta 1994, 66/67 , 285.

Nagano, T.; Mitamura, H.; Nakayama, S.; Nakashima, S. Clays Clay Minerals 1999, 47(6), 748.

Schwertmann, U.; Cornell, R.M. Iron Oxides in the Laboratory (Preparation and Characterization); VCH Verlagsgesellschaft mbH: Weinheim, 1991; p 137.

Loeppert, R.H.; Inskeep, W.P. In Methods in Soil Analysis. Part 3. Chemical Methods, J.M. Bartels, Ed.; SSAS & ASA, Inc.: Madison, WI, 1996; Vol. 5, pp 639.

Artinger, R.; Kienzler, B.; Schüssler, W.; Kim, J.I. J. Contam. Hydrol. 1998, 35 , 261.

Liang, L.; Morgan, G.G. Aquatic Sci. 1990, 52 (1), 32.

V.   Actinide Migration Experiment in Äspö HRL

(B. Kienzler, P. Vejmelka, J. Römer, E. Fanghänel, F. Geyer, E. Soballa, M. Fuß, T. Kisely, INE)

Abstract

Within the scope of a bilateral cooperation between Svensk Kärnbränslehantering AB (SKB) and Forschungszentrum Karlsruhe, Institut für Nukleare Entsorgung (FZK-INE), an Actinide Migration Experiment is currently being performed at the Äspö Hard Rock Laboratory (HRL) in Sweden. Batch and migration experiments were performed in laboratory at INE. For the in-situ experiments in the underground laboratory, the CHEMLAB 2 probe developed by SKB was used. The experimental setup as well as the breakthrough of inert tracers and of the actinides Am, Np, and Pu are presented. The breakthrough curves of inert tracers were analyzed to determine hydraulic properties of the fractured samples. Post-mortem analyses of the solid samples were performed to characterize the flow path and the sorbed actinides. In the experiments only breakthrough of Np(V) was observed.

Zusammenfassung

Im Rahmen einer bilateralen Kooperation zwischen der Svensk Kärnbränslehantering AB (SKB) und dem Forschungszentrum Karlsruhe, Institut für Nukleare Entsorgung (FZK-INE) wird derzeit ein Actiniden Migration Experiment im schwedischen Unter-tagelabor Äspö durchgeführt. Begleitende Sorptions- und Migrationsexperimente erfolgten im INE. Für die in-situ Experimente wurde die von SKB entwickelte Bohrlochsonde CHEMLAB 2 verwendet. Im vorliegenden Bericht werden der experimentelle Aufbau und die Durchbruchskurven für inerte Tracer (HTO) und die Actiniden Am, Np und Pu vorgestellt. Der Durchbruch des inerten Tracers wird zur Bestimmung der hydraulischen Eigenschaften geklüfteten Gesteinsprobe verwendet. Nach Abschluss der Experimente wurden die Gesteinsproben hinsichtlich des Fließweges und der sorbierten Actinden analysiert. Es konnte jeweils nur der Durchbruch von Np gemessen werden. Der Wiedererhalt lag deutlich unter 40 %.

Objectives

The FZK/INE investigations are focusing on sorption and migration of radionuclides, esp. actinides, in fractured rock. To guarantee conditions as realistic as possible, the

experiments are designed to be compatible with the CHEMLAB 2 probe. The objectives of the experiment are directed to the applicability of radionuclide retention coefficients measured in laboratory batch experiments for in-situ conditions, the validation of radionuclide retardation measured in laboratory by data from in-situ experiments in rock and the reduction of uncertainties in the retardation properties americium, neptunium and plutonium.

Experimental concept

In a first step, the experimental set-up was designed and some preliminary sorption experiments with fracture filling material and granite, respectively, and with groundwater from the area of CHEMLAB 2 were conducted in the laboratory at INE. For the in-situ migration experiments, a drill core sample with a fracture concealed in an autoclave (see Fig. 1) was placed in CHEMLAB 2. The first experiment was conducted in 2000, the second was started in November 2001.

The hydraulic properties of fractured rock samples were investigated at INE. HTO was used as inert tracer and dependences of the breakthrough from the applied flow rates were recorded. The actinide breakthrough was measured and the actinide recovery as a function of the eluted groundwater volume.

Different techniques were applied in order to investigate the retention of the actinides along the flow path. After termination of the migration experiments, a fluorescent
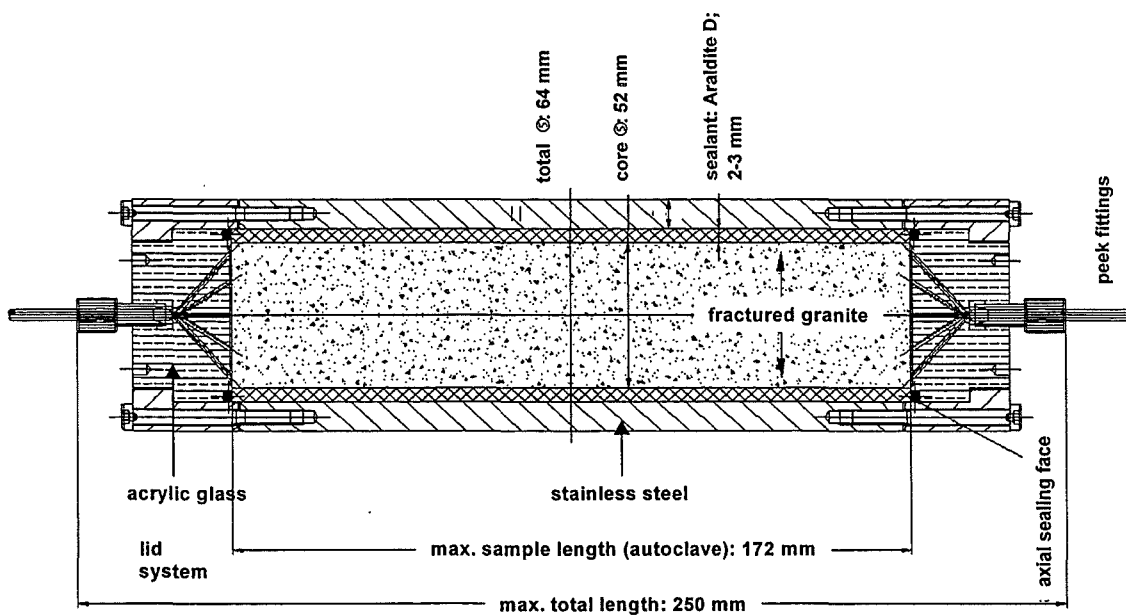
Fig.1: Design of the autoclave for the fractured granite cores

epoxy was injected and the cores were cut perpendicular to the cylinder axis. The geometry of the flow path was analyzed by scanning of the slices optically and discrimination of colors with respect to the fluorescent resin. The volumes and the inner surface areas of the fracture could be determined from the scans by means of pixel counting and numerical evaluation. Additional information on the flow path was obtained by 3D visualization of the fracture.

The actinide concentrations on each surface of the slices were analyzed by spatially resolved α-radiography and by coupled laser ablation ICP-MS techniques. The abraded material gained by cutting the slices was dissolved and actinide concentrations were measured by ICP-MS.

Results

In laboratory and in the in-situ experiment, an unretarded breakthrough of Np was observed. Total recovery of Np was obtained between 20 and 40%. Breakthrough of Am and Pu was not measured. The open fracture of core #1 (used in a laboratory migration experiment) was analyzed. Its cross sections varied between 38 and 87 mm^2 (mean value 53 mm^2) and the circumferences of the fracture at top and bottom of each slice were determined between 72 and 96 mm (mean value 80 mm). In contrast to core #1, in the CHEMLAB core #2 no continuous flow path could be detected. Structures which could be seen in the scans of core #2 slices were attributed to a healed fracture system. Volumes filled with fluorescent resin were generally too small to be identified by the scanning technique, however, single spots of fluorescent resin could be identified visually throughout many slices of the core.

In the abraded material gained by cutting of the slices of core #1, Np was found by ICP-MS measurements between $9x10^{-3}$ and $2x10^{-2}$ nmol/g, for core #2, Np concentrations varied between $6x10^{-3}$ and $7x10^{-2}$ nmol/g. Pu was in the range of the detection limit ($3x10^{-4}$ nmol/g). Am was detected in core #1 only, its concentration was in the range of $6x10^{-4}$ to $2x10^{-3}$ nmol/g.

For core #1, it was possible to combine measured Np and Am distributions with the geometrical information of the fracture obtained by evaluation of the slices. Spatially resolved α-radiography showed clearly that the actinides were sorbed onto the surfaces of the fractures. The surface loading of the fracture could be calculated. For Np, a continuous decrease of the loading from the injection to a distance of 23 mm was found. At a distance of 4.35 mm from the injection plane, the Np loading was

about 4×10^{-4} nmol/mm^2. Between 23 and 56 mm, the Np loading was found to scatter between about 2×10^{-4} and 1×10^{-4} ng/mm^2. Integration over the surface loading of Np yielded in 1.1 nmol Np which reflected the amount the of totally injected ^{237}Np and the observed recovery.

A similar analysis was carried out for ^{243}Am. Am recovery in all experiments was below the detection limit indicating that almost the total amount of Am injected remained in the core. A first maximum of the Am loading was determined at a distance of 18.5 mm from injection (4×10^{-5} nmol/mm^2). The Am loading dropped to 2×10^{-5} nmol/mm^2 at 37.3 mm. The Am distribution over this distance showed a well pronounced peak. Comparing the groundwater velocity with the migration velocity of Am, a retardation of Am against water of approx. 40 was calculated.
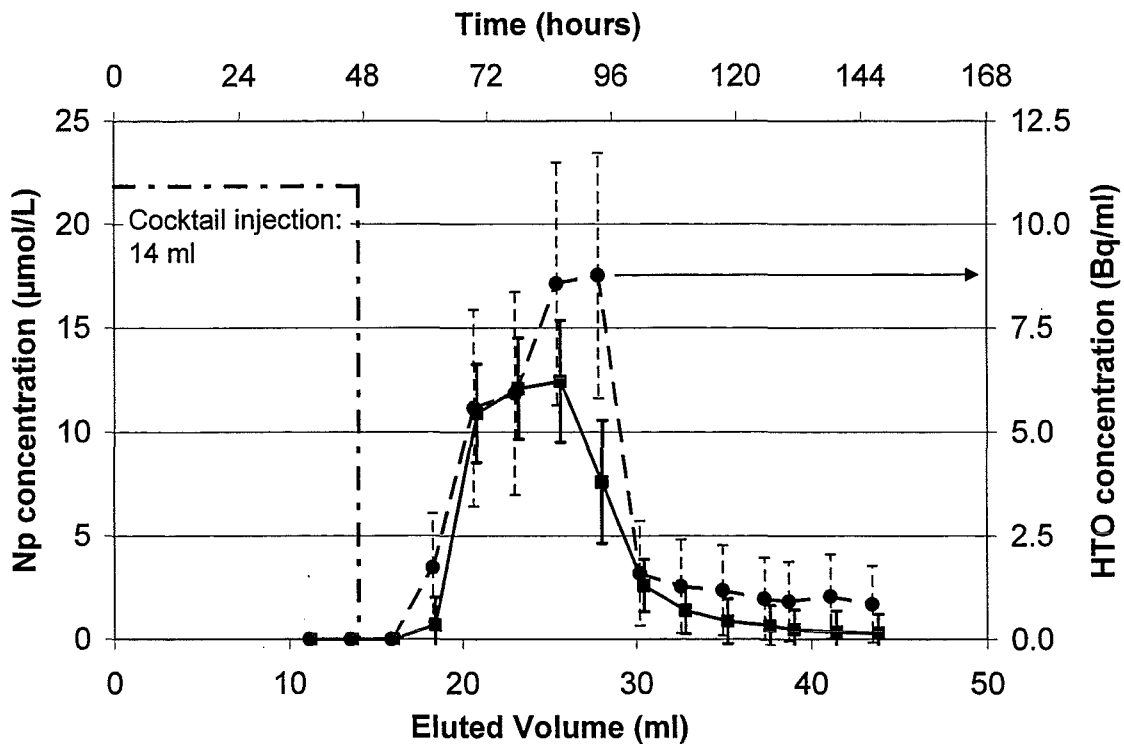
Fig. 2 Breakthrough of Np and HTO determined in the CHEMLAB 2 experiment (core #2) (dot: HTO, square: Np)

VI.   Colloid and Radionuclide Retention Experiment at the Grimsel HRL

(W. Hauser, H. Geckeis, R. Götz, F. Geyer, Th. Schäfer, Th. Rabung, J.I. Kim, INE)

Abstract

The Colloid and Radionuclide Retardation Experiment (CRR) aims to the understanding of processes leading to the colloid-mediated transport of radionuclides in a granitic groundwater ($I=10^{-3}$ mol/l, pH=9.6). The project is conducted in the frame of an international cooperation where the participants are NAGRA (Switzerland), ENRESA, CIEMAT, QuantiSci (Spain), ANDRA (France), JNC (Japan), SNL (USA) and FZK-INE, (Germany). The experimental scenario considers the bentonite backfill/groundwater interface as a source for colloids. The migration behaviour of Hf(IV), Th(IV) and Tb(III) as actinide homologues in absence and presence of smectitic colloids is investigated in various *in-situ* experiments in a granitic fracture zones. For the first time the colloid breakthrough is determined on-line by a mobile laser-induced breakdown detection (LIBD) arrangement. The breakthrough of the metal ions analysed by ICP-MS follows the colloid breakthrough indicating the colloid-mediated migration under the natural aquatic conditions.

Zusammenfassung

Das Colloid and Radionuclide Retardation Experiment (CRR) im Grimsel Felslabor wird durchgeführt, um den Kolloideinfluss auf die Radionuklidmigration unter weitgehend naturnahen Bedingungen in einem granitischen Grundwasser ($I=10^{-3}$ mol/l, pH=9.6) zu untersuchen. Das Experiment findet im Rahmen einer internationalen Kooperation mit NAGRA (Schweiz), ENRESA, CIEMAT, QuantiSci (Spanien), ANDRA (Frankreich), JNC (Japan), SNL (USA) und FZK-INE (Deutschland) statt. Das experimentelle Szenario betrachtet die Grenzfläche zwischen dem Bentonit Versatzmaterial und dem Grundwasser als mögliche Kolloidquelle. Die Migration von Hf(IV), Th(IV) und Tb(III) als Actinidenhomologen in An- und Abwesenheit von smektitischen Kolloiden wird in *in-situ* Experimenten in einer granitischen Kluft untersucht. Zum ersten Mal werden Kolloide on-line mit einer mobilen Laser-induzierten Breakdown Anlage (LIBD) bestimmt. Die Migration der Metallionen, die mittels ICP-MS detektiert wurden, erfolgt simultan mit dem Kolloiddurchbruch und damit kolloidgetragen.

Introduction

Aquatic colloids are ubiquitous in natural water and play a carrier role for the aquifer migration of metal ions with higher charges (Z > 3+), particularly actinide ions. The average size of predominant aquatic colloids is in general less than 50 nm and their number density exceeds 10^9 particles per liter water. The hitherto available non-invasive method for the characterization of such colloids is a light scattering technique with different detection modes. As the light scattering on particles of less than 100 nm decreases with the size as a function of the inverse power of 6, aquatic colloids of dilute concentrations are often not detectable by this technique. Contrary to this, the plasma generation on colloids by the focused laser beam can be conveniently used for the characterization of the number density and average size of small colloids without perturbation of sample solutions.

The laser-induced breakdown detection (LIBD) method has been developed particularly for the characterization of aquatic colloids of small size in dilute concentrations. In this work a mobile set of LIBD is presented, which is developed for the field study of the aquatic colloid migration under non-perturbed conditions [1]. The first direct application is made at the Grimsel Test Site (GTS) tunnel for investigating the bentonite colloid migration in a rock fracture with a dipole distance of 5 m. With and without spiking of heavy metal ions on colloids, their migration behavior is directly monitored on-line with respect to the size change and recovery. The study is performed within the Colloid and Radionuclide Retention project (CRR) in order to study the role of colloids on the radionuclide migration in such a system. In the preliminary study clay colloids released from a bentonite barrier system in the near field of a nuclear repository in granite are identified as relevant stable colloid species in the low mineralized groundwater.

Instrumentation of the mobile LIBD

The principle of LIBD is based on the generation of a dielectric breakdown in the focus region of a pulsed laser beam. As the threshold energy (irradiance) to incite breakdown for solid is lower than for liquid or gas, the breakdown can be generated selectively on particles dispersed in solution at suitable pulse energy. A schematic diagram of the mobile LIBD set-up used in the present work is shown Fig. 1. The similar instrumentation for the laboratory use is described in earlier work. A pulsed
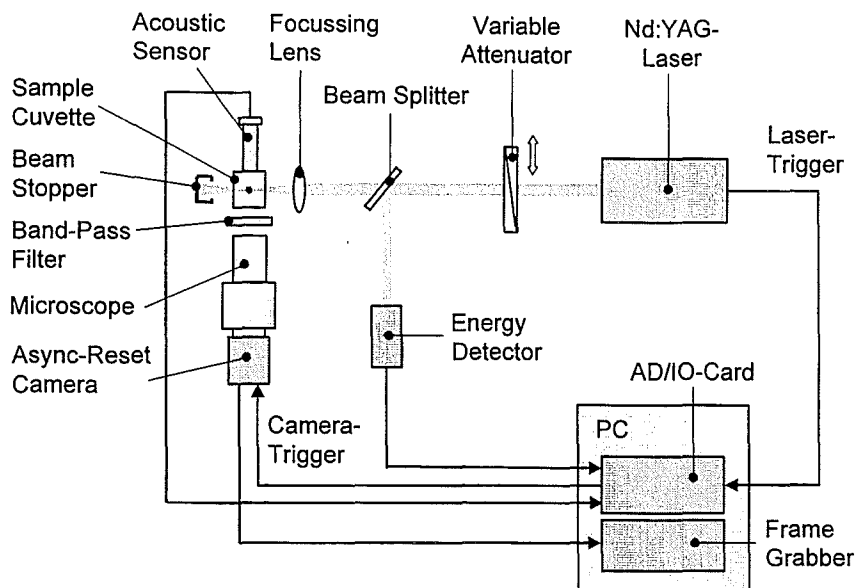
Fig. 1:   A schematic diagram for the mobile laser-induced breakdown detection
system

laser beam with a frequency of 15 Hz at 532 nm wavelength from a small Nd:YAG-laser (Continuum Minilite I) is focused (15 mm focal length) into the center of a flow-through silica cell, after passing through a variable attenuator and a beam splitter. The plasma generated at a breakdown event is monitored by a microscope equipped with a CCD monochrome camera triggered by the incident laser pulse and recorded by a PC controlled picture processing system. A breakdown shock wave propagated in the sample solution is detected simultaneously by an acoustic sensor (piezoelectric transducer) that is connected to the surface of the cell. Both the energy and acoustic signal are recorded by an analog-digital converter interface in a PC. The mobile instrumentation of LIBD is combined with a Millipore ultra-pure water processing unit for on-line cleaning the flow-through detection cell of LIBD. The whole system, which is set up to a compact mobile unit, is transported by a van for the field experiment.

In situ colloid migration experiment

The migration experiment is carried out in the Grimsel Test Site (GTS), where a dipole flow field is established between the injection and extraction boreholes. The hydraulic flow along the dipole is directed towards the gallery, following the natural groundwater flow at the site.

Experimental setup

The mobile LIBD system is positioned close to the in-situ experimental area with a natural fracture zone. A schematic view of the dipole experiment is shown in Fig. 2 (a). The injection is made through the borehole BOMI 87.008 into the dipole fracture zone with a migration path of 5 m length. Extraction takes place through the borehole BOMI 87.010. Both the injection and extraction boreholes are lined with stainless steel tubes. The flow through detection cell of LIBD is connected by a PEEK capillary tube with the extraction line of the experimental dipole, which extends about 3 m below the drift axis. Fig. 2 (b) presents a picture of the experimental set-up of LIBD in the GTS field laboratory, where the injection and extraction tubes are marked by file.

a)   b)
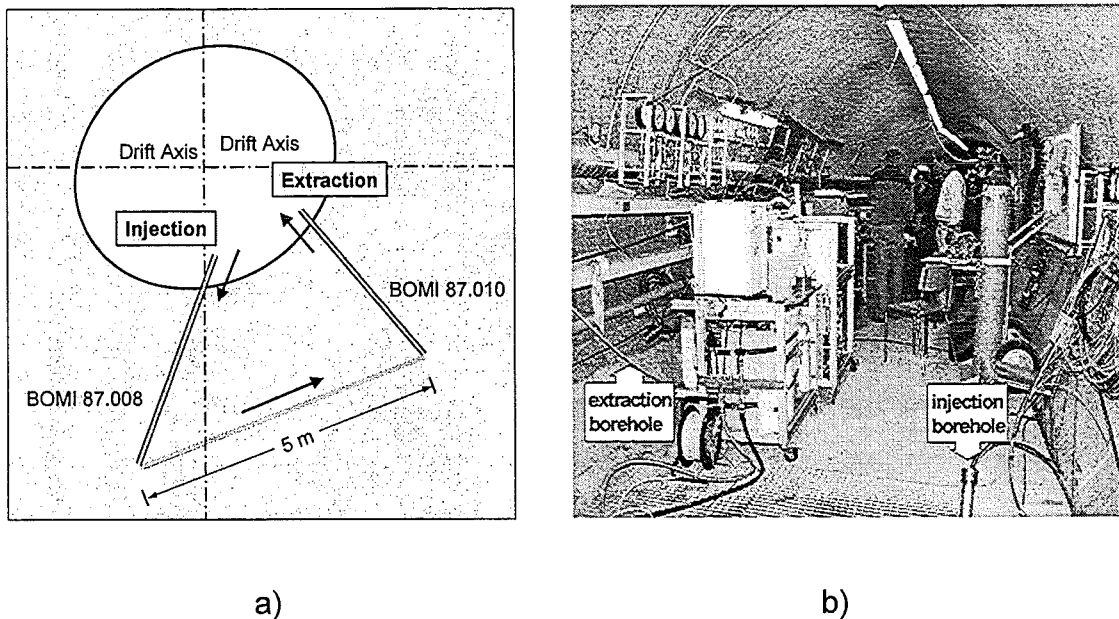
Fig. 2:   Field experiment for the colloid migration: (a) a schematic illustration of dipole 3 configuration; (b) mobile LIBD instrumentation in the Grimsel laboratory drift

The experimental set-up consists of packer systems for the injection and extraction boreholes with tubing connections from and to the gallery. The packers are equipped with pressure and flow control units. The injection solution is put in a high-density polyethylene bottle and kept under Ar-atmosphere before the injection. By applying the pressure from a bottle of nitrogen gas, the colloid solution injected into the PEEK tubing (PEEK: polyether etherketone) of the injection line. The actual injection flow rate (10 ml/min) is controlled by balancing the mass loss from the bottle. The extraction flow (150 ml/min) is provided by a pump device. All parts of the packer

system exposed to groundwater are coated with PEEK to minimize the surface sorption of trace elements.

Migration of bentonite colloids

A batch solution of colloids is prepared from FEBEX bentonite by repeatedly washing with the groundwater of the Grimsel Test Site (GTS) and used as a stock solution. The FEBEX (Full-scale Engineered Barriers Experiment) bentonite used in this study is proposed as a potential backfill material in a granite repository. FEBEX bentonite is mainly composed of Ca smectite (>90 wt%) with accessory minerals quartz, cristobalite, feldspar and calcite. The colloid dispersion is remained stable for several weeks as confirmed by photon correlation spectroscopy. A 200 ml of the injection solution is prepared by diluting the stock solution to a final colloid concentration of 20 µg/ml under Ar-atmosphere. The colloid solution remained at pH 9.5, being same as the value of original groundwater (pH 9.6). The injection of colloid dispersion is made to a volume of 101 ml, corresponding to a total amount of colloid 2.02 mg.

The colloid quantification in the extracted water is made continuously on-line and occasionally off-line. Prior to the breakthrough of injected colloids, the background colloids present in groundwater are quantified for the purpose of comparison. After the colloid injection, the breakdown probability is detected in the range of 5 –10%. These signals are attributed to the natural colloid background in the Grimsel groundwater under the given flow condition and appear significantly above the value of the ultra-pure water. The migration of bentonite colloids is observed first at 40 min after the injection. After the maximum colloid concentration is reached at 60 min, the concentration of extracted bentonite colloids decreases slowly to the background level of groundwater colloids at about 250 min. The background levels before the injection and after the completion of bentonite colloid extraction are found to be the same.

Based on a 2-D spatial distribution of breakdown events along the laser beam axis as determined by image-processing of the data obtained by off-line measurements, the average colloid size and concentration are appraised quantitatively. For the calculation of the colloid concentration a particle density $\rho_P = 3.7$ g/cm^3 is taken for FEBEX bentonite colloids. The measurements are made off-line partly in situ and partly in laboratory for the collected sample fractions. The results are illustrated in Fig. 3. In the groundwater extracted before the breakthrough of injected colloids, the

background colloids are found to be a concentration of about 5 ppb with an average size of 202 ± 12 nm. Such a large colloid size infers that a forced hydrodynamic flow of groundwater in the fracture zone may induce the mechanical stress on the rock matrix surface and hence colloids of larger size are generated by dispersion. The average size of the extracted bentonite colloids is found to be at 116 ± 12 nm, which is lower than the value of the initial colloid dispersion at 148 ± 8 nm. The maximum concentration of the extracted colloids is found at 175 ± 20 ppb. The batch samples collected during the field-experiment are later analyzed by ICP-MS for the element Al present as one of the major component in bentonite colloids.

The breakthrough patterns of the colloid concentration determined by both LIBD and CP-MS are in good agreement with each other, as shown in Fig. 3 (down part). Integrating the breakthrough curve after subtracting the natural background level of colloids in groundwater, the extracted bentonite colloid fraction relative to the injected
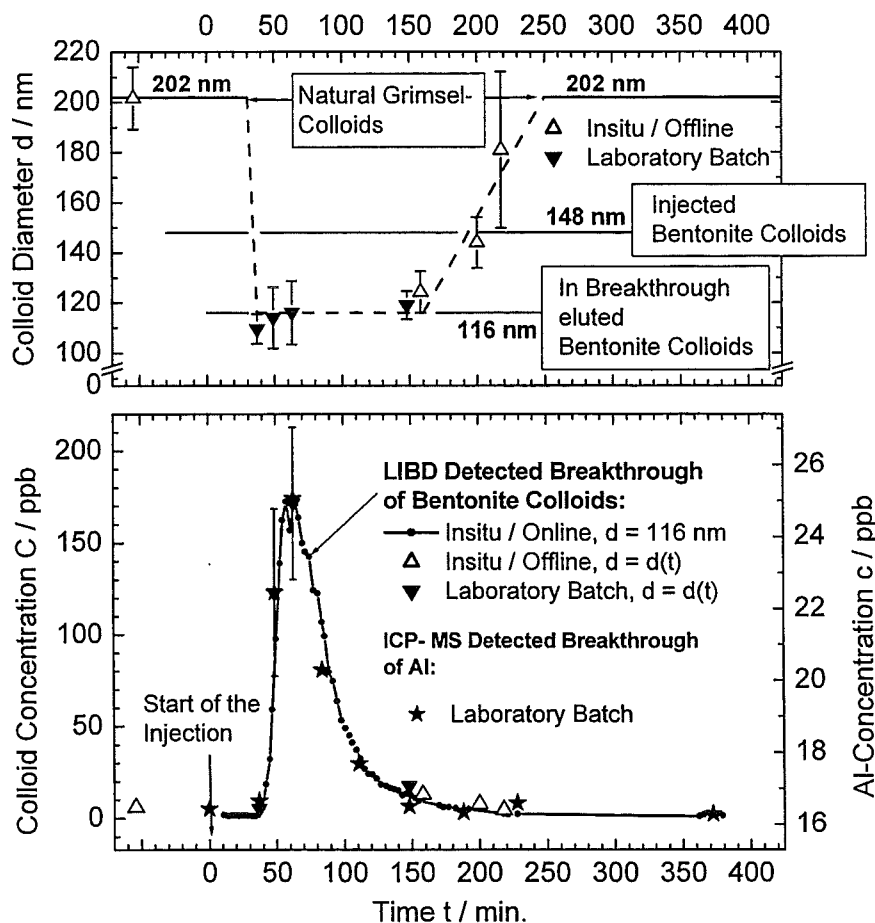
Fig. 3: Particle diameter and concentration in the migration breakthrough of bentonite colloids

mass concentration is evaluated. A recovery obtained from both LIBD and ICP-MS is calculated to be identical at 55 + 5 %. This is interpreted that a fraction of larger sized bentonite colloids is filtered out in the fracture zone, while the smaller sized colloids with an average size of 116 ± 12 nm are mobile under the experimental conditions.

Migration of tracered bentonite colloids

The second injection solution is prepared identically but spiked with Hf(IV), Th(IV) and Tb(III) to a final concentration of 30 ppb for each element. For spiking, a solution containing 1000 μg/ml of each element in 1 M HNO_3 is diluted with water in 50 folds to pH 1.7 for using as a stock solution. To a 200 ml of the groundwater containing 20 ppm bentonite colloids, a 300 μl of the stock solution is added on shaking, thus resulting in the final molar concentration of 1.3×10^{-7} mol/l for Th, 1.7×10^{-7} mol/l for Hf and 1.9×10^{-7} mol/l for Tb. The groundwater pH is not changed by adding the tracer solution (remained the same within 0.2 units). According to the thermodynamic solubility of each tracer element, the final concentrations of these elements are, in the absence of colloids in a state of over saturation at the given pH. Therefore, it is presumed that they are interacted with bentonite colloids in both ionic and colloidal forms. However, all tracer elements are found as sorbed quantitatively onto bentonite colloids after spiking, though their chemical states are not known. The injected volume of traced colloidal dispersion is 82.5 ml.
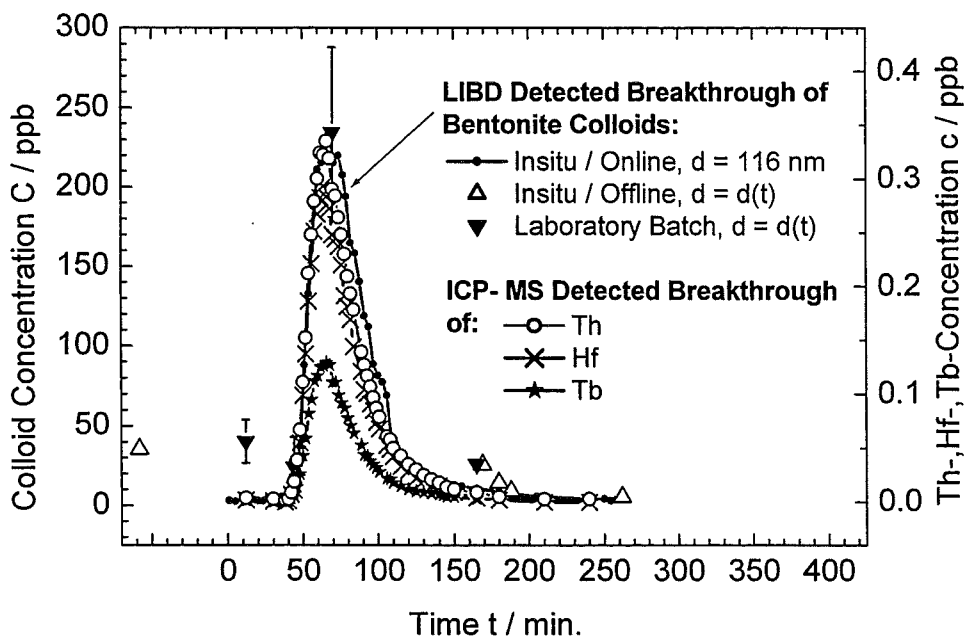
Fig. 4: Bentonite colloid and Th(IV), Hf(IV), Tb(III) concentrations in the migration breakthrough of bentonite colloids

The extraction flow from the dipole is analyzed on-line by LIBD for colloids alone and occasionally off-line as well. Different batches of extracted groundwater are sampled via a sampling valve. Then they are transported to laboratory for analyzing the traced elements and Al by ICP-MS after acidifying with HNO_3. As shown in Fig. 4, each of the breakthrough patterns of Al, Th, Hf and Tb determined by ICP-MS are in good agreement with one another and also in good accordance with the bentonite colloid breakthrough determined by LIBD. The results indicate that the polyvalent metal ion migration in the presence of colloids under the present experimental conditions is facilitated by bentonite colloids acting as a carrier.

The calculated colloid recovery is 56 ± 6 %, which corresponds to the value of the first migration experiment. Recoveries for both tetra-valent elements, Th and Hf, are found to be 78 + 8 % which is significantly higher than the recovery of bentonite colloid mass. This discrepancy can be explained by the fact that the metal ion loading onto colloids depends on their surface area. As is found in this experiment, bentonite colloids are undergone the change in their average size somewhat to smaller one and hence the larger surface area is resulted in for the same mass concentration. In order to corroborate this assumption, the total 'recovered colloid surface' is compared with the total surface of the injected particles. Assuming a spherical geometry for the injected colloids (148 nm) of a total mass of 1.65 mg, their total surface of 2.5×10^{-8} cm^2 is calculated. For the extracted bentonite colloid fraction (56 ± 6 %) with an average colloid size of 116 nm, the total surface is found as 1.8×10^{-8} cm^2, which corresponds to a recovered surface area of ~ 72 %. This value is very close to the recovery of Th and Hf, which may thus explain the discrepancy between the mass fraction recovery obtained for colloids and the concentration fraction recovered for Th and Hf.

The recovery for Tb is found at a considerably lower value of 33 + 3 %. The trivalent Tb ion has a sorption affinity towards bentonite colloids somewhat less than tetra-valent metal ions and, for this reason, the Tb ion sorbed onto colloids may be dissociated in the course of migration and undergone to sorption interactions on the rock matrix surface as well as on the surface of experimental devices. For the moment, this may explain the low recovery obtained for this metal ion. As for the chemical effects of metal ion oxidation states on their colloid-bone migration, further detailed investigations are necessary. They are for the moment in progress.

Conclusions

The present paper demonstrates the application of a mobile LIBD system for the on-line analysis of colloids in the field migration experiment. The instrumentation is robust enough for the field application. The high sensitivity of LIBD allows a direct quantification of colloids even at the low natural background level. A 2-D optical monitoring of the spatial distribution of breakdown events in the laser beam focus region provides information on the average particle size of colloids of the prevalent concentration. A combination of on-line LIBD and off-line ICP-MS measurements facilitates the field study of the colloid-borne migration of trace metal ions. The present method is applicable for understanding the migration behavior of radionuclides in natural aquifer systems, in which aquatic colloids play a carrier role for the migration of heavy element radionuclides, especially actinides.

As the main objective of the present study is to demonstrate the applicability of a mobile LIDB for the field experiment, the hydrodynamic groundwater flow rate is enhanced more than the ordinary situation and the chemical interaction processes of trace metal ions with bentonite colloids are not presented in detail. The present study, however, shows clearly the migration behavior of bentonite colloids and their carrier role for the migration of heavy metal ions.

References

1.   W. Hauser, H. Geckeis, J.I. Kim, Th. Fierz, A mobile laser-induced break-down detection system and its application for the in situ-monitoring of colloid migration, Colloids & Surfaces (A) 203 (2002), 37 - 45

VII.   Initial results on changes in humic colloid content through drainage of wetland in the Gorleben south-east area

(G. Buckau, R. Artinger J.I. Kim, INE; M. Wolf, GSF-IfH, S. Geyer, P. Fritz, UFZ)

Abstract

Chemical and isotopic data are analyzed from groundwater of the Gorleben aquifer system, south, south-east and east of the underlying salt-dome. Comparison with the development of land-use, including drainage of wetland around 250 years ago, shows that agricultural activities and drainage has a considerable impact on the groundwater composition. It is shown that part of the deep groundwater originates from previous wetland recharge. In the past around 250 years, groundwater has been exchanged down to a depth of about 70 meters. This is a key parameter for hydrological modeling. In groundwater originating from previous wetland recharge, elevated concentrations of humic substances are found. These humic substances appear to originate from past wetland recharge, and thus remain stable and mobile over several hundreds of years.

Introduction

Drainage of wetland leads to changes in groundwater recharge, both with respect to amounts and isotopic composition. Through surface evaporation, heavy water isotope (Oxygen-18 (^{18}O) and Deuterium (^{2}H)) are enriched. Thereby, a deviation from the global meteoric water line occurs. Consequently groundwater from wetland recharge conditions and after surface drainage can be distinguished from each other.

The Gorleben aquifer system has the main recharge south-east and south of the position of the underlying Gorleben salt dome as well as over the central part of the salt dome (Fig. 1). In addition to this, recharge also takes place in the north at the Höbeck hill. Discharge takes place into the Elbe river flowing from east to west in the northern part of the area. The recharge situation has changed in the past due to drainage of wet-land. There is a large number of drainage channels carrying surface water into the Elbe. In the south-east part of the area, drainage channels were constructed between around 1710 and 1750. This previous wetland recharge area thus has changed to a relatively dry area with net discharge (Fig. 1). Change in isotopic composition (^{18}O /^{2}H) is used to identify the existence of groundwater origi-

nating from recharge under previous wet-land conditions. Chemical composition and isotopic data (^{14}C) are analyzed and conclusions are drawn with respect to the origin of aquatic humic substances. For this purpose data are evaluated from own investigations, the BfS ("Bundesamt für Strahlenschutz") data base and [1].

Coordinate (44... (km))
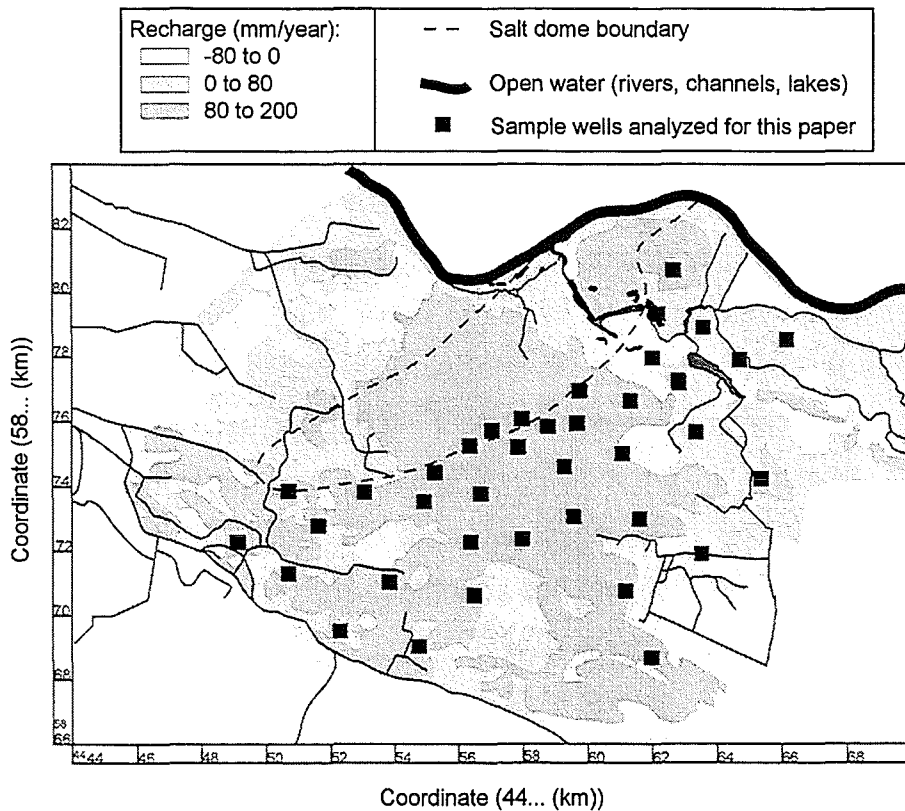
Fig. 1: Gorleben site with position of sampling wells used for the present study.

Results

Analytical data are used from the part of the Gorleben aquifer system stretching from the salt-dome boundary towards the south, south-east and east (positions of sampling wells are shown in Fig. 1). Groundwater originating from previous wetland recharge conditions is identified by deviation from the global meteoric water line. The global meteoric water line reflects the isotopic composition of precipitation at different distance from the sea, altitude and climatic conditions [2] (Fig. 2). Deviation from this global meteoric water line is found where surface evaporation is of considerable magnitude. Such waters are also found in the Gorleben aquifer system (Fig. 2). There is a limited number of deuterium data for groundwaters from the investigation area. Through surface evaporation, however, ^{18}O isotope data become enriched

compared to groundwater not influenced by surface evaporation. On this basis surface evaporated groundwater can be identified. In Fig. 3, positions of these waters are shown. Three such waters are found near the surface. These may be the result of local processes or result from uplift of deep groundwater. More important is that nine such groundwaters cluster in a region to the south-east of the salt dome at depth between approximately 70 and 170 meters. Above these groundwaters, groundwater is not affected by surface evaporation processes. This shows that (i) the deep groundwaters influenced from surface evaporation have been recharged before drainage had taken place, and (ii) during the past approximately 250 years, groundwater has been replaced down to a depth of about 70 meters. This is a key parameter for hydrological modeling of the aquifer system.
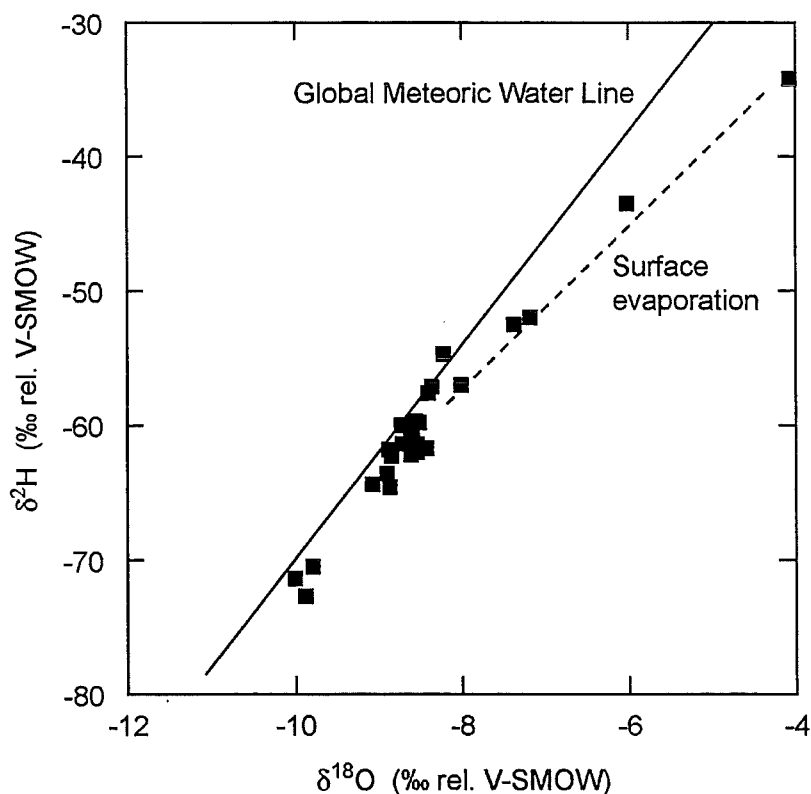
Fig. 2: Deuterium and ^{18}O for investigated Gorleben groundwaters.

With changes in the humidity of land surface and variation in land-use, the chemical composition of recharge groundwater changes. This includes changes in inorganic carbon inventory and ^{14}C concentration of the dissolved inorganic carbon (DIC). In Fig. 4, the ^{14}C concentration (given as pmc (percent modern carbon)) is plotted against the inverse of the DIC concentration. Data fall on a straight line where there

is a common origin of groundwater and the DIC concentration is increasing through geochemical reactions releasing ^{14}C free carbonate [3]. With such increase in the DIC concentration, the ^{14}C concentration from recharge will also decrease. For infinite dilution of the recharge DIC (1/[DIC] -> 0) through dissolution/generation of DIC in the aquifer, the line will also approach zero for the ^{14}C concentration. Most of the data in Fig. 4 fall on a straight line. These groundwaters represent recharge under forest conditions as found today and dilution of DIC with ^{14}C free carbonate from geochemical reactions. Contrary to this, data for near surface groundwater under land used for agriculture scatter and show higher DIC concentrations in recharge in combination with higher ^{14}C concentrations. This reflects the higher turnover of organic matter in agriculture soil compared to forests.
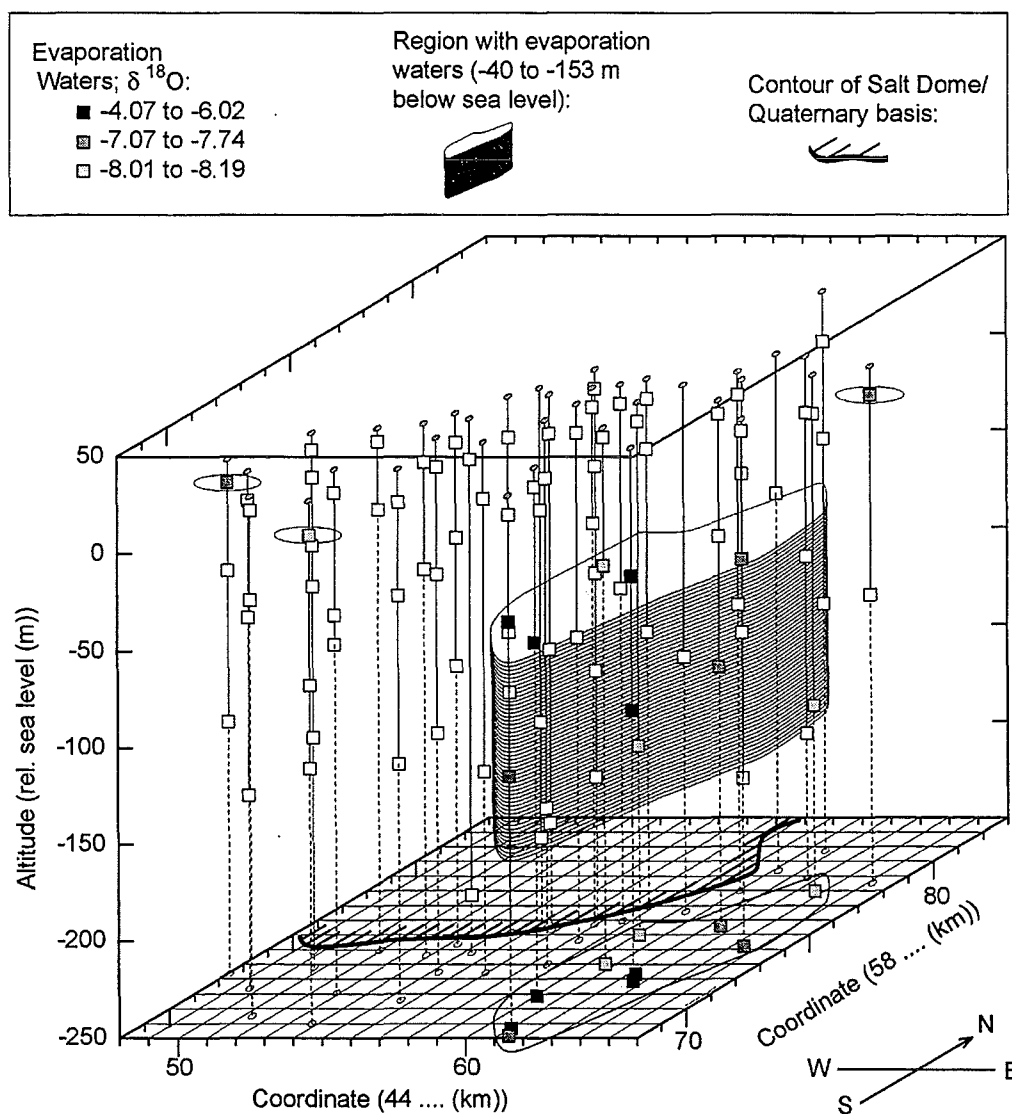
Fig. 3: Position of groundwater sampling (cf. Fig. 1) and occurrence of groundwater affected by surface evaporation prior to recharge.
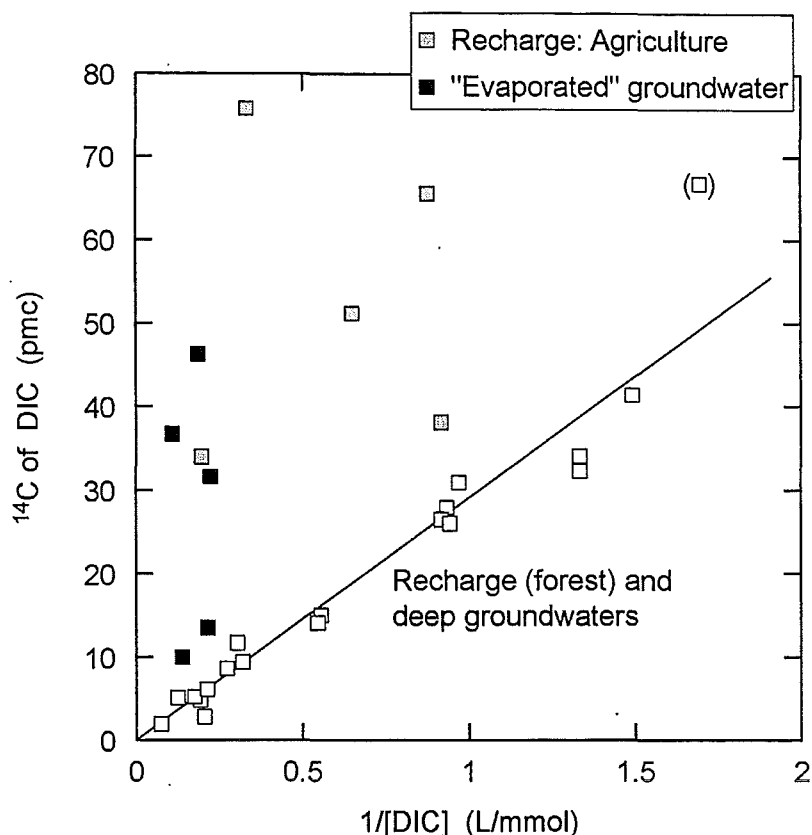
Fig. 4: ^{14}C concentration of DIC plotted against the inverse DIC concentration.

Even higher recharge DIC concentrations and original ^{14}C concentrations are found for the deep groundwater originating from former wet-land recharge. At least half of the DIC in deep groundwater can be expected to originate from carbonate dissolution through carbonic acid in recharge [3]. Consequently, the ^{14}C concentration of the biogenic recharge DIC in some of these groundwaters approaches 100 pmc. This high DIC content and ^{14}C concentration of biogenic DIC of recharge is expected for high turnover of organic matter in wetland.

High concentrations of dissolved organic carbon (DOC, especially humic substances) are also found with high turnover of organic matter in wetland. This is also true for groundwater influenced by in-situ generation of DOC through partial oxidation of sedimentary organic carbon [4]. The DOC concentrations of groundwaters of different origin are shown in Fig. 5. The DOC concentrations under forest recharge and in the deep brines is less than or around 2 mgC/L. Through in-situ generation, elevated DOC concentrations are found. The same is true for the deep groundwater recharged from previous wetland. The combination of relatively high ^{14}C concentration of the DIC (cf. Fig. 4) and the high DOC concentrations suggest that the elevated DOC

concentrations originate from the wetland recharge of such waters. This implies that the DOC has a high mobility and long residence time in the aquifer.
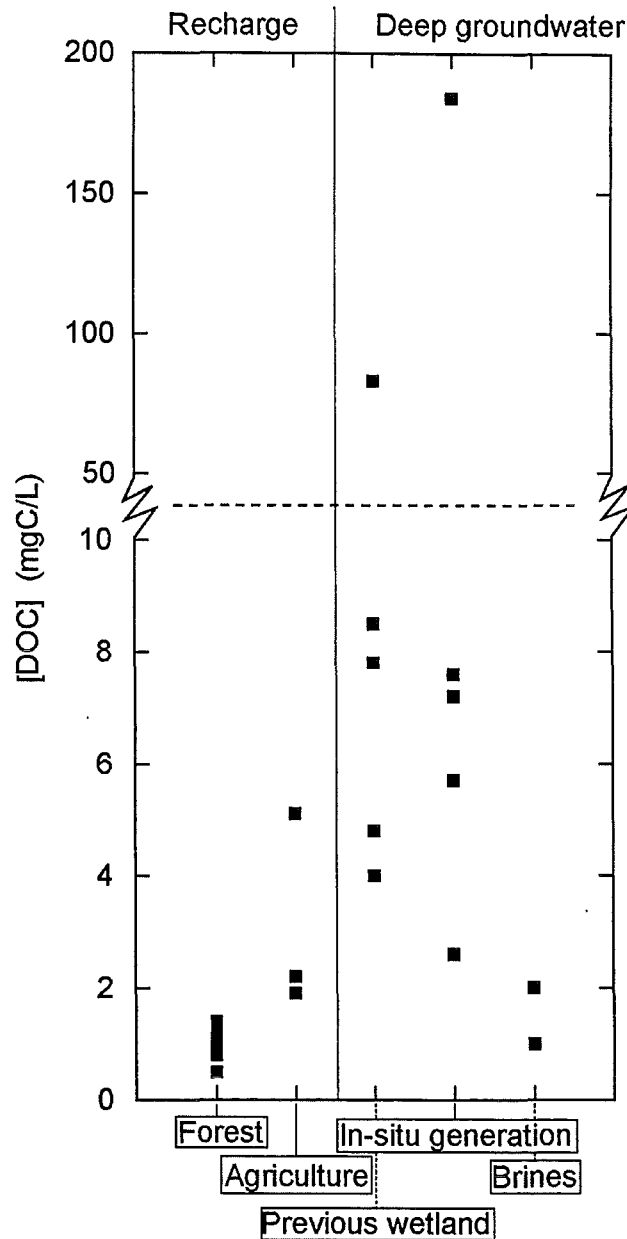
Fig. 5: DOC concentrations in groundwater of different origin (Forest: near-surface groundwater under forest; Agriculture: near surface groundwater under agricultural land; Previous wetland: deep groundwater (approximately 70 – 170 m depth) originating from wet-land recharge; In-situ generation: Deep groundwaters originating from recharge comparable to present forest conditions where elevated DOC concentrations arise from DOC in-situ generation [2]; Brines: Saline groundwater in the vicinity of the salt-dome) .

Acknowledgement

References

Suckow A. (1993) "Isotopenhydrologische und Edelgaspaleotemperatur-Untersuchungen im Deckgebirge über dem Salzstock Gorleben, Thesis, Universität Heidelberg.

Craig H. (1961) "Isotopic variations in meteoric waters", Science, 133, 1702-1703.

Buckau G, Artinger R., Geyer S., Wolf M., Fritz P. and Kim J.I. (2000) "14C dating of Gorleben groundwater", Applied Geochemisty, 15, 583-587.

Buckau G., Artinger R., Geyer S., Wolf M., Kim J.I., Fritz P. (2000) "Groundwater in-situ Generation of Aquatic Humic and Fulvic Acids and the Mineralization of Sedimentary Organic Carbon", Applied Geochemistry, 15, 819-32.

32.25.04 Aquatische Chemie der Actiniden und langlebiger Spaltprodukte

I. Aquatic Chemistry and Thermodynamic of tetravalent Actinides

(V. Neck, M. Altmaier, R. Müller, M. Bouby, Th. Fanghänel, J.I. Kim, INE)

Abstract

The investigations in the field of the aquatic chemistry and thermodynamics of long-lived actinides and fission products are focussed on the solubility, hydrolysis and colloid formation of Th, U, Np and Pu in the tetravalent oxidation state. In order to determine accurate solubility data for oxide and hydroxide solid phases an alternative method was developed by combining coulometric pH titration with the laser-induced breakdown detection (LIBD). Applying this method together with other laser-spectroscopic methods (LPAS, EXAFS) led to considerable progress in the determination and validation of thermodynamic data for the solid phases and hydroxide complexes of the tetravalent actinides.

Zusammenfassung

Die Arbeiten zum Vorhaben "Aquatische Chemie und Thermodynamik langlebiger Actiniden und Spaltproduke" konzentrieren sich auf die Löslichkeit, Hydrolyse und Kolloidbildung von Th, U, Np und Pu in der tetravalenten Oxidationsstufe. Eine am INE entwickelte Methode zur Bestimmung akkurater Löslichkeitsdaten für oxidische und hydroxidische Festphasen basiert auf coulometrischer Titration in Kombination mit der Laser-induzierten Breakdown-Detektion (LIBD). Mit Hilfe dieser Methode sowie anderer Laser-spektroskopischer Methoden (LPAS, EXAFS) konnten erhebliche Fortschritte erzielt werden bei der Bestimmung bzw. Validierung von thermodynamischen Daten zur Löslichkeit und Hydrolyse der tetravalenten Actiniden.

Introduction

The thermodynamic data reported in the literature for the actinides Th, U, Np and Pu in the tetravalent oxidation state are largely discrepant and partly based on contradictory chemical models. This implies large uncertainties for the geochemical modeling of actinides in natural aquatic systems. The difficulties are related to the strong tendency toward hydrolysis and colloid formation, the low solubility, and the limited spectroscopic possibilities for aqueous speciation. The results of classical solubility studies are widely scattered and imply a certain ambiguity, because the

chemical form of the solubility limiting oxidic or hydroxidic solid is not clear. Possibly they have a non-unique composition, $AnO_n(OH)_{(4-2n)}xH_2O(s)$ with $0 < n < 2$, depending on pretreatment and ageing of the solid.

Our recent literature review as well as the published experimental studies on the solubility, hydrolysis and colloid formation of tetravalent actinides are listed below, together with the abstracts of these papers. In addition to spectroscopic and classical solubility studies we developed an alternative method to determine more accurate solubility data for oxides and hydroxides [1]. This method is based on coulometric pH titration combined with the LIBD to detect the initial colloid formation as a function the H^+ and metal ion concentration. Considering colloids as small solid particles, their formation indicates that the solubility is just exceeded during the titration. The H^+ and actinide concentrations at the onset of colloid formation define the solubility of the corresponding oxide or hydroxide excluding colloidal species. As an unexpected result, the titrations of $2.8 \cdot 10^{-2}$ - $8.9 \cdot 10^{-5}$ M thorium nitrate solutions in the pH range 1.5 - 2.5 led to the formation of small $ThO_2(s)$ colloids with a mean diameter of 16 - 23 nm [1], which subsequently agglomerate to a microcrystalline precipitate. The same titration-LIBD method is applied in the higher pH range of 3 - 5, where hydrolysis and polynucleation lead to the formation of amorphous thorium hydroxide colloids as demonstrated by EXAFS measurements [2]. The latter titration-LIBD experiments and the evaluation of the solubility product of amorphous Th(IV) hydroxide are reported in detail.

Solubility and hydrolysis of tetravalent actinides

V. Neck and J.I. Kim, Radiochimica Acta 89 (2001), 1 - 16

The solubility and hydrolysis of Th(IV), U(IV), Np(IV), and Pu(IV) are critically reviewed and a comprehensive set of thermodynamic constants at I = 0 and 25°C is presented. The hydrolysis constants are selected preferentially from experimental studies at actinide trace concentrations, where the interference of colloid formation can be excluded. Unknown formation constants of mononuclear complexes $An(OH)_n^{4-n}$ are estimated by applying a semi-empirical electrostatic model and an empirical correlation with the known constants of other actinide ions. Based on the known and estimated hydrolysis constants, the solubility products of $An(OH)_4(am)$ or $AnO_2 \cdot xH_2O(am)$ are calculated from experimental solubility data available in the literature. The SIT is used for ionic strength corrections.

The solubilities of U(IV), Np(IV), and Pu(IV) hydroxides or hydrous oxides can be calculated by accounting only for mononuclear hydrolysis species. The considerably higher solubilities of amorphous Th(IV) precipitates at pH < 5 include major contributions of polynuclear species. The solubility data in acidic solutions depend strongly on the preparation and crystallinity of the solid phase. In neutral and alkaline solutions, where $An(OH)_4(aq)$ are the predominant aqueous species, the solubilities of $AnO_2(cr)$ become equal to those of the amorphous solids. This indicates that the crystalline dioxides are covered by amorphous hydroxide layers.

Solubility, Hydrolysis and Colloid Formation of Plutonium(IV)

R. Knopp, V. Neck and J.I. Kim, Radiochimica Acta 86 (1999), 101 – 108

The solubility and hydrolysis behaviour of Pu(IV) is critically reviewed taking into account the effect of colloid formation. Literature data on mononuclear Pu(IV) hydrolysis constants, determined from a solvent extraction study with Pu(IV) trace concentrations, are used to calculate the solubility product of $Pu(OH)_4(am)$ from the available experimental solubility data. Applying the SIT approach, the thermodynamic constant is calculated to be log K°_{sp} = -58.7 ± 0.9. The evaluated solubility product agrees well with the literature value determined recently by an indirect method, independent of Pu(IV) hydrolysis reactions. The generation of Pu(IV) colloids is investigated by chemical reduction of Pu(VI) as a function of the Pu concentration in 0.1 M $HClO_4$. Ultrafiltration and Laser induced breakdown detection (LIBD) measurements demonstrate that colloid formation is the predominant reaction, when the solutions are oversaturated with respect to the thermodynamic solubility of $Pu(OH)_4(am)$. In undersaturated solutions, the contribution of Pu(IV) colloids is negligible. The thermodynamic calculation of the solubility is consistent with the present results on colloid formation.

Application of LIBD to the determination of the solubility product of thorium(IV)-colloids

T. Bundschuh, R. Knopp, R. Müller, J. I. Kim, V. Neck and Th. Fanghänel
Radiochimica Acta 88 (2000), 625 - 629

A new experimental method is presented for the determination of solubility data, which is based on the laser-induced breakdown detection (LIBD). The method is capable of monitoring the initial colloid generation when the metal ion concentration reaches or just exceeds the solubility at given pH. The application is made to

determine the solubility of Th(IV) in acidic solutions at I = 0.5 M (NaCl) and 25°C. The initial colloid formation is determined as a function the H^+ concentration in a series of $2.8 \cdot 10^{-2}$ - $8.9 \cdot 10^{-5}$ M thorium solutions. The conditional solubility product (log K'_{sp} = = - 49.54 ± 0.22) obtained in this study corresponds to an equilibrium between solution and colloidal thorium dioxide particles. The solubility product at I = 0 (log $K°_{sp}$ = - 52.8 ± 0.3) is calculated with the SIT coefficients of the NEA-TDB. It corresponds to the known value for crystalline ThO_2(cr), in particular if the small particle size of about 20 nm is taken into account.

A spectroscopic study of the hydrolysis, colloid formation and solubility of Np(IV)

V. Neck, J.I. Kim, B.S. Seidel, C.M. Marquardt, K. Dardenne, M.P. Jensen and W. Hauser

The hydrolysis, colloid formation and solubility of Np(IV) are investigated in aqueous $HClO_4$-$NaClO_4$ solutions (log [H^+] = 0 to -2.5) by absorption spectroscopy in the wavelength range of 680 - 1000 nm. Applying Laser induced photoacoustic spectroscopy (LPAS) in the range of 680 - 760 nm, the study is extended to low Np(IV) concentrations of 10^{-6} mol/l in $DClO_4$-$NaClO_4$-D_2O solutions up to log [D^+] = -3.3. Laser induced breakdown detection (LIBD) demonstrates the formation of Np(IV) colloids when the Np(IV) concentration exceeds the solubility of Np(OH)$_4$(am) at given pH. The simultaneous decrease of the Np(IV) absorption bands at 723 and 960 nm cannot be ascribed to the formation of the mononuclear complex $Np(OH)^{3+}$ as assumed in the literature. It is found to be caused by polynucleation. In undersaturated Np(IV) solutions below 10^{-4} mol/l, the position and intensity of the absorption maximum at 723 nm are practically insensitive to the pH change. In oversaturated solutions the absorption band decreases significantly. The spectroscopically determined pH-dependent equilibrium concentration of mono-nuclear Np(IV) species upon freshly formed solid or colloidal Np(IV) particles indicates that $Np(OH)_2^{2+}$ is the predominant species in the pH range of 1.5 - 3. This finding is in agreement with the Np(IV) hydrolysis constants reported in the literature from a solvent extraction study with [239]Np(IV) trace concentrations. The solubility product of freshly formed Np(OH)$_4$(am) particles is determined to be log K'_{sp} = -54.4 ± 0.4 in 0.1 M $HClO_4$-$NaClO_4$ and log $K°_{sp}$ = -56.5 ± 0.4 (converted to I = 0 by applying the SIT).

Application of LIBD to determine the solubility product of Th(OH)$_4$(am)

V. Neck, R. Müller, M. Bouby, M. Altmaier and J.I. Kim

Summary

The solubility of amorphous Th(IV) hydroxide is investigated in acidic 0.5 M NaCl solutions at 25°C. The laser-induced breakdown detection (LIBD) is used to monitor the initial formation of Th(OH)$_4$(am) colloids during the coulometric titration of $1.2 \cdot 10^{-2}$ - $1.0 \cdot 10^{-5}$ M thorium solutions in the pH range of 2.7 - 4.5. The accurate solubility limit determined by this method is comparable with data measured from undersaturation with an x-ray amorphous solid precipitated at higher pH and dried at room temperature. Based on the hydrolysis constants selected in our recent review, the solubility product of Th(OH)$_4$(am) in 0.5 M NaCl is calculated to be log K'$_{sp}$ = - 44.48 ± 0.24 corresponding to log K°$_{sp}$ = - 47.8 ± 0.3 (converted to I = 0 with the SIT coefficients of the NEA-TDB).

Introduction

The solubility of amorphous Th(IV) precipitates, called either amorphous hydroxides Th(OH)$_4$(am) or hydrous oxides ThO$_2$·xH$_2$O(am), has been investigated by Nabivanets and Kudritskaya [3] at 17°C in 0.1 M NaClO$_4$, by Moon [4] at 18°C in 0.5 M NaClO$_4$, and by Rai et al. at 22 - 25°C in 0.1 M NaClO$_4$ [5], 0.6 M NaCl and KCl [6, 7] concentrated NaCl and MgCl$_2$ solutions [7], and in 0.1 M NaCl [8]. In these studies, the amorphous precipitates were not dried or treated at higher temperature but only washed with water. Although relatively widely scatted, the solubilities determined in these studies at pH 3.5 - 5 are reasonably consistent. Using a precipitate dried at room temperature for one week in a vacuum desiccator, Östhols et al. [9] measured the solubility at 25°C in 0.5 M NaClO$_4$. Their results are 3 - 4 orders of magnitude lower than those in [3, 4, 6 - 8] but still about 6 orders of magnitude higher than expected for crystalline ThO$_2$(cr) according to the solubility product calculated from thermochemical data, log K°$_{sp}$(ThO$_2$(cr)) = - 54.2 ± 1.3 [10] .

The hitherto available data on the solubility and hydrolysis of tetravalent actinides have been critically discussed in our recent review [11]. The thermodynamic data for Th(IV) are summarized in Table 1. Activity coefficients are calculated with the

Table 1. Thermodynamic constants at I = 0 and ion interaction (SIT) coefficients for Th(IV) species at 25°C (from [11])

Solubility products: $\log K^\circ{}_{sp} = -54.2 \pm 1.1$ for $ThO_2(cr)$

$\log K^\circ{}_{sp} = -47.0 \pm 0.8$ for $Th(OH)_4(am)$

Formation constants $\log \beta^\circ{}_{xy}$ and hydrolysis constants $\log K^\circ{}_{xy}$ for the complexes $Th_x(OH)_y{}^{4x-y}$ [a]

$\log \beta^\circ{}_{1,1} = 11.8 \pm 0.2$ $\quad \log K^\circ{}_{1,1} = -2.2 \pm 0.2$

$\log \beta^\circ{}_{1,2} = 22.0 \pm 0.6$ $\quad \log K^\circ{}_{1,2} = -6.0 \pm 0.6$

$\log \beta^\circ{}_{1,3} = 31.0 \pm 1.0$ $\quad \log K^\circ{}_{1,3} = -11.0 \pm 1.0$

$\log \beta^\circ{}_{1,4} = 38.5 \pm 1.0$ $\quad \log K^\circ{}_{1,4} = -17.5 \pm 1.0$

$\log \beta^\circ{}_{2,2} = 22.3$ $\qquad\quad \log K^\circ{}_{2,2} = -5.7$

$\log \beta^\circ{}_{4,8} = 91.6$ $\qquad\quad \log K^\circ{}_{4,8} = -20.4$

$\log \beta^\circ{}_{4,12} = 141.3$ $\qquad\, \log K^\circ{}_{4,12} = -26.7$

$\log \beta^\circ{}_{6,15} = 176.0$ $\qquad\, \log K^\circ{}_{6,15} = -34.0$

Ion interaction (SIT) coefficients:

i	j	ε_{ij}	j	ε_{ij}
H^+	ClO_4^-	0.14 ± 0.02 [b]	Cl^-	0.12 ± 0.01 [b]
OH^-	Na^+	0.04 ± 0.01 [b]		
Th^{4+}	ClO_4^-	0.67 ± 0.1 [c]	Cl^-	0.25 ± 0.03 [b]
$Th(OH)^{3+}$	ClO_4^-	0.45 ± 0.1 [c]	Cl^-	0.2 ± 0.1 [c]
$Th(OH)_2{}^{2+}$	ClO_4^-	0.3 ± 0.1 [c]	Cl^-	0.1 ± 0.1 [c]
$Th(OH)_3{}^+$	ClO_4^-	0.15 ± 0.1 [c]	Cl^-	0.05 ± 0.1 [c]
$Th(OH)_4{}^\circ$	ClO_4^-	0 [b]	Cl^-	0 [b]
$Th(OH)_4{}^\circ$	Na^+	0 [b]		
$Th_2(OH)_2{}^{6+}$	ClO_4^-	1.3 [d]		
$Th_4(OH)_8{}^{8+}$	ClO_4^-	1.7 [d]		
$Th_4(OH)_{12}{}^{4+}$	ClO_4^-	0.4 [d]		
$Th_6(OH)_{15}{}^{9+}$	ClO_4^-	5.6 ± 1.9 [d]		

[a] $\log \beta^\circ{}_{xy}$ refers to the reaction: $x\,Th^{4+} + y\,OH^- \Longleftrightarrow Th_x(OH)_y{}^{4x-y}$

$\log K^\circ{}_{xy}$ refers to the reaction: $x\,Th^{4+} + y\,H_2O \Longleftrightarrow Th_x(OH)_y{}^{4x-y} + y\,H^+$

[b] From the NEA-TDB [12]

[c] Estimated according to the analogies pointed out in the NEA-TDB [12]

[d] Calculated from the $\Delta\varepsilon$ values derived in [11].

specific ion interaction theory (SIT) [12]. As the total Th(IV) equilibrium concentration is given by

$$[Th]_{tot} = [Th^{4+}] + \Sigma \, x \, [Th_x(OH)_y^{4x-y}]$$

(1)

$$= K'_{sp}[OH^-]^{-4} + \Sigma \, x \, (K'_{sp}[OH^-]^{-4})^x \, \beta'_{xy} \, [OH^-]^y)$$

the calculated solubility product is directly correlated with the hydrolysis constants used in Eq.(1). The solubility products reported in the literature for Th(OH)$_4$(am) or ThO$_2$·xH$_2$O(am) differ by orders of magnitude, even if the experimental solubilities are in reasonable agreement: e.g. Rai et al. calculated log K°_{sp} = - 45.5 [6, 7]) and - 44.9 [8], whereas Nabivanets and Kudritskaya calculated log K'_{sp} = - 41.1 (corresponding to - 43.2 at I = 0) and Moon calculated log K'_{sp} = -50.52 in 0.5 M NaClO$_4$ [4] (corresponding to - 53.6 at I = 0). The main reason for these discrepant numbers are the different hydrolysis constants applied by the authors. Rai et al. [6 - 8] even neglect hydrolysis. If the solubility products are re-calculated from the experimental data at pH < 5 with the hydrolysis constants and SIT coefficients in Table 1, the log K°_{sp} values lie within the range of - 46.2 to - 47.3. The considerably lower solubility product given in [9], log K°_{sp} = - 48.7 (based on the hydrolysis constants in [13]), becomes - 48.2 if recalculated with the hydrolysis constants in [11]. In the present study an attempt is made to elucidate by LIBD, whether the higher solubilities measured in other studies are due to chemical differences in the solids or to the inclusion of colloids.

Experimental

Th(NO$_3$)$_4$·5H$_2$O (p.a.), NaCl (p.a.) and HCl (ultrapure) are purchased from Merck. For further purification, NaCl is recristallized twice. Colloid-free thorium solutions for the titration-LIBD experiments are obtained by double ultrafiltrations (Amicon 10 kD). All solutions are prepared with ultrapure water (Milli-Q-academic). Thorium concentrations are determined photometrically by the arsenazo-method [9] and by ICP-MS (ELAN 6100, Perkin Elmer). Combination pH electrodes (type ROSS, Orion Co.) are used to determine the H$^+$ concentration in 0.5 M NaCl solution. They are calibrated against standard pH buffers (pH 1 - 10, Merck) and standard solutions x M HCl / (0.5 - x) M NaCl with x = 0.001 - 0.1.

The coulometric titration of 1.2·10^{-2} to 1.0·10^{-6} M thorium nitrate solutions (60 ml) at I = 0.5 M (NaCl) and initial H$^+$ concentrations in the range -log [H$^+$] = 2.7 - 4.1 is

performed in a double-walled titration vessel, thermostated at 25°C, with the equipment described in [1]. A peristaltic pump is used to pump the titration solution through a flow-through cuvette for simultaneous colloid detection by LIBD. Since titrations performed with a current of 0.3 - 1 mA lead to local oversaturation, provoking the formation of unstable colloids, the current is reduced to 0.05 mA (corresponding to the addition of $4.48 \cdot 10^{-2}$ mmol OH^- per day to 60 ml solution). The pH electrode is freshly calibrated before and re-calibrated at the end of each experiment. In the case of titrations lasting more than 2 days, the electrode is re-calibrated after 2 - 3 days. The measured values of log $[H^+]$ are corrected for the electrode potential shift (usually below 0.03 pH-units per day). In each experiment, the thorium concentration is determined in unfiltered aliquots taken at the beginning and at the end, in some experiments also during the titration, to elucidate sorption effects. In addition, 1 kD filtration (Filtron, pore size ca. 1.2 nm) is applied to quantify the fraction of Th(IV) colloids.

The experimental setup of the LIBD apparatus used in the present study and its calibration with reference colloids have been described previously [1, 14, 15]. The laser pulse energy of the Nd-YAG laser (Continuum; Surelite, I_{em} = 532 nm, repetition rate 20 Hz) is adjusted to a constant value of 0.35 mJ and a CCD camera is used to record the plasma light emission, magnified by a macro-microscope. The breakdown probability is derived from 3000 laser shots.

Results and discussion

The results of the titration-LIBD experiments, i.e. the breakdown probability measured as a function of the H^+ and initial Th concentration, are shown in Fig.1. The onset of colloid formation during the titration is recognized by the increase of the breakdown probability (number of breakdown events per laser pulse). The formation of appreciable amounts of colloids (10 - 70% of $[Th]_{tot}$) is corroborated by 1 kD filtration at the end of the titration experiments.

The titration experiment at the initial thorium concentration of $[Th]° = 5.0 \cdot 10^{-3}$ mol/l (Fig.1a) is performed with a current of 1 mA (corresponding to the addition of $3.73 \cdot 10^{-2}$ mmol OH^- per hour to 60 ml solution). A small increase of the breakdown probability occurs already at -log $[H^+]$ = 3.15, i.e., considerably before the formation of a large amount of colloids in the range of -log $[H^+]$ = 3.35 - 3.40 leads to a breakdown probability of 100%. In several further titration experiments performed with a current of 0.3 - 1 mA, the breakdown probability of $1.0 \cdot 10^{-4}$ M thorium solutions

at - log $[H^+]$ = 2.8 to 3.2 increases continuously, starting from the beginning of the titration. As Th(IV) has an extremely high tendency toward polynucleation in this pH range, even a small local oversaturation provokes the formation of unstable colloids below the solubility limit. However, these colloids re-dissolve within a few days. In the other experiments shown in Fig.1a, the titration is performed with a current of 0.05 mA to avoid colloid formation caused by local pH gradients. As a consequence of the low titration velocity, the titration of solutions with high thorium concentrations of $[Th]°$ = $1.2 \cdot 10^{-2}$ mol/l and $3.0 \cdot 10^{-3}$ mol/l requires long times of 35 and 11 days, respectively (Fig. 1b). The largest part of the OH⁻ ions is consumed by the hydrolysis reactions of thorium and only a small part remains for increasing the pH.

Despite the slow titration, the initiation of colloid formation below the solubility limit is not completely avoided at these high thorium concentrations. However, upon stopping the titration or reducing the current to values < 0.01 mA overnight or over the weekend (filled points in Fig.1b), these unstable colloids re-dissolve. In order to exclude such artefacts, the long-time stability of the thorium colloids present at the end of the titration experiment is ascertained by measuring the breakdown probability in aliquots of the final solutions over a period of 1 - 3 months.
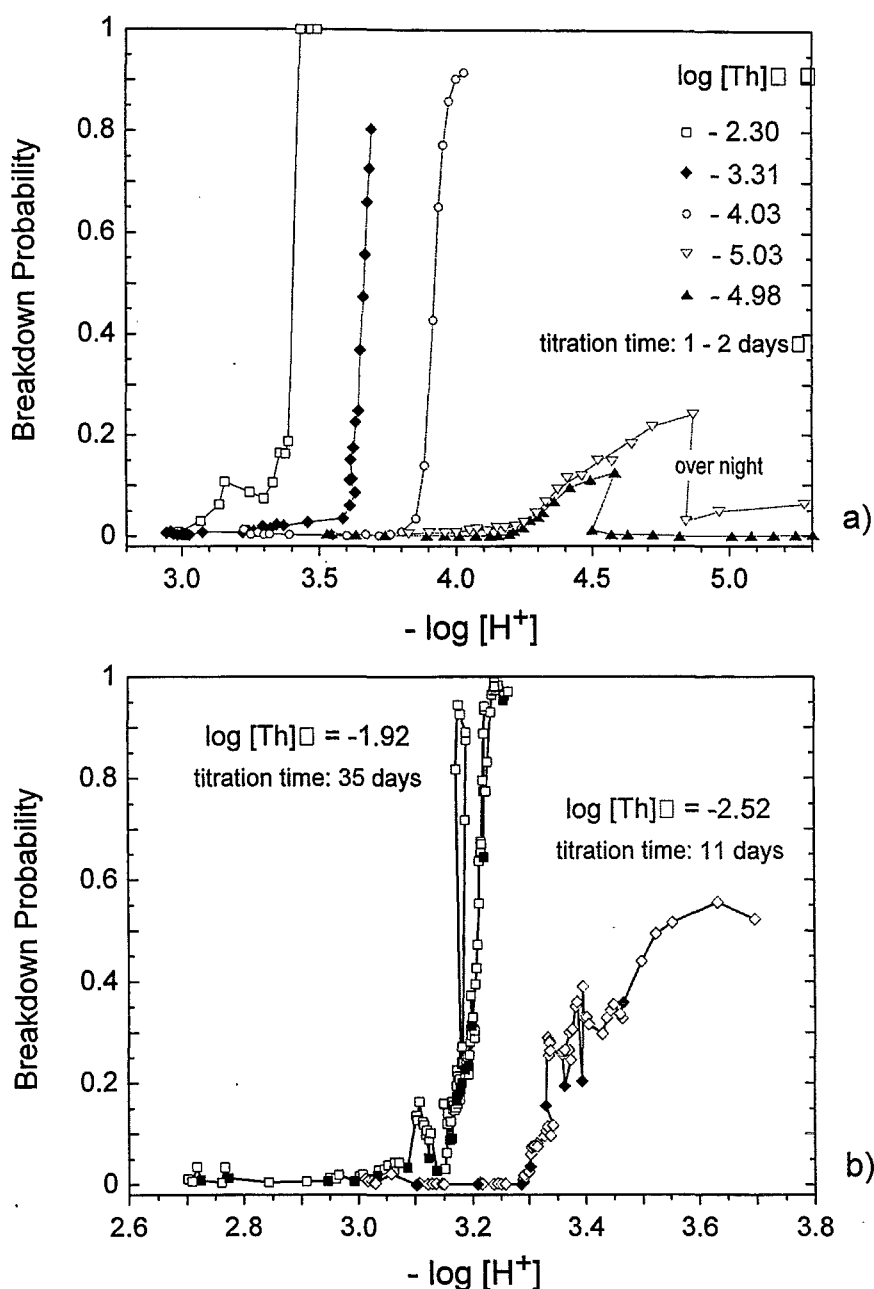
Fig. 1: Titration-LIBD experiments at 25°C: breakdown probability as a function of the H^+ concentration during the coulometric titration of $1.2 \cdot 10^{-2} - 1.0 \cdot 10^{-5}$ M thorium nitrate solutions in 0.5 M NaCl.

Sorption of thorium onto the glass surface of the reaction vessel is a problem, particularly in the experiments at low thorium concentrations. At $[Th]° > 10^{-4}$ mol/l, the observed decrease of the thorium concentrations is less than 20%. However, during the titration experiments at $[Th]° = 10^{-5}$ mol/l and pH > 4, the thorium concentrations decrease to 10^{-7} mol/l and the breakdown probability decreases to

the background level when the titration is stopped overnight (Fig.1a). The applicability of the present method and equipment is restricted to [Th] = 10^{-5} mol/l.

The results of the titration-LIBD experiments, i.e. the H^+ and Th(IV) concentrations at the onset of colloid formation, are comparable with the solubility data measured by Östhols et al. [9] and in the present study with amorphous precipitates dried at room temperature (Fig.2). This finding gives rise to the conclusion that the high solubilities determined at -log $[H^+]$ = 3.5 - 5 with precipitates not dried but only washed with water include large amounts of small colloids, in spite of the fact that Moon [4] and Rai et al. [5 - 8] determined the thorium concentration after filtration at a pore size of about 2 nm. Amorphous precipitates only washed with water may include small particles, which easily become suspended in the solubility experiment, whereas dehydration of the solid by drying may lead to larger agglomerates in the solid and, hence, to less colloids in the solubility experiment.

The solubility data defined by the onset of colloid formation are used to calculate the solubility product of Th(OH)$_4$(am). As the experimental data do not allow to determine the solubility product independently of the hydrolysis constants, the log β°_{xy} values in [11] are converted to I = 0.5 M and used as fixed values in Eq.(1). Considering also the uncertainties in the selected hydrolysis constants, the following solubility product is obtained for Th(OH)$_4$(am):

$$\log K'_{sp} = -44.48 \pm 0.24 \text{ (in 0.5 M NaCl)}$$

and

$$\log K^{\circ}_{sp} = -47.8 \pm 0.3 \text{ (converted to I = 0 with the SIT)}$$

The speciation calculated along this solubility curve predicts Th(OH)$^{3+}$ as the predominant complex in the range -log $[H^+]$ = 3.6 - 4.3. This is consistent with the experimental data, which decrease with a slope of about -3. At -log $[H^+]$ < 3.5 and [Th] >10^{-3} mol/l, polynuclear species become predominant. For the titrations at [Th] >10^{-3} mol/l, this is confirmed by the balance between the total OH$^-$ added coulometrically and the fraction of OH$^-$ consumed for increasing the pH. Appreciable amounts of small polynuclear species are formed already prior to the onset of colloid formation.

Th(OH)$_4$(am)□

✕ Moon, 0.5 M NaClO$_4$

╀ Rai et al., 0.6 M NaCl

▽ ...sthols et al.,
0.5 M NaClO$_4$

○ p.w., 0.5 M NaCl

Th(OH)$_4$(coll.)□

■ LIBD (p.w.)
0.5 M NaCl

ThO$_2$(coll.)□

◆ LIBD

Bundschuh et al.
0.5 M NaCl

log [Th(IV)]

- log [H$^+$]
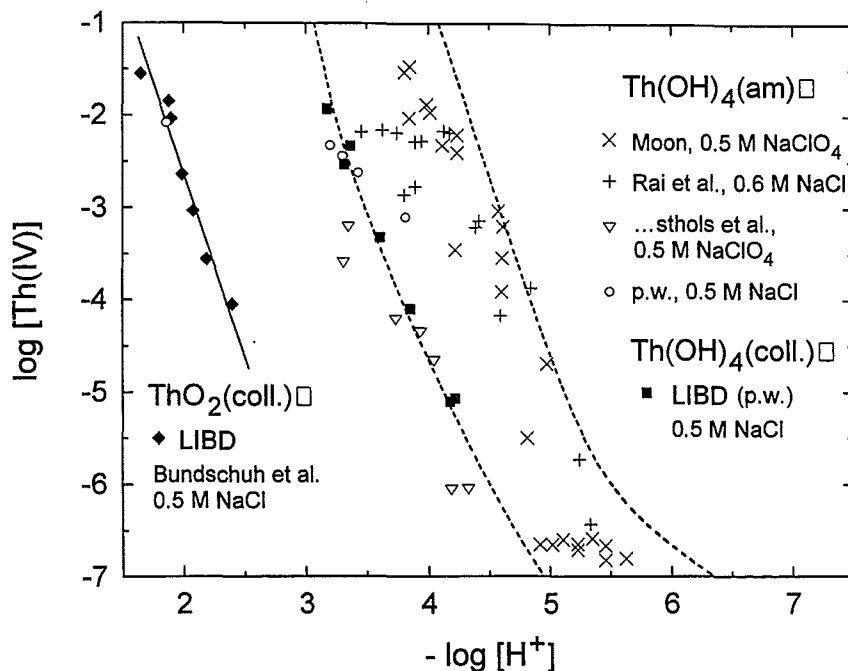
Fig 2: Comparison of the titration-LIBD data at the onset of Th(OH)$_4$(am) colloid formation with classical solubility data for amorphous Th(IV) solids at comparable ionic strength of I = 0.5 - 0.6 M). The lower and upper dashed curves are calculated with log K°$_{sp}$ = - 47.8 and - 46.2, respectively, and the hydrolysis constants in Table 1. The considerably lower solubility data from the initial formation of ThO$_2$(colloids) in the pH range 1.5 - 2.5 [1] are shown for comparison.

It must be emphasized that the present titration-LIBD experiment, although performed with the same equipment, is not comparable with the previous study of Bundschuh et al. [1]. In that previous paper, the titration in the range pH = 1.5 - 2.5 led to the formation of thorium oxide colloids, which subsequently agglomerate and form precipitates after some weeks. At these low pH values, the solid particles are formed in solutions where Th^{4+}(aq) is the predominant aqueous species. The titrations at pH > 3 lead to hydrolysis of the Th^{4+}(aq) ion and polynucleation up to the formation of amorphous hydroxide colloids. The chemical and structural differences between the microcrystalline ThO$_2$ particles formed at pH 1.5 - 2.5 and the amorphous hydroxide colloids formed at pH 3 - 4 are explicitly demonstrated and discussed in the EXAFS study of Rothe et al. [2].

Acknowledgements

References

1. Bundschuh, T., Knopp, R., Müller, R., Kim, J.I., Neck, V., Fanghänel, Th., Radiochim. Acta 88, 625 (2000).

2. Rothe J., Denecke, M.A., Neck, V., Müller, R., Kim, J.I.,
    Inorganic Chemistry (2002), in print

3. Nabivanets, B.I., Kudritskaya, L.N., Ukr. Khim. Zh. 30, 891 (1964).

4. Moon, H.C.; Bull. Korean Chem. Soc. 10, 270 (1989).

5. Ryan, J.L., Rai, D.; Inorg. Chem. 26, 4140 (1987).

6. Felmy, A.R., Rai, D., Mason, M.J.; Radiochim. Acta 55, 177 (1991).

7. Rai, D., Felmy, A.R., Sterner, S.M., Moore, D.A., Mason, M.J., Novak, C.F, Radiochim. Acta 79, 239 (1997).

8. Rai, D., Moore, D.A., Oakes, C.S., Yui, M.,
    Radiochim. Acta 88, 297 (2000).

9. Östhols, E., Bruno, J., Grenthe, I.,
    Geochim. Cosmochim. Acta 58, 613 (1994).

10. Rai, Swanson, J.L., Ryan, J.L.; Radiochim. Acta 42, 35 (1987).

11. Neck, V., Kim, J.I., Radiochim. Acta, 89, 1 (2001).

12. Grenthe, I., Fuger, J., Konings, R.J.M., Lemire, R.J., Muller, A.B., Nguyen-Trung, C., Wanner, H. (OECD, NEA-TDB): Chemical Thermo-dynamics of Uranium, Elsevier, North-Holland, Amsterdam, 1992

13. Grenthe, I., Lagermann, B.; Acta Chem. Scand. 45, 231 (1991).

14. Scherbaum, F., Knopp, R., Kim, J.I, Appl. Physics, B63, 299 (1996).

15. Bundschuh, T., Knopp, R., Kim, J.I., Colloids Surf. A 177, 47 (2001).

II.　　Study of Cm(III) Sorption onto γ-Al$_2$O$_3$ and clay minerals by Time-Resolved Laser Fluorescence Spectroscopy

(Th. Rabung, H. Geckeis, M.-C. Pierret, A. Bauer, R. Klenze, J.I. Kim, INE; Th. Stumpf, Institut für Radiochemie, FZ Rossendorf)

Abstract

The sorption of Cm(III) onto γ-Al$_2$O$_3$, illite and Ca-montmorillonite is investigated by time-resolved laser fluorescence spectroscopy (TRLFS) at a constant ionic strength (0.1 M NaClO$_4$ for γ-Al$_2$O$_3$, illite and 0.066 M CaClO$_4$ for Ca-montmorillonite). Sorption experiments are carried out in a glove box under an argon atmosphere in the pH range between 3.5 and 13 and at a Cm(III) concentration of 2.5×10^{-7} mol/L. Three different Cm(III) species are identified at the γ-Al$_2$O$_3$ and illite–surface with their pH dependent appearance being very similar. No change in the time dependence of the emission decay can be observed for the three sorbed species at γ-Al$_2$O$_3$ and Ca-montmorillonite (constant lifetimes of 110 μs) so that subsequent hydrolysis of the sorbed monodentate surface complex with increasing pH is deduced. The Cm(III) sorption to γ-Al$_2$O$_3$ is described by surface complexation modeling.

Zusammenfassung

Die Sorption von Cm(III) an γ-Al$_2$O$_3$, Illit and Ca-Montmorillonit wurde mit Hilfe der zeitaufgelösten Laserfluoreszenzspektroskopie bei einer konstanten Ionenstärke untersucht (0.1 M NaClO$_4$ für γ-Al$_2$O$_3$, Illit und 0.066 M CaClO$_4$ for Ca-montmorillonite). Die Sorptionsexperimente wurden unter Inertgasatmosphäre in einem pH-Bereich von 3.5 and 13 bei einer Cm(III) Gesamtkonzentration von 2,5 x 10^{-7} mol/l durchgeführt. Drei unterschiedliche Cm(III)-Spezies konnten an der γ-Al$_2$O$_3$- und Illitoberfläche identifiziert werden. Für die an γ-Al$_2$O$_3$ und Ca-Montmorillonit sorbierten Spezies wurde eine konstante Fluoreszenzlebensdauer (110 μs) festgestellt. Daraus lässt sich die mit steigendem pH fortschreitende Bildung ternärer Hydrolysekomplexe aus dem monodentat gebundenen Cm(III) Oberflächen-komplex schlussfolgern. Die Cm(III) Wechselwirkung mit γ-Al$_2$O$_3$ wurde mit einem Oberflächenkomplexierungsmodell beschrieben.

Introduction

The sorption of radionuclides onto natural mineral surfaces has attracted much interest in conjunction with the long-term performance assessment of nuclear waste repositories. Due to their strong interactions with mineral surfaces, multivalent radionuclides can be considerably retarded by sorption, precipitation or mineralisation reactions. On the other site sorption/incorporation reactions with natural groundwater colloids may lead to an enhanced radionuclide mobility, especially when the desorption reactions are kinetically hindered. Therefore, the underlying sorption mechanisms and the surface species involved must be clearly identified for a thermodynamic description of radionuclide sorption reactions. Various surface complexation models (SCM) have been developed for a thermodynamic modeling of experimental sorption data most of them implementing the electrostatic potential which is due to surface charges. Nevertheless, in most cases the surface complexes derived are the result of fitting experimental data as a function of metal ion concentration, pH, and ionic strength without direct experimental confirmation of the surface speciation assumed. The present work is dedicated to the speciation of surface sorbed actinides by using the laser fluorescence spectroscopy (TRLFS). Spectroscopy provides insight into sorption mechanisms and the speciation of the surface sorbed Cm(III) and thus, can be used to substantiate the development of SCM.

The sorption of the trivalent actinides, Am(III) and Cm(III), and their lanthanide homologues onto different mineral phases has been described by various authors [1-8]. It was found that the sorption behavior of Eu(III) and Am(III) is very similar [2]. The sorption properties of γ-Al_2O_3 resembles that of hematite, and surface aluminol groups are assumed to be mainly responsible for the Cm(III) sorption onto clay minerals based on the similarity of TRLFS spectra [4, 8]. The quantification of the Cm(III) interaction with the aluminol sites of the γ-Al_2O_3 might, therefore, allow the modeling of sorption processes for a wide range of minerals. Clay minerals as illite and smectite are present in the geosphere and are components of possible backfill materials in a nuclear repository. The sorption of REE and Cm(III) onto kaolinite and smectite has already been studied [8, 9]. Outer-sphere complexation by an ion exchange mechanism has been spectroscopically (TRLFS) identified to prevail at low pH and inner-sphere surface complex formation has been found to be relevant at neutral and high pH [8]. The present work aims to study the interaction of trivalent

actinides with the clay surface and γ-Al_2O_3 spectroscopically over a wide pH range up to the alkaline region (pH ~ 13).

1. Sorption of Cm(III) onto γ-Al_2O_3

Fig. 1 shows the evolution of the TRLFS spectra with increasing pH. Spectra are normalized to the same peak area. A red shift of the Cm(III) fluorescence emission band up to pH=13.2 indicates the formation of inner-sphere surface complexes. The
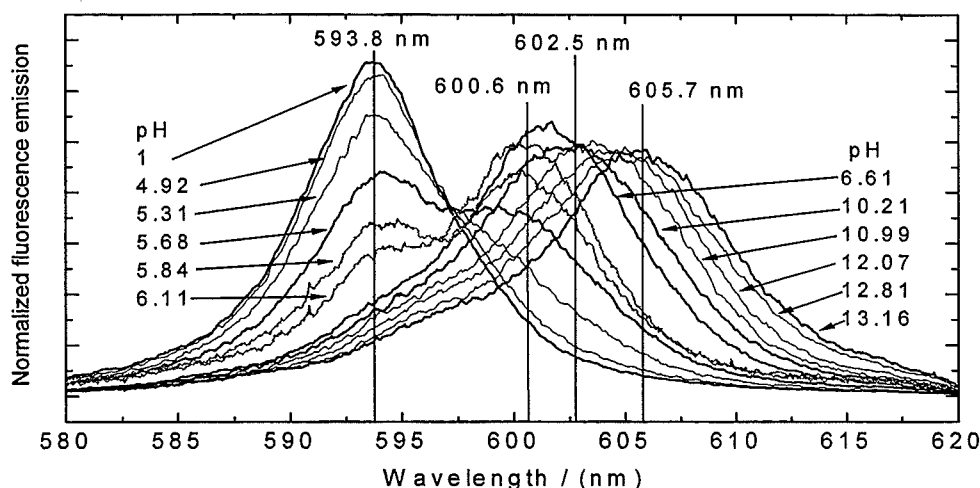
Fig. 1: Fluorescence emission spectra of 2.5 $\times$ 10^{-7} mol/L Cm(III) in 0.57 g/L aqueous γ-Al_2O_3 suspension (0.1 M $NaClO_4$) at various pH; spectra are scaled to the same peak area.

emission band of the Cm(III) aquo ion at 593.8 nm begins to decrease at pH 4.9 and a shoulder indicates the formation of a first inner-sphere surface complex. At increasing the pH to pH=6.1 this first sorbed Cm(III) species becomes dominant. Between pH=6.1 and 6.6 a further clear red shift of the emission band appears. This fact directs to a noticeable change in the Cm(III) speciation within a narrow pH range. Small changes in the spectra from pH=6.6 to 10.2 indicate the presence of a relatively constant species distribution under the given conditions. The appearance of another surface complex at pH>10.2 can be deduced by the progressing shift of the emission band to higher wavelengths.

Three different Cm(III) species are derived from the set of spectra by deconvolution. Emission band maxima lie at 600.6 nm, 602.5 nm and 605.7 nm. All mixed spectra are deconvoluted using these three single component spectra plus the well known spectrum of the aquo ion. Taking the relative fluorescence intensity factors (*FI*) of each Cm(III) species depending on the molar absorptivity, ε_i, at the excitation

wavelength, the fluorescence quantum yield, Φ_i, and the overall efficiency of the instrumentation into account (fluorescence intensity factors relative to the intensity of the free aquo ion: *FI* (Cm(III)complex 1) = 0.45 ± 0.05, *FI* (Cm(III)complex 2) = 0.29 ± 0.02, *FI* (Cm(III)complex 3) = 0.26 ± 0.02), the Cm(III) species distribution can be calculated on the basis of the spectral data (Fig.2).
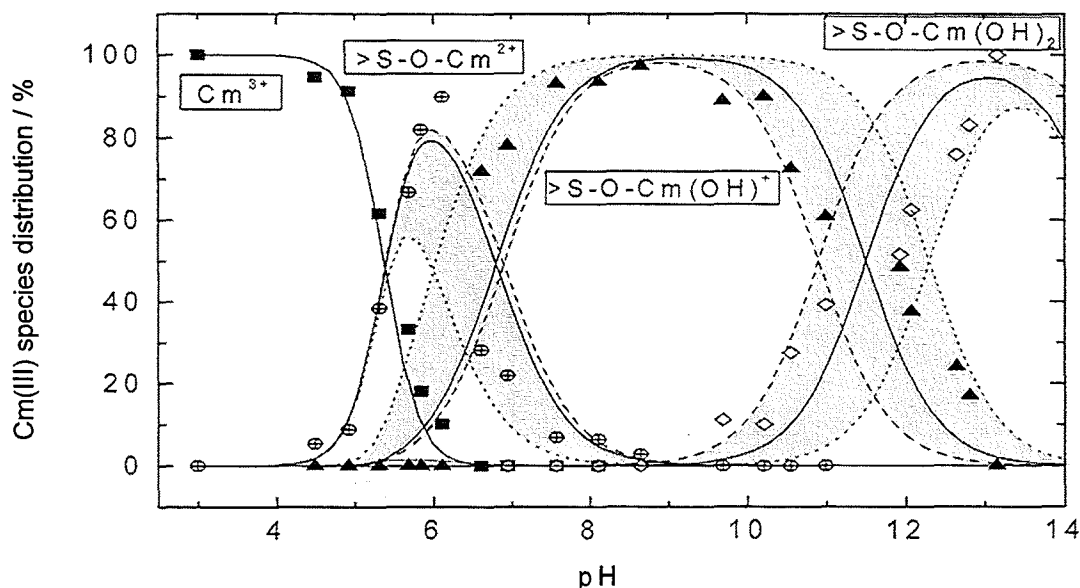
Fig. 2: Calculated Cm(III) species distribution for the sorption of 2.5×10^{-7} mol/L Cm(III) onto γ-Al$_2$O$_3$ (0.57 g/L aqueous γ-Al$_2$O$_3$ suspension in 0.1 M NaClO$_4$). Lines and shaded area correspond to surface complexation model calculations

The sorption reaction of Cm(III) as determined by TRLFS is in good agreement with earlier batch experiments with Am(III) and Eu(III) illustrating the consistent sorption behaviour. The constant fluorescence lifetime of τ= 110 μs for the surface sorbed Cm(III) indicates the presence of 5±1 H$_2$O molecules or OH$^-$ ions in the first coordination sphere. The following chemical surface sorption model is, therefore, suggested:

$[\equiv Al\text{-}O\text{-}H] + Cm(H_2O)_9^{3+} \Leftrightarrow [\equiv Al\text{-}O\text{-}Cm]^{2+}(H_2O)_5 \Leftrightarrow [\equiv Al\text{-}O\text{-}Cm(OH)]^+(H_2O)_4 \Leftrightarrow [\equiv Al\text{-}O\text{-}Cm(OH_2)](H_2O)_3$

$\quad\quad\quad\quad\quad\quad\quad\quad - 4H_2O; -H^+ \quad\quad\quad\quad\quad -H^+ \quad\quad\quad\quad\quad\quad\quad -H^+$
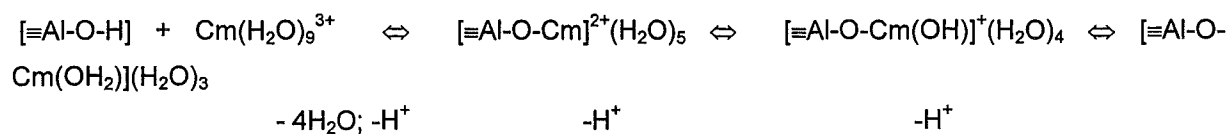
The respective results of the surface complexation modeling are given in Tab. 1.

Tab. 1: Results of the surface complexation model calculations; the results of the calculations are plotted in Fig. 2

reaction	log K		
	dotted line	solid line	dashed line
$\equiv$Al-OH + Cm^{3+} $\Leftrightarrow$ $\equiv$Al-O-Cm^{2+} + H^{+}		2.5 [2]	
$\equiv$Al-OH + Cm^{3+} + H$_2$O $\Leftrightarrow$ $\equiv$Al-O-Cm(OH)$^{+}$ + 2H^{+}	-3.5	-4.3	-4.4
$\equiv$Al-OH + Cm^{3+} + 2H$_2$O $\Leftrightarrow$ $\equiv$Al-O-Cm(OH)$_2$ + 3H^{+}	-15.8	-15.8	-15.3

2. Sorption of Cm(III) onto illite and Ca-montmorillonite

Clay materials play an important role in potential radioactive waste repositories. So is illite the most abundant clay mineral in the Opalinus clay and in the clay formation in Bure, France. Therefore, Cm(III) sorption onto a purified and well characterized illite (illite du Puy, supplied by CEA-Saclay) at I= 0.1 M NaClO$_4$ and an illite concentration of 0.25 g/L was also studied by TRLFS. Only inner-sphere sorbed Cm(III) can be differentiated spectroscopically from the free aquo ion by a peak shift to higher wavelengths and increasing fluorescence lifetime. Outer-sphere complexation which generally plays an important role for the permanent negatively charged clay materials is dominant at low pH and low ionic strength. Spectra evaluation and peak deconvolution results in three distinct surface sorbed complexes at 598.8 nm, 602.3 nm and 605.5 nm. The species distribution shown in Fig. 3 is quite similar to that obtained for the γ-Al$_2$O$_3$ (see Fig. 2) measured under comparable conditions (total Cm(III) and solid concentration, ionic strength). This observation supports the assumption that sorption onto clay materials is dominated be the aluminol groups and not by the silanol groups.

The sorption of Cm(III) onto Ca-montmorillonite as a major constituent of bentonite backfill is also studied. TRLFS spectra of Cm(III) sorbed on the Ca-montmorillonite suggest the similar mechanisms as found for γ-Al$_2$O$_3$ and illite. The study will be continued.
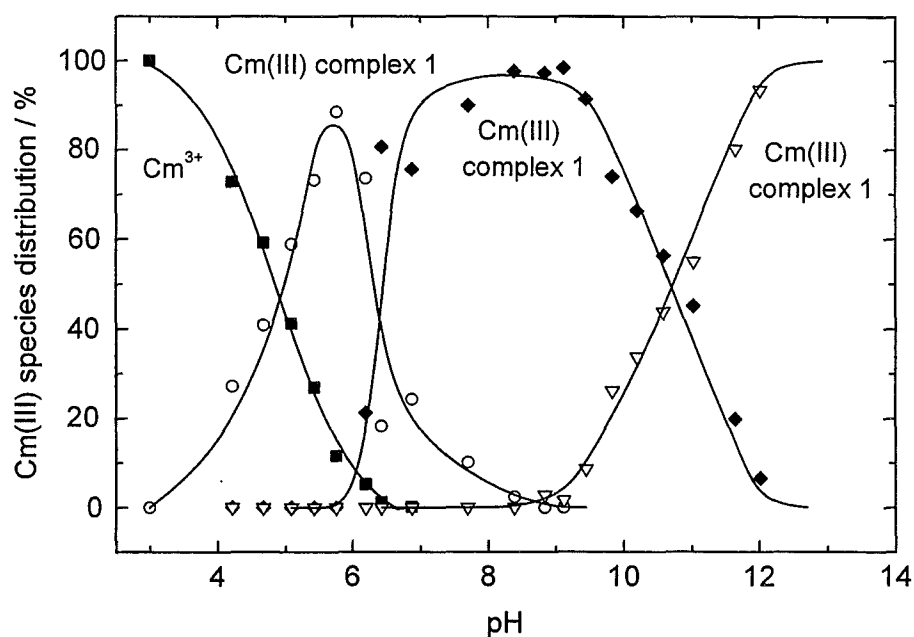
Fig. 3: Speciation plot for the Cm(III) sorption onto illite at =0.1 M NaClO₄

References

1. Stumpf, Th., Rabung, Th., Klenze, R., Geckeis, H., Kim, J.I.: Spectroscopic study of Cm(III) sorption onto γ-alumina, J. Colloid Interface Sci. **238**, 219-224 (2001)

2. Rabung, Th., Stumpf, Th., Geckeis, H., Klenze, R., Kim J.I.: Sorption of Am(III) and Eu(III) onto γ-alumina: experiment and modelling, Radiochim. Acta **88**, 711-716 (2000)

3. Rabung, Th., Geckeis, H., Kim, J. I., Beck, H. P.: Sorption of Eu(III) on a Natural Hematite: Application of a Surface Complexation Model, J. Colloid Interface Sci. **208**, 153-161 (1998)

4. Geckeis, H., Klenze, R., Kim, J. I.: Solid Water Interface Reaction of Actinides and Homologues: Sorption onto Mineral Surfaces, Radiochim. Acta **87**, 13-21 (1999)

5. Nordén, M., Ephraim, J. H., Allard, B.: The Influence of a Fulvic Acid on the Adsorption of Europium and Strontium by Alumina and Quartz: Effect of pH and Ionic Strength, Radiochim. Acta **65**, 265-270 (1994)

6. Xiangke W., Wenming, D., Xiongxin, D., Aixia, W., Jinzhou, D., Zuyi, T.: Sorption of Eu and Yb on alumina: mechanisms and effect of fulvic acid, Appl. Radiat. Isot. **52**, 165-173 (2000)

7. Kosmulski, M.: Standard Enthalpies of Adsorption of Di- and Trivalent Cations on Alumina, J. Colloid Interface Sci. **192**, 215-227 (1997)

8. Stumpf Th., Bauer A., Coppin F., Kim J.I., Time-resolved laser fluorescence spectroscopy study of the sorption of Cm(III) onto smectite and kaolinite. Environmental Science and Technology, **35**, 3691-94 (2001)

9. F. Coppin, G. Berger, A. Bauer, S. Castet, M. Loubet, Sorption of lanthanides on smectite and kaolinite, Chemical Geology **182**, 57-68 (2002)

III.   <u>In situ Speciation von Actiniden mit Synchrotronstrahlung</u>

(K. Dardenne, M.A. Denecke, P. Lindqvist-Reis, J. Rothe, INE)

Abstract

X-ray absorption fine structure (XAFS, the general term for both EXAFS and NEXAFS or XANES) spectroscopy provides information concerning oxidation state, electronic structure, coordination geometry and metric parameters (e.g., bond distances, coordination numbers) for describing actinide ion speciation. Analysis of XAFS data aids interpretation of experimental results from actinide spectroscopic, solubility and sorption studies. In 2001, INE has applied the XAFS method for determining the coordination of actinides complexed with humic substances[1], sorbed onto amorphous iron oxyhydroxides and their transformation products[2], in polynuclear hydrolysis products and eigencolloids[3], embedded in silica glasses[4] and sorbed onto silica and alumina surfaces[5]. In addition to these studies with X-ray energies at core ionization energies of the actinide elements, soft X-ray NEXAFS investigations at the ionization energy of carbon, combined with microscopic imaging for characterizing the interaction of actinides with humic colloids and mixed-colloids are performed[6]. Without exception, these investigations are accompanied by complementary spectroscopic/microscopy studies. This provides us insight into actinide coordination structures, their reactions in solution, in the solid state and at the water-solid interface, as well as the reaction mechanisms involved.

Zusammenfassung

Die Röntgenabsorptionsspektroskopie (XAFS, die allgemeine Bezeichnung für EXAFS und NEXAFS oder XANES) liefert Informationen bezüglich Valenzzustand, elektronischer Struktur und Koordinationsgeometrie sowie metrischer Parameter (z.B. Bindungslängen, Koordinationszahlen), die die Actinid-Speziation beschreiben. Die XAFS-Analyse unterstützt die Interpretation von spektroskopischen Studien, Löslichkeitsdaten und Sorptionsuntersuchungen an Actiniden. Im Jahr 2001 wurde die XAFS-Methode im INE zur Bestimmung der Koordination von Actinid-Fulvat-Komplexen[1], Actinidkationen sorbiert auf amorphem Eisenoxyhydroxid und dessen Transformationsprodukten[2], polynuklearen Hydrolyseprodukten von Actiniden, Actinid-Eigenkolloiden[3] sowie Actiniden eingebettet in Silica-Gläser[4] und sorbiert auf Silica-

und Alumina-Oberflächen[5] angewendet. Zusätzlich zu diesen Untersuchungen im Röntgenbereich, in dem sich die Innerschalen-Ionisationsenergien der Actinid-elemente befinden, werden auch NEXAFS-Untersuchungen im Weich-Röntgen-bereich durchgeführt. Dies wird mit mikroskopischen Abbildungsmethoden kombi-niert, um die Wechselwirkung von Actiniden mit Huminkolloiden und gemischten Humin-Mineral-Kolloiden zu charakterisieren[6]. Alle diese Studien werden von komplementären spektroskopischen bzw. mikroskopischen Untersuchungen begleitet. Die kombinierten Ergebnisse tragen zum Verständnis der Actinid-Koordi-nation, deren Reaktionen in Lösung, in der festen Phase und an der Wasser-Fest-stoff-Grenzfläche sowie den zugehörigen Reaktionsmechanismen bei.

1. XAFS study of actinide coordination structure in Np(IV)-fulvates

The coordination environment surrounding tetravalent neptunium complexed with two different naturally occurring fulvic acids (FA) at H^+ concentrations of $10^{-1.0}$ and $10^{-1.5}$ M are determined from analysis of their Np L3 edge EXAFS spectra. The k^3-weighted EXAFS and their corresponding Fourier transforms (FT) are shown in Fig. 1. The change in the oscillation fingerprint near $k = 8\text{-}9$ Å^{-1}, the distinct shoulder on the high R side of the first FT peak and the beat mode interference pattern in Fourier filtered data (not shown) indicates that two Np(IV)-O distances are present. Modeling the data with the EXAFS equation shows that the shorter distance is in the range 2.24 to 2.27 Å; the second, longer Np(IV)-O distance 2.41 to 2.44 Å. From comparison to
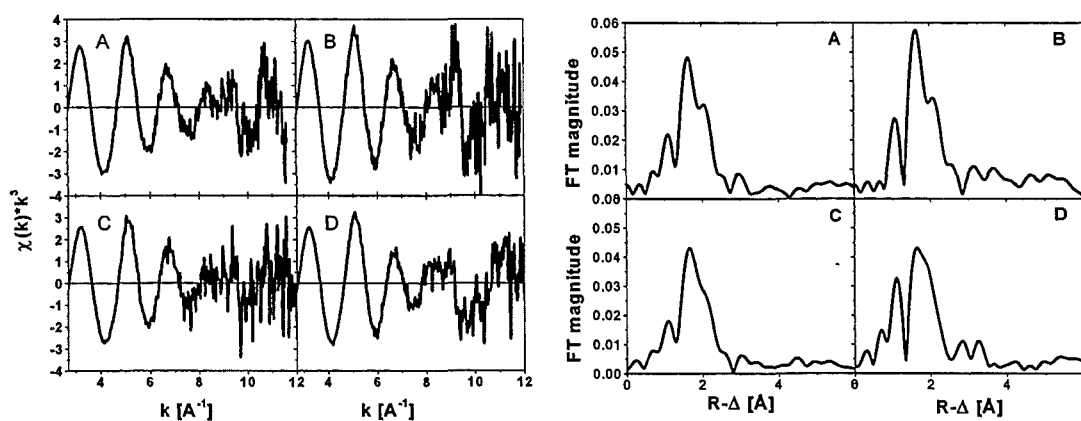
Fig. 1: k^3-weighted EXAFS (left) and their corresponding FT (right) of the Np(IV)-fulvates studied. A: Np(IV):Gorleben-FA, $-\log[H^+]= 1.5$; B: Np(IV):Gorleben-FA, $-\log[H^+]= 1.0$; C: Np(IV):Boom clay-FA, $-\log[H^+]= 1.5$; D: Np(IV):Boom clay-FA, $-\log[H^+]= 1.0$.

Np(IV)-O distances in known hydroxo complexes, the shorter distance is attributed to a hydroxyl ligand; the longer one is an average Np-O distance for coordinating water molecules and carboxyl groups from the fulvate. No Np-Np scattering peak is observed in the EXAFS spectra, i.e., polynuclear species or eigencolloids do not form. The anomalous increase in loading capacity7 of humic substances for Np(IV) with increasing pH, compared to that for actinyl ions and trivalent actinides is, according to these results, due to the presence of $Np(OH)_xFA(4-x)$. The loading capacity is calculated assuming a charge neutralization of the Np(IV) cation through formation of a Np(IV)-FA4 complex, where the FA(4) denotes four functional groups from fulvate neutralizing the Np(IV) cation charge.8 For each coordinating hydroxyl group, one less functional group from the fulvate is needed to neutralize the Np(IV) cation charge. If this is not known or included in the calculation of the loading capacity, its value will be erroneously high.

The coordination number determination associated with the hydroxyl ligands from fits to the data has a shallow minimum, so that it is difficult to determine how many of these ligands are actually bound to Np(IV). However, interpretation of optical spectroscopy results9 to determine the formation constant for the complex suggests x=2 of $Np(OH)_2FA(2)$.

2. Low temperature XAFS investigation on the lutetium binding changes during the 2line-ferrihydrite alteration process

The time dependent changes of Lu(III) speciation, initially sorbed onto two-line ferrihydrite (2LFh) at pH 5.9, during tempering (70°C) and leading to stable crystalline transformation products is studied at the Lu L3 absorption edge. Lu(III) is used as a analogue for the trivalent actinides. Samples are tempered for 0, 84, 155 and 238 hours. Complementary microscopic studies (AFM, SEM), XRD and FTIR spectroscopy confirm transformation of Lu(III):2LFh (pH 6) to both goethite and hematite, with a predominance of hematite. XRD investigation of a transformation series at pH 8 shows that the cell volume of hematite product increases slightly, suggesting the incorporation of Lu(III) in the structure. The EXAFS results aim at determining the fate of the Lu(III) during transformation.

Fig. 2 shows the experimental and the best fit results and their corresponding FT's. The initial sorption sample (temper time = 0) is fit using two coordination shells, an

oxygen and an iron shell. The fit yields (Table 1) seven oxygen atoms (O') at a mean bond distance of 2.31Å and a Lu-Fe' distance of 3.41Å. This is in good agreement with previous results10.

The other samples are fit to structural models including the two possible end products (hematite-like and goethite-like models), with an isotropic expansion of interatomic distances to simulate Lu(III) incorporation into iron position of the crystal-lattice. The coordination numbers are kept constant at expected values during the fits. Results of the best fit are listed in Table 1. The fit to the 238h tempered sample data is only possible using the hematite-like model. It requires inclusion of a Lu-Fe distance near 3.9Å (Fe4). This distance is absent in the goethite-like cluster. No good fit is possible using solely the goethite-like cluster model. If Lu(III) is incorporated into goethite, its EXAFS contribution is completely masked by Lu(III) in hematite.

Data from the 84 and 155h tempered samples is modeled with a combination of the temper time = 0 and 238h species. The first coordination shell bond lengths and coordination numbers are fixed to the values obtained for samples with temper times

0 and 238h and scaled with a ratio factor, rf. The rf is the proportion of the Lu(III) incorporated into hematite species (temper time = 238h). Results of the fits are also given Table 1. EXAFS for both 84h and 155h tempered samples is very well modeled with this combination of species. This shows that both species, Lu(III) sorbed onto 2LFh and Lu(III) incorporated into hematite crystal structure, coexist in the inter-mediate temper time samples.
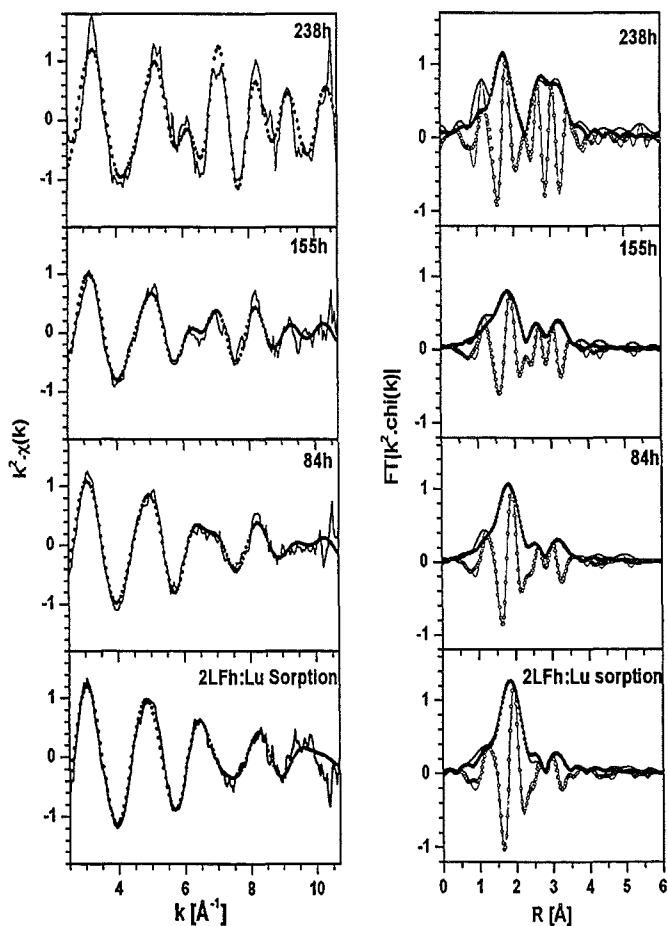
Fig. 2: Left: k^2-weighted Lu L3 edge EXAFS (lines) and best fit results. (dots). Right: corresponding FT.

Table 1: Coordination number (N), interatomic distance (R), relative ionization energy shift (ΔE_0), mean-square-displacement (σ^2) and relative amount Lu incorporated into hematite (rf) obtained from fits to the EXAFS shown in Fig. 2.

Sample Temper time (h)	Neighbor	N**	R [Å]	ΔE_0 [eV]	σ^2 [10^{-3} Å^2]	rf
0	O'	7.2	2.31	7.64	7.44	0
	Fe'	1*	3.41	4.8	5.10	
84h	O	1.54	2.19	6.79	7.46	0.26
	O'	5.20	2.31	6.79	7.37	
	Fe1 + Fe2	1.02	3.17	0.80	15.03	
	Fe3 + Fe'	1.51	3.42	0.80	5.60	
	Fe4	1.54	3.93	0.80	10.7	
155h	O	3.98	2.19	6.79	14.68	0.66
	O'	2.61	2.31	6.79	5.23	
	Fe1 + Fe2	2.65	3.12	0.01	13.14	
	Fe3 + Fe'	2.32	3.42	0.01	5.60	
	Fe4	3.98	3.89	0.01	17.2	
238h	O	6*	2.19	6.74	7.22	1.00
	Fe1 + Fe2	4*	3.08	0.01	10.17	
	Fe3	3*	3.41	0.01	2.12	
	Fe4	6*	3.88	0.01	12.1	

* fixed at this value   **N(O')=(1-rf)*7.2, N(O)=rf*6 and, N(Fe3+Fe')=(1-rf)*1+ rf*3

These results corroborate XRD results on a transformation series at pH 8 that Lu(III) sorbed onto 2LFh is incorporated into the transformation product hematite crystal lattice, as opposed to being occluded or remaining a sorbed species on the surface.

3. XAFS investigation of the structure of aqueous Th(IV) species, colloids, and solid Th(IV) oxide/hydroxide

XAFS studies at the Th L3 edge are performed on a series of Th(IV) solutions with varying pH and concentration for aqueous speciation of thorium, in order to help elucidate the reason for the discrepancy between solubility data reported in the literature. Solubility data reported for amorphous Th(IV) precipitates, called either amorphous hydroxides Th(OH)$_4$(am) or hydrous oxides ThO$_2$·xH$_2$O(am), show considerable discrepancies.[11,12,13,14,15,16] This may be due to the fact that the reported solubilities do not refer to a well-defined solid phase but to hydrated

oxyhydroxide $ThO_n(OH)_{4-2n}\cdot xH_2O(am)$ with $0 \leq n \leq 2$[12,16,17,18] or the presence of colloids in the solutions studied[19].
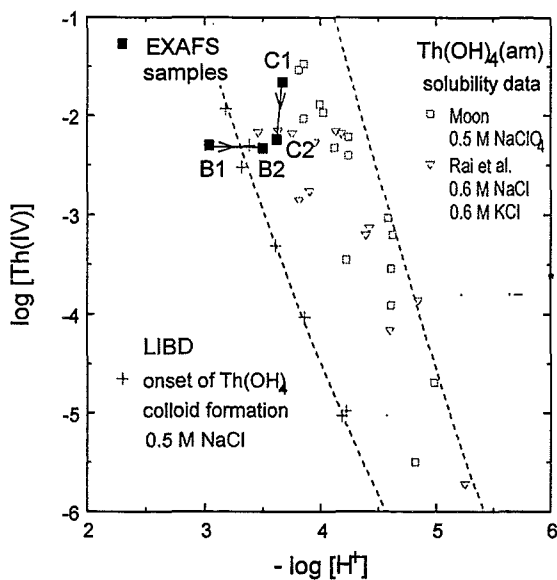
Fig. 3 H^+ and $Th(IV)$ concentrations of the EXAFS solutions (filled squares) compared to solubilities.

The H^+ and $Th(IV)$ concentrations in the EXAFS solution samples are depicted as filled squares in Fig 3, together with the solubility determined by LIBD[20] and literature data[12,14]. Samples B1 and B2 are taken at the beginning and end of the titration of a specific LIBD experiment. Sample B1 is a solution below the onset of colloid formation; sample B2 is above the onset of colloid formation. Sample C1 and C2 are non-filtered and filtered colloid suspensions. Sample C1 is prepared by titrating a $Th(IV)$ solution from $-log\ [H^+] = 2.6$ to $-log\ [H^+] = 3.7$. The presence of colloids is confirmed by LIBD. Colloids are still detected in sample C2 prepared by 1 kD filtration of sample C1 (Filtron, pore size ca. 1.2 nm). Reformation of colloids immediately after filtration shifts the pH. For comparison, EXAFS spectra of Th^{4+}(aq) in 1.5 M $HClO_4$ (sample A) and of a freshly precipitated amorphous $Th(IV)$ solid (sample D) are recorded.

The EXAFS spectra of the samples are shown in Fig. 4. Metrical parameters (N, R, σ^2 and ΔE_0 values) obtained in theoretical fits to the data are listed in Table 2. The major solution species in sample B1 is the mononuclear species Th^{4+}(aq) so that its spectrum is similar to that of sample A. The fit results for both these samples are also the same,
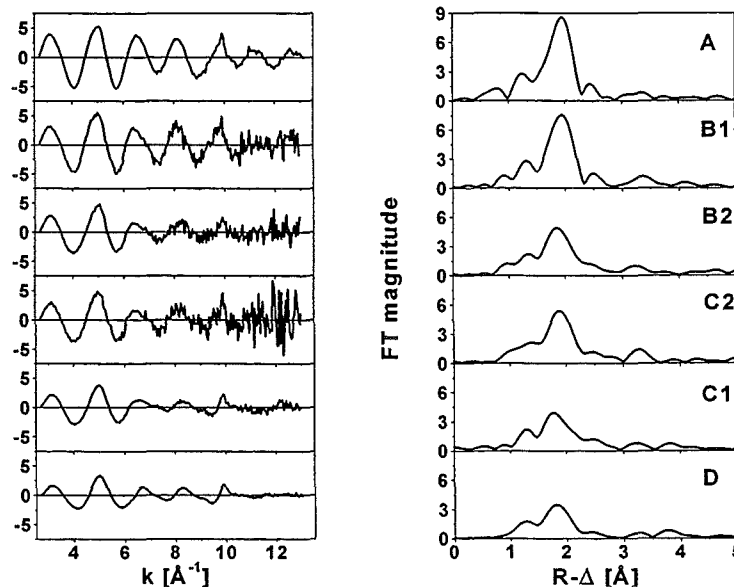
Fig. 4: k^2-weighted Th L3 edge EXAFS (left) and their corresponding FT (right).

within experimental uncertainty. The EXAFS spectra of samples B2, C2 (with similar

H$^+$ and Th(IV) concentrations, both above the onset of colloid formation) and particularly sample C1 (with H$^+$ and thorium concentrations exceeding the solubility determined by LIBD) are significantly different from that of A and B1. This demonstrates the presence of polynuclear species or Th(IV) colloids. The highly asymmetric Th-O coordination exhibited by all these samples, i.e., a broad asymmetric Th-O FT peak, is also indicative of this. The observed asymmetry makes inclusion of an inharmonic correction to the phase21 in the fits to the Th-O shell in all these samples necessary. An additional oxygen shell (O2) must also be included in the fit to the spectrum of sample C1 and sample D. Both the EXAFS spectra of these two samples and the metrical parameters describing their Th(IV) coordination are very similar. This indicates that the suspended solid particles in sample C1 have a structure similar to the amorphous precipitate, sample D. Note that the Th-Th distance in sample C1 disappears following filtration, as it is not observed in the spectrum of sample C2. Removing larger colloids via the filtration step shifts the H$^+$ and thorium concentration so that the spectrum of this sample C2 is more similar to sample B2.

Table 2: Metrical parameters extracted by least squares fitting analysis of EXAFS spectra in Fig. 4.

ID	Shell	R [Å]	N	σ^2 [Å^2]	ΔE_0 [eV]
A	O	2.45	12.7	0.0072	4.1
B1	O	2.46	11.6	0.0074	3.9
B2	O	2.51	10.6	0.0121^{C3}	7.5
C1	O1	2.50	9.4	0.0140^{C3}	6.9
	O2	3.09	1.2	0.0007	6.9
	Th	3.99	0.7	0.0032	11.0
C2	O	2.51	10.5	0.0103^{C3}	7.5
D	O1	2.46	6.6	0.0106^{C3}	6.7
	O2	3.13	4.4	0.0109	15.8
	Th	3.96	1.5	0.0065	8.9

^{C3} with inharmonic correction

The EXAFS results from solutions above and below the onset of colloid detection by LIBD demonstrate that the variations in reported solubilities of 3 - 4 orders for amorphous Th(OH)$_4$(am) precipitates are due to the presence of small amorphous colloids in the analyzed solutions.

4. XAFS and TRLFS investigation on Cm(III) and Eu(III) in amorphous silica

The local structure of Cm(III) and Eu(III) cations incorporated into sol-gel derived silica (SiO_2) is studied with XAFS. The structural changes in the metal cation coordination associated with dehydrating the silica by annealing at 20 °C, 200 °C, 400 °C and 800 °C are determined. Results are compared to the $Cm(III)_{aq}$ and $Eu(III)_{aq}$ ions.

The Cm L3 edge k^3-weighted EXAFS and corresponding FT are shown in Fig. 5. The FT of the 20°C sample is featureless for interatomic distances further distant than the first oxygen coordination shell. The spectrum at 800 °C shows a significant EXAFS pattern at indicating the presence of more than one shell.

From fits to the data (cf. Fig. 5), the following changes in metal coordination with increasing annealing are observed. In the porous silica structure, the Cm(III) {(EuIII)} cations are surrounded by approximately nine {nine} water molecules with a mean distance between the metal cations and the water oxygen atoms of ~2.48 Å {~2.45 Å}. These distances are similar to those of the aquo ions. Time resolved laser fluorescence determination of emission lifetimes confirms that the hydration number of Cm(III) and Eu(III) is the same as the hydration number for their aquo ions. As the
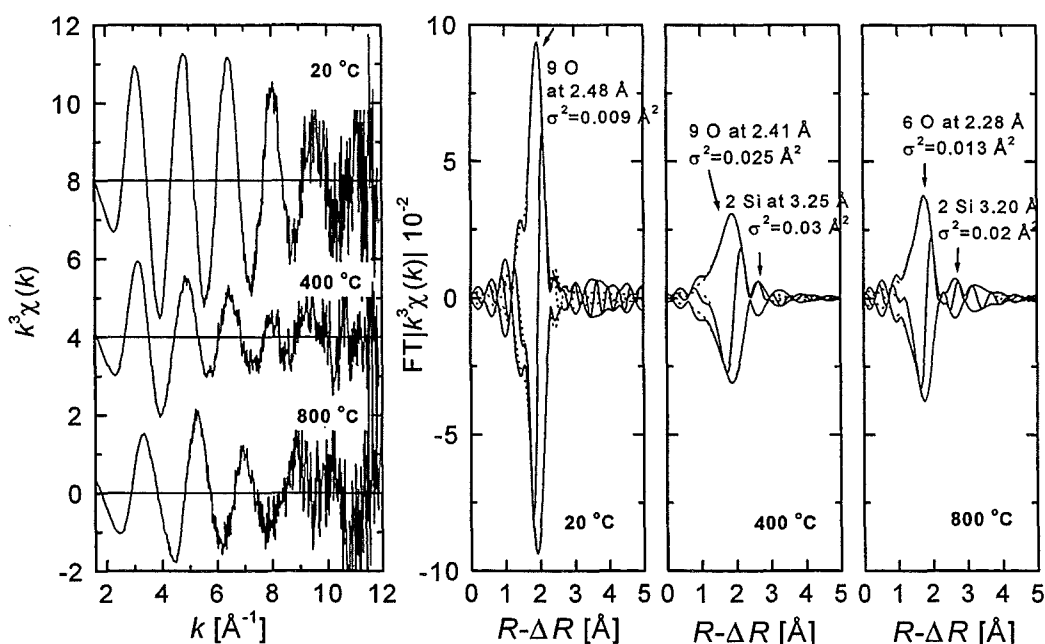
Fig. 5: k^3-weighted Cm L3 data (left) and corresponding FT (right). Model functions are dotted, experimental data continuous lines.

silica samples are heated, bound water molecules are released and the cation coordination structure changes. The reduced EXAFS amplitude for the 400°C annealed sample results from the presence of a spread of metal-O distances. Modeling both Cm(III) and Eu(III) data for this annealing temperature requires including an inharmonic correction to the phase to account for asymmetry[21] of the metal-O shell. At the highest annealing temperature studied, the coordination number decreases from nine {nine} to 6-7 {~7}. In the 800 °C annealed sample with Eu(III), the metal-O shell is split into two distances, 2.33 Å and 2.50 Å. The Cm(III) sample annealed at 800 °C does not show two defined distances, but must be modeled with an inharmonic correction. Ordering of the metal cation coordination sphere at higher annealing temperatures is observed, as indicated by the presence of a metal-Si interaction at 3.20 Å {3.28 Å}.

5. Grazing incidence (GI) XAFS measurements of metal cation sorption onto mineral surfaces

Surface sensitive grazing incidence XAFS (GIXAFS) measurements of mineral sorbed metal cations are used to characterize the metal sorbed at reactive surface sites. Two different systems are studied: 1) Hf(IV) sorbed onto the (001) basal plane of freshly cleaved mica and a surface oxidized silicon disk and 2) U(VI) sorbed onto the (110) surface of α-Al$_2$O$_3$ measured at two different orientations of the crystal surface plane to the polarization vector of the incident synchrotron radiation.
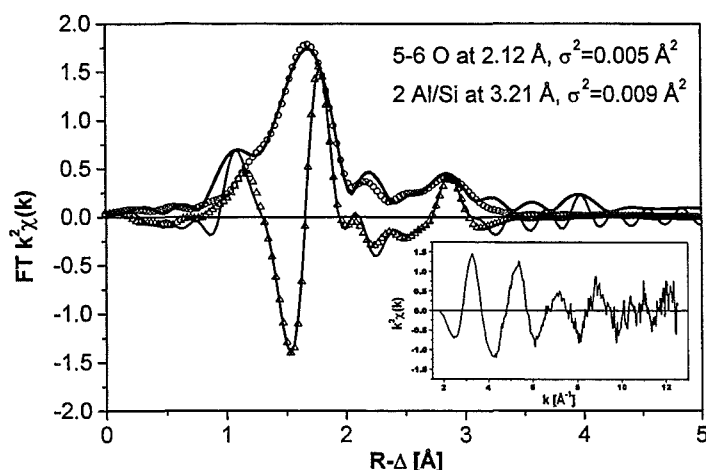
Fig. 6: Hf L3 GIXAFS measurement of Hf(IV) sorbed onto (001) mica plane at pH 4 Experimental points are continuous lines, fit results symbols.

The Hf L3 EXAFS and fit results for Hf(IV) sorbed onto the (001) mica surface at pH ~4 is depicted in Fig. 6. The results for the oxidized silicon wafer (not shown) are in qualitative agreement to those for mica. In accordance to previous bulk measurements22, the short ~2.1 Å Hf(IV)-O distance indicates the primary inter-

action of the metal cations with the mica surface occurs *via* links to corners of Si/Al-oxygen polyhedra, i.e., a monodentate species forms with Hf(IV) bound to silanol or aluminol groups of Si/Al-tetrahedra/octahedra. The observation of a second Al/Si neighbor shell also suggests that the Hf(IV) cations partly lose their coordinating water sphere, binding directly to the surface. The Hf-Si/Al distance is that expected for a monodentate interaction; a bidentate distance would be near 3 Å. As the (001) or basal plane of mica has no silanol/aluminol groups to bind the metal cations, the binding must take place at surface imperfections such as steps and kinks.

Considering the difference in ionic radii, these findings are in agreement with a previous GI-FluoXAFS study on the sorption of Cu(II) onto the mica-(001) surface23. In contrast to the Cu(II) study, the Hf(IV) surface species is mononuclear; no Hf-Hf interaction is observed.

The U L3 edge XANES spectrum of the (110) α-Al_2O_3 surface sorbed U(VI) uranyl moiety exhibits only a small polarization dependency (not shown). The dependency of the EXAFS is remarkable (Fig. 7). In the initial orientation of the crystal surface to the polarization vector of the incident synchrotron radiation (denoted as 0°), the axial oxygen shell dominates the spectrum. In the EXAFS measured after rotating the sample disc 90°, both axial and equatorial coordinating shells are evident in the FT.

Comparison of the spectral trends with data recorded for $UO_2(CH_3CO_2)_2 {}^* 2H_2O$ single crystals24 allows identification of the general orientation of uranyl units on the surface. The orientation of the disc denoted as 0° has $O=U^{2+}=O$ units more parallel to the incident radiation polarization vector; the 90° spectrum is more perpendicular.

Because a polarization dependence is observed, we may exclude mono-dentate binding sites and surface imperfections as reactive surface sorption sites. There are two possible candidates for bidentate sorption on the (110) α-Al_2O_3 surface (corundum structure). One is at AlO_6 octahedra edges
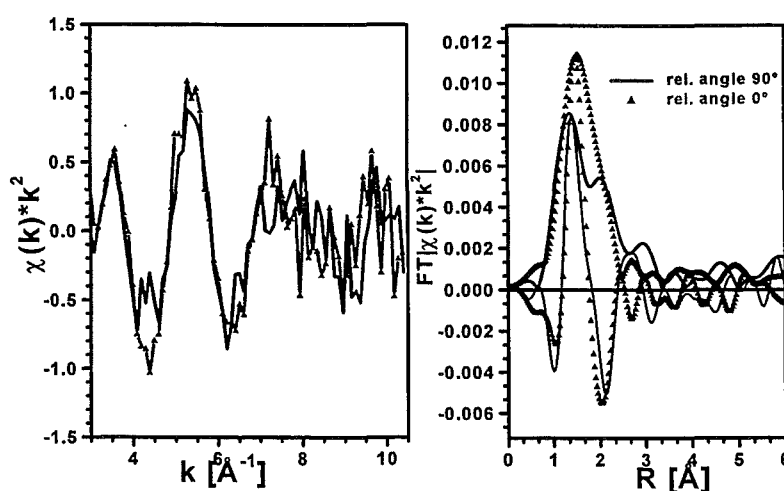
Fig. 7: U L3 GIXAFS measurement of U(VI) sorbed onto a (110) α-Al_2O_3 surface at pH ~6. Symbols are the spectrum at a relative angle = 0°; continuous lines at 90°.

and the other bridging two adjacent AlO$_6$ apices. The angle between these surface sites is near 55°, so that differentiation between edge and apices sites or determination of any a preferential sorption onto one site over the other is likely not possible with measurements at two right angles. Future experiments are underway to measure other specific α-Al$_2$O$_3$ surfaces and at several relative angles of orientation.

6. Combined AFM and STXM *in situ* study of the influence of Eu(III) on the agglomeration of humic acid

Aldrich humic acid (HA) agglomerates formed in aqueous solutions in the presence of Eu(III) cations as analogue to the trivalent actinides (10^{-5} mol/L, pH~5.5) are investigated *in situ* with a combination of atomic force microscopy (AFM), having high spatial resolution, and scanning transmission x-ray microscopy (STXM), with chemical sensitivity. Both methods together disclose regions
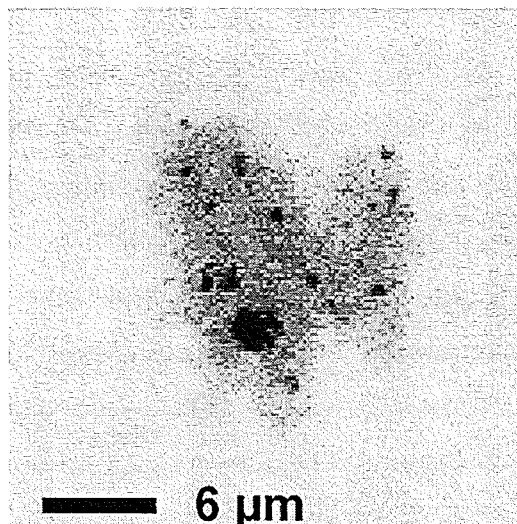
Fig. 8: STXM image of Aldrich HA agglomerate formed after addition of Eu(III), recorded at 288.7 eV.
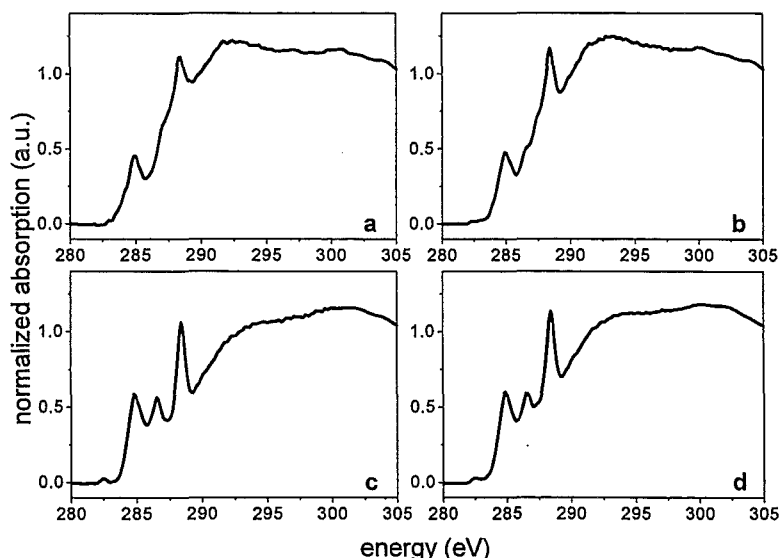
Fig. 9: C K-NEXAFS of **a**: HA / 6LFh aggregates **b**: HA agglomerates formed following Eu(III) complexation (dark regions in Fig. 8), **c**: HA agglomerates formed following Eu(III) complexation (light regions in Fig. 8), **d**: spatially averaged spectrum (extracted from the entire agglomerate in Fig. 8).

in samples containing Eu(III)-HA complexes, which markedly differ in their micromorphology and chemical functionality. STXM micrographs of Eu(III)-HA agglomerates reveal zones of high and low optical density (Fig. 8; 150×150 pixel, 200 nm x/y step width) with markedly distinct C K-NEXAFS (Fig. 9b,c), indicative of different humic functionalities. The

dark patches exhibit a NEXAFS spectrum (Fig. 9b) similar to both that recorded for a suspension of 6-line ferrihydrite (6LFh) and HA (Fig. 9a) and for HA alone25. Two additional absorption peaks (Fig. 9c) appear at 282.4 and 286.5 eV in the NEXAFS extracted from the lighter regions of the Eu(III)-HA agglomerate in Fig. 8. The intensity of the carboxylate peak at 288.4 eV remains almost unaffected by the Eu(III) complexation. For comparison, an average spectrum, as it would have been recorded with a spatial resolution less than 200 nm, is shown in Fig. 9d. Had the NEXAFS been extracted from the agglomerate at a lower resolution, only a change in the spectra following Eu(III) complexation would have been observed; the similarity of the dark region NEXAFS to the HA NEXAFS and the observed pseudo-phase separation into regions of differing chemical functionality would have remained undetected Typical HA morphologies in the presence of Eu(III) observed in AFM images are particulate agglomerates and fibrous structures (not shown). The particulate agglomerates are likely correlated to the dense zones in STXM images, fibrous structures associated with low density areas. Because the Eu(III) cation distribution within the agglomerates cannot be unambiguously deduced from their C K-NEXAFS spectra, one may not yet speculate if there is a difference in metal cation affinity associated with HA of different morphologies/optical densities.

References

1   M. A. Denecke, C.M. Marquardt, J. Rothe, K. Dardenne, M.P. Jensen, *J. Nuclear Science Technology* (submitted).

2   Dardenne, K. Schäfer, T., Lindqvist-Reis, P., Denecke, M.A., Plaschke, M. Rothe, J., Kim, J.I., submitted to *Environ. Sci. Technol.*

3   Rothe, J., Denecke, M.A., Neck, V., Müller, R., Kim, J.I. *Inorg. Chem.* (in print).

4   Lindqvist-Reis, P., Denecke, M.A., Rothe, J., Dardenne, K., Panak, P., Klenze, R., in preparation.

5   Rothe, J., Denecke, M.A., Dardenne, K., Lindqvist-Reis, P., *HASYLAB Annual Report 2001*, to appear at http://www-hasylab.desy.de/science/annual_reports/2001_report/index.html.

6   Plaschke, M., Rothe, J., Denecke, M.A., Dardenne, K., Pompe, S., Heise, K.-H., *Colloids Surfaces* A **197**, 245-256 (2002).

7   Marquardt, C.M., Pirlet, V., Kim, J.I., *Wissenschaftliche Berichte Forschungszentrum Karlsruhe*, **6524**, 45 (2000)

8   Kim, J.I., Czerwinski, K.R., *Radiochim. Acta* **73**, 5 (1996).

9   Marquardt, C.M., Pirlet, V., Kim, J.I., in preparation

10 Dardenne, K., Schäfer, T., Denecke, M.A., Rothe, J., Kim, J.I., *Radiochim. Acta* **89**, 469-479 (2001).

11 Nabivanets, B. I., Kudritskaya, L. N. *Ukr. Khim. Zh.* **30**, 891-895 (1964).

12 Moon, H. C. *Bull. Korean Chem. Soc.* **10**, 270 (1989)

13 Ryan, J. L., Rai, D. *Inorg. Chem.* **26**, 4140-4142 (1987).

14 Felmy, A. R., Rai, D., Mason, M. J. *Radiochim. Acta* **55**, 177-185 (1991).

15 Rai, D., Felmy, A. R., Sterner, S. M., Moore, D. A., Mason, M. J., Novak, C.F. *Radiochim. Acta* **79**, 239-247 (1997).

16 Rai, D., Moore, D. A., Oakes, C. S., Yui, M. *Radiochim. Acta* **88**, 297-306 (2000).

17 Grenthe, I., Fuger, J., Konings, R. J. M., Lemire, R. J., Muller, A. B., Nguyen-Trung, C., Wanner, H. *Chemical Thermodynamics Vol. 1. Chemical Thermodynamics of Uranium*; Elsevier (OECD, NEA-TDB), North-Holland: Amsterdam, 1992.

18 Greiling, H.-D., Lieser, K. H. *Radiochim. Acta* **35**, 79-89 (1984).

19 Neck, V., Kim, J. I. *Radiochim. Acta*, 89, 1-16 (2001).

20 Neck, V., Müller, R., Bouby-Laliron, M., Altmaier, M., Rothe, J., Denecke, M.A. Kim, J.I., *Radiochim. Acta* (submitted).

21 Bunker, G., *Nucl. Instrum. and Methods* **207**, 437 (1983).

22 Denecke, M.A., Geckeis, H., Pohlmann, C., Rothe, J. Degering, D., *Radiochim. Acta* 88, 639 (2000).

23 Farquhar, M.L., Charnock, J.M., England, K.E.R., Vaughan, D.J., *J. Colloid Interface Sci.* 177, 561 (1996).

24   Hudson, E. A., Allen, P. G., Terminello, L. J., Denecke, M. A., Reich, T., *Phys. Rev.* B **54** (1996) 156-65.

25   Rothe, J., Denecke, M.A., Dardenne, K., *J. Colloid Interface Sci.* **231**, 91-97 (2000).

32.25.05 Geochemische Transportmodellierung sowie Untersuchung der Übertragbarkeit

I.   Application of geochemical modeling in site selection process for radio-active waste repositories

(V. Metz, B. Kienzler, W. Schüßler, INE)

Abstract

An integrated source term for the disposal of radioactive waste forms was developed. The project was coordinated by FZK-INE and most of the detailed investigations were performed at our institute. The actinide source term has been applied in the current study for the evaluation of different groundwater – host rock systems. The geochemical environment of a deep bedrock repository is mainly characterized by the composition of the groundwater influencing radionuclide solubility, chemical buffer capacity, radionuclide retention and chemical compatibility with waste forms, containers and backfill materials. Evaluation of different groundwater – host rock systems is performed by modeling of the various geochemical environments and resulting radionuclide concentrations. In a first step, it is analyzed if the groundwater composition is in equilibrium with the mineral phases of the geological formation. In addition, corrosion reactions of waste forms in the different groundwaters are taken into account. These reactions may change the solution compositions and pH, resulting in significant changes of the radionuclide solubilities. In order to demonstrate the evaluation method, model calculations are applied to data sets available for various geological formations, such as granite, clay and rocksalt formations. The results demonstrate that geochemical modeling proves to be a feasible tool in a site selection process with respect to deep underground repositories.

Introduction

The geological disposal in deep bedrock repositories has been the preferred option for the management of high-level radioactive waste. Many countries have initiated research programs to identify suitable geological formations and select potential repository sites. In the beginning of such a program, requirements and preferences are defined [1]. Besides geological, hydrological, seismic and rock mechanic characteristics of a host formation, its geochemical characteristics determine if the

formation is suitable for disposal of radioactive waste. The geochemical environment of such a formation must fulfill following requirements: high radionuclide retention capacity, high chemical buffering capacity, and favorable composition of formation water with respect to radionuclide solubility. With regard to the geochemical requirements, it is desireable to derive a catalog of environmental variables (such as pH, Eh, ionic strength) and favorable ranges of these variables and to develop tools for comparison of potential host formations.

The aim of the current study is to demonstrate the use of geochemical modeling as a tool for evaluation of groundwater – rock systems with respect to their suitability for radioactive waste disposal. Case studies are presented to exemplify the applicability of the developed method.

Geochemical tools for evaluation of groundwater – host rock systems

Since many potential sites for repositories are situated in water-saturated formations, slow water transport or even better stagnant formation water is considered to be a preferable condition. A long residence time of water is indicated by saturation or oversaturation of the formation water with respect to the solid phases of the bedrock. Moreover, geochemically stable conditions within a formation, which are reflected by an equilibrium between formation water and host rock, are considered as positive. The contrary reasoning is not valid, because a calculated disequilibrium (undersaturation) of the site-specific rock-water system may result from solution mixing with groundwater of other formations, dissolution of the bedrock by non-stagnant groundwater, metastable equilibria, heterogeneous occurrence of mineral phases, or inadequate knowledge about the mineral phases. Because of large uncertainties involved in determining the saturation state of the rock-water system, calculation may facilitate the appraisal of non-stagnant formation water conditions. Still, calculated (over-) saturation of groundwater with respect to the host rock is a reasonable indicator for favorable conditions. The generation of mobile radionuclide species and their migration are determined by various geochemical reactions. These reactions are influenced by environmental variables, especially by pH, redox conditions, ionic strength, content of organic matter and pCO_2. In general, the definition of geochemically favorable conditions is not straightforward, because the mentioned reactions are rather complex and interdependent.

By means of geochemical modeling, it is possible to deal comprehensively with the complex reactions and the variety of involved species. Therefore modeling should be examined as an evaluation tool to determine the site specific geochemical environment and the radionuclide concentrations depending on the environmental conditions. Moreover, for evaluation of the radionuclide retention capacity and solubility in the specific geochemical environment of an underground repository, the chemical properties of the groundwater – host rock system including radioactive waste forms, containers and backfilling materials has to be considered. The corrosion of the waste form changes the solution compositions, resulting in significant changes of radionuclide solubilities [2, 3]. Such an evaluation cannot be done on a sole experimental basis due to the large variety of possible conditions governed by the repository site, waste and backfilling materials. To resolve this problem, reaction path modeling can be used to simulate corrosion of radioactive waste and the associated radionuclide release in the geochemical environment governed by the specific conditions of the repository, e.g. [2 - 7].

Modeling methods

Determination of saturation states of rock formation – groundwater systems

In the first step of evaluation, a potential host formation is geochemically characterized, i.e., analysis of the formation water composition and the bedrock is performed. Using the measured concentrations of dissolved elements and the mineralogical composition of solid, speciation in solution and subsequently the saturation state of formation water with respect to the mineral phases are calculated.

Modeling of compatibility of radioactive waste forms with site-specific environments

Compatibility of a groundwater – host rock system for a radioactive waste derives from the impact of the groundwater and the geomatrix on radionuclide release from the corroding waste form. Reaction path modeling of waste corrosion at specific conditions is used to examine compatibility. A fundamental assumption for the application of reaction path modeling to describe waste corrosion in a deep bedrock repository is the existence of local thermodynamic equilibrium. Due to the effective function of near-field barriers, a "quasi closed" system can be adopted [3]. Exchange processes between the quasi closed system and the open natural system are limited and controlled by slow diffusive processes. Thus, local thermodynamic equilibrium

between the solution and solid phases is established at pertinent time scales. The validity and limitations of this assumption are discussed in [8, 9]. The benefit from the quasi closed system approach lies in the fact that thermodynamic reaction path modeling effectively describes the systems under consideration. Kinetically controlled radionuclide release processes account only for easily soluble radionuclides (e.g. Sr) but not for long-term behavior of actinides. In a study on long-term leaching of full-scale cemented radioactive waste forms [2] reaction path modeling was successfully applied to describe the experimental results.

Program codes and databases

Modeling is carried out using the Geochemist's Workbench code [10] and the EQ3/6 software package [11]. Application of different thermodynamic databases (e.g., databases with Debye-Hückel or Pitzer parameters) allows comparisons between sites of different salinities. The original EQ3/6 thermodynamic databases (data0.com and data0.pit for diluted and saline solutions, respectively) are extended for the considered radionuclides, Si, Al and Fe and checked for consistency. The same databases are applied for both EQ3/6 and Geochemist's Workbench calculations.

Application of evaluation methods

In order to demonstrate the use of geochemical modeling within a evaluation process, representative case studies are performed on (1) determining the saturation state of rock formation – groundwater systems and (2) simulating interactions between radioactive waste and groundwater.

Case studies regarding saturation state of the rock formation – groundwater system

In the current study several granitic and argillaceous rock-water systems are assessed with respect to their saturation states. The saturation state index, SI, of a solution with respect to a solid phase is defined by $SI = log(IAP/K_{sp})$, where IAP denotes the ion activity product of the solution, and K_{sp} denotes the solubility product of the solid phase. The studied granite solutions (Table 1) originated from Äspö, Sweden and Böttstein, Switzerland.

The studied granitic groundwater from Äspö and Böttstein are considerably undersaturated with respect to the vast majority of primary minerals. The Böttstein groundwater samples are saturated or close to saturation with respect to a large variety of secondary minerals, e.g., calcite, dolomite, siderite, hematite, fluorite phases and

Tab. 1: Compositions of granite groundwater, argillaceous porewater and NaCl brine.

	Böttstein 400 m[a]	Böttstein 618 m[a]	Äspö 530 m[b]	Opalinus SOPW2[c]	FEBEX s/l 3.3[d]	granite EGW[e]	NaCl brine[f]
conctr.	[molal]	[molal]	[molal]	[molal]	[molal]	[molal]	[molal]
Na^+	1.5E-02	1.7E-02	9.1E-02	2.5E-01	8.0E-01	4.1E-03	6.23
K^+	2.2E-04	2.5E-04	2.1E-04	5.8E-03	7.5E-03	5.1E-05	0
Mg^{++}	1.1E-05	9.9E-06	1.7E-03	2.1E-02	3.9E-01	n.d.	0
Ca^{++}	2.4E-04	2.7E-04	9.6E-03	2.9E-02	3.0E-01	6.0E-05	0
Sr^{++}	4.7E-06	5.1E-06	4.0E-04	3.0E-04	6.2E-03	n.d.	0
Ba^{++}	2.9E-07	1.8E-07	n.d.	n.d.	n.d.	n.d.	0
Mn^{++}	2.2E-06	3.3E-06	5.3E-06	n.d.	n.d.	n.d.	0
Fe(tot)	7.3E-05	4.1E-05	4.4E-06	4.0E-06	n.d.	n.d.	0
F^-	6.6E-04	6.6E-04	7.9E-05	n.d.	n.d.	3.0E-04	0
Cl^-	3.4E-03	3.5E-03	1.8E-01	n.d.	1.2E-01	2.9E-03	6.23
Br^-	1.0E-05	1.3E-05	5.0E-04	n.d.	4.9E-03	n.d.	0
SO_4^-	3.2E-03	3.5E-03	5.8E-03	2.8E-02	6.0E-01	n.d.	0
HCO_3^-	4.8E-03	6.3E-03	1.6E-04	n.d.	6.7E-02	4.6E-04	0
Al^{+++}	3.3E-07	5.1E-07	1.0E-06	6.0E-06	3.4E-04	n.d.	0
$SiO_2(aq)$	1.2E-03	1.4E-03	1.5E-04	2.9E-04	1.1E-02	2.1E-03	0
pH	8.	8	8.1	8	7.49	8.7	7.0

n.d. = not determined. (a) Granitic groundwater from Böttstein borehole [14]. (b) Granitic groundwater from Äspö borehole KAS02 [12]. (c) Synthetic Opalinus clay porewater conditioned with crushed Opalinus clay [17]. (d) FEBEX bentonite porewater extracted by squeezing; solid/liquid ratio (s/l) of 3.3:1 [16]. (e) Synthetic equilibrated granite water [18]. (f) NaCl brine [18].

with respect to quartz, mica (annite), chlorite. The studied Äspö groundwater is close to saturation only with respect to quartz and to secondary minerals saponitic smectite and calcite. In granites from Äspö and Böttstein, quartz has been found in the primary mineral assemblage and in the fracture fillings as well [12 - 14]. Chlorite is identified as the major mineral of fracture fillings in Äspö granite [12 - 13]. Hence, it is likely that secondary quartz and chlorite rather than primary quartz and chlorite are in equilibrium or close to equilibrium in the solutions. Though the granitic groundwater samples are saturated with respect to fracture filling minerals, undersaturation of major primary minerals may be explained by considerable groundwater transport and continued dissolution of geomatrix. The results are in agreement with geohydrological observations at both sites [13, 15]. Based on the geohydrological situation at the Böttstein site, it appears that this site is not suitable for disposal of radioactive waste [15]. In research programs on waste disposal in a granite, it is envisioned to embed radioactive waste within bentonitic backfilling material in order

to prevent radionuclide migration by groundwater flow, e.g., [19, 20]. Since smectite, the major mineral of bentonite, is close to saturation with the Äspö groundwater, it dissolves very slowly in the studied solution. The effect of saturation state on smectite dissolution kinetics is discussed in detail by [21, 22].

(In-situ) compositions of porewater extracted from various argillaceous rocks have been published in recent studies ([17, 23] and references therein). However, the reported porewater compositions in these studies do not comprise all the elements needed for reliable calculations of the saturation state with respect to clay minerals and other alumosilicates, which are the dominant phases of argillaceous rocks. A comprehensive composition of Opalinus clay porewater (Table 1) is given by [24]. The Mont Terri Opalinus clay consists mostly of clay minerals (illite, illite/smectite, kaolinite and chlorite) and minor amounts of quartz, carbonates and feldspars [24]. In addition to the Opalinus porewater, a porewater extracted from the reference bentonite of the Full Scale Engineered Barriers Experiment, FEBEX, was used in this study (Table 1). FEBEX bentonite is composed of a mixed layer illite/smectite with 85-90% montmorillonitic smectite, and minor amounts of quartz, cristobalite and feldspars [21].

In contrast to the studied granitic groundwater, the Opalinus and FEBEX porewater samples were taken from closed-system equilibration experiments. The calculations demonstrate both porewater samples are in equilibrium with the dominant mineral smectite. Accessory cristobalite is close to equilibrium in the FEBEX system and phlogopite in equilibrium in the Opalinus system. Other minerals are undersaturated in Opalinus and FEBEX porewater.

For the Opalinus and FEBEX porewater as well as for Äspö granite groundwater, equilibrium is calculated with respect to saponitic smectite, whereas montmorillonitic smectite is calculated to be undersaturated. However, mineralogical characterizations of the FEBEX and Äspö fracture filling material show that in both cases the smectite content is of montmorillonitic and not of saponitic composition [21, 12]. Concerning the uncertainty in determining solubility constants (K_{sp}) of various smectites [22], differences between saturation states of both smectites have to be considered as insignificant.

Case studies regarding compatibility of radioactive waste with a site-specific environment

Evaluation of the compatibility of a site specific geochemical environment with a radioactive waste form is demonstrated using the case studies on spent UO_2 fuel corrosion, namely, corrosion of spent UO_2 fuel in granite groundwater and in NaCl brine. Interactions were studied in experiment at FZK-INE [18] and by reaction path modeling. Parallel experiments were carried out with addition of iron powder and without iron. Details on the static corrosion experiments are presented in [18]. Compositions of the used synthetic granite groundwater and NaCl brine are given in Tab. 1. Tab. 2 presents the composition of the used UO_2 fuel from the Gösgen power plant (Switzerland). Besides their difference in ionic strength, the two solutions differ with respect to their content of dissolved inorganic carbon. The release of Sr, Cs, U, Np, Pu and Am have been investigated. Since the focus of this communication is on evaluation of different groundwater – host rock systems, the results of Am and Np are presented as examples.

Tab. 2: Composition of spent UO_2 fuel [25]).

	Am	Cs	Mo	Nd	Np	Pu	Sr	U
concentration [mol kg^{-1}]	0.01	0.02	0.03	0.03	0.04	0.05	0.01	3.91

Spent fuel corrosion in granite groundwater and in NaCl brine show different evolution of the solution compositions and consequently different solubilities of radionuclides. In the NaCl brine, the pH increased from 7 to 9.7. In contrast, a decrease of less than 0.5 pH units was observed in the experiment with granite groundwater. Fig. 1 shows the variation of Np and Am concentrations as a function of the reaction progress in units of dissolved spent fuel mass per mass H_2O. Concentrations of both actinides in the granite groundwater experiment differ significantly from the concentrations in the NaCl brine experiment.

(a)

(b)
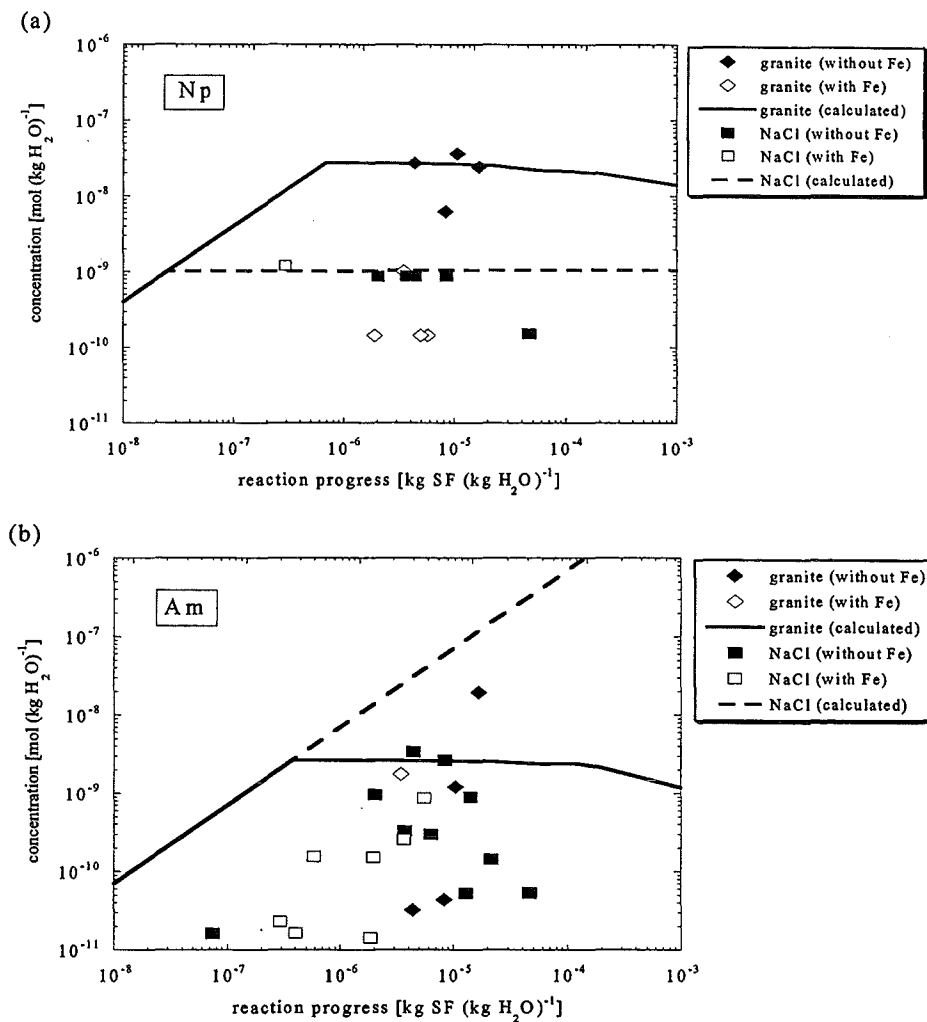
Fig. 1: Corrosion of spent UO2 fuel in granite groundwater and NaCl brine. Measured and calculated variation of Np (a) and Am (b) concentration as a function of corrosion progress.

In NaCl brine a Np concentration of 10^{-9} molal and in granite groundwater of around $3 \cdot 10^{-8}$ molal (Fig. 1a) is computed applying $Np(OH)_4$(am) as solubility limiting phase. The relative high neptunium concentration in the granite groundwater is due to the formation of aqueous Np-carbonato species, predominantly $Np(OH)_3(CO_3)^-$. Experiments in NaCl brine were free of CO_2, and the dominant aqueous species was $Np(OH)_4$(aq). Calculated Np concentrations correspond reasonably to measured concentrations in NaCl brine experiments as well as in granite groundwater experiments without iron powder. In granite groundwater experiments with Fe, measured Np concentrations were below the $Np(OH)_4$(am) solubility concentration. Probably after the release of Np from corroding spent fuel, it was sorbed onto surfaces of iron corrosion products.

In granite groundwater, precipitation of $AmCO_3OH$(cr) is calculated to control americium concentration at $3 \cdot 10^{-9}$ molal (Fig. 1b), and the dominant aqueous species

is $Am(CO_3)_2^-$. In contrast, the Am speciation in carbonate free NaCl brine is dominated by $Am(OH)_2^+$, and Am concentration is not limited by precipitation of any solid phase within the range of computed reaction progress (Fig. 1b). Measured americium concentrations in granite groundwater scatter between 10^{-12} and 10^{-9} molal. Only one Am concentration value was determined significantly above the calculated solubility concentration (Fig. 1b). Similarly, measured Am concentrations in NaCl brine are in the range of 10^{-12} to $3 \cdot 10^{-8}$ molal (Fig. 1b). Since Am is sorbed to some extent onto surfaces of iron corrosion products in experiments with iron [18], measured Am concentrations are partly lower than computed concentrations.

In order to assess the compatibility of a site specific environment with radioactive waste, one has to take into account the chemical development of all relevant radionuclides. At this point, it is emphasized that application of reaction path modeling enables us to deal with the evolution of pH and the aqueous and solid species of the radionuclides. Hence this tool provides necessary information to evaluate compatibility.

Conclusions

A catalog of environmental variables and their favorable ranges is needed for evaluation of potential repository formations. However, selection of suitable conditions is generally not a straightforward process, because of the multitude and complexity of the reactions involved. In order to evaluate different groundwater – host rock systems, modeling can be sued to comprehensively describe geochemical environments and their impacts on radionuclide mobilization. Geochemical modeling is a tool feasible of assessing the effect of environmental variables and handling complex processes such as corrosion of radioactive waste forms.

The saturation of a groundwater with respect to the host rock and the compatibility of a groundwater – host rock system for a waste form are important properties to the evaluation process. Groundwater saturation is considered a positive indicator for a quasi-closed system. It is shown that the comparison of different groundwater – rock systems based on mineral saturation states can be used to identify suitable host formations. Reaction path modeling is an essential tool for evaluation of the geochemical compatibility of a host rock for radioactive waste. Calculations show the significant dependence of radionuclide mobilization on both the waste form and the groundwater – host rock system. In subsequent site selection process, geochemical

modeling must be based on detailed information about the geological site, the waste form, the planned repository structure and the backfilling concept, in order to yield site specific predictions of radionuclide mobilization.

References

1. Andersson, J., Ström, A., Svemar, C., Almén, K. E. and Ericsson, L. O., 2001. Proc. 9th Int. High-Level Radioactive Waste Management Conf., Las Vegas, USA.

2. Kienzler, B., Vejmelka, P., Herbert, H. J., Meyer, H. and Altenhein-Haese, C., 2000. Nucl. Technol., 129, 101-118.

3. Kienzler, B. and Metz, V., 2001. Proc. 9th Int. High-Level Radioactive Waste Management Conf., Las Vegas, USA, p. 2.1/1-4.

4. Bourcier, W. L., 1990. Mat. Res. Soc. Symp. 1990, 176, 209-216.

5. Kienzler, B., Luckscheiter, B., Wilhelm, S., 2001. Waste Management (in press).

6. Kim, J.-I., and Grambow, B., 1999. Eng. Geol., 52, 221-230.

7. Metz, V., Kienzler, B. and Schüßler, W., 2002. J. Contam. Hydrology (submitted).

8. Brown, P. L. and Lowson, R. T., 1997. J. Contam. Hydrol. 26, 27-34.

9. van der Lee, J. and De Windt, L., 2001. J. Contam. Hydrol. 47, 265-282.

10. Bethke, C., 2000. The Geochemist's Workbench. University of Illinois.

11. Wolery, T. J., 1992. EQ3/6, A Software Package for Geochemical Modeling. Lawrence Livermore National Laboratory, Livermore.

12. Ekberg, C., 1999. Ph. D. thesis, Chalmers University of Technology, Göteborg.

13. Laaksoharju, M. and Wallin, B., 1997. Proc. 2nd Äspö Int. Geochemistry Workshop, June 1995. Svensk Kärnbränslehantering AB, Stockholm.

14. Wittwer, C., 1986. NTB 85-49 report, NAGRA, Wettingen.

15. HSK, 1996. Hauptabteilung der Sicherheit der Kernanlagen des Bundesamtes für Energie, Villigen.

16. ENRESA, 2000. Publicación Técnica 1/2000, Madrid, Spain.

17. Bradbury, M. H. and Baeyens, B., 1998. Geochim. Cosmochim. Acta 62, 783-795.

18. Grambow, B., Loida, A., Martinez-Esparza, A., Diaz-Arocas, P., de Pablo, J., Paul, J.L., Marx, G., Glatz, J.P., Lemmens, K., Ollila, K. and Christensen, H., 2000. FZKA 6420, Karlsruhe, Germany.

19. SKB, 1997. Technical Report 96-25. Svensk Kärnbränslehantering AB, Stockholm.

20. SKB, 1999. Technical Report TR-99-28. Svensk Kärnbränslehantering AB, Stockholm.

21. Cama, J., Ganor, J., Ayora, C. and Lasaga, A. C., 2000. Geochim. Cosmochim. Acta 64, 2701-2717.

22. Metz, V., 2001. Ph.D. thesis, Ben-Gurion University of the Negev, Beer Sheva.

23. Bradbury, M. H. and Baeyens, B., 2000. J. Contam. Hydrol. 42, 141-163.

24. Lauber, M., Baeyens, B. and Bradbury, M. H., 2000. Paul Scherrer Institut Bericht PSI 00-10, Villigen.

25. Grambow, B., Loida, A., Dressler, P., Geckeis, H., Gago, J., Casas, I., de Pablo, J., Giménez, J. and Torrero, M. E., 1996. FZKA 5702, Karlsruhe.

II.   Comparison of double layer models in transport problems

(J. Lützenkirchen, B. Kienzler, INE)

Abstract

Experimental data for ion adsorption to minerals surfaces can be fitted using a wide range of models, although the description of acid-base properties of the mineral surfaces may be very bad. In transport problems with variations of pH, such model short comings are shown to be crucial for the ion breakthrough.

Zusammenfassung

Experimentelle Daten zur Ionen Adsorption an mineralischen Oberflächen können mit einer ganzen Bandbreite von Modellen beschrieben, obwohl die Beschreibung der Säure-Base Eigenschaften der Mineraloberfläche sehr schlecht ist. Bei Transportvorgängen mit variierenden pH Werten sind schlechte Eigenschaften des Säure-Base Models von Bedeutung für den Durchbruch des Ions.

Introduction

For the description of adsorption phenomena on oxide minerals a wide range of (semi)mechanistic surface complexation models are available. They have in common that they separate the free energy of adsorption into an intrinsic chemical and a coulombic contribution. By defining surface species in terms of surface chemical reactions and reactivities the intrinsic contribution is qualitatively defined. The coulombic term is determined by the structure of the electrical double layer, which forms at charged solid/water interfaces. The contributions to the overall free energy of the formation of surface species can be computed if one assumes a picture for the two aspects.

Unfortunately, a wide range of pictures exist how surface species are defined and how the electrical double layer is envisioned. This may for example be due to different objectives of the modelling i.e. a simple or a comprehensive model may be used to either just describe data or to attempt a structural representation on the macroscopic level, respectively.

There is at present no way to experimentally distinguish quantitatively between the contributions of the two terms and modellers are free to combine different

complexities of the various components of surface complexation theory, which results in a wide range of model variations.

Theory

Thus the various existing models differ in the way the different components of the surface complexation approach are treated. The fundamental model is usually decided on when the sorbent acid-base properties are described, although some features still can be added in the subsequent modelling of the contaminant adsorption data. On the simplest level of surface complexation theory possible components of any model encompass decisions on:

- The proton ad(de)sorption mechanism: one may assume a 1-pK or a 2-pK protonation mechanism. The 1-pK approach involves only one proton ad(de)sorption step within the usual range of pH, so that surface groups will be present in no more than two states. The 2-pK approach generally involves two consecutive protonation steps (3 states) within a relatively narrow range of pH (the range is dependent on model parameterisation).

- The treatment of surface heterogeneity: one may distinguish between discrete and continuous heterogeneity. Discrete heterogeneity involves the allocation of a specific affinity to a specific type. The simplest case would be a one site model with a defined stability constant for all species formed on this site. Continuous heterogeneity involves a distribution function for the reactivities. The most complex case would be a multi-site model with distribution functions for all species formed on all sites.

- Electrical double layer: one has to account for the contribution of charge formation at the oxide/electrolyte interface. This is possible by defining a model for the structure of this interface. Different models of various degree of complexity exist which allow a more or less detailed picture (see figure 1).

With the complexity of the model, the number of parameters required usually increases. From various modelling exercises it has become clear that parameters are frequently correlated with each other and that a unique model parameter set can rarely be obtained. Combination of methods (i.e. macroscopic adsorption data with structural "microscopic" data) may improve that issue to some extent in particular for well-defined sorbents.
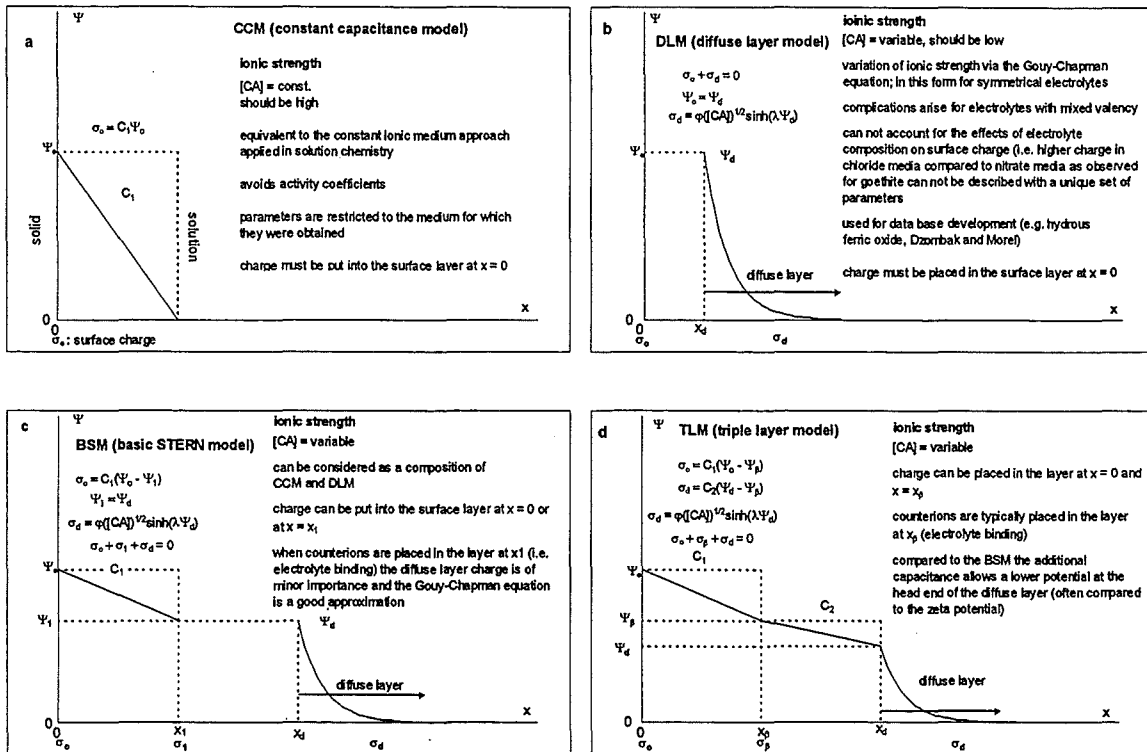
Fig. 1: Electrostatic standard models as they are used in standard speciation codes handling surface complexation models

Results

In general many models will yield good descriptions of one data set. This is shown for goethite surface charge in figure 2. In this example two advanced approaches to handle multi-site features (discrete heterogeneity) with predicted proton affinities (Hiemstra et al. [1] based on goethite bulk structure; Rustad et al. [2] based on molecular modelling) allow a very similar description of goethite surface charge, although the individual contributions to the charge are very different in the two models.

Approaches to compare the respective model performances are desirable. In this contribution an attempt is made to compare the performance of various models in transport problems. This attempt encompasses model calibration on available batch adsorption data and subsequent application in predicting breakthrough curves with the individual models under identical hydrodynamic conditions.

In a first step the surface complexation models tested is applied to a set of adsorption data. This encompasses the respective modelling of the acid-base properties of the sorbent and the use of the extracted model parameters in the fitting of the adsorption data.
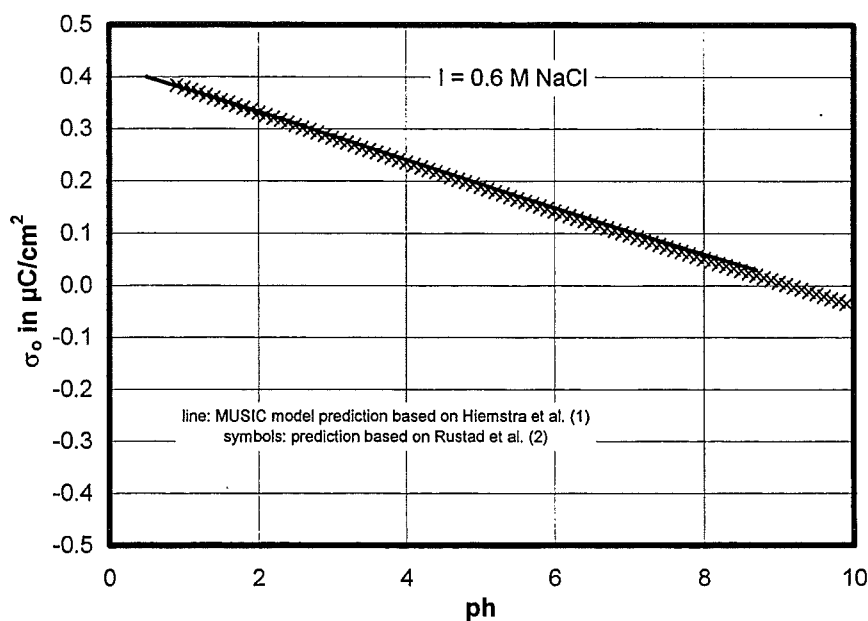
Fig. 2: Prediction of goethite surface charge based on two different approaches. ph is the negative logarithm of the free proton concentration.

The descriptions of the adsorption data are usually in good agreement. However, the underlying proton data (i.e. surface charge vs. pH curves) may show differences concerning the goodness of fit. In the description of static batch adsorption experiments this is not crucial since the outcome of interest (i.e. the description of the adsorption curves) is similar. However, concerning dynamic column experiments two situations may be discussed:

- situations where the system is buffered with respect to the pH: here it is expected that models which are equally successful in describing batch experimental data will result in comparable breakthrough curves.

- situations where a pH front moves through the system: in such cases it is expected that the quality of the underlying acid-base model (i.e. the description of surface charge vs. pH curves) will strongly influence the breakthrough curve.
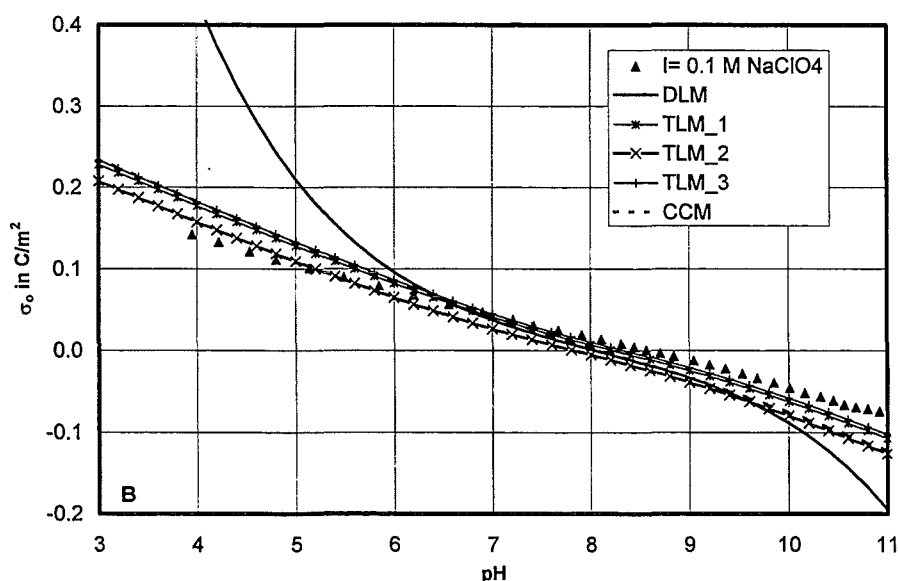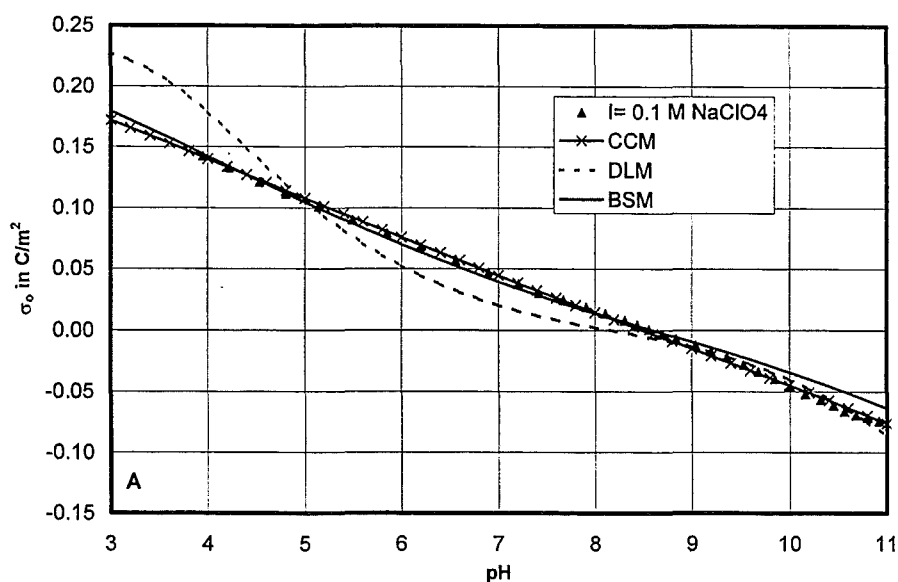
Fig. 3: Model adjustment to surface charge data from Rabung et al. (3) with differentsurface complexation models. CCM: constant capacitance model.

Different surface complexation models have been used to obtain a good model for batch titration of γ-Al_2O_3 (3) and model data sets for metal ion adsorption comparable to Eu sorption have been obtained and described within the framework of both the above mentioned models and predictions based on work by Sverjensky and co-workers [4].

The results for the acid-base properties are shown in figures 3 (model adjustment, best fit, A) and 4 (predictions based on (4) without adjustment, B).

It can be seen as has been stated in previous comparisons that the DLM is typically much less successful compared to other models on a best fit basis (figure 3A). The predictions (figure 3B) are by far less successful in describing the data set compared to the best fit results. In particular the prediction by the DLM is very poor.

Figure 4 shows the model data set (created on the basis of Eu adsorption data for Eu onto γ-Al$_2$O$_3$ (3) and the CCM in figure 3A and the best fit based on the "worst case" model from figure 3B. It is obvious that despite the very poor acid-base model the model adsorption data can be very accurately reproduced. The different electrostatic contributions are adjusted through the respective intrinsic contributions such that the overall free energy of adsorption remains the same for these cases.
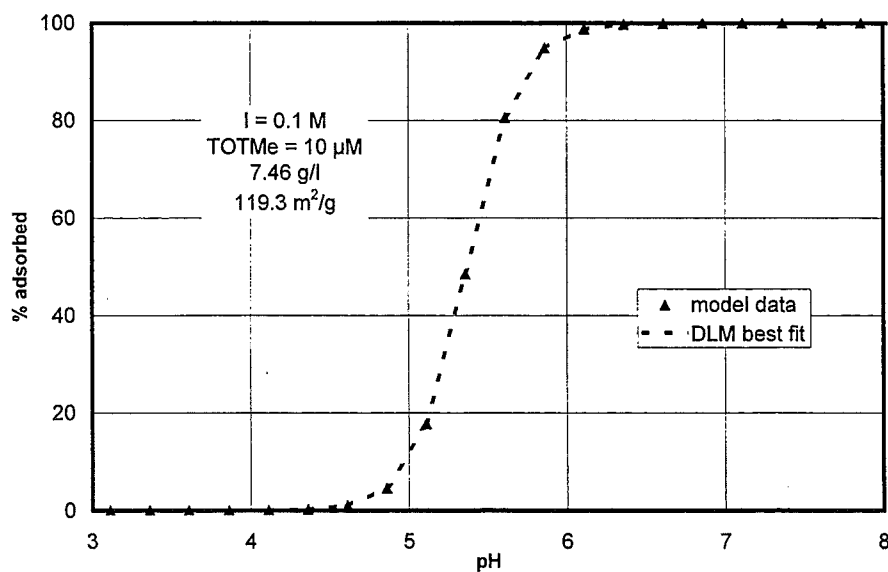
Fig. 4: Description of a model adsorption data set (filled triangles, created by a CCM, comparable to Eu sorption onto γ-Al$_2$O$_3$) by the DLM model given in Fig. 3B.

While the batch adsorption modelling does not allow to single out inappropriate metal adsorption models, reactive transport codes applied with the different model variations applied to variable pH conditions make the difference between a good and an inappropriate model (results not shown).

References

1. Hiemstra, T., Venema, P., and Van Riemsdijk, W.H. 1996, J. COLLOID INTERFACE SCI. *184*, 680. Venema, P., Hiemstra, T., Weidler, P. G. and van Riemsdijk, W.H. 1998. J. COLLOID INTERFACE SCI. *198*, 282.

2. Rustad, J.R., Felmy, A.R., and Hay, B.P. 1996, GEOCHIM. COSMOCHIM. ACTA *60*, 1553. Rustad, J.R., Felmy, A.R. , and Hay, B.P. 1998, GEOCHIM. COSMOCHIM. ACTA *60*, 1563. Felmy, A.R. , and Rustad, J.R. 1996, GEOCHIM. COSMOCHIM. ACTA *62*, 25.

3. Rabung, T., Stumpf, T., Geckeis, H., Klenze, R. and Kim J.I. 2000, Radiochim. Acta *88*, 711.

4. Sverjensky, D.A. GEOCHIM. COSMOCHIM. ACTA *65*, 3643. Sahai, N. and Sverjensky, D.A. GEOCHIM. COSMOCHIM. ACTA *61*, 2801. Sahai, N. and Sverjensky, D.A. GEOCHIM COSMOCHIM ACTA *61*, 2827. Sverjensky, D.A. and Sahai, N. GEOCHIM COSMOCHIM ACTA *60*, 3773.

32.26 IMMOBILISIERUNG VON HOCHRADIOAKTIVEM ABFALL

(W. Grünewald, G. Roth, INE)

Zusammenfassung

Neben den Forschungsarbeiten zur Langzeitsicherheit werden vom INE Planungs-arbeiten für den Hauptprozessbereich der zwischenzeitlich im fortgeschrittenen Baustadium befindlichen Verglasungseinrichtung Karlsruhe (VEK) durchgeführt. Diese Arbeiten beinhalten u. a. Auslegung und Design von Apparatekomponenten inkl. des Schmelzofens. Der aktuelle Schwerpunkt der Arbeiten lag im Berichtsjahr auf der Ausarbeitung der Genehmigungsunterlagen für den aktiven Schmelzofen der VEK, der vom INE gebaut und geliefert wird. Hierbei wurden u.a. die aus 18 Baugruppen bestehenden Vorprüfunterlagen des Schmelzofens als Teil der 3. Teil-errichtungsgenehmigung (TEG) erstellt. Die 3. TEG wurde Mitte November erteilt. Ein weiterer Schwerpunkt bildete die verantwortliche Prüfung der Realisierung der E- und Leittechnik-Konzeption für die Gewerke Prozessleitsystem, Maschinentechnik, Verfahrenstechnik und Raumlufttechnik inklusive der gewerkespezifischen Prüfung der Vorprüfunterlagen. Neben den Tätigkeiten zur Anlagentechnik erfolgte die Bearbeitung des Handbuchs zur Verfahrensqualifikation zur Absicherung des erzeugten Glasproduktes. Das Handbuch wurde zusammen mit begleitenden Berichtsunterlagen über die Glasentwicklung fertiggestellt und vom FZK im Dezember 2001 an die Bundesanstalt für Strahlenschutz (BfS) als Genehmigungs-behörde eingereicht.

Weitere Arbeiten des INE betreffen die Anwendung der Verglasungstechnologie des Forschungszentrums Karlsruhe für eine von UKAEA (United Kingdom Atomic Energy Authority) in Dounreay/Schottland geplante Verglasungsanlage für hochradioaktive Spaltproduktlösungen aus der Wiederaufarbeitung von Schnellbrüterbrennstoff. Bei der von UKAEA Dounreay durchgeführten neuerlichen Ausschreibung zur Auswahl einer Hauptprozesstechnologie (Core Technology) für die Dounreay Vitrification Plant (DVP) hat sich das Forschungszentrum im Verbund mit der britischen Firma AEAT vorqualifiziert. In einer anschließenden Prozedur zur Bewertung der Technologie und zur Entscheidungsfindung wurde ein umfangreicher Fragenkatalog beantwortet und im November die Technologie im Rahmen einer Präsentation in Dounreay vorgestellt. Eine Entscheidung wird für Frühjahr 2002 erwartet. Bei positivem Ausgang für die FZK Technologie würde das Konzeptdesign in der zweiten Hälfte 2002 beginnen.

32.26.01 Technologie zur Verglasung der hochradioaktiven Spaltprodukt-lösungen der WAK in einer Standortverglasungsanlage

Die Beiträge des INE für das VEK-Projekt umfassten im Berichtsjahr drei Themen-schwerpunkte: Erstellung der genehmigungsrelevanten Ausführungsunterlagen für den Bau des keramischen Schmelzofens, Planungsüberwachung der elektro- und leittechnischen Einrichtungen und ihrer Realisierung sowie Ausarbeitung der Genehmigungsunterlagen zum Glasprodukt (Verfahrensqualifikation).

VEK-Schmelzofen

Die Ausführung der 3. Teilerrichtungsgenehmigung für die VEK beinhaltet die Installation der technischen Gewerke wie z. B. die verfahrenstechnischen und maschinentechnische Einrichtungen. Hauptbeitrag des INE ist hierbei die Lieferung des keramischen Schmelzofen und einer baugleichen Reservekomponente. Der Gesamtauftrag umfasst die Erstellung aller technischen Unterlagen, die für die Genehmigung und Fertigung erforderlich sind, die Fertigung sowie die Abwicklung von Unteraufträgen an Zulieferfirmen. Zur Qualitätssicherung der kerntechnischen Komponenten war nach den gültigen kerntechnischen Regularien folgende Vor-gehensweise erforderlich:

Erstellung einer Sonderspezifikation für den Schmelzofen

Die Sonderspezifikation beinhaltet eine detaillierte technische Beschreibung des Schmelzofens und seiner Komponenten. Die qualitätssichernden Maßnahmen für die Fertigung sind beschrieben und der genaue Auftragsumfang ist definiert. Diese Unterlage muss vom Gutachter (TÜV Südwest) begutachtet und freigegeben werden.

Erstellung der Vorprüfunterlagen (VPU) für die Fertigung

Der Schmelzofen gliedert sich in 18 Baugruppen. Für jede einzelne Baugruppe muss eine separate Vorprüfunterlage erstellt werden. Inhalt jeder Vorprüfunterlage ist :

- Auslegung und Konstruktion in Form von Datenblättern, Fertigungs-Zeich-nungen, Schweißplänen und Stücklisten
- Nachweise durch Berechnungen auch im Hinblick auf die Ereignisse Flugzeug-absturz und Bemessungserdbeben
- Spezifizierung der Werkstoffe anhand von Werkstoffprüfplänen

- Bauüberwachung durch einen Bauprüfplan
- Weitere Unterlagen bzw. Spezifikationen wie Werkstoffprüfblätter und technische Datenblätter

Diese Unterlagen gehen ebenfalls zum Gutachter und müssen für die Fertigung freigegeben werden.

Fertigung gemäß genehmigter VPU

Die Fertigung folgt nach den genehmigten Vorgaben in den Vorprüfunterlagen. Darüber hinaus wird eine umfassende Dokumentation erstellt.

Bis Juli 2001 wurden die für den Bau des Schmelzofens wesentlichen Baugruppen 1 bis 16 (Schmelzofenkeramik, Edelstahlgehäuse, Elektroden sowie alle Anbauteile) erstellt und dem Gutachter übergeben. Die Prüfung ist abgeschlossen und eine vorgezogene Fertigungsfreigabe erteilt. Die restlichen beiden Baugruppen betreffen Hilfseinrichtungen und Verbindungsteile für den Einbau des Schmelzofens und wurden bis Dezember 2001 fertiggestellt. Die schmelzofenbezogenen Arbeiten des INE liegen im vorgegebenen Zeitrahmen des VEK-Projektes.

E- und Leittechnik

Innerhalb des VEK-Projektes führt INE verantwortlich die Abwicklung der Vorprüfung für die Elektro- und Leittechnik durch. Dies betrifft hauptsächlich die Fachtechnik für die Elektro- und Leittechnik, die Verfahrenstechnik, die Maschinentechnik, die Sicherheitstechnik, die Raumluft- und Kernstrahlungsmesstechnik sowie für die Kommunikationsanlagen. Die Prüfergebnisse der Planungsfirmen der einzelnen Gewerke der VEK und des späteren Betreibers sowie INE-eigene fachtechnische Prüfergebnisse werden zusammengeführt und gegebenenfalls Überarbeitungen durchgeführt bzw. veranlasst. In diesem Zusammenhang ist INE Ansprechpartner aller projektexternen Prüfstellen und Auftragnehmer für die VEK im Bereich der Elektro- und Leittechnik. Diese Arbeiten wurden dieses Jahr begonnen und dauern bis Ende 2002 an.

Glasproduktuntersuchungen und Verfahrensqualifikation

Das bei der Verglasung des WAK-HAWC in der VEK produzierte nukleare Abfallglas unterliegt einem separaten Genehmigungsverfahren, das vom Bundesamt für Strahlenschutz durchgeführt wird. Hauptsächliche Genehmigungsunterlage ist hierbei das Handbuch zur Verfahrensqualifikation, das im wesentlichen eine Beschreibung und Bewertung des Verfahrens im Hinblick auf die Erzeugung von spezifikationsgerechten Glaskokillen enthält. Die Klassifikation der Kokillen erfolgt auf der Basis einer Liste von 16 endlagerrelevanten Parametern/Garantiewerten. Im Hinblick auf die Einhaltung der Garantieparameter werden neben den verfügbaren Analysendaten des HAWC (nominelle Zusammensetzung) auch hiervon abweichende Zusammensetzungen betrachtet, wie sie betriebsbedingt auftreten könnten (z. B. bei der Restentleerung eines LAVA-Lagertanks, bei der eine höhere Konzentration an ungelösten Feststoffen eventuell zu erwarten ist). Zur Unterstützung des Genehmigungsverfahrens wurde zwei Wege beschritten: (1) Mit Hilfe des Testbetriebs der Prototypverglasungsanlage (PVA) konnte der Nachweis erbracht werden, dass dieses Verfahren geeignet ist, Glasgebinde herzustellen, die den Spezifikationen entsprechen. Dies wurde auch für abweichende Simulatlösungen demonstriert. Die Untersuchungen wurden durch zerstörungsfreie Prüfung des Glaszustandes in der Kokille ergänzt. Im Rahmen eines Technologieprogramms wurden Glasuntersuchungen an Laborgläsern und an Produktionsgläsern aus dem Testbetrieb der PVA durchgeführt, um den notwendigen Datensatz für das Qualifizierungsverfahren des VEK-Glasproduktes zu erhalten.

Computertomographische Untersuchungen einer Glaskokille

Bedingt durch die begrenzte Kapazität des Schmelzofens müssen die Glaskokillen (Inhalt 400 kg) in der VEK mit vier Chargen zu je 100 kg befüllt werden. Dieser Befüllmodus hat zur Folge, dass zwischen erstem und letztem Glasabstich ca. 2 Tage vergehen. Der Glasinhalt in der unbeheizten Kokille unterliegt in diesem Zeitraum Temperaturänderungen (Abkühlung zwischen den Abstichen und teilweise Wiederaufheizung durch die jeweils folgende Charge). Die Fragestellung war, wie sich diese Prozedur auf den Zustand auf des Glases auswirkt. Die zerstörungsfreie Untersuchung einer Glaskokille aus dem PVA-Betrieb erlaubte die Beurteilung der internen makroskopischen Struktur des Glasblocks und die Ermittlung seiner Ober-

flächenvergrößerung in Bezug zu einem monolithischen Block. Hierzu wurden zwei Methoden eingesetzt: Digitale Radiographie (DR) und Computertomographie (CT). Letztere erlaubt, die Existenz von Rissen und deren Verteilung im Glas festzustellen und daraus die Oberflächenvergrößerung zu ermitteln. Die DR gibt einen qualitativen Überblick über den Glasblockzustand. Die Ergebnisse der Untersuchungen eines Glasblocks aus dem PVA-Betrieb zeigt Abb. 1.

Die DR-Aufnahme zeigt, dass die Glaskokille im unteren Bereich zwei Lunker enthält. Die CT Aufnahmen zeigen, dass das Glas, das in 4 Teilchargen im Zeitabstand von ca. 15 h in die Kokillen abgefüllt wurde, nur wenige Risse enthält. Die durch Lunker und Risse bedingte Oberflächenvergrößerung relativ zum monolithischen Block betrug 6,8. Im Vergleich zu den üblichen Annahmen eines Oberflächenvergrößerungsfaktors von 20 ist dieser Wert relativ gering.

Glasproduktuntersuchungen

Das Ziel der Arbeiten war, die notwendige Datenbasis für das Qualifizierungsverfahren des VEK-Glasproduktes zu erhalten. An inaktiven Laborglasproben nominaler Zusammensetzung wurde ein Datensatz ermittelt, der die Viskosität, den spez. el. Widerstand, den Kristallisationsgrad, thermische Eigenschaften sowie Kurzzeit- und Langzeitkorrosionstests in verschiedenen Medien umfasste. Darüber hinaus wurden Proben untersucht, die Auswirkung transferbedingt variierender Feststoffgehalte im HAWC auf das Glasprodukt simulierten. Zur Vervollständigung wurden Gläser mit Sonderzusammensetzungen ebenfalls in das Untersuchungsprogramm einbezogen. Die Untersuchungsergebnisse zeigen, dass das Glasprodukt bis auf wenige Ausnahmen im Falle der Extremzusammensetzung die geforderten schmelztechnischen und qualitätsrelevanten Eigenschaften aufweist.

Glasbeladungsschwankungen bei der Nominalzusammensetzung innerhalb der vorgegebenen Grenzen von 16 ±3 Gew.% haben auf die relevanten Glaseigenschaften praktisch keine bzw. vernachlässigbare Auswirkungen. Mit steigender Beladung wird das Glas etwas dünnflüssiger und elektrisch leitfähiger und zeigt eine leicht erhöhte Kristallisationstendenz. Bei der Glaskorrosion liegen die Unterschiede innerhalb der Messgenauigkeit der normierten Massenverluste von Einzelelementen.

Vergleiche der Messdaten von Laborglasproben mit solchen von technisch herge-
stelltem Glasprodukt zeigen, dass die Laborglasdaten ohne Einschränkungen auf
das technisch hergestellte Produkt übertragbar sind. Ergebnisse hierzu sind in
Tabelle 1 gegeben. Sie enthält neben dem Vergleich der Glasprodukteigenschaften
für die Nominalzusammensetzung auch Eigenschaften von technisch hergestellten
Gläsern, die aus Simulatlösungen mit minimalem bzw. maximalen Gehalt an unge-
lösten Feststoffen erschmolzen wurden.
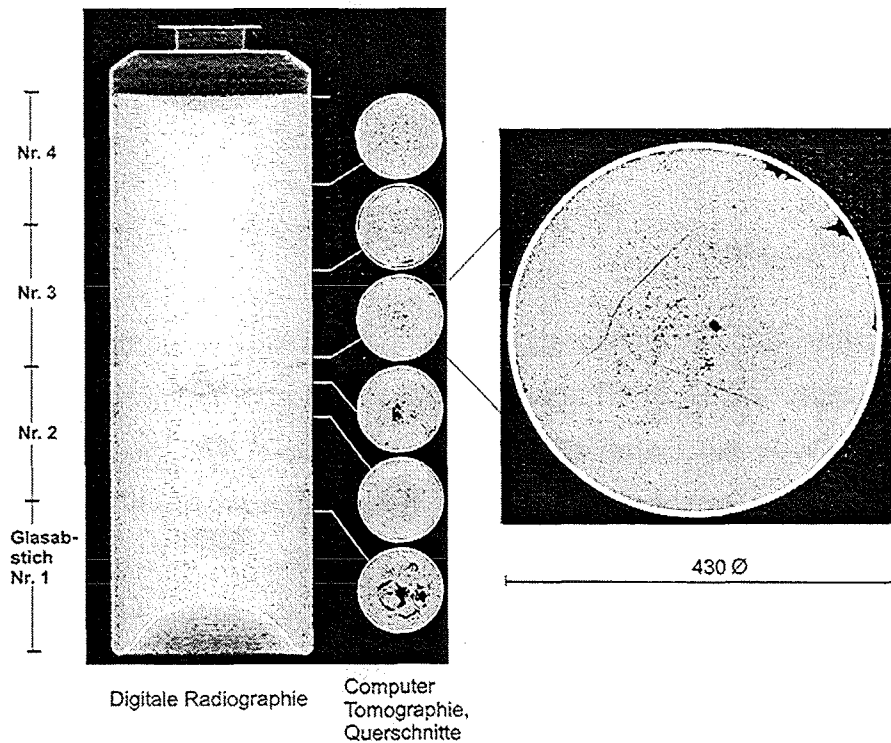
Abb. 1: Digitale Radiographie eines Glasblocks und typisches Aussehen von computer-
tomographischen Querschnitten in verschiedenen Höhen der Kokille.

Tab. 1: Vergleich der an technischen Glasprodukten aus dem PVA-Betrieb ermittelten physikalischen/ chemischen Daten mit Laborglasdaten

Eigenschaften	Labor-Glasprodukt (nominal)	Technische Glasprodukte PVA-1, HAWC$_{nom}$ [1]	PVA-3, HAWC$_{min}$ [2]	PVA-4, HAWC$_{max}$ [3]
Glasbeladung HAW-Simulatoxide	16 Gew.-%	16,4 Gew.-%	16,3 Gew.-%	16,3 Gew.-%
Viskosität bei 1150°C	47 dPa·s	42 dPa·s	36 dPa·s	48 dPa·s
Viskosität bei 950°C	530 dPa·s	450 dPa·s	330 dPa·s	519 dPa·s
Spez.elektr. Widerstand,1150°C	7 Ω·cm	6,8 Ω·cm	6,5 Ω·cm	6,8 Ω·cm
Spez.elektr. Widerstand, 950°C	21 Ω·cm	18,1 Ω·cm	17,5 Ω·cm	18,1 Ω·cm
Transformationstemperatur	504 °C	498-506 °C	486°C	493°C
Erweichungstemperatur	554 °C	531-544 °C	536°C	545°C
Therm.Ausdehnungskoeffizient (100-400°C)	9,6E-6 /°C	9,2-9,9E-6 /°C	10,6E-6 /°C	10,5E-6 /°C
Kristallisation (nach Temperung)	~ 3 Vol%	~ 5 Vol%	< 1 Vol%	< 1 Vol%

Auslaugresistenz Auslaugmedium, Zusammensetzung 1[1] (110°C, 112 Tage)

	Normierter Masseverlust g/m²	Normierter Masseverlust g/m²	Normierter Masseverlust g/m²	Normierter Masseverlust g/m²
Si	0,006	0,0075	0,0091	0,0057
B	1,43	1,48	1,02	0,99
Li	2,08	1,86	1,66	1,45
Ca	0,375	0,58	0,89	0,73
Sr	0,37	0,29	0,35	0,37
Mo	0,82	0,30	1,10	0,74
Ce	0,004	-	< 0,03	0,016
Nd	0,008	-	0,036	0,011
pH[**]	4,95	5,3	5,05	5,1

(190°C, 112 Tage)

Si	0,02	0,01	0,0276	0,0173
B	4,29	3,04	5,67	3,73
Li	8,67	5,0	8,39	6,59
Ca	3,2	1,72	3,96	4,04
Sr	2,4	0,79	2,28	3,35
Mo	1,27	0,66	1,82	1,02
Ce	0,36	0,088	0,66	0,78
Nd	0,34	0,062	0,61	0,72
pH	3,7	4,8	4,05	4,15

[1] Auslaugmedium NaCl-KCl-MgCl$_2$-MgSO$_4$-H$_2$O mit hohem MgCl$_2$-Gehalt   [**] pH in Auslaugmedium nach 112 d

Auslaugmedium, Zusammensetzung 2[***] (110°C, 112 Tage)

	g/m²	g/m²	g/m²	g/m²
Si	0,017	0,017	0,029	0,017
B	0,95	1,0	1,12	1,12
Li	1,79	1,5	2,29	2,09
Ca	-	-	-	-
Sr	0,6	0,58	0,71	0,76
Mo	0,18	0,24	0,5	0,16
Ce	< 0,02	< 0,02	0,098	< 0,02
Nd	< 0,02	< 0,02	0,036	< 0,02
pH	7,8	7,9	8,3	8,2

(190°C, 112 Tage)

Si	0,04	0,025	0,048	0,041
B	1,13	1,2	5,3	1,21
Li	6,15	2,85	7,52	4,63
Ca	-	-	-	-
Sr	0,94	0,7	0,41	0,83
Mo	0,29	0,23	6,62	0,12
Ce	< 0,02	< 0,02	0,1	< 0,02
Nd	< 0,02	< 0,02	0,025	< 0,02
pH	7,8	7,5	8,6	7,9

[***] Auslaugmedium NaCl-MgSO$_4$-CaSO4-K$_2$SO$_4$-H$_2$O mit hohem NaCl-Gehalt

1) HAWC-Simulat nominaler Zusammensetzung
2) HAWC-Simulat mit vermindertem Gehalt an Feststoffen (Zr, Mo, Nd)
3) HAWC-Simulat mit erhöhtem Gehalt an Feststoffen

32.26.02 UKAEA Dounreay Projekt, Verglasung hochradioaktiver Spaltprodukte aus der Schnellbrüterbrennstoff-Wiederaufarbeitung

In Dounreay/Schottland lagern mehrere 100 m^3 hochradioaktive Flüssigabfälle unterschiedlicher Zusammensetzung, die aus der Wiederaufarbeitung von Schnellbrüterbrennstoff stammen. Die Absicht des Betreibers UKAEA Dounreay ist es, die Abfälle in Borosilikatglas einzuschmelzen. Grundlagen für die Verglasung der Abfälle wurden im INE geschaffen. Die hierzu durchgeführten F+E-Arbeiten umfassten Schritte von der Entwicklung von Glasrezepturen für die unterschiedlichen Abfälle bis hin zum inaktiven Verglasungstest in einer technischen Anlage des INE, bei dem 10000 l einer spezifischen Zusammensetzung verglast wurde. Neben der Demonstration der Verglasbarkeit diente dieser Langzeittest zur Erstellung einer Datenbasis für eine Dounreay-Verglasungsanlage und eines Anlagenkonzeptes durch das INE.

Das von UKAEA Dounreay in 1998 erstmals durchgeführte europaweite Ausschreibungsverfahren zur Erstellung einer Dounreay Vitrification Plant (DVP) wurde in 2001 durch ein modifiziertes Verfahren ersetzt, das der zwischenzeitlich geänderten Kontraktstrategie von UKAEA besser entsprach (Auswahl der Core Technology vor Abschluss eines Kontraktes). Daher war ein neuerliches Vorqualifizierungsverfahren notwendig geworden. Dieses wurde von FZK zusammen mit der britischen Firma AEA Technology im Juni 2001 erfolgreich abgeschlossen. Die nachfolgende Vorgehensweise von UKAEA/Dounreay diente zur detaillierteren Bewertung der Core Technologien der vorqualifizierten Bewerber und zur endgültigen Auswahl. UKAEA/ Dounreay legte dazu den Bewerbern einen umfangreichen Fragenkatalog mit insgesamt 54 Fragenkomplexen vor, der bis Mitte Oktober 2001 beantwortet sein musste. Anschließend fand hierzu in Dounreay am 6. November 01 eine Präsentation statt. Die Beantwortung des Fragenkataloges und die Präsentation wurden durch ein UKAEA-Gremium bewertet, dem auch externe Gutachter angehörten. Bis Ende des Jahres 2001 soll von diesem Gremium eine Empfehlung an den Vorstand von UKAEA und das Londoner Ministerium DTI (Department of Trade and Industry) erfolgen. Bei positivem Ausgang könnte Mitte 2002 mit dem „Conceptional design" für eine DVP begonnen werden.

Veröffentlichte Berichte

Schriftliche Veröffentlichungen

AKTAA, J.; HÄDRICH, H.J.; JULISCH, P.;
KLOTZ, M.; SCHMITT, R.
Investigations to size effects on plastic
deformation and failure behavior of
inhomogeneously loaded structures.
Matzen, V.C. [Hrsg.]
Transactions of the 16th Internat.Conf.on
Structural Mechanics in Reactor Technology
(SMiRT 16), Washington, D.C., Aug. 12-17,2001
Madison, Wis.: Omnipress, 2001 CD-ROM Paper
1891   (50661)

AKTAA, J.; KLOTZ, M.; PFEIFENROTH, M.;
SCHMITT, R.
Investigations to size effects on deformation
and failure behavior of specimens including a
center hole.
Programm Nukleare Sicherheitsforschung.
Jahresbericht 2000
Wissenschaftliche Berichte, FZKA-6653
(September 2001) S.357-58   (50568)

ALBRECHT, G.; BRÜGGEMANN, H.;
CHERDRON, W.; JENES, E.; KAISER, A.;
PROTHMANN, N.; RAUPP, D.; SCHÜTZ, W.;
WILL, H.
ECO-Experimente zur Energiekonversion bei
Dampfexplosionen.
Programm Nukleare Sicherheitsforschung.
Jahresbericht 2000
Wissenschaftliche Berichte, FZKA-6653
(September 2001) S.55-60   (50542)

ALBRECHT, G.; BRÜGGEMANN, H.; JENES, E.;
RAUPP, D.; SCHÜTZ, W.
Untersuchungen zum EPR-Konzept - KAJET-
Versuche.
Programm Nukleare Sicherheitsforschung.
Jahresbericht 2000
Wissenschaftliche Berichte, FZKA-6653
(September 2001) S.153-59   (50549)

ALBRECHT, G.; CHERDRON, W.; IMKE, U.;
JACOBS, H.; KAISER, A.; SCHÜTZ, W.; WILL, H.
Experiments on melt-coolant interaction
processes, including steam explosions.
Matzen, V.C. [Hrsg.]
Transactions of the 16th Internat.Conf.on
Structural Mechanics in Reactor Technology
(SMiRT 16), Washington, D.C., Aug. 12-17,2001
Madison, Wis.: Omnipress, 2001 CD-ROM Paper
1383   (49562)

ALBRECHT, G.; CHERDRON, W.; IMKE, U.;
JACOBS, H.; KAISER, A.; SCHÜTZ, W.; WILL, H.
Experiments on melt-coolant interaction
processes, including steam explosions.
Matzen, V.C. [Hrsg.]
Transactions of the 16th Internat.Conf.on
Structural Mechanics in Reactor Technology
(SMiRT 16), Washington, D.C., Aug. 12-17,
2001
Madison, Wis.: Omnipress, 2001 CD-ROM Paper
1383   (49562)

ALSMEYER, H.; CRON, T.; SCHMIDT-STIEFEL,
S.;SCHNEIDER, H.; TROMM, W.; WENZ, T.;
ADELHELM, C.; DILLMANN, H.G.; PASLER, H.;
SCHÖCK, W.; GREHL, C.; MERKEL, G.;
RATAJCZAK, W.
COMET-Konzept.
Programm Nukleare Sicherheitsforschung.
Jahresbericht 2000
Wissenschaftliche Berichte, FZKA-6653
(September 2001) S.109-39   (50547)

ARTINGER, R.; MARQUARDT, C.M.; KIM, J.I.;
SEIBERT, A.; TRAUTMANN, N.; KRATZ, J.V.
Humic colloid-borne Np migration: influence
of the oxidation state.
MIGRATION'99 : 7th Internat.Conf.on the
Chemistry and Migration Behavior of Actinides
and Fission Products in the Geosphere, Lake
Tahoe, Calif., September 26 - October 1, 1999
Radiochimica Acta, 88(2000) S.609-12(46593)

BAUER, A.; COPPIN, F.; BERGER, G.;
CASTET, S.; STUMPF, T.; LOUBET, M.
Adsorption of lanthanides on smectite and
kaolinite.
79.Jahrestagung der Deutschen Mineralogischen
Gesellschaft, Potsdam, 9.-14.September 2001 :
Referate der Vorträge und Poster
Berichte der Deutschen Mineralogischen
Gesellschaft, No.1, 2001 S.20
(Beihefte zum European Journal of Mineralogy,
Vol. 13, 2001)   (50234)

BAUER, A.; SCHÄFER, T.; DOHRMANN, R.;
HOFFMANN, H.; KIM, J.I.
Smectite stability in acid salt solutions and
the fate of Eu, Th and U in solution.
Clay Minerals, 36(2001) S.93-103   (49648)

BAUER, G.S.; SALVATORES, M.; HEUSENER, G.
MEGAPIE, a 1 MW pilot experiment for a liquid
metal spallation target.
Proc.of the 4th Internat.Workshop on
Spallation Materials Technology (IWSMT-4),
Schruns, A, October 8-13, 2000
Journal of Nuclear Materials, 296(2001)
S.17-33   (50275)

BAUMUNG, K.; BLUHM, H.; KANEL, G.I.;
MÜLLER, G.; SINGER, J.
Measurement of the adhesive strength of 200
µm thick turbine blade coatings by a dynamic
method.

PPA 2001 : Internat.Conf.on Pulsed Power
Applications, Gelsenkirchen, March 27-29,
2001
Proc. S.E.14/1-5 Gelsenkirchen :
Fachhochschule Gelsenkirchen, 2001
(Vorgetragen ; Bd.2)   (49459)

BAUMUNG, K.; MÜLLER, G.; SINGER, J.;
KANEL, G.I.; RAZORENOV, S.V.
Strength of plasma sprayed turbine-blade
coatings using an advanced spallation
technique.
Journal of Applied Physics, 89(2001)
S.6523-29   (49834)

BENZ, G.; EHRHARDT, J.; FISCHER, F.;
HALLER, CH.; HASEMANN, I.;
HESSELSCHWERDT, E.; LANDMANN, C.;
LORENZ, A.; PÄSLER-SAUER, J.; RAFAT, M.;
RASKOB, W.; SCHICHTEL, T.; STEIDLINGER,
A.
Entwicklung von Methoden zur Abschätzung und
Minimierung der radiologischen Folgen von
Reaktorunfällen.
Programm Nukleare Sicherheitsforschung.
Jahresbericht 2000
Wissenschaftliche Berichte, FZKA-6653
(September 2001) S.317-25   (50562)

BIELERT, U.
Dreidimensionale Simulation von Explosions-
abläufen in großen Räumen.
Sichere Handhabung brennbarer Stäube :
Kolloquium, Nürnberg, 27.-29.März 2001 = Safe
Handling of Combustible Dusts.
Düsseldorf : VDI-Verl., 2001 S.677-88
(VDI-Berichte ; 1601)   (49281)

BIELERT, U.; BREITUNG, W.; KOTCHOURKO,
A.; ROYL, P.; SCHOLTYSSEK, W.; VESER, A.;
BECCANTINI, A.; DABBENE, F.; PAILLERE, H.;
STUDER, E.; HULD, T.; WILKENING, H.;
EDLINGER, B.; PORUBA, C.; MOVAHED, M.
Multidimensional simulation of hydrogen
distribution and turbulent combustion in
severe accidents.
Van Goethem, G. [Hrsg.]
FISA 99 : EU Research in Reactor Safety ;
Conclusion Symp.on Shared-Cost and Concerted
Actions, Luxembourg, L, Nov. 29 – Dec. 1, 1999
Luxembourg : Office for Official Publ.of the
European Communities, 2000 S.450-58
EUR-19532-EN
Nuclear Engineering and Design, 209(2001)
S.165-72   (46698)

BIELERT, U.; KOTCHOURKO, A.; BREITUNG,
W.
Numerische Simulationen als Beitrag zur
Sicherheit von Wasserstoffanlagen.
Technische Überwachung, 42(2001) Nr.7/8,
S.11-16   (50420)

BIELERT, U.; KOTCHOURKO, A.; BURGETH, B.;
BREITUNG, W.
Numerical simulation of large scale hydrogen
explosions in complex geometries.
Jahrestagung der Gesellschaft für Angewandte
Mathematik und Mechanik, Göttingen,
2.-7.April 2000
Zeitschrift für Angewandte Mathematik und
Mechanik, 81(2001) Suppl.3, S.S519-S520
          (47268)

BIELERT, U.; KOTCHOURKO, A.; VESER, A.;
BREITUNG, W.
Numerical simulation of combustion with COM3D
and B0B.
Programm Nukleare Sicherheitsforschung.
Jahresbericht 2000
Wissenschaftliche Berichte, FZKA-6653
(September 2001) S.25-38   (50539)

BIELERT, U.; SICHEL, M.
Numerische Simulation von Staubexplosionen in
pneumatischen Saug-Flug-Förderanlagen.
Sichere Handhabung brennbarer Stäube :
Kolloquium, Nürnberg, 27.-29.März 2001 = Safe
Handling of Combustible Dusts
Düsseldorf : VDI-Verl., 2001 S.449-72
(VDI-Berichte ; 1601)   (49282)

BLUHM, H.; MÜLLER, G.; SCHUMACHER, G.;
STRAUSS, D.; ZIMMERMANN, F.; ENGELKO, V.
Design and application of pulsed electron beam
facility GESA for surface treatment of materials.
Displays and Vacuum Electronics :
Contributions to the 9th ITG-Conf.,
Garmisch-Partenkirchen, May 2-3, 2001
Berlin [u.a.] : VDE-Verl., 2001 S.309-14
(ITG-Fachbericht ; 165)   (49262)

BOCK, M.; EHRHARD, P.
Theoretische Untersuchung zum fernen,
turbulenten Nachlauf über einer beheizten
Kugel.
Wissenschaftliche Berichte, FZKA-6571
(November 2001)   (50835)

BOSBACH, D.
Linking molecular-scale barite precipitation
mechanisms with macroscopic crystal growth
rates.
Hellmann, R. [Hrsg.]
Water-Rock Interactions, Ore Deposits and
Environmental Geochemistry : A Tribute to
David A. Crerar
St.Louis, Mo. : Geochemical Society, 2001
(The Geochemical Society Special Publications
; 7)   (50935)

BOSBACH, D.; CHARLET, L.; PERETYASHKO, T.
Heterogene Oxidation von Fe(II) auf Schicht-
silikatoberflächen.

79.Jahrestagung der Deutschen Mineralogischen Gesellschaft, Potsdam, 9.-14.September 2001 : Referate der Vorträge und Poster
Berichte der Deutschen Mineralogischen Gesellschaft, No.1, 2001 S.26
(Beihefte zum European Journal of Mineralogy, Vol. 13, 2001)   (50235)

BRANDT, F.; BOSBACH, D.
Bassanite ($CASO_4.0.5H_2O$) dissolution and gypsum ($CaSO_4.2H_2O$) precipitation in the presence of cellulose ethers.
Journal of Crystal Growth, 233(2001) S.837-45
                    (50705)

BRANDT, F.; BOSBACH, D.; ARNOLD, T.; KRAWCZYK-BAERSCH, E.; BERNHARD, G.
Verwitterung von Chlorit im sauren pH-Bereich: ein kombinierter makroskopischer und mikroskopischer Ansatz.
79.Jahrestagung der Deutschen Mineralogischen Gesellschaft, Potsdam, 9.-14.September 2001 : Referate der Vorträge und Poster
Berichte der Deutschen Mineralogischen Gesellschaft, No.1, 2001 S.27
(Beihefte zum European Journal of Mineralogy, Vol. 13, 2001)   (50236)

BROEDERS, C.H.M.; DAGAN, R.; MERK, B.; SANCHEZ, V.; BROEDERS, I.; STEIN, E.
Physics investigations for innovative nuclear systems.
Programm Nukleare Sicherheitsforschung. Jahresbericht 2000
Wissenschaftliche Berichte, FZKA-6653
(September 2001) S.431-41   (50579)

BUCKEL, G.; FUJITA, S.; GÖTZMANN, W.; KIEFHABER, E.; RINEISKI, A.; THIEM, D.; WIESE, H.W.; WOLL, D.
Upgrading of tools for core design studies and safety analyses.
Programm Nukleare Sicherheitsforschung. Jahresbericht 2000
Wissenschaftliche Berichte, FZKA-6653
(September 2001) S.381-85   (50573)

BUNDSCHUH, T.; HAUSER, W.; KIM, J.I.; KNOPP, R.; SCHERBAUM, F.J.
Determination of colloid size by 2-D optical detection of laser induced plasma.
Colloids and Surfaces A, 180(2001) S.285-93
                    (49484)

BUNDSCHUH, T.; KNOPP, R.; KIM, J.I.
Laser-induced breakdown detection (LIBD) of aquatic colloids with different laser systems.
Colloids and Surfaces A, 177(2001) S.47-55
                    (49034)

BUNDSCHUH, T.; KNOPP, R.; MÜLLER, R.; KIM, J.I.; NECK, V.; FANGHÄNEL, T.

Application of LIBD to the determination of the solubility product of thorium(IV)-colloids.
Radiochimica Acta, 88(2000) S.625-29(49545)

BUNK, M.; EHRHARD, P.; KING, J.R.
Spreading flows with solidification – top crusting.
Ehrhard, P. [Hrsg.]
Interactive Dynamics of Convection and Solidification : Proc.of the EUROMECH Colloquium 408, Chamonix, F, March 18-22, 2000
Dordrecht [u.a.] : Kluwer Acad.Publ., 2001
S.155-64   (50271)

BURGETH, B.; VESER, A.
Ein strukturdynamisches Modell zur Interpretation realer dynamischer Drucklasten.
Programm Nukleare Sicherheitsforschung. Jahresbericht 2000
Wissenschaftliche Berichte, FZKA-6653
(September 2001) S.39-48   (50540)

CACUCI, D.G.
Dimensionally adaptive dynamic switching and adjoint sensitivity analysis: new features of the RELAP5/PANBOX/COBRA code system for reactor safety transients.
Nuclear Engineering and Design, 202(2000) S.325-38   (49174)

CACUCI, D.C.; IONESCU-BUJOR, M.; HERING, W.; SANCHEZ, V.H.
Untersuchungen zur Reaktor- und Anlagen-dynamik.
Programm Nukleare Sicherheitsforschung. Jahresbericht 2000
Wissenschaftliche Berichte, FZKA-6653
(September 2001) S.339-44   (50565)

CAMA, J.; METZ, V.; GANOR, J.; ALMERA, J.
Modeling kaolinite dissolution at acidic pH.
79.Jahrestagung der Deutschen Mineralogischen Gesellschaft, Potsdam, 9.-14.September 2001 : Referate der Vorträge und Poster
Berichte der Deutschen Mineralogischen Gesellschaft, No.1, 2001 S.33
(Beihefte zum European Journal of Mineralogy, Vol. 13, 2001)   (50237)

CARTECIANO, L.N.; DORR, B.; OLBRICH, W.; GRÖTZBACH, G.; JIN, X.
Entwicklung des Rechenprogramms FLUTAN für thermo- und fluiddynamische Anwendungen. Two and three-dimensional thermal and fluid-dynamical analysis of the complete MEGAPIE-module with the computer code FLUTAN.
Programm Nukleare Sicherheitsforschung. Jahresbericht 2000
Wissenschaftliche Berichte, FZKA-6653
(September 2001) S.443-58   (50580)

CHAWLA, R.; HAGER, H.; PARATTE, J.M.;
SEILER, R.; WILLIAMS, T.; BERGER, H.D.;
BÖHME, R.
Analysis of fuel enrichment effects investigated in
the PROTEUS-LWHCR phase II experiments.
ICENES 2000 : The 10th Internat.Conf.on
Emerging Nuclear Energy Systems, Petten, NL,
September 24-28, 2000
Petten : NRG, 2000 CD ROM S.289-95 (48760)

CHENG, X.; BAZIN, P.; CORNET, P.;
HITTNER, D.; JACKSON, J.D.;
LOPEZ JIMENEZ, J.; NAVIGLIO, A.; ORIOLO,
F.; PETZOLD, H.
Experimental data base for containment
thermalhydraulic analysis.
Proc.of the 9th Internat.Topical Conf. on
Nuclear Reactor Thermal Hydraulics
(NURETH-9), San Francisco, Calif., October
3-8, 1999
La Grange Park, Ill. : American Nuclear
Society, 1999
CD-ROM
Nuclear Engineering and Design, 204(2001)
S.267-84   (46106)

CHENG, X.; JACOBS, H.; KIEFHABER, E.;
SCHULENBERG, T.
Thermal-hydraulics of a supercritical pressure
light water reactor.
Programm Nukleare Sicherheitsforschung.
Jahresbericht 2000
Wissenschaftliche Berichte, FZKA-6653
(September 2001) S.371-78   (50572)

CHENG, X.; PETTAN, C.; KNEBEL, J.U.;
SCHULENBERG, T.; HEUSENER, G.
Experimental and numerical studies on
thermal-hydraulics of spallation targets.
Proc.of the 4th Topical Meeting on Nuclear
Applications of Accelerator Technolgy (AccApp
'00), Washington, D.C., November 12-15, 2000
La Grange Park, Ill. : ANS, 2001 S.141-53
                        (48471)

CHENG, X.; SCHULENBERG, T.
Heat transfer at supercritical pressures.
Literature review and application to an HPLWR.
Wissenschaftliche Berichte, FZKA-6609 (Mai
2001)
http://bibliothek.fzk.de/zb/berichte/FZKA6609.pdf.
                        (49813)

CHENG, X.; TAK, N.I.
Numerical design of the MEGAPIE target.
Jahrestagung Kerntechnik 2001, Dresden,
15.-17.Mai 2001
Bonn : INFORUM GmbH, 2001 S.671-75
(Auch auf CD-ROM)   (49709)

CHERDRON, W.; KAISER, A.; SCHÜTZ, W.;
WILL, H.
ECO steam explosion experiments on the
conversion of thermal into mechanical energy.
Jahrestagung Kerntechnik 2001, Dresden,
15.-17.Mai 2001
Bonn : INFORUM GmbH, 2001 S.223-26
(Auch auf CD-ROM)   (49755)

DAGAN, R.; SCHIKORR, M.; BROEDERS, C.H.
The kinetic and dynamic behavior of ADS
versus critical systems.
Jahrestagung Kerntechnik 2001, Dresden,
15.-17.Mai 2001
Bonn : INFORUM GmbH, 2001 S.683-86
(Auch auf CD-ROM)   (49713)

DARDENNE, K.; DENECKE, M.A.; ROTHE, J.;
SCHAEFER, T.
XAFS investigation of lanthanide sorption
onto ferrihydrite and transformation products
tempered at 75^0C.
Jahresbericht 2000 = Annual Report Hamburger
Synchrotronstrahlungslabor HASYLAB am
Deutschen Elektronen-Synchrotron DESY Part I
S.825-26
Hamburg : DESY   (49643)

M.A.; ROTHE, J.; KIM, J.I.
Identification and characterization of sorbed
lutetium species on 2-line ferrihydrite by sorption
data modeling, TRLFS and EXAFS.
Radiochimica Acta, 89(2001) S.469-79(50230)

DENECKE, M.A.; GECKEIS, H.; POHLMANN, C.;
ROTHE, J.; DEGERING, D.
Extended X-ray absorption fine structure and time
differential perturbed angular correlation study of
hafnium(IV) sorbed onto amorphous silica.
MIGRATION'99 : 7th Internat.Conf.on the
Chemistry and Migration Behavior of Actinides
and Fission Products in the Geosphere, Lake
Tahoe, Calif., September 26 - October 1, 1999
Radiochimica Acta, 88(2000) S.639-43(45765)

DENECKE, M.A.; MOSER, H.
Synchrotron radiation techniques in the
environmental sciences workshop.
Synchrotron Radiation News, 14(2001) Nr.1,
S.11-12   (50946)

DIEGELE, E.; HOFER, D.
Versagen des Reaktordruckbehälters infolge
thermoviskoplastischer Instabilität.
Programm Nukleare Sicherheitsforschung.
Jahresbericht 2000
Wissenschaftliche Berichte, FZKA-6653
(September 2001) S.71-79   (50544)

DOLENSKY, B.; GÖLLER, B.; JORDAN, T.;
KRIEG, R.; LUX, M.; MESSEMER, G.; RIEGER,
H.; SIDOR, M.
Reactor pressure vessel head loaded by a slug
impact.
Programm Nukleare Sicherheitsforschung.
Jahresbericht 2000
Wissenschaftliche Berichte, FZKA-6653
(September 2001) S.181-95   (50552)

DOLENSKY, B.; GÖLLER, B.; KRIEG, R.;
BREITUNG, W.; REDLINGER, R.; ROYL, P.
Assessment of loading and response of a
spherical PWR steel containment to a
postulated hydrogen detonation.
Proc.of the SMIRT-16 Post-Conf.Seminar
Containment of Nuclear Reactors, Albuquerque,
N.M., August 20-21, 2001 S.141-52   (51100)

DOLENSKY, B.; GÖLLER, B.; KRIEG, R.;
BREITUNG, W.; REDLINGER, R.; ROYL, P.
Assessment of loading and response of a
spherical PWR steel containment to a
postulated hydrogen detonation.
Proc.of the SMIRT-16 Post-Conf.Seminar
Containment of Nuclear Reactors, Albuquerque,
N.M., August 20-21, 2001 S.141-52   (51100)

DOLENSKY, B.; JORDAN, T.; KRIEG, R.;
MALMBERG, T.; MESSEMER, G.; RIEGER, H.;
AKTAA, J.; DIEGELE, E.; SCHMITT, R.;
PLITZ, H.
Limit strains for severe accident conditions.
Description of an European program and first
results.
Programm Nukleare Sicherheitsforschung.
Jahresbericht 2000
Wissenschaftliche Berichte, FZKA-6653
(September 2001) S.197-211   (50553)

EHRHARD, P.; RICHTER, F.
Axisymmetric spreading of melts with basal
solidification.
Ehrhard, P. [Hrsg.]
Interactive Dynamics of Convection and
Solidification : Proc.of the EUROMECH
Colloquium 408, Chamonix, F, March 18-22,
2000
Dordrecht [u.a.] : Kluwer Acad.Publ., 2001
S.187-94   (48131)

EHRHARD, P.; RILEY, D.S.; STEEN, P.H.;
[HRSG.]
Interactive Dynamics of Convection and
Solidification.
Proc.of the EUROMECH Colloquium 408,
Chamonix, CH, March 18-22, 2000
Dordrecht [u.a.] : Kluwer Acad.Publ., 2001
                (50270)

EHRHARDT, J.
Verbesserung des Notfallschutzmanagements in

Europa: das Entscheidungshilfesystem RODOS.
Radioaktivität und Kernenergie
Karlsruhe : Forschungszentrum Karlsruhe GmbH,
2001 S.85-101   (50083)

ENGELKO, V.; MÜLLER, G.
Influence of particle fluxes from a target on
the characteristics of intense electron beams.
6th Internat.Conf.on Electron Beam
Technologies (EBT '2000), Varna, BG, June
4-7, 2001
Vaccum, 62(2001) S.97-103   (49899)

ENGELKO, V.; MÜLLER, G.; BLUHM, H.
Influence of particle fluxes from target on
characteristics of intense electron beams.
13th Internat.Conf.on High-Power Particle
Beams, Nagaoka, J, June 25-30, 2000
Proc.on CD-ROM S.188-91   (47993)

ENGELKO, V.; YATSENKO, B.; MÜLLER, G.;
BLUHM, H.
Pulsed electron beam facility (GESA) for
surface treatment of materials.
6th Internat.Conf.on Electron Beam
Technologies (EBT '2000), Varna, BG, June
4-7, 2001
Vaccum, 62(2001) S.211-16
                (49900)

EPPINGER, B.; FELLMOSER, F.; FIEG, G.;
TROMM, W.
KAPOOL experiments to simulate molten corium
- sacrificial concrete interaction.
Proc.of the 9th Internat.Conf.on Nuclear
Engineering (ICONE-9), Nice, F, April 8-12,
2001
Paris : SFEN, 2001 CD-ROM   (49276)

EPPINGER, B.; FIEG, G.; MASSIER, H.;
SCHÜTZ, W.; STEGMAIER, U.; STERN, G.
Simulationsexperimente zum Ausbreitungs-
verhalten von Kernschmelzen: KATS-8 bis KATS-
17.
Wissenschaftliche Berichte, FZKA-6589 (März
2001)
http://bibliothek.fzk.de/zb/berichte/FZKA6589.pdf
                (49659)

EPPINGER, B.; FIEG, G.; MASSIER, H.;
SCHÜTZ, W.; STEGMAIER, U.; STERN, G.
Criteria for the spreading of oxide melts: test series
miniKATS-1 to -5.
Wissenschaftliche Berichte, FZKA-6656
(September 2001)
http://bibliothek.fzk.de/zb/berichte/FZKA6656.pdf
                (50535)

EPPINGER, B.; FIEG, G.; SCHMIDT-STIEFEL, S.;
TROMM, W.
KAPOOL experiments to simulate gate opening
in the EPR core catcher concept.

Jahrestagung Kerntechnik 2001, Dresden,
15.-17.Mai 2001
Bonn : INFORUM GmbH, 2001 S.227-30
(Auch auf CD-ROM)   (49278)

EPPINGER, B.; FIEG, G.; SCHMIDT-STIEFEL,
S.; TROMM, W.; STERN, G.
Investigations for the EPR concept - KAPOOL
experiments.
Programm Nukleare Sicherheitsforschung.
Jahresbericht 2000
Wissenschaftliche Berichte, FZKA-6653
(September 2001) S.141-52   (50548)

EPPINGER, B.; FIEG, G.; SCHÜTZ, W.;
STEGMAIER, U.
KATS experiments to simulate corium spreading
in the EPR core catcher concept.
Proc.of the 9th Internat.Conf.on Nuclear
Engineering (ICONE-9), Nice, F, April 8-12,
2001
Paris : SFEN, 2001 CD-ROM   (49277)

ERSHOV, B.G.; GORDEEV, A.V.; JANATA, E.;
KELM, M.
Radiation-chemical oxidation of bromide ions
and formation of tribromide ions in weakly
acidic aqueous solutions.
Mendeleev Communications, (2001) No.4,
S.149-50   (50379)

EYINK, J.; MOVAHED, M.; PETZOLD, K.G.;
KOTCHOURKO, A.; ROYL, P.; TRAVIS, J.R.
Thermal and dynamic loads on the EPR
containment due to hydrogen combustion.
Proc.of the 9th Internat.Conf.on Nuclear
Engineering (ICONE-9), Nice, F, Apr. 8-12, 2001
Paris : SFEN, 2001 CD-ROM   (51040)

FENTER, P.; MCBRIDE, M.T.; SRAJER, G.;
STURCHIO, N.C.; BOSBACH, D.
Structure of barite (001)- and (210)-water
interfaces.
Journal of Physical Chemistry B, 105(2001)
S.8112-19   (50380)

FLEISCH, J.; KUTTRUF, H.; LUMPP, W.;
PFEIFER, W.; SCHWANZER, S.;
WEISENBURGER, S.
Umsetzung von Sicherheitsstandards beim Bau
der Verglasungseinrichtung Karlsruhe (VEK).
Jahrestagung Kerntechnik 2001, Dresden,
15.-17.Mai 2001
Bonn : INFORUM GmbH, 2001 S.291-94
(Auch auf CD-ROM)   (49875)

FOIT, J.J.
Analysis of KATS experiments.
Jahrestagung Kerntechnik 2001, Dresden,
15.-17.Mai 2001
Bonn : INFORUM GmbH, 2001 S.235-38
(Auch auf CD-ROM)   · (49708)

FOIT, J.J.
Analysis of KATS experiments with two
different melt release conditions.
Programm Nukleare Sicherheitsforschung.
Jahresbericht 2000
Wissenschaftliche Berichte, FZKA-6653
(September 2001) S.161-65   (50550)

FRITZ, P.; CLOSS, K.D.; KUCZERA, B.;
ERLENWEIN, P.; LANGETEPE, G.; WEISS, F.P.;
WOLFERT, K.
Vorauseilender Ausstieg aus der Kernenergie
an den deutschen Hochschulen und Forschungs-
zentren?
ATW - Internationale Zeitschrift für Kernenergie ,
46(2001) S.88-94   (49169)

GARGALLO, M.; GREULICH, M.; KIRSTAHLER,
M.; MEYER, L.; SCHWALL, M.; WACHTER, E.;
WÖRNER, G.
Experimente zur Dispersion von Corium.
Programm Nukleare Sicherheitsforschung.
Jahresbericht 2000
Wissenschaftliche Berichte, FZKA-6653
(September 2001) S.81-100   (50545)

GARGALLO, M.; MEYER, L.
Experimental simulation of melt dispersion at
low pressure in an annular cavity.
Matzen, V.C. [Hrsg.]
Transactions of the 16th Internat.Conf.on
Structural Mechanics in Reactor Technology
(SMiRT 16), Washington, D.C., Aug. 12-17, 2001
Madison, Wis.: Omnipress, 2001 CD-ROM Paper
1865   (49654)

GEIST, A.; KIM, J.I.; PLUCINSKI, P.; NITSCH, W.
Hollow fibre modules as novel phase contactors
for the separation of multi-cation ixtures by chemical
extraction.
Cox, M. [Hrsg.]
Proc. of the Internat.Solvent Extraction
Conf. (ISEC '99), Barcelona, E, July 11-16, 1999
London : Society of Chemical Industry, 2001
S.1517-22   (46561)

GEIST, A.; WEIGL, M.; GOMPPER, K.
Actinide(III)/lanthanide(III) separation in a
hollow fiber module with a synergistic
mixture of bis(chlorophenyl)dithiophosphinic
acid and TOPO.
Internat.Meeting on the Back End of the Fuel
Cycle: From Research to Solutions (GLOBAL
2001), Paris, F, September 9-13, 2001
Proc.on CD-ROM, Paper 049   (50586)

GEIST, A.; WEIGL, M.; MÜLLICH, U.;
GOMPPER, K.
Actinide(III)/lanthanide(III) partitioning
using n-Pr-BTP as extractant: extraction
kinetics and extraction test in a hollow
fiber module.

6th Information Exchange Meeting on Actinide and Fission Product Partitioning and Transmutation, Madrid, E, December 11-13, 2000
EUR-19783 EN (2001) S.641-47   (50117)

GEIST, A.; WEIGL, M.; MÜLLICH, U.; GOMPPER, K.
Abtrennverfahren für Aktiniden aus hoch-radioaktiven Abfällen.
Programm Nukleare Sicherheitsforschung.
Jahresbericht 2000
Wissenschaftliche Berichte, FZKA-6653
(September 2001) S.387-92   (50574)

GLASBRENNER, H.; KONYS, J.; MÜLLER, G.; RUSANOV, A.
Corrosion investigations of steels in flowing lead at 400°C and 550°C.
Proc.of the 4th Internat.Workshop on Spallation Materials Technology (IWSMT-4), Schruns, A, October 8-13, 2000
Journal of Nuclear Materials, 296(2001)
S.237-42   (48498)

GLASBRENNER, H.; STEIN-FECHNER, K.; KONYS, J.
Scale structure of aluminised Manet steel after HIP treatment.
9th Internat.Conf.on Fusion Reactor Materials (ICFRM-9), Colorado Springs, Colo., October 10-15, 1999
Journal of Nuclear Materials, 283-287(2000)
Part II, S.1302-05   (49052)

GOMPPER, K.
Zur Abtrennung langlebiger Radionuklide.
Radioaktivität und Kernenergie
Karlsruhe : Forschungszentrum Karlsruhe GmbH, 2001 S.153-67   (50087)

GRAMBOW, B.; MÜLLER, R.
First-order dissolution rate law and the role of surface layers in glass performance assessment.
Journal of Nuclear Materials, 298(2001)
S.112-24   (50381)

GRÜNEWALD, W.; ROTH, G.; TOBIE, W.; WEISENBURGER, S.; SCHWANZER, S.
Inaktive Simulation des Verglasungsprozesses.
Ein Beitrag zum Sicherheitskonzept der VEK.
Jahrestagung Kerntechnik 2001, Dresden, 15.-17.Mai 2001
Bonn : INFORUM GmbH, 2001 S.327-30
(Auch auf CD-ROM)   (49874)

GUDOWSKI, W.; ARZHANOV, V.; BROEDERS, C.; BROEDERS, I.; CETNAR, J.; CUMMINGS, R.; ERICSSON, M.; FOGELBERG, B.; GAUDARD, C.; KONING, A.; LANDEYRO, P.; MAGILL, J.; PAZSIT, I.; PEERANI, P.;

PHLIPPEN, P.; PIONTEK, M.; RAMSTRÖM, E.; RAVETTO, P.; RITTER, G.; SHUBIN, Y.; SOUBIALE, S.; TOCCOLI, C.; VALADE, M.; WALLENIUS, J.; YOUNIOU, G.
Review of the European project - impact of accelerator-based technologies on nuclear fission safety (IABAT).
Progress in Nuclear Energy, 38(2001) S.135-51
(49336)

HARMS, M.; GOSCHNICK, J.
Einsatz von Gassensorik zur sicherheits-technischen Überwachung.
Programm Nukleare Sicherheitsforschung.
Jahresbericht 2000
Wissenschaftliche Berichte, FZKA-6653
(September 2001) S.49-54   (50541)

HENNEGES, G.
Parametric studies in an advanced PWR-containment.
Proc.of the 9th Internat.Conf.on Nuclear Engineering (ICONE-9), Nice, F, April 8-12, 2001
Paris : SFEN, 2001 CD-ROM   (49549)

HERING, W.
Investigation of in-vessel core degradation for the European pressurised water reactor with SCDAP/RELAP5 mod 3.2.
Wissenschaftliche Berichte, FZKA-6567 (März 2001)
http://bibliothek.fzk.de/zb/berichte/FZKA6567.pdf
(49655)

HERING, W.; HOMANN, C.; SANCHEZ-ESPINOZA, V.H.
Reflood simulation of design and beyond design basis accident conditions.
Jahrestagung Kerntechnik 2001, Dresden, 15.-17.Mai 2001
Bonn : INFORUM GmbH, 2001 S.203-06
(Auch auf CD-ROM)   (49711)

HERING, W.; HOMANN, CH.; SENGPIEL, W.; STRUWE, D.; MESSAINGUIRAL, CH.
Severe accident investigations.
Programm Nukleare Sicherheitsforschung.
Jahresbericht 2000
Wissenschaftliche Berichte, FZKA-6653
(September 2001) S.305-16   (50561)

HERING, W.; SENGPIEL, W.
Theoretische Interpretation der experimentellen Ergebnisse.
Programm Nukleare Sicherheitsforschung.
Jahresbericht 2000
Wissenschaftliche Berichte, FZKA-6653
(September 2001) S.327-31   (50563)

JACOBS, H.; RUATTO, P.; STEHLE, B.;
STEIN, E.; BÖTTCHER, M.; IMKE, U.;
STRUWE, D.; MARTEN, H.
Theoretische Arbeiten zur Schmelze-Kühlmittel-
Wechselwirkung.
Programm Nukleare Sicherheitsforschung.
Jahresbericht 2000
Wissenschaftliche Berichte, FZKA-6653
(September 2001) S.61-69   (50543)

JANSSENS-MAENHOUT, G.; DAUBNER, M.;
UMEKAWA, H.; SCHULENBERG, T.
Two-dimensional geysering in the test
facility SUCOT.
Programm Nukleare Sicherheitsforschung.
Jahresbericht 2000
Wissenschaftliche Berichte, FZKA-6653
(September 2001) S.167-80   (50551)

JANSSENS-MAENHOUT, G.; UMEKAWA, H.;
SCHULENBERG, T.
Criteria for flashing in a two-dimensional
channel under low mass flux condition.
Matsui, G. [Hrsg.]
Proc.of the 2nd Japanese-European Two-Phase
Flow Group Meeting, Tsukuba, J, September
25-29, 2000
CD ROM Paper C-4   · (47829)

JIN, X.
Rechenverfahren zur Diskretisierung von
Strömungen in komplexer Geometrie mittels
körperangepaßter Gitter.
Wissenschaftliche Berichte, FZKA-6596 (April
2001)
Dissertation, Universität Karlsruhe 2001
http://bibliothek.fzk.de/zb/berichte/FZKA6596.pdf
          (49808)

KAISER, A.; SCHÜTZ, W.; WILL, H.
PREMIX experiments PM12-PM18 to investigate
the mixing of a hot melt with water.
Wissenschaftliche Berichte, FZKA-6380 (Juli
2001)
http://bibliothek.fzk.de/zb/berichte/FZKA6380.pdf
          (50172)

KELM, M.; BOHNERT, E.; PASHALIDIS, I.
Products formed from alpha radiolysis of
chloride brines.
Research on Chemical Intermediates, 27(2001)
S.503-07   (50384)

KESSLER, G.
Requirements for nuclear energy in the 21st
century.
2nd Fujihara Internat.Seminar on Advanced
Nuclear Energy Systems Towards 0 Release of
Radioactive Wastes, Susono, J, November 6-9,
2000
ATW - Internationale Zeitschrift für
Kernenergie, 46(2001) S.118-25   (48771)

KESSLER, G.; GOMPPER, K.; BROEDERS, C.;
KIEFHABER, E.
Moderne Strategien zur Beseitigung von
Plutonium.
ATW - Internationale Zeitschrift für
Kernenergie, 46(2001) S.32-39   (49495)

KIENZLER, B.; LOIDA, A.
Endlagerrelevante Eigenschaften von hoch-
radioaktiven Abfallprodukten.Charakterisierung
und Bewertung. Empfehlung des Arbeitskreises
HAW-Produkte.
Wissenschaftliche Berichte, FZKA-6651
(September 2001)
http://bibliothek.fzk.de/zb/berichte/FZKA6651.pdf
          (50533)

KIENZLER, B.; LUCKSCHEITER, B.; WILHELM, S.
Waste form corrosion modeling: comparison
with experimental results.
Waste Management, 21(2001) S.741-52
          (50934)

KIENZLER, B.; METZ, V.
Status of source term modeling for radioactive
wastes in Germany.
Proc.of the 9th Internat High-Level
Radioactive Waste Management Conference
(IHLRWM), Las Vegas, Nev., Apr. 29 - May 3,
2001
CD ROM   (49172)

KIENZLER, B.; METZ, V.; SCHÜSSLER, W.
Geochemically based source term modeling.
DisTec 2000 : Disposal Technologies and
Concepts 2000 ; Proc.of the Internat.Conf.on
Radioactive Waste Disposal, Berlin, September
4-6, 2000
Hamburg : KONTEC, Gesellschaft für technische
Kommunikation mbH, 2000 S.478-83   (50232)

KIENZLER, B.; VEJMELKA, P.; METZ, V.
Near field radionuclide concentrations: sorption or
solubility constrained?
ICEM'01 : The 8th Internat.Conf.on Radioactive
Waste Management and Environmental
Remediation, Bruges, B, Sept. 30 – Oct. 4, 2001
Book of Abstracts S.83
Proc.on CD-ROM   (50006)

KIM, J.I.
Is the thermodynamic approach appropriate to
describe natural dynamic systems? (Status and
limitations).
Nuclear Engineering and Design, 202(2000)
S.143-55   (49970)

KIM, J.I.; GOMPPER, K.; GECKEIS, H.
Forschung zur Langzeitsicherheit der
Endlagerung hochaktiver Abfälle.
Radioaktivität und Kernenergie
Karlsruhe : Forschungszentrum Karlsruhe GmbH,

2001 S.117-29 (50085)

KLEYKAMP, H.
Phase equilibria in the UO_2-PuO_2 system
under a temperature gradient.
Proc.of the 10th Symp.on Thermodynamics of
Nuclear Materials, Halifax, CDN, August 6-11,
2000
Journal of Nuclear Materials, 294(2001)
S.8-12 (48586)

KLEYKAMP, H.
Thermodynamic studies on chromium carbides
by the electromotive force (emf) method.
Discussion Meeting on Thermodynamics of
Alloys, Stockholm, S, May 8-11, 2000
Book of Abstracs S.17
Journal of Alloys and Compounds, 321(2001)
S.138-45 (48588)

KLEYKAMP, H.
Post-irradiation studies on the (U,Pu)O_2
cluster experiment POUSSIX in the PHENIX
reactor.
Wissenschaftliche Berichte, FZKA-6679
(Oktober 2001)
http://bibliothek.fzk.de/zb/abstracts/6679.htm
(50642)

KNEBEL, J.U.; ADELHELM, CH.; MÜLLER, G.;
KONYS, J.; GRÖTZBACH, G.
HGF strategy fund project 99/16:
thermalhydraulic and material specific
investigations into the realization of an
accelerator driven system (ADS) to transmute
minor actinides.
Programm Nukleare Sicherheitsforschung.
Jahresbericht 2000
Wissenschaftliche Berichte, FZKA-6653
(September 2001) S.483-521 (50582)

KNEBEL, J.U.; CHENG, X.; MÜLLER, G.;
SCHUMACHER, G.; KONYS, J.; WEDEMEYER,
O.; GRÖTZBACH, G.; CARTECIANO, L.
Thermalhydraulic and material specific
investigations into the realization of an
accelerator driven system (ADS) to transmute
minor actinides. 2000 status report.
Wissenschaftliche Berichte, FZKA-6618
(September 2001) (50532)

KNEBEL, J.U.; HEUSENER, G.
Untersuchungen zur Transmutation und zu
Beschleuniger getriebenen Systemen (ADS) im
Forschungszentrum Karlsruhe.
Radioaktivität und Kernenergie
Karlsruhe : Forschungszentrum Karlsruhe GmbH,
2001 S.169-86 (50088)

KNEBEL, J.U.; MÜLLER, G.; KONYS, J.
Karlsruher Flüssigmetalllabor KALLA.
Karlsruhe : Forschungszentrum Karlsruhe GmbH,

2001 (50266)

KONDO, S.; YAMANO, H.; SUZUKI, T.;
TOBITA, Y.; FUJITA, S.; CAO, X.;
KAMIYAMA, K.; MORITA, K.; FISCHER, E.A.;
BREAR, D.J.; SHIRAKAWA, N.; MIZUNO, M.;
HOSONO, S.; KONDO, T.; MASCHEK, W.;
KIEFHABER, E.; BUCKEL, G.; RINEISKI, A.;
FLAD, M.; COSTE, P.; PIGNY, S.; LOUVET, J.;
CADIOU, T.
SIMMER-III: A computer program for LMFR core
disruptive accident analysis. Version 2.H
model summary and program description.
JNC TN9400 2001-002 (November 2000)
(49714)

KONDO, S.; YAMANO, H.; TOBITA, Y.;
FUJITA, S.; KAMIYAMA, H.; MASCHEK, W.;
COSTE, P.; PIGNY, S.; LOUVET, J.
Phase 2 code assessment of SIMMER-III, a
computer program for LMFT core disruptive
accident analysis.
JNC TN9400 2000-105 (September 2000)
(49681)

KONYS, J.; GLASBRENNER, H.; MÜLLER, G.;
HEINZEL, A.; RUSANOV, A.
Liquid metal corrosion.
Programm Nukleare Sicherheitsforschung.
Jahresbericht 2000
Wissenschaftliche Berichte, FZKA-6653
(September 2001) S.421-30 (50578)

KONYS, J.; MUSCHER, H.; VOSS, Z.;
WEDEMEYER, O.
Development of oxygen meters for the use in
lead-bismuth.
Proc.of the 4th Internat.Workshop on
Spallation Materials Technology (IWSMT-4),
Schruns, A, October 8-13, 2000
Journal of Nuclear Materials, 296(2001)
S.289-94 · (48499)

KOROVIN, YU.A.; KONOBEYEV, A.YU.;
PERESLAVTSEV, P.E.; STANKOVSKY, A.YU.;
BROEDERS, C.; BROEDERS, I.; FISCHER, U.;
MÖLLENDORFF, U.VON
Evaluated nuclear data files for accelerator
driven systems and other intermediate and
high-energy applications.
Nuclear Instruments and Methods A, 463(2001)
S.544-56 (49850)

KRAUSS, W.; SCHANZ, G.; STEINER, H.
Einzeleffekt-Untersuchungen zum
Reaktionsverhalten von Zircaloy-4 in Luft und
zur Oxidation von B_4C.
Programm Nukleare Sicherheitsforschung.
Jahresbericht 2000
Wissenschaftliche Berichte, FZKA-6653
(September 2001) S.287-304 (50560)

KRAUTSCHICK, V.; SCHMUCK, P.
Contributions of Forschungszentrum Karlsruhe
to PHEBEN2 first yearly progress report.
Müller, K. [Hrsg.]
Minutes of PHEBEN2 2nd Progress Meeting,
Belgirate, I, March 13, 2001
Technical Note No.I.01.59/SAM-PHEBEN2-M003
(May 2001) Annex 8   (49475)

KRAUTSCHICK, V.; SCHMUCK, P.
Contribution to PHEBEN2 - validating severe
accident codes against PHEBUS FP for plant
applications.
Programm Nukleare Sicherheitsforschung.
Jahresbericht 2000
Wissenschaftliche Berichte, FZKA-6653
(September 2001) S.333-37   (50564)

KRIEG, R.; DEVOS, J.; CAROLI, C.;
SOLOMOS, G.; ENNIS, P.J.; KALKHOF, D.
On the prediction of the reactor vessel
integrity under severe accident loadings
(RPVSA).
FISA-99 : EU Research in Reactor Safety,
Luxembourg, L, November 29 - December 1,
1999
Preprints S.126-35
Luxembourg : Commision of the European
Communities, 1999
Nuclear Engineering and Design, 209(2001)
S.117-25   (46716)

KRIEG, R.; DOLENSKY, B.; GÖLLER, B.;
HAILFINGER, G.; JONATZKE, O.; MALMBERG,
T.; MESSEMER, G.; STRATMANNS, E.;
VORBERG, G.; BENZ, H.; RATAJCZAK, W.
Load carrying capacity of a reactor vessel
head under a coriuum slug impact from a
postulated in-vessel steam explosion.
Nuclear Engineering and Design, 202(2000)
S.179-96   (49173)

KRIEG, R.; JULISCH, P.; KALKHOF, D.;
TALJA, H.; SOLOMOS, G.; AIFANTIS, E.;
CIZELJ, L.; CAROLI, C.; FOKKENS, J.;
BHANDARI, S.; VERON, P.; SCHRAMM, K.;
KIESELBACH, R.
Limit strains for severe accident conditions.
FISA-2001 : EU Research in Reactor Safety,
Mid-Term Symp.on Shared-Cost and Concerted
Actions, Luxembourg, L, November 12-14, 2001
Pre-Proc. S.396-407   (51110)

KUCZERA, B.   ·
Thirty years of LWR safety research at Karlsruhe.
Nuclear Engineering and Design, 202(2000)
S.129-42   (49166)

KUCZERA, B.
Karlsruher Forschungsbeiträge zur
Sicherheitvorsorge in Kernkraftwerken mit
Leichtwasserreaktoren.

Radioaktivität und Kernenergie
Karlsruhe : Forschungszentrum Karlsruhe GmbH,
2001 S.65-82   (50082)

KUCZERA, B.
Vom Nutzen der Kernenergie bei der
Stromerzeugung.
Radioaktivität und Kernenergie
Karlsruhe : Forschungszentrum Karlsruhe GmbH,
2001 S.189-200   (50089)

KUNZE, S.
Inerte Atmosphäre mindert radioaktive
Beschichtungsalterung.
Farbe und Lack, 107(2001) Nr.2, S.66-68
          (50598)

KUNZE, S.
In Luft und sauerstofffreier Atmosphäre
bestrahlte Beschichtungen für kerntechnische
Anlagen.
Elektrizitätswirtschaft, 100(2001) Nr.11,
S.46-50   (50599)

LEFHALM, C.H.; KNEBEL, J.U.; MACK, K.J.
Kinetics of gas phase oxygen control systems
(OCS) for stagnant and flowing Pb-Bi systems.
Proc.of the 4th Internat.Workshop on Spallation
Materials Technology (IWSMT-4), Schruns, A,
October 8-13, 2000
Journal of Nuclear Materials, 296(2001)
S.301-04   (50280)

LEFHALM, C.H.; KNEBEL, J.U.; MACK, K.J.
Kinetik des Sauerstoffkontrollsystems (OCS)
für stagnierende Blei-Wismut Systeme.
Wissenschaftliche Berichte, FZKA-6610
(September 2001)
http://bibliothek.fzk.de/zb/berichte/FZKA6610.pdf
          (50531)

LOIDA, A.; [HRSG.]
Nukleare Entsorgung. F&E-Aktivitäten 2000.
Sammlung der Vorträge anläßlich des internen
INE Mitarbeiterseminars am 5.-6.Dez. 2000.
Wissenschaftliche Berichte, FZKA-6629 (August
2001)   (50412)

LOIDA, A.; GRAMBOW, B.; GECKEIS, H.
Congruent and incongruent radionuclide release
during matrix dissolution of partly oxidized high
burnup spent fuel.
Hart, K.P. [Hrsg.]
Scientific Basis for Nuclear Waste Management:
24.Symp., Sydney, AUS, August 27 - 31, 2000
Warrendale, Pa. : MRS, 2001 S.417-28
(Materials Research Society Symposium
Proceedings ; 663)   (47635)

LOIDA, A.; GRAMBOW, B.; GECKEIS, H.
Spent fuel corrosion behavior in salt solution in the
presence of hydrogen overpressure.

ICEM'01 : The 8th Internat.Conf.on Radioactive Waste Management and Environmental Remediation, Bruges, B,Sept. 30 – Oct. 4, 2001 Book of Abstracts S.48 Proc.on CD-ROM (50584)

LUCKSCHEITER, B.; KIENZLER, B. Determination of sorption isotherms for Eu, Th, U and Am on the gel layer of corroded HLW glass. Journal of Nuclear Materials, 298(2001) S.155-62 (50386)

LÜTZENKIRCHEN, J. A discussion of the surface complexation modeling in the paper by Sarkar et al. (1999). Soil Science Society of America Journal, 65(2001) S.1348-49 (50925)

MADIC, C.; LECOMTE, M.; TESTARD, F.; HUDSON, M.J.; LILJENZIN, J.O.; SÄTMARK, B.; FERRANDO, M.; FACCHINI, A.; GEIST, A.; MODOLO, G.; GONZALES-ESPARTERO, A.; DE MENDOZA, J. PARTNEW. An European research programme for the partitioning of minor actinides from high level liquid wastes. Internat.Meeting on the Back End of the Fuel Cycle: From Research to Solutions (GLOBAL 2001), Paris, F, September 9-13, 2001 Proc.on CD-ROM, Paper 300 (50588)

MALMBERG, T.; TSAGRAKIS, I.; ELEFTHERIADIS, I.; AIFANTIS, E.C. On the gradient plasticity approach to size effects. Part II: applications. Wissenschaftliche Berichte, FZKA-6322 (März 2001) (49507)

MALMBERG, T.; TSAGRAKIS, I.; ELEFTHERIADIS, I.; AIFANTIS, E.C. On the gradient plasticity approach to size effects. Part I: reviews. Wissenschaftliche Berichte, FZKA-6321 (März 2001) (49508)

MARQUARDT, C.M.; ARTINGER, R.; BUCKAU, G.; DARDENNE, K.; DENECKE, M.A.; GECKEIS, H.; KIM, J.I.; MONSALIER, J.M.; THANG, N.M.; PLASCHKE, M.; ROTHE, J.; SEIBERT, A.; SCHÄFER, T.; SCHÜSSLER, W. Wechselwirkung von Actiniden mit Huminstoffen. Untertägige Entsorgung. Fünftes Statusgespräch zu FuE-Vorhaben auf dem Gebiet der Entsorgung gefährlicher Abfälle in tiefen geologischen Formationen am 15. und 16.Mai 2001 in Leipzig. Wissenschaftliche Berichte, FZKA-PTE Nr. 7 (Juli 2001) S. 519-40 (50968)

MASCHEK, W.; RINEISKI, A.; MORITA, K.; KIEFHABER, E.; BUCKEL, G.; FLAD, M.;

COSTE, P.; PIGNY, S.; RIMPAULT, G.; LOUVET, J.; CADIOU, T.; KONDO, S.; TOBITA, Y.; SUZUKI, T.; YAMANO, H.; FUJITA, S. SIMMER-III code development for analyzing transients and accidents in accelerator driven systems (ADS). Proc.of the 4th Topical Meeting on Nuclear Applications of Accelerator Technolgy (AccApp '00), Washington, D.C., November 12-15, 2000 La Grange Park, Ill. : ANS, 2001 S.131-40 (48492)

MASCHEK, W.; RINEISKI, A.; MORITA, K.; FLAD, M. Safety investigations for accelerator driven transmutation systems. Jahrestagung Kerntechnik 2001, Dresden, 15.-17.Mai 2001 Bonn : INFORUM GmbH, 2001 S.677-81 (Auch auf CD-ROM) (49283)

MASCHEK, W.; RINEISKI, A.; MORITA, K.; FLAD, M. Inherent and passive safety measures in accelerator driven systems: a safety strategy for ADS. GLOBAL 2001 : Internat.Conf.on the Back End of the Fuel Cycle: From Research to Solutions, Paris, F, September 9-13, 2001 Proc.on CD-ROM Paper 001 American Nuclear Soc., French Section, 2001 (49967)

MASCHEK, W.; RINEISKI, A.; MORITA, K.; FLAD, M. Analysis of safety behavior of accelerator driven transmutation systems. Programm Nukleare Sicherheitsforschung. Jahresbericht 2000 Wissenschaftliche Berichte, FZKA-6653 (September 2001) S.393-400 (50575)

METZ, V.; GANOR, J. Effect of crystallinity on Kaolinite solubility and dissolution kinetics. 79.Jahrestagung der Deutschen Mineralogischen Gesellschaft, Potsdam, 9.-14.September 2001 : Referate der Vorträge und Poster Berichte der Deutschen Mineralogischen Gesellschaft, No.1, 2001 S.119 (Beihefte zum European Journal of Mineralogy, Vol. 13, 2001) (50161)

METZ, V.; GANOR, J. Stirring effect on kaolinite dissolution rate. Geochimica et Cosmochimica Acta, 65(2001) S.3475-90 (50781)

MEYER, L.; GARGALLO, M. Experiments on melt dispersion with lateral failure in the bottom head of the pressure vessel.

Proc.of the 9th Internat.Conf.on Nuclear
Engineering (ICONE-9), Nice, F, April 8-12,
2001
Paris : SFEN, 2001 CD-ROM   (49275)

MIASSOEDOV, A.; PIEL, D.; SEPOLD, L.;
STEINBRÜCK, M.; STEINBOCK, L.;
STEGMAIER, U.
Results of the QUENCH-05 and QUENCH-06
bundle experiments on the investigation of cool-
down behaviour of overheated PWR fuel rod
simulators (QUENCH-Programme).
Programm Nukleare Sicherheitsforschung.
Jahresbericht 2000
Wissenschaftliche Berichte, FZKA-6653
(September 2001) S.239-50   (50556)

MINGES, J.; SCHÜTZ, W.; KOCH, M.K.
KAREX-Experimente zum radiologischen
Quellterm infolge Resuspension.
Programm Nukleare Sicherheitsforschung.
Jahresbericht 2000
Wissenschaftliche Berichte, FZKA-6653
(September 2001) S.231-38   (50555)

MONSALLIER, J.M.; SCHERBAUM, F.J.;
BUCKAU, G.; KIM, J.I.; KUMKE, M.U.;
SPECHT, C.H.; FRIMMEL, F.H.
Influence of photochemical reactions on the
complexation of humic acid with europium(III).
Journal of Photochemistry and Photobiology A,
138(2001) S.55-63   (49055)

MORITA, K.; RINEISKI, A.; KIEFHABER, E.;
MASCHEK, W.; FLAD, M.; RIMPAULT, G.;
COSTE, P.; PIGNY, S.; KONDO, S.; TOBITA, Y.;
FUJITA, S.
Mechanistic SIMMER-III analyses of severe
transients in accelerator driven systems (ADS).
Proc.of the 9th Internat.Conf.on Nuclear
Engineering (ICONE-9), Nice, F, April 8-12, 2001
Paris : SFEN, 2001 CD-ROM   (49273)

MUSCHER, H.; KONYS, J.; VOSS, Z.;
WEDEMEYER, O.
Measurement of oxygen activities in eutectic
lead-bismuth by means of the EMF method.
Wissenschaftliche Berichte, FZKA-6690
(Dezember 2001)
http://bibliothek.fzk.de/zb/berichte/FZKA6690.pdf
        (51037)

MÜHL, B.; [HRSG.]
Programm Nukleare Sicherheitsforschung.
Jahresbericht 2000.
Wissenschaftliche Berichte, FZKA-6653
(September 2001)   (50536)

MÜLLER, G.; BLUHM, H.; ENGELKO, V.
The pulsed electron beam facilities GESA I
and GESA II for surface treatment of materials.
PPA 2001 : Internat.Conf.on Pulsed Power

Applications, Gelsenkirchen, March 27-29, 2001
Proc. S.E.19/1-6
Gelsenkirchen : Fachhochschule Gelsenkirchen,
2001
(Vorgetragen ; Bd.2)   (49705)

MÜLLER, G.; ENGELKO, D.V.; ANDREEV, A.;
KOMAROV, O.; STRAUSS, G.; SCHUMACHER,
G.; ZIMMERMANN, F.; BLUHM, H.
Conceptional design of the pulsed electron
beam facility GESA II.
13th Internat.Conf.on High-Power Particle
Beams, Nagaoka, J, June 25-30, 2000
Proc.on CD-ROM S,398-401   (47994)

MÜLLER, G.; HUBER, R.; SCHUMACHER, G.;
STRAUSS, D.; ZIMMERMANN, F.; ENGELKO, V.
Behandlung von MCrAIY-Schutzschichten mit
Grundlagenuntersuchungen zur Strahlerzeugung.
Programm Nukleare Sicherheitsforschung.
Jahresbericht 2000
Wissenschaftliche Berichte, FZKA-6653
(September 2001) S.363-68   (50570)

MÜLLER, G.; SCHUMACHER, G.; STRAUSS,
D.;ZIMMERMANN, F.; BLUHM, H.; ENGELKO, V.
Improvement of the corrosion resistance of
steels and MCrAIY coatings by application of
a pulsed electron beam.
13th Internat.Conf.on High-Power Particle
Beams, Nagaoka, J, June 25-30, 2000
Proc.on CD-ROM S.216-21   (47992)

MÜLLER, G.; STRAUSS, D.; SCHUMACHER, G.;
ZIMMERMANN, F.; BLUHM, H.; ENGELKO, V.
Improvement of the corrosion resistance of
MCrAIY turbine blade coatings by large area
pulsed electron beam treatment.
PPA 2001 : Internat.Conf.on Pulsed Power
Applications, Gelsenkirchen, March 27-29,
2001
Proc. S.E.20/1-6
Gelsenkirchen : Fachhochschule Gelsenkirchen,
2001
(Vorgetragen ; Bd.2)   (49706)

NAKAZAWA, T.; KIMURA, H.; KOMATSU, H.;
KAGUCHI, H.; KOTO, H.; SCHIRRA, M.
Creep rupture properties and microstructure
of European and Japanese type low carbon
medium nitrogen 316 steel.
Karyoku Genshiryoku Hatsuden, 49(1998)
S.342-48 (in japan.Sprache)   (49456)

NECK, V.; KIM, J.I.
An electrostatic approach for the prediction
of actinide complexation constants with
inorganic ligands-application to carbonate
complexes.
MIGRATION'99 : 7th Internat.Conf.on the
Chemistry and Migration Behavior of Actinides
and Fission Products in the Geosphere, Lake

Tahoe, Calif., September 26 - October 1, 1999
Radiochimica Acta, 88(2000) S.815-22(46597)

NECK, V.; KIM, J.I.
Solubility and hydrolysis of tetravalent actinides.
Radiochimica Acta, 89(2001) S.1-16 (49374)

NECK, V.; KIM, J.I.; SEIDEL, B.S.;
MARQUARDT, C.M.; DARDENNE, K.; JENSEN,
M.P.; HAUSER, W.
A spectroscopic study of the hydrolysis,
colloid formation and solubility of Np(IV).
Radiochimica Acta, 89(2001) S.439-46
                          (50114)

PIEPER, H.; BOSBACH, D.; BAUER, A.
Die Auflösung von Illit: Nanomorphologie und
Reaktionskinetik.
79.Jahrestagung der Deutschen Mineralogischen
Gesellschaft, Potsdam, 9.-14.September 2001 :
Referate der Vorträge und Poster
Berichte der Deutschen Mineralogischen
Gesellschaft, No.1, 2001 S.139
(Beihefte zum European Journal of Mineralogy,
Vol. 13, 2001)   (50238)

PIERRET, M.C.; BAUER, A.; RABUNG, T.;
GECKEIS, H.; KLENZE, R.; KIM, J.I.;
BRADBURY, M.H.; BAEYENS, B.
Interaction of Cm(III) and Eu(III) with
Ca-montmorillonite: surface complexation
modelling and spectroscopic studies.
79.Jahrestagung der Deutschen Mineralogischen
Gesellschaft, Potsdam, 9.-14.September 2001 :
Referate der Vorträge und Poster
Berichte der Deutschen Mineralogischen
Gesellschaft, No.1, 2001 S.140
(Beihefte zum European Journal of Mineralogy,
Vol. 13, 2001)   (50239)

PLASCHKE, M.; SCHÄFER, T.; BUNDSCHUH,
T.; NGO MANH, T.; KNOPP, R.; GECKEIS, H.;
KIM, J.I.
Size characterization of bentonite colloids
by different methods.
Analytical Chemistry, 73(2001) S.4338-47
                          (50392)

PLITZ, H.
Bestrahlungsexperimente zur Transmutation von
Aktiniden im HFR.
Programm Nukleare Sicherheitsforschung.
Jahresbericht 2000
Wissenschaftliche Berichte, FZKA-6653
(September 2001) S.401-03   (50576)

PUDEWILLS, A.
Numerical analysis of long-term
thermomechanical behavior of repository
structures.
Matzen, V.C. [Hrsg.]
Transactions of the 16th Internat.Conf.on

Structural Mechanics in Reactor Technology
(SMiRT 16), Washington, D.C., August 12-17,
2001
Madison, Wis.: Omnipress, 2001 CD-ROM Paper
1055   (49547)

PUDEWILLS, A.; KRAUSS, M.
Analysis of coupled flow, heat and brine transport
in the far field of a nuclear waste repository.
Bathe, K.J. [Hrsg.]
Computational Fluid and Solid Mechanics :
Proc. of the 1st MIT Conf., Boston, Mass.,
June 12-15, 2001 Vol.2 S.1349-52
Amsterdam [u.a.] : Elsevier, 2001
Auch auf CD ROM   (50794)

RABUNG, T.; STUMPF, T.; GECKEIS, H.;
KLENZE, R.; KIM, J.I.
Sorption of Am(III) and Eu(III) onto
γ-alumina: experiment results and modeling.
MIGRATION'99 : 7th Internat.Conf.on the
Chemistry and Migration Behavior of Actinides
and Fission Products in the Geosphere, Lake
Tahoe, Calif., September 26 - October 1, 1999
Radiochimica Acta, 88(2000) S.711-16(46602)

RICHTER, F.; EHRHARD, P.
Experiments on the axisymmetric spreading of
a metallic melt in presence of basal solidification.
Wissenschaftliche Berichte, FZKA-6577 (Juni
2001)   (50174)

RINEISKI, A.; KIEFHABER, E.; MERK, B.;
MASCHEK, W.; FLAD, M.
Neutron kinetics developments of the
SIMMER-III safety code for ADS application.
Utilization and Reliability of High Power
Proton Accelerators : Workshop Proc.,
Aix-en-Provence, F, November 22-24, 1999
Paris : OECD, 2001 S.335-44
(Nuclear Science)   (46763)

ROTH, G.; WEISENBURGER, S.
Verglasungstechnologie des Forschungszentrums
Karlsruhe für hochradioaktive flüssige Abfälle.
Radioaktivität und Kernenergie
Karlsruhe : Forschungszentrum Karlsruhe GmbH,
2001 S.103-15   (50084)

ROTH, G.; WEISENBURGER, S.; GRÜNEWALD,
W.; GAUTHIER, Y.
Effect of canister filling by multiple pouring batches
on quality properties of HLW glass product.
ICEM'01 : The 8th Internat.Conf.on
Radioactive Waste Management and
Environmental Remediation, Bruges, B,
September 30 - October 4, 2001
Book of Abstracts S.99
Proc.on CD-ROM   (50585)

ROTHE, J.; DENECKE, M.A.; DARDENNE, K.; NECK, V.
XAFS investigations of the structure of aquatic thorium oxide/hydroxide colloids.
Jahresbericht 2000 = Annual Report Hamburger Synchrotronstrahlungslabor HASYLAB am Deutschen Elektronen-Synchrotron DESY Part I S.829-30
Hamburg : DESY   (49642)

ROYL, P.; NECKER, G.; TRAVIS, J.R.
GASFLOW simulation of hydrogen recombination with radiation transport from catalytic foils in the recombiner foil test HDR E 11.8.1.
Jahrestagung Kerntechnik 2001, Dresden, 15.-17.Mai 2001
Bonn : INFORUM GmbH, 2001 S.211-14
(Auch auf CD-ROM)   (49279)

ROYL, P.; TRAVIS, J.R.; NECKER, G.
Model development and validation of GASFLOW II.
Programm Nukleare Sicherheitsforschung.
Jahresbericht 2000
Wissenschaftliche Berichte, FZKA-6653
(September 2001) S.1-16   (50537)

SABISCH, W.; WÖRNER, M.; GRÖTZBACH, G.; CACUCI, D.G.
Dreidimensionale Numerische Simulation von aufsteigenden Einzelblasen und Blasen-schwärmen mit einer Volume-of-Fluid Methode.
Tagung des GVC-Fachausschusses CFD, Bamberg, 28.Februar - 1.März 2000
Chemie Ingenieur Technik, 73(2001) S.368-73
          (49736)

SABISCH, W.; WÖRNER, M.; GRÖTZBACH, G.; CACUCI, D.G.
3D volume-of-fluid simulation of a wobbling bubble in a gas-liquid system of low Morton number.
Michaelides, E.E. [Hrsg.]
Proc.of the 4th Internat.Conf.on Multiphase Flow, New Orleans, La., May 27 - June 1, 2001
CD-ROM   (49829)

SCHANZ, G.; HECK, M.; STEGMAIER, U.
Metallographic post-test examination of QUENCH test bundles and phenomenological interpretation.
Programm Nukleare Sicherheitsforschung.
Jahresbericht 2000
Wissenschaftliche Berichte, FZKA-6653
(September 2001) S.251-58   (50557)

SCHANZ, G.; STEINBRÜCK, M.; STEGMAIER, U.; MIASSOEDOV, A.
Post-test examination results of the water-quenched bundles QUENCH-01, QUENCH-02 and QUENCH-03.
Jahrestagung Kerntechnik 2001, Dresden,

15.-17.Mai 2001
Bonn : INFORUM GmbH, 2001 S.197-201
(Auch auf CD-ROM)   (49877)

SCHIKORR, M.
Assessment of the transient behavior of sub-critical systems (ADS) in comparison to critical reactor systems.
Programm Nukleare Sicherheitsforschung.
Jahresbericht 2000
Wissenschaftliche Berichte, FZKA-6653
(September 2001) S.459-82   (50581)

SCHILD, D.; MARQUARDT, C.M.
Analysis of Th(IV)-humate by XPS.
MIGRATION'99 : 7th Internat.Conf.on the Chemistry and Migration Behavior of Actinides and Fission Products in the Geosphere, Lake Tahoe, Calif., September 26 - October 1, 1999
Radiochimica Acta, 88(2000) S.587-91(46609)

SCHIRRA, M.
Long-term studies on the creep behaviour of the structural material 316 L (N) in the low-stress range at 550 and 600°C.
Parker, J.D. [Hrsg.]
Proc.of the 9th Internat.Conf.on Creep and Fracture of Engineering Materials and Structures, Swansea, April 1-6, 2001
London : The Institute of Materials, 2001
S.669-78   (49662)

SCHIRRA, M.; GRAF, P.; FALKENSTEIN, A.; HEGER, S.; MATERNA-MORRIS, E.
Untersuchungen an Strukturmaterialien der Kerntechnik.
Programm Nukleare Sicherheitsforschung.
Jahresbericht 2000
Wissenschaftliche Berichte, FZKA-6653
(September 2001) S.353-55   (50567)

SCHMUCK, P.; MIETTINEN, J.
The STEPS process tracking model for fast calculations of accidental radioactive releases.
Programm Nukleare Sicherheitsforschung.
Jahresbericht 2000
Wissenschaftliche Berichte, FZKA-6653
(September 2001) S.213-30   (50554)

SCHÄFER, T.; BAUER, A.; CLARET, F.; LANSON, B.; WIRICK, S.; JACOBSEN, C.; KIM, J.I.
Soft X-ray spectromicroscopy investigations of natural organic matter (NOM)-clay interaction in high pH solutions.
79.Jahrestagung der Deutschen Mineralogischen Gesellschaft, Potsdam, 9.-14.September 2001 : Referate der Vorträge und Poster
Berichte der Deutschen Mineralogischen Gesellschaft, No.1, 2001 S.160
(Beihefte zum European Journal of Mineralogy, Vol. 13, 2001)   (50240)

SCHÜSSLER, W.; ARTINGER, R.; KIM, J.I.;
BRYAN, N.D.; GRIFFIN, D.
Numerical modeling of humic colloid borne
americium (III) migration in column
experiments using the transport/speciation
code K1D and the KICAM model.
Journal of Contaminant Hydrology, 47(2001)
S.311-22   (49339)

SCHÜSSLER, W.; KIENZLER, B.; WILHELM, S.;
KIM, J.I.
Geochemical properties of buffer and backfill
materials for radioactive waste disposal in
salt formations.
DisTec 2000 : Disposal Technologies and
Concepts 2000 ; Proc.of the Internat.Conf.on
Radioactive Waste Disposal, Berlin, September
4-6, 2000
Hamburg : KONTEC, Gesellschaft für technische
Kommunikation mbH, 2000 S.602-05   (49645)

SCHÜSSLER, W.; KIENZLER, B.; WILHELM, S.;
NECK, V.; KIM, J.I.
Modeling of near field actinide concentrations in
radioactive waste repositories in salt formations:
effect of buffer materials.
Smith, R. [Hrsg.]
Scientific Basis for Nuclear Waste Management:
23.Symp., Boston, Mass., November 29 -
December 2, 1999
Warrendale, Pa. : MRS, 2000 S.791-98
(Materials Research Society Symposium
Proceedings ; 608)   (50792)

SCHÜSSLER, W.; NEUEBRT, R.; LEVIN, I.;
FISCHER, N.; SONNTAG, C.
Determination of microbial versus root-produced
CO_2 in an agricultural ecosystem by means of
$\delta^{13}CO_2$ measurement in soil air.
Tellus B, 52(2000) S.909-18   (49644)

SEIBERT, A.; MANSEL, A.; MARQUARDT, C.M.;
KELLER, E.; KRATZ, J.V.; TRAUTMANN, N.
Complexation behaviour of neptunium with
humic acid.
Radiochimica Acta, 89(2001) S.505-10(50350)

SEPOLD, L.; HOFMANN, P.; LEILING, W.;
MIASSOEDOV, A.; PIEL, D.; SCHMIDT, L.;
STEINBRÜCK, M.
Reflooding experiments with LWR-type fuel rod
simulators in the quench facility.
Proc.of the 9th Internat.Topical Conf. on
Nuclear Reactor Thermal Hydraulics
(NURETH-9), San Francisco, Calif., October
3-8, 1999
La Grange Park, Ill. : American Nuclear
Society, 1999
CD-ROM
Nuclear Engineering and Design, 204(2001)
S.205-20   (44978)

SFAR, K.; AKTAA, J.
Mikromechanische Modellierung von
Wärmedämmschichten.
Programm Nukleare Sicherheitsforschung.
Jahresbericht 2000
Wissenschaftliche Berichte, FZKA-6653
(September 2001) S.369   (50571)

SFAR, K.; AKTAA, J.; MUNZ, D.
Crack assessment in TBC systems using FEM and
taking mode mixity into account.
Proc.of the 25th Annual Conf.on Composites,
Advanced Ceramics, Materials, and Structures,
Cocoa Beach, Fla., January 21-27, 2001
Ceramic Engineering and Science Proceedings,
22(2001) S.397   (50702)

SHEPHERD, I.; HASTE, T.; KOURTI, N.;
ORIOLO, F.; LEONARDI, M.; KNORR, J.;
KRETSCHMER, S.; UMBREIT, M.; ADROGUER,
B.; HOFMANN, P.; MIASSOEDOV, A.; NOACK,
V.; STEINBRÜCK, M.; HOMANN, C.; PLITZ, H.;
VESHCHUNOV, M.; JAEGER, M.; MEDALE, M.;
TURLAND, B.; HILES, R.; BANDINI, G.; EDERLI,
S.; LINNEMANN, T.; KOCH, M.; UNGER, H.;
MÜLLER, K.; FERNANDEZ BENITEZ, J.
Investigation of core degradation (COBE).
Nuclear Engineering and Design, 209(2001)
S.107-16   (51155)

SILDE, A.; REDLINGER, R.
Three-dimensional simulation of hydrogen
detonations in the Olkiluoto BWR reactor building.
VTT Energy Reports 13/2000 (December 2000)
                                 (49288)

SMAILOS, E.
Corrosion behaviour of the candidate HLW/spent
fuel container material TStE355 carbon steel in
granitic environments.
Proc.of the Internat.Conf.'Corrosion Odyssey
2001', Edinburgh, GB, September 18-20, 2001
CD ROM   (49646)

SMAILOS, E.
Influence of gamma radiation on corrosion of
Cu-base materials in NaCl-rich brine.
Proc.of the 9th Internat.High-Level
Radioactive Waste Management Conf.(IHLRWM),
Las Vegas, Nev., April 29 - May 3, 2001
CD ROM (Session E-5)   (49647)

STEINBOCK, L.
Messung von optischen Eigenschaften an
Reaktorwerkstoffen.
Jahrestagung Kerntechnik 2001, Dresden,
15.-17.Mai 2001
Bonn : INFORUM GmbH, 2001 S.407-10
(Auch auf CD-ROM)   (49872)

STEINBOCK, L.; DUSTMANN, C.H.
Investigation of the inner structure of ZEBRA

cells with a microtomograph.
Journal of the Electrochemical Society,
148(2001) Issue 2, S.A132-A136
(49382)

STEINBRÜCK, M.; MEIER, A.; STEGMEIER, U.;
STEINBOCK, L.; STUCKERT, J.
Oxidation of B_4C at high temperatures.
Jahrestagung Kerntechnik 2001, Dresden,
15.-17.Mai 2001
Bonn : INFORUM GmbH, 2001 S.193-96
(Auch auf CD-ROM)   (49878)

STEINBRÜCK, M.; STEINBOCK, L.; MEIER, A.;
STEGMAIER, U.; STUCKERT, J.; SCHANZ, G.;
KRAUSS, W.
Separate-effects tests.
Programm Nukleare Sicherheitsforschung.
Jahresbericht 2000
Wissenschaftliche Berichte, FZKA-6653
(September 2001) S.269-85   (50559)

STEINER, H.
Post test calculations for QUENCH-04 with the
FZK bundle code CALUMO.
Jahrestagung Kerntechnik 2001, Dresden,
15.-17.Mai 2001
Bonn : INFORUM GmbH, 2001 S.397-402
(Auch auf CD-ROM)   (49873)

STEINER, H.; HECK, M.
Recalculation of the temperature transient in
QUENCH-03 with the code CALUMO.
Programm Nukleare Sicherheitsforschung.
Jahresbericht 2000
Wissenschaftliche Berichte, FZKA-6653
(September 2001) S.259-67   (50558)

STRAUSS, D.; MÜLLER, G.; SCHUMACHER,
G.; ENGELKO, V.; STAMM, W.; CLEMENS, D.;
QUADAKKERS, W.J.
Oxide scale growth on MCrAlY bond coatings
after pulsed electron beam treatment and
deposition of EBPVD-TBC.
Internat.Conf.on Metallurgical Coatings and
Thin Films (ICMCTF-2000), San Diego, Calif.,
April 10-14, 2000
Surface and Coatings Technology, 135(2001)
S.196-201   (48590)

STRUWE, D.; PFRANG, W.; ZIMMERER, W.
Theoretische Interpretation der Ergebnisse
des CABRI-Programms.
Programm Nukleare Sicherheitsforschung.
Jahresbericht 2000
Wissenschaftliche Berichte, FZKA-6653
(September 2001) S.359-62   (50569)

STUCKERT, J.; STEINBRÜCK, M.; STEGMAIER,
U.
Single rod Quench tests with Zr-1Nb cladding.
Comparison with zircaloy-4 cladding tests and
modelling.
Wissenschaftliche Berichte, FZKA-6604 (Juni
2001)
http://bibliothek.fzk.de/zb/berichte/FZKA6604.pdf
(49997)

STUMPF, T.; BAUER, A.; COPPIN, F.; KIM, J.I.
Time-resolved laser fluorescence spectroscopy
(TRLFS) study of the sorption of Cm(III) onto
smectite and kaolinite.
79.Jahrestagung der Deutschen Mineralogischen
Gesellschaft, Potsdam, 9.-14.September 2001 :
Referate der Vorträge und Poster
Berichte der Deutschen Mineralogischen
Gesellschaft, No.1, 2001 S.184
(Beihefte zum European Journal of Mineralogy,
Vol. 13, 2001)   (50242)

STUMPF, T.; BAUER, A.; COPPIN, F.; KIM, J.I.
Time-resolved laser fluorescence spectroscopy
study of the sorption of Cm(III) onto smectite and
kaolinite.
Environmental Science and Technology,
35(2001) S.3691-94   (50397)

STUMPF, TH.; RABUNG, TH.; KLENZE, R.;
GECKEIS, H.; KIM, J.I.
Spectroscopic study of Cm(III) sorption onto
γ-alumina.
Journal of Colloid and Interface Science,
238(2001) S.219-24   (49855)

TAK, N.I.; CHENG, X.
Numerical design of the active part of the
MEGAPIE target.
Wissenschaftliche Berichte, FZKA-6611 (Juni
2001)
http://bibliothek.fzk.de/zb/berichte/FZKA6611.pdf
(49998)

TAK, N.I.; CHENG, X.; KNEBEL, J.U.
Thermalhydraulic layout of the MEGAPIE
spallation target.
Programm Nukleare Sicherheitsforschung.
Jahresbericht 2000
Wissenschaftliche Berichte, FZKA-6653
(September 2001) S.405-19   (50577)

TAN, S.S.; LENG, G.J.; NEITZEL, H.J.;
SCHMIDT, H.; CHENG, X.
Investigations on the passive containment
cooling system of an advanced Chinese PWR.
Wissenschaftliche Berichte, FZKA-6622
(Dezember 2001)
http://bibliothek.fzk.de/zb/berichte/FZKA6622.pdf
(51086)

THANG, N.M.; GECKEIS, H.; KIM, J.I.;
BECK, H.P.
Application of the flow field flow
fractionation (FFFF) to the characterization
of aquatic humic colloids: evaluation and
optimization of the method.
Colloids and Surfaces A, 181(2001) S.289-301
(49590)

THANG, N.M.; KNOPP, R.; GECKEIS, H.;
KIM, J.I.; BECK, H.P.
Detection of nanocolloids with flow-field
flow fractionation and laser-induced
breakdown detection.
Analytical Chemistry, 72(2000) S.1-5
(50956)

TROMM, W.; ALSMEYER, H.; CRON, T.;
SCHMIDT-STIEFEL, S.; WENZ, T.; ADELHELM,
C.; DILLMANN, H.G.; PASLER, H.; SCHÖCK,
W.; GREHL, C.; MERKEL, G.; FERDERER, F.;
SCHUMACHER, G.
Experimente zur Kühlung von Kernschmelzen
durch das CometPC-Konzept.
Jahrestagung Kerntechnik 2001, Dresden,
15.-17.Mai 2001
Bonn : INFORUM GmbH, 2001 S.239-42
(Auch auf CD-ROM)   (49707)

TROMM, W.; ALSMEYER, H.; CRON, T.;
FERDERER, F.; SCHMIDT-STIEFEL, S.;
WENZ, T.
Ex-vessel corium cooling by passive water
addition through porous concrete.
Proc.of the 9th Internat.Conf.on Nuclear
Engineering (ICONE-9), Nice, F, Apr. 8-12, 2001
Paris : SFEN, 2001 CD-ROM   (49724)

VASILE, A.; RIMPAULT, G.; TOMMASI, J.;
DE SAINT JEAN, C.; DELPECH, M.; HESKETH,
K.; BEAUMONT, H.M.; SUNDERLAND, R.E.;
NEWTON, T.; SMITH, P.; MASCHEK, W.; HAAS,
D.; DE RAEDT, C.; VAMBENEPE, G.; LEFEVRE,
J.C.
Fast reactors fuel cycle core physics results
from the CAPRA-CADRA programme.
GLOBAL 2001 : Internat.Conf.on the Back End
of the Fuel Cycle: From Research to
Solutions, Paris, F, September 9-13, 2001
Proc.on CD-ROM Paper 095
American Nuclear Soc., French Section, 2001
(49965)

VEJMELKA, P.; KIENZLER, B.; RÖMER, J.;
MARQUARDT, CH.; SOBALLA, E.; GEYER, F.;
KISELY, T.; HEATHMAN, D.
Actinide migration experiment in the HRL
ÄSPÖ, Sweden: results of laboratory and in
situ experiments (part I).
Wissenschaftl. Berichte, FZKA-6652 (Aug.2001)
http://bibliothek.fzk.de/zb/berichte/FZKA6652.pdf
(50413)

VEJMELKA, P.; KIENZLER, B.; RÖMER, J.;
MARQUARDT, CH.; SOBALLA, E.; GEYER, F.;
KISELY, T.; HEATHMAN, D.
Actinide migration experiment in the HRL
ÄSPÖ, Sweden: results of laboratory and in
situ experiments (part I).
Wissenschaftliche Berichte, FZKA-6652 (August
2001)
http://bibliothek.fzk.de/zb/berichte/FZKA6652.pdf
(50413)

VESER, A.; STERN, G.; GRUNE, J.;
BREITUNG, W.
Combustion tests at FZK 12m tube.
Programm Nukleare Sicherheitsforschung.
Jahresbericht 2000
Wissenschaftliche Berichte, FZKA-6653
(September 2001) S.17-23   (50538)

WALTHER, C.; HERLERT, A.; KIM, J.I.;
SCHERBAUM, F.J.; SCHWEIKHARD, L.; VOGEL,
M.
Absolute cross-sections for the nonresonant
multi-photon ionization of toluene and xylene
in the gas phase.
Chemical Physics, 265(2001) S.243-50
(49592)

WEIGL, M.; GEIST, A.; GOMPPER, K.; KIM, J.I.
Kinetics of lanthanide/actinide co-extraction with
N,N-dimethyl-N,N'-dibutyltetradecylmalonic
diamide (DMDBTDMA).
Solvent Extraction and Ion Exchange, 19(2001)
S.215-30   (49593)

WEIGL, M.; GEIST, A.; GOMPPER, K.
The DIAMEX process, first step in a partitioning
strategy: a kinetic study of lanthanide(III)/
actinide(III) co-extraction with N,N'-dimethyl-N,N'-
dibutyltetradecylmalonic diamide (DMDBTDMA).
Internat.Meeting on the Back End of the Fuel
Cycle: From Research to Solutions (GLOBAL
2001), Paris, F, September 9-13, 2001
Proc.on CD-ROM, Paper 146   (50587)

WEIGL, M.; NITSCH, W.
Control of interfacial reactions at liquid/liquid
interfaces by amphiphilic layers.
Transportmechanisms Across Fluid Interfaces :
Papers of the Final Meeting of a Priority
Program of the Deutsche Forschungs-
gemeinschaft, München, Nov. 29-Dec. 1, 1999
Weinheim [u.a.] : Wiley-VCH, 2000 S.339-56
(DECHEMA-Monographien ; 136)   (48348)

WEIGL, M.; NITSCH, W.
Kinetics of mass transfer and the different
effects of surfactants.
Cox, M. [Hrsg.]
Proc. of the Internat.Solvent Extraction
Conf. (ISEC '99), Barcelona, E, July 11-16,
1999

London : Society of Chemical Industry, 2001
S.853-58   (48349)

WILHELM, D.
Analysis of a thermite experiment to study
low pressure corium dispersion.
Wissenschaftliche Berichte, FZKA-6602 (August
2001)
http://bibliothek.fzk.de/zb/berichte/FZKA6602.pdf
                        (50410)

WILHELM, D.
Rechnungen zur Dispersion der Kernschmelze.
Programm Nukleare Sicherheitsforschung.
Jahresbericht 2000
Wissenschaftliche Berichte, FZKA-6653
(September 2001) S.101-07   (50546)

WINTRUFF, I.; GÜNTHER, C.
An adaptive moving grid model for convective
melting and solidification problems.
Ehrhard, P. [Hrsg.]
Interactive Dynamics of Convection and
Solidification : Proc.of the EUROMECH
Colloquium 408, Chamonix, F, March 18-22,
2000
Dordrecht [u.a.] : Kluwer Acad.Publ., 2001
S.235-42   (50272)

WINTRUFF, I.; GÜNTHER, C.; CLASS, A.G.
An interface-tracking control-volume
finite-element method for melting and
solidification problems. Part II:
Verification and application.
Numerical Heat Transfer B, 39(2001) S.127-49
                        (49355)

WINTRUFF, I.; GÜNTHER, C.; CLASS, A.G.
An interface-tracking control-volume
finite-element method for melting and
solidification problems. Part I: Formulation.
Numerical Heat Transfer B, 39(2001) S.101-25
                        (49356)

WÖRNER, M.; CACUCI, D.G.; GHIDERSA, B.;
GRÖTZBACH, G.; SABISCH, W.
Entwicklung von Methoden zur
Grobstruktursimulation turbulenter
Zweiphasenströmungen.
Theoretische Untersuchungen.
Programm Nukleare Sicherheitsforschung.
Jahresbericht 2000
Wissenschaftliche Berichte, FZKA-6653
(September 2001) S.345-52   (50566)

WÖRNER, M.; SABISCH, W.; GRÖTZBACH, G.;
CACUCI, D.G.
Volume-averaged conservation equations for
volume-of-fluid interface tracking.
Michaelides, E.E. [Hrsg.]
Proc.of the 4th Internat.Conf.on Multiphase
Flow, New Orleans, La., May 27 - June 1, 2001

CD-ROM   (49830)

XU, Z.; KOTCHOURKO, A.
Development, implementation and verification
of a reduced hydrogen-air chemistry model for
the COM3D computer code.
Wissenschaftliche Berichte, FZKA-6675
(November 2001)
http://bibliothek.fzk.de/zb/berichte/FZKA6675.pdf
                        (50842)

YUN, J.; BUNDSCHUH, T.; NECK, V.; KIM, J.I.
Selective determination of europium(III)
oxide and hydroxide colloids in aqueous
solution by laser-induced breakdown
spectroscopy.
Applied Spectroscopy, 55(2001) S.273-78
                        (49595)

YUN, J.I.
Entwicklung einer Laser-induzierten
Breakdown-Spektroskopie zur Charakterisierung
von Glasschmelzen und aquatischen Kolloiden.
Wissenschaftliche Berichte, FZKA-6586
(Februar 2001)
Dissertation, Universität Aachen 2000
http://bibliothek.fzk.de/zb/berichte/FZKA6586.pdf
                        (49353)

ZIMMER, P.; BOHNERT, E.; KIM, J.I.;
ALTHAUS, E.
Formation of secondary phases after longterm
corrosion of simulated HAW glass in brine
solutions at 190°C.
79.Jahrestagung der Deutschen Mineralogischen
Gesellschaft, Potsdam, 9.-14.September 2001 :
Referate der Vorträge und Poster
Berichte der Deutschen Mineralogischen
Gesellschaft, No.1, 2001 S.204
(Beihefte zum European Journal of Mineralogy,
Vol. 13, 2001)   (50243)

ZIMMER, P.; KIM, J.I.; ALTHAUS, E.
Einfluss von Eisen auf die Auslaugungsrate
von simulierten, radioaktiven Abfallgläsern.
79.Jahrestagung der Deutschen Mineralogischen
Gesellschaft, Potsdam, 9.-14.September 2001 :
Referate der Vorträge und Poster
Berichte der Deutschen Mineralogischen
Gesellschaft, No.1, 2001 S.205
(Beihefte zum European Journal of Mineralogy,
Vol. 13, 2001)   (50244)

Vorträge, die nicht in gedruckter Form vorliegen

ADROGUER, B.; CHATELARD, P.;
VAN DORSSELAERE, J.P.; DURIEZ, C.;
COCUAUD, N.; BELLENFANT, L.;
BOTTOMLEY, D.;
VRTILKOVA, V.; MUELLER, K.; HERING, W.;
HOMANN, C.; KRAUSS, W.; MIASSOEDOV, A.;
STEINBRÜCK, M.; HOZER, Z.; BANDINI, G.;
BIRCHLEY, J.; BERLEPSCH, T.VON; BUCK, M.;
BENITEZ, J.A.F.; VIRTANEN, E.; MARGUET, S.;
AZARIAN, G.; PLANK, H.; VESHCHUNOV, M.;
ZVONAREV, Y.
Core loss during a severe accident (COLOSS)
FISA-2001 Symp.on EU Research on Severe
Accidents and Post-FISA-2001 Workshop
Session, Luxembourg, L, November 12-15, 2001
(V50940)

ANDREEV, A.D.; ENGELKO, V.I.; MÜLLER, G.
Multipoint explosive emission cathode
operation in external magnetic field.
13th IEEE Internat.Pulsed Power Conf., Las
Vegas, Nev., June 17-22, 2001
http://bibliothek.fzk.de/zb/veroeff/49897.htm
(V49897)

ARTINGER, R.; BUCKAU, G.; ZEH, P.;
GERAEDTS, K.; VANCLUYSEN, J.; MAES, A.;
KIM, J.I.
Humic colloid mediated transport of
tetravalent actinides and technetium.
8th Internat.Conf.on Chemistry and Migration
Behaviour of Actinides and Fission Products
in the Geosphere (Migration '01), Bregenz, A,
September 16-21, 2001
Book of Abstracts S.70   (V50735)

ARTINGER, R.; SCHÜSSLER, W.; GECKEIS,
H.;
KIM, J.I.
^{241}Am migration in a sandy aquifer studied
by long-term column experiments.
8th Internat.Conf.on Chemistry and Migration
Behaviour of Actinides and Fission Products
in the Geosphere (Migration '01), Bregenz, A,
September 16-21, 2001
Book of Abstracts S.85   (V50739)

BARBOT, C.; DURAND, J.P.; PIERI, J.;
GOUDARD, F.; KIM, J.I.; BUCKAU, G.;
CZERWINSKI, K.; VIAL, M.; MOULIN, V.
Complexation of Eu(III) with humic acid
coated epoxy silica gel.
8th Internat.Conf.on Chemistry and Migration
Behaviour of Actinides and Fission Products
in the Geosphere (Migration '01), Bregenz, A,
September 16-21, 2001
Book of Abstracts S.136   (V50748)

BERNOTAT, W.; LE GAL, X.; CROVISIER, J.L.
Retention of LREE and HREE by smectite in
altered basaltic glass.
8th Internat.Conf.on Chemistry and Migration
Behaviour of Actinides and Fission Products
in the Geosphere (Migration '01), Bregenz, A,
September 16-21, 2001
Book of Abstracts S.103   (V50740)

BIELERT, U.; BREITUNG, W.; BURGETH, B.;
KOTCHOURKO, A.; SCHOLTYSSEK, W.;
PAILHORIES, P.; PETIT, M.; STUDER, E.;
EYINK, J.; MOVAHED, M.; PETZOLD, K.G.;
HEITSCH, M.; ALEKSEEV, V.; DOROFEEV, S.;
EFIMENKO, A.; KUZNETSOV, M.; OKUN, M.;
YANKIN, Y.; HULD, T.
Integral large scale experiments on hydrogen
combustion for severe accident code
validation HYCOM.
FISA-2001 : EU Research in Reactor Safety,
Mid-Term Symp.on Shared-Cost and Concerted
Actions, Luxembourg, L, November 12-14, 2001
(V51139)

BITEA, C.; KIM, J.I.; SCHERBAUM, F.;
WALTHER, C.
On the agglomeration behaviour of
ZrO_2-colloids at trace concentrations.
8th Internat.Conf.on Chemistry and Migration
Behaviour of Actinides and Fission Products
in the Geosphere (Migration '01), Bregenz, A,
September 16-21, 2001
Book of Abstracts S.57   (V50732)

BITEA, C.; WALTHER, C.
Zeitaufgelöste Beobachtung der Agglomeration
von ZrO_2-Partikeln.
Frühjahrstagung des Arbeitkreises Atome,
Moleküle Quantenoptik und Plasmen der DPG,
Berlin, 2.-6.April 2001
Verhandlungen der Deutschen Physikalischen
Gesellschaft, R.6, Bd.36 (2001) MP 1.30
http://bibliothek.fzk.de/zb/veroeff/49133.htm
(V49133)

BOSBACH, D.
Die Reaktivität von
Schichtsilikatoberflächen.
Geowissenschaftliches Kolloquium, Karlsruhe,
11.Dezember 2001   (V51097)

BOSBACH, D.
Kristallwachstum im molularen Maßstab:
Mechanismen und Kinetik.
Freiberger Forschungsforum - Kristallisation
und Technik, Freiberg, 21.Juni 2001 (V51098)

BOUBY, M.; NGO-MANH, T.; GECKEIS, H.;
SCHERBAUM, F.; KIM, J.I.
Characterization of colloidal actinide
species in groundwater by LIBD and ICP-MS
with size fractionation.

8th Internat.Conf.on Chemistry and Migration
Behaviour of Actinides and Fission Products
in the Geosphere (Migration '01), Bregenz, A,
September 16-21, 2001
Book of Abstracts S.73   (V50738)

BREITUNG, W.; NECKER, G.; KAUP, B.;
VESER, A.
Numerical simulation of hydrogen release in a
private garage.
4th Internat.Symp.on Hydrogen Power -
Theoretical and Engineering Solutions
(HYPOTHESIS IV), Stralsund, September 9-14,
2001   (V50072)

BUCKAU, G.
Groundwater humic substances: origin,
mobility and impact on radionuclide
transport.
Vortr.: University of Cyprus, Nikosia, CY,
18.Oktober 2001   (V50949)

BUCKAU, G.
Huminstoff-Kolloide: Herkunft, Mobilität und
ihr Einfluß auf den Transport von Actiniden.
Vortr.: Hydrologisches Kolloquium,
Universität München, 11.Dezember 2001
                          (V50952)

BUCKAU, G.
General information to nuclear power and
radioactive waste management in Germany and
impact of colloids on the mobility of actinide ions
in groundwater.
Vortr.: Massachusetts Institute of Technology,
Boston, Mass., 22.März 2001   (V50953)

BUCKAU, G.
Humic colloids: origin, mobility and impact
on actinide migration.
8th Internat.Conf.on Chemistry and Migration
Behaviour of Actinides and Fission Products
in the Geosphere (Migration '01), Bregenz, A,
September 16-21, 2001   (V51213)

BUCKAU, G.; HAUSER, W.; GECKEIS, H.;
KIM, J.I.; DEGUELDRE, C.; KERSTING, A.B.
Impact of colloids on long-term safety in
performance assessment of nuclear waste
disposal.
GEOTRAP 5 Workshop (Geological Evidence
and Theoretical Bases for Radionuclide-
Retention
Processes in Heterogeneous Media), Äspö, S,
May 29, 2001   (V50951)

BURGETH, B.
Accurate and efficient evaluation of
integrals involving the beta distribution.
Jahrestagung der Gesellschaft für Angewandte
Mathematik und Mechanik, Zürich, CH, February
12-15, 2001   (V50069)

CLASS, A.
An interface-tracking control-volume
finite-element method for melting and
solidification problems.
Vortr.: Northwestern University, Evanston,
Ill., 15.Januar 2001   (V51106)

COPPIN, F.; BAUER, A.; BERGER, G.;
CASTET, S.; STUMPF, T.; LOUBET, M.
Adsorption of lanthanides on smectite and
kaolinite.
8th Internat.Conf.on Chemistry and Migration
Behaviour of Actinides and Fission Products
in the Geosphere (Migration '01), Bregenz, A,
September 16-21, 2001
Book of Abstracts S.65   (V50734)

DAGAN, R.; CACUCI, D.G.; BROEDERS, C.H.M.
On the use of perturbation theory for dynamic
simulation of accelerator driven systems
(ADS).
17th Internat.Conf.on Transport Theory,
London, July 8-14, 2001
Book of Abstracts S.124   (V50483)

DARDENNE, K.; SCHÄFER, T.;
LINDQVIST-REIS, P.; DENECKE, M.A.;
PLASCHKE, M.; ROTHE, J.; KIM, J.I.
Low temperature XAFS investigation on the
mineralization of lutetium in the HFO
alteration process.
8th Internat.Conf.on Chemistry and Migration
Behaviour of Actinides and Fission Products
in the Geosphere (Migration '01), Bregenz, A,
September 16-21, 2001
Book of Abstracts S.194   (V50757)

DENECKE, M.A.
X-ray absorption fine structure
investigations for actinide speciation.
8th Internat.Conf.on Chemistry and Migration
Behaviour of Actinides and Fission Products
in the Geosphere (Migration '01), Bregenz, A,
September 16-21, 2001   (V50947)

DENECKE, M.A.; MARQUARDT, C.M.; ROTHE,
J.; NECK, V.; MÜLLER, R.; DARDENNE, K.;
JENSEN, M.P.
XAFS studies of actinide coordination structure.
Actinides-2001 : Internat.Conf., Hayama, J,
November 4-9, 2001
Abstracts S.125   (V50869)

DENECKE, M.A.; ROTHE, J.
X-ray absorption fine structure (XAFS)
spectroscopy as a speciation tool.
Workshop 'How to Use Synchrotron Radiation
Techniques in Environmental Science',
Karlsruhe, October 1-2, 2001   (V50945)

DOLENSKY, B.; GÖLLER, B.; JORDAN, T.;
KRIEG, R.; LUX, M.; MESSEMER, G.; RIEGER,
H.; SIDOR, M.
Reactor pressure vessel head loaded by a
corium slug impact.
16th Internat.Conf.on Structural Mechanics in
Reactor Technology (SMiRT 16), Washington,
D.C., August 12-17, 2001   (V50489)

EHRHARD, P.; BUNK, M.
Spreading flows with solidification: model
for top crusting.
Jahrestagung der Gesellschaft für Angewandte
Mathematik und Mechanik, Zürich, CH, February
12-15, 2001   (V50030)

EHRHARDT, J.
Installation des RODOS Systems im
Europäischen Raum.
4.Seminar Notfallschutz 'Messen und Rechnen
im Notfallschutz', München, 28.-30.März 2001
          (V49274)

FISCHER, K.; BROECKERHOFF, P.; AHLERS,
G.; GUSTAVSSON, V.; POLO, J.; DOMINGUEZ,
T.; ROYL, P.
Hydrogen removel from LWR containments by
catalytic coated thermal insulation elements
(THINCAT).
FISA-2001 : EU Research in Reactor Safety,
Mid-Term Symp.on Shared-Cost and Concerted
Actions, Luxembourg, L, November 12-14, 2001
          (V51024)

FRITZ, P.
Kompetenzverbund Kerntechnik - Perspektiven
in Forschung und Lehre.
ILK: Chancen und Risiken der Kernenergie,
Bühler Höhe, Baden-Baden, 26.April 2001
Jahrestagung Kerntechnik 2001, Dresden,
15.-17.Mai 2001
KTG-Workshop 'Kernenergie hat Zukunft',
Erlangen, 11.Oktober 2001   (V51211)

FRITZ, P.
Maintenance of competence in the R&D field of
nuclear energy - a German perspective.
Policy Debate: Infrastructure and the
Maintenance of Competence in the Field of
Nuclear Energy, OECD-Nuclear Energy Agency,
Paris, F, May 4, 2001   (V51212)

FUSS, M.; FANGHÄNEL, E.; GECKEIS, H.;
GOMPPER, K.; PLASCHKE, M.; HAUSER, W.;
GÖRTZEN, A.; KIM, J.I.
Anwendung der Laserablation zur Analytik von
Radionukliden.
Fachtagung Nuklearchemie, Würzburg,
September
24-26, 2001   (V50933)

GANOR, J.; METZ, V.
To stir or not to stir - implications for silicate
dissolution experiments.
10th Internat.Symp.on Water-Rock Interaction,
Villasimus, I, June 10-15, 2001   (V50231)

GECKEIS, H.; HAUSER, W.; GEYER, F.W.;
GÖTZ, R.; SCHÄFER, TH.; RABUNG, T.;
BAUER, A.; PLASCHKE, M.; NGO-MANH, T.;
KIM, J.I.
Kolloidgetragener Radionuklidtransport in einer
granitischen Kluft. Erkenntnisse aus Labor- und in-
situ Experimenten.
Fachtagung Nuklearchemie, Würzburg, September
24-26, 2001   (V50932)

GECKEIS, H.; RAMAROSON, V.; GÖRTZEN, A.;
PORZELT, C.
Determination of Sr-90, Fe-55 and Ni-63 in
waste samples by extraction chromatography.
Internat.Conf.on Advances in Liquid
Scintillation Spectrometry (LSC-2001),
Karlsruhe, May 7-11, 2001   (V50931)

GEIST, A.
Einsatz der nichtdispersiven Flüssig-Flüssig-
Extraktion im Minor-Actinide-Partitioning.
Tagung des GVC-Fachausschusses 'Extraktion',
Bremen, 7.-8.September 2000   (V49640)

GEIST, A.; WEIGL, M.; GOMPPER, K.
Aufbau und Betrieb einer Hohlfaser-Microplant
für die Flüssig-Flüssig-Extraktion.
Deutsche Vereinigung für Chemie und Verfahrens-
technik (DVCV),
Gemeinschaftsausschuss Extraktion, Frankfurt,
27.-28.September 2001   (V50591)

GEIST, A.; WEIGL, M.; MÜLLICH, U.;
GOMPPER, K.
Hochselektive Abtrennung von Actiniden(III) von
den Spaltlanthaniden aus salpetersauren
Lösungen mittels nichtdispersiver Flüssig-Flüssig-
Extraktion.
Jahrestagung der Gesellschaft Deutscher
Chemiker (GDCh), Würzburg, 24.-26.September
2001   (V50592)

GEIST, A.; WEIGL, M.; MÜLLICH, U.;
GOMPPER, K.
Separation of actinides(III) from fission
lanthanides by non-dispersive liquid-liquid
extraction.
Actinides-2001 : Internat.Conf., Hayama, J,
November 4-9, 2001   (V50867)

GLAUS, M.A.; BAEYENS, B.; LAUBER, M.;
RABUNG, T.; VAN LOON, L.R.
The effect of organic matter extracted from
Mont Terri and Benken Opalinus clay on the
speciation of radionuclides.
8th Internat.Conf.on Chemistry and Migration

Behaviour of Actinides and Fission Products
in the Geosphere (Migration '01), Bregenz, A,
September 16-21, 2001
Book of Abstracts S.91   (V50971)

GRAMBOW, B.; MÜLLER, R.; MARQUARDT,
C.M.; BUNDSCHUH, T.; SCHUBERT, P.
Monomer-oligomer-colloid - solid transitions
in the precipitation of UO_2 from aqueous
solutions.
8th Internat.Conf.on Chemistry and Migration
Behaviour of Actinides and Fission Products
in the Geosphere (Migration '01), Bregenz, A,
September 16-21, 2001
Book of Abstracts S.113   (V50742)

GRÖTZBACH, G.
Simulation der Konvektion bei mittleren und
kleinen Prandtl-Zahlen.
Treffen zum DFG-Projekt 'Interdisziplinäre
Turbulenzinitiative', Universität Ilmenau,
5.-7.September 2001   (V50367)

GRÖTZBACH, G.
Numerical analysis of LWR sump cooling
experiments.
Seminar, Research Laboratory for Nuclear
Reactors, Tokyo Institute of Technology
(TIT), Tokyo, J, September 24-25, 2001
                    (V50603)

GRÖTZBACH, G.; CARTECIANO, L.N.; DORR,
B.; JIN, X.
Analysis of an LWR sump cooling concept.
IAHR Congress, Special Seminar on Advances in
Industrial Hydraulics and Applications to
Energy Production, Beijing, China, September
17-21, 2001   (V50486)

HAUSER, W.
Online-Quantifizierung von Kolloiden im
Felslabor Grimsel mit der Laser-induzierten
Breakdown-Detektion.
Vortr.: Forschungszentrum Rossendorf,
Dresden, 21.März 2001   (V50229)

HAUSER, W.; GECKEIS, H.; KIM, J.I.;
FIERZ, T.
Online-monitoring of colloid migration with
laser-induced breakdown detection at the
Grimsel test site.
8th Internat.Conf.on Chemistry and Migration
Behaviour of Actinides and Fission Products
in the Geosphere (Migration '01), Bregenz, A,
September 16-21, 2001
Book of Abstracts S.72   (V50736)

HERING, W.; HOMANN, CH.; SANCHEZ, V.;
SENGPIEL, W.; STRUWE, D.;
MESSAINGUIRAL, CH.
Code validation and core degradation analyses
with S/R5 and ICARE2.

CSARP Meeting (CSARP = Cooperative Severe
Accidents Research Programme), Bethesda, Md.,
May 7-10, 2001   (V50484)

JANATA, E.; KELM, M.; GORDEEV, A.V.;
ERSHOV, B.G.
Radiation-chemical effects in the near-field
of a final disposal site: role of bromine on
the radiolytic processes in NaCl-solutions.
8th Internat.Conf.on Chemistry and Migration
Behaviour of Actinides and Fission Products
in the Geosphere (Migration '01), Bregenz, A,
September 16-21, 2001
Book of Abstracts S.140   (V50749)

JANSSENS-MAENHOUT, G.; UMEKAWA, H.;
SCHULENBERG, T.
Geysering with two-dimensional effects.
4th Internat.Conf.on Multiphase Flow
(ICFM-2001), New Orleans, La., May 27 - June
1, 2001   (V49968)

JONES, A.V.; DICKINSON, S.; DE PASCALE, C.;
HANNIET, N.; HERRANZ, L.; DE ROSA, F.;
HENNEGES, G.; LANGHANS, J.; HOUSIADAS,
C.; WICHERS, V.; BIRCHLEY, J.; PACI, S.;
MARTIN-FUERTES, F.
Validation of severe accident codes against
phebus FP for plant applications (PHEBEN2).
FISA-2001 : EU Research in Reactor Safety,
Mid-Term Symp.on Shared-Cost and Concerted
Actions, Luxembourg, L, November 12-14, 2001
                    (V51025)

KELM, M.; BOHNERT, E.
Radiolysis and corrosion of ^{238}Pu doped UO_2
pellets in chloride brine.
Internat.Spent Fuel Workshop, Helsinki, SF,
September 13-14, 2001   (V50595)

KIENZLER, B.
Geochemisches Verhalten von Plutonium in
einem Endlager. Mobilität und Kritikalität.
Vortr.: Reaktorsicherheitskommission,
Ausschuss Ver- und Entsorgung, Bonn,
20.Februar 2001   (V50226)

KIENZLER, B.
Near field geochemistry. Overview of German
activities.
USDOE-CBFO German Workshop, Carlsbad,
N.M.,
April 25-27, 2001   (V50227)

KIENZLER, B.
Actinide and colloid migration experiments in
granite.
Vortr.: Bundesanstalt für Geowissenschaften
und Rohstoffe (BGR), Hannover, 30.Mai 2001
                    (V50228)

646

KIENZLER, B.; VEJMELKA, P.; RÖMER, J.;
FANGHÄNEL, E.; WIKBERG, P.; JANSSON, M.;
ERIKSEN, T.E.
Swedish-German actinide migration experiment
at ÄSPÖ HRL.
8th Internat.Conf.on Chemistry and Migration
Behaviour of Actinides and Fission Products
in the Geosphere (Migration '01), Bregenz, A,
September 16-21, 2001
Book of Abstracts S.160   (V50751)

KIM, J.I.
Anforderungen an die Trennchemie und deren
Möglichkeiten.
527.DECHEMA-Kolloquium 'Ein neuer Weg zur
Entsorgung von abgebrannten Kernbrennstoffen?
Trennchemie und Transmutation', Frankfurt,
8.Februar 2001   (V49641)

KIM, J.I.
Aquatic colloids of actinides: how are they
generated and do they migrate.
221st Nat.Meeting of the American Chemical
Society, San Diego, Calif., April 1-5, 2001
Abstracts Nr.94   (V49971)

KIM, J.I.
Is thermodynamics of actinides applicable to
natural dynamic systems?
3rd NUCEF Internat.Symp., Scientific Basis
for Criticality Safety, Separation Process
and Waste Disposal, Tokai Mura, J, October 31
- November 2, 2001   (V50863)

KIM, J.I.
Nanoscopic speciation of aquatic actinides by
laser spectroscopy.
2.Mainzer Symp.über Spurenanalytik, Mainz,
9.November 2001   (V50864)

KIM, J.I.
Chemical behaviour of Pu and minor actinides
in natural aquifer systems: solubility,speciation
and migration.
Du Combustible Nucleaire aux Dechets :
Recherches Actuelles, Academie des Sciences,
Paris, F, 6-8 Decembre 2001   (V51013)

KIM, M.A.; KÖHLER, K.; PANAK, P.; KLENZE,
R.
Interaction of actinides with alumina-silica-
colloids in statu nascendi.
8th Internat.Conf.on Chemistry and Migration
Behaviour of Actinides and Fission Products
in the Geosphere (Migration '01), Bregenz, A,
September 16-21, 2001
Book of Abstracts S.113   (V50741)

KLENZE, R.; CHUNG, K.H.; PARK, K.K.;
PAVIET-HARTMANN, P.; LINDQVIST-REIS, P.;
KIM, J.I.
Incorporation of Eu(III) and Cm(III) in

silica studied by time-resolved laser
fluorescence spectroscopy.
8th Internat.Conf.on Chemistry and Migration
Behaviour of Actinides and Fission Products
in the Geosphere (Migration '01), Bregenz, A,
September 16-21, 2001
Book of Abstracts S.56   (V50731)

KLENZE, R.; KIM, J.I.; MORI, M.;
MIYAJIMA, T.
A complexation study of Cm(III) with fulvic
acid of different origin by time-resolved
laser fluorescence spectroscopy (TRLFS).
Actinides-2001 : Internat.Conf., Hayama, J,
November 4-9, 2001
Abstracts S.92   (V50870)

KNEBEL, J.U.
HGF strategy fund project: innovative
technology to reduce radiotoxicity.
Vortr.: Japan Atomic Energy Research
Institute (JAERI), Tokai Mura, J, 11.Dezember
2000
Vortr.: Korean Atomic Energy Research
Institute (KAERI), Taejan, Korea, 18.Dezember
2000   (V49284)

KNEBEL, J.U.; CHENG, X.; TAK, N.I.
Thermalhydraulic design of the MEGAPIE
spallation target.
5th Topical Meeting on Nuclear Applications
of Accelerator Technology (AccApp '01), Reno,
Nev., November 11-15, 2001   (V50600)

KNEBEL, J.U.; KLEIN, J.C.; GORSE, D.;
AGOSTINI, P.; GRÖSCHEL, F.; KUPSCHUS, P.;
KIRCHNER, T.; VOGT, J.B.
MEGAPIE-TEST: A European project on
spallation target testing.
5th Topical Meeting on Nuclear Applications
of Accelerator Technology (AccApp '01), Reno,
Nev., November 11-15, 2001   (V50601)

KNEBEL, J.U.; MÜLLER, G.; KONYS, J.
ADS test facilities in the European Union.
Pb-Bi Internat.Meeting of the Japan Nuclear
Cycle Development Institute, O'Arai, J,
12.Dezember 2000   (V49285)

KNEBEL, J.U.; MÜLLER, G.; KONYS, J.
Development of Pb-Bi application technologies
at Forschungszentrum Karlsruhe.
Pb-Bi Internat.Meeting of the Japan Nuclear
Cycle Development Institute, O'Arai, J,
13.Dezember 2000   (V49436)

KONYS, J.
Corrosion investigations in lead and
lead-bismuth at Forschungszentrum Karlsruhe.
Scientific Advisory Committee Reactor Safety,
Fuel and Reactor Materials-Meeting, Mol, B,
February 9, 2001   (V49543)

KOTCHOURKO, A.; BURGETH, B.;
DOROFEEV, S.B.; BREITUNG, W.
Turbulent reactive flow simulation with
presumed β-PDF combustion model.
18th Internat.Colloquium on the Dynamics of
Explosions and Reactive Systems, Seattle,
Wash., July 29 - August 3, 2001   (V51028)

KRIEG, R.; JORDAN, T.; DOLENSKY, B.;
MALMBERG, T.; AKTAA, J.; PLITZ, H.;
JULISCH, P.; SEIDENFUSS, M.; TALJA, H.;
SOLOMOS, G.; AIFANTIS, E.; CIZELJ, L.;
CAROLI, C.; FOKKENS, J.; BJANDARI, S.B.;
VERON, P.; TRAUTH, M.
Limit strains for severe accident conditions,
description of an European research program
and first results.
16th Internat.Conf.on Structural Mechanics in
Reactor Technology (SMiRT 16), Washington,
D.C., August 12-17, 2001   (V50490)

KUCZEWSKI, B.; GECKEIS, H.; KRATZ, J.V.;
SEIBERT, A.; TRAUTMANN, N.
Investigations on the redox behaviour of
plutonium in the presence of humic acid.
8th Internat.Conf.on Chemistry and Migration
Behaviour of Actinides and Fission Products
in the Geosphere (Migration '01), Bregenz, A,
September 16-21, 2001
Book of Abstracts S.142   (V50750)

LOIDA, A.; GRAMBOW, B.; GECKEIS, H.
Spent fuel corrosion behavior in salt solution in
the presence of hydrogen overpressure.
ICEM'01 : The 8th Internat.Conf.on Radioactive
Waste Management andEnvironmental
Remediation, Bruges, B, September 30 - October
4, 2001   (V50594)

LOIDA, A.; MÜLLER, N.
High burn-up spent fuel dissolution studies
in salt brine: effects of the near field.
Internat.Spent Fuel Workshop, Helsinki, SF,
September 13-14, 2001   (V50596)

LOIDA, A.; MÜLLER, N.
Post irradiation examinations of high burnup
spent fuel samples: corrosion test procedures,
sampling and sample treatment.
Technical Workshop 'Hot Laboratories and
Remote Handling', Madrid, E, October 22-24,
2001   (V50597)

LUCKSCHEITER, B.; NESOVIC, M.
Sorption behaviour of Am on precorroded HLW
glass in water and brines.
8th Internat.Conf.on Chemistry and Migration
Behaviour of Actinides and Fission Products
in the Geosphere (Migration '01), Bregenz, A,
September 16-21, 2001   (V50116)

LÜTZENKIRCHEN, J.; WERSIN, P.
The influence of temperature on sorption in a
high level waste environment: a preliminary
assessment.
8th Internat.Conf.on Chemistry and Migration
Behaviour of Actinides and Fission Products
in the Geosphere (Migration '01), Bregenz, A,
September 16-21, 2001
Book of Abstracts S.165   (V50753)

MALMBERG, T.; KROMPHOLZ, K.; SOLOMOS,
G.; AIFANTIS, E.C.
Size effects in deformation and fracture of a
ferritic reactor pressure vessel steel.
16th Internat.Conf.on Structural Mechanics in
Reactor Technology (SMiRT 16), Washington,
D.C., August 12-17, 2001   (V50487)

MALMBERG, T.; TSAGRAKIS, I.;
ELEFTHERIADIS, I.; AIFANTIS, E.C.;
KROMPHOLZ, K.; SOLOMOS, G.
Gradient plasticity approach to size effects.
16th Internat.Conf.on Structural Mechanics in
Reactor Technology (SMiRT 16), Washington,
D.C., August 12-17, 2001   (V50488)

MARQUARDT, C.M.; ARTINGER, R.; BUCKAU,
G.; DARDENNE, K.; DENECKE, M.A.; GECKEIS,
H.; MONSALIER, J.M.; THAN, N.M.; PLASCHKE,
M.; ROTHE, J.; SCHÄFER, T.; SCHÜSSLER, W.
FuE-Arbeiten zur Huminstoff-Radionuklid-
Wechselwirkung.
5.Projektstatusgespräch zu FuE-Vorhaben auf
dem Gebiet der Entsorgung gefährlicher
Abfälle in tiefen geologischen Formationen,
Leipzig, 15.-16.Mai 2001   (V50957)

MARQUARDT, C.M.; KIM, J.I.; PIRLET, V.
Complexation of tetravalent neptunium with
fulvic acid.
Actinides-2001 : Internat.Conf., Hayama, J,
November 4-9, 2001
Abstracts S.140   (V50866)

MARQUARDT, C.M.; SEIBERT, A.; KIM, S.S.;
GECKEIS, H.
Trennung von Plutonium(III-VI)-Ionen mittels
Ionenaustauschchromatographie.
Jahrestagung Chemie 2001, Würzburg,
23.-29.September 2001   (V50958)

MASCHEK, W.
The SIMMER-III code: applications to
subcritical accelerator driven systems.
Topical Day on Reactor Physics Computational
Methods, Mol, B, October 16, 2001
Book of Abstracts S.15   (V50891)

MASCHEK, W.
Review of safety issues of waste incinerating
ADSs: severe accidents with core degradation.
GEDEON Workshop Simulation Applied to

Innovative Systems for Transmutation, Paris,
F, October 2-3, 2001   (V50892)

MASCHEK, W.; RINEISKI, A.; WANG, S.;
FLAD, M.; MORITA, K.
Safety improvements for ADS transmuters with
dedicated fuel.
Nuclear Applications in the New Millenium
(ADDTA '01), Reno, Nev., November 11-15,
2001   (V50268)

MATERNA-MORRIS, E.; GRAF, P.;
ZIMMERMANN, H.
Quantitative Fraktographie am Beispiel von
geprüften Zugversuchsproben.
Metallographie-Tagung, Neu-Ulm,
19.-21.September 2001   (V51000)

METZ, V.; CAMA, J.; GANOR, J.;
WEINGARTEN, B.
Affinity effect on smectite dissolution rate
at acidic and basic conditions.
79.Jahrestagung der Deutschen Mineralogischen
Gesellschaft, Potsdam, 9.-13.September 2001
        (V50162)

METZ, V.; KIENZLER, B.; SCHÜSSLER, W.;
KIM, J.I.
Evaluation of different groundwater – host rock
systems with respect to actinide mobilization.
8th Internat.Conf.on Chemistry and Migration
Behaviour of Actinides and Fission Products
in the Geosphere (Migration '01), Bregenz, A,
September 16-21, 2001
Book of Abstracts S.104   (V50589)

METZ, V.; KIENZLER, B.; SCHÜSSLER, W.
Geochemische Modellierung der Korrosion von
radioaktiven Abfallprodukten.
Jahrestagung der Gesellschaft Deutscher
Chemiker (GDCh), Würzburg, 24.-26.September
2001   (V50593)

METZ, V.; KIENZLER, B.; SCHÜSSLER, W.;
KIM, J.I.
Geochemical modeling in context of site
evaluation.
8th Internat.Conf.on Chemistry and Migration
Behaviour of Actinides and Fission Products
in the Geosphere (Migration '01), Bregenz, A,
September 16-21, 2001   (V50783)

MEYER, L.; GARGALLO, M.
Low pressure corium dispersion experiments
with lateral failure in the bottom head of the
pressure vessel.
16th Internat.Conf.on Structural Mechanics in
Reactor Technology (SMiRT-16), Post
Conf.Seminar 'Containment of Nuclear
Reactors', Albuquerque, N.M., August 20-21,
2001   (V50330)

MONSALLIER, J.M.; ARTINGER, R.; DENECKE,
M.A.; SCHERBAUM, F.; BUCKAU, G.; KIM, J.I.
Spectroscopic study (TRLFS and EXAFS) on the
kinetic availability of humate complexes of
TRI- and tetravalent actinide ions.
8th Internat.Conf.on Chemistry and Migration
Behaviour of Actinides and Fission Products
in the Geosphere (Migration '01), Bregenz, A,
September 16-21, 2001
Book of Abstracts S.129   (V50746)

MÖRI, A.; GECKEIS, H.; FIERZ, T.
Field tracer migration tests at the Grimsel test site.
Studying the colloid migration in a granitic fracture.
8th Internat.Conf.on Chemistry and Migration
Behaviour of Actinides and Fission Products
in the Geosphere (Migration '01), Bregenz, A,
September 16-21, 2001
Book of Abstracts S.161   (V50752)

MÖRI, A.; GECKEIS, H.; MISSANA, T.; GUIMERA,
J.; DEGUELDRE, C.; MEYER, P.; OTA, K.;
PAPENGUTH, H.; ALEXANDER, W.R.;HERNAN,
P.
The colloid and radionuclide retardation
experiment (CRR) at the Grimsel test site first
evidences for the colloid-mediated radionuclide
transport in a granitic fracture.
8th Internat.Conf.on Chemistry and Migration
Behaviour of Actinides and Fission Products
in the Geosphere (Migration '01), Bregenz, A,
September 16-21, 2001   (V50916)

MÜLLER, G.; BLUHM, H.; ENGELKO, V.;
KOMAROV, O.
Improvement of the spatial current density
distribution of intense pulsed electron beams.
13th IEEE Internat.Pulsed Power Conf., Las
Vegas, Nev., June 17-22, 2001
http://bibliothek.fzk.de/zb/veroeff/49774.htm
        (V49774)

MÜLLER, G.; HEINZEL, A.; SCHUMACHER, G.;
WEISENBURGER, A.; ZIMMERMANN, F.; KONYS,
J.; ENGELKO, V.; RUSANOV, A.; MARKOV, V.
Results of steel corrosion tests in flowing liquid
Pb/Bi at 420-600^{0}C after 2000 h.
Pb/Bi Internat.Workshop, ENEA, Brasimone, I,
April 18-20, 2001
http://bibliothek.fzk.de/zb/veroeff/49775.htm
        (V49775)

MÜLLER, G.; HEINZEL, A.; SCHUMACHER, G.;
WEISENBURGER, A.; ZIMMERMANN, F.;
KONYS, J.; ENGELKO, V.; RUSANOV, A.;
MARKOV, V.
Results of steel corrosion tests in flowing
liquid Pb/Bi at 420-600^{0}C after 2000 h.
Pb/Bi Internat.Workshop, ENEA, Brasimone, I,
April 18-20, 2001
http://bibliothek.fzk.de/zb/veroeff/49775.htm
        (V49775)

NECK, V.
Aquatische Chemie tetravalenter
Actiniden-Datenbasis und experimentelle
Arbeiten am Forschungszentrum Karlsruhe INE.
Vortr.: Forschungszentrum Rossendorf,
Dresden, 9.Mai 2001   (V50855)

NECK, V.; ALTMAIER, M.; MÜLLER, R.;
BUNDSCHUH, T.; ROTHE, J.; DENECKE, M.A.;
KIM, J.I.; FANGHÄNEL, T.
Solubility of thorium dioxide and hydroxide.
8th Internat.Conf.on Chemistry and Migration
Behaviour of Actinides and Fission Products
in the Geosphere (Migration '01), Bregenz, A,
September 16-21, 2001
Book of Abstracts S.43   (V50730)

NECK, V.; ALTMAIER, M.; MÜLLER, R.;
BUNDSCHUH, T.; ROTHE, J.; DENECKE, M.A.;
KIM, J.I.; FANGHÄNEL, T.
Untersuchungen zur Löslichkeit und
Kolloidbildung von Thorium(IV)-Dioxid und
Hydroxid.
GDCh-Jahrestagung Chemie 2001, Würzburg,
23.-29.September 2001
Kurzreferate S.66   (V50854)

NECK, V.; KIM, J.I.
Thermodynamics of tetravalent actinides in
aqueous solution: a critical assessment of
uncertainties.
Actinides-2001 : Internat.Conf., Hayama, J,
November 4-9, 2001
Abstracts S.105   (V50853)

NECK, V.; KIM, J.I.; BUNDSCHUH, T.;
MÜLLER, R.; SEIDEL, B.S.; MARQUARDT,
C.M.; HAUSER, W.; DARDENNE, K.; JENSEN,
M.P.; FANGHÄNEL, T.
Determination of thermodynamic solubilities
of An(IV) oxides/hydroxides from their initial
colloid formation.
8th Internat.Conf.on Chemistry and Migration
Behaviour of Actinides and Fission Products
in the Geosphere (Migration '01), Bregenz, A,
September 16-21, 2001
Book of Abstracts S.30   (V50728)

NOSECK, U.; SCHÜSSLER, W.
Impact of colloids on actinide migration with
regard to performance assessment.
8th Internat.Conf.on Chemistry and Migration
Behaviour of Actinides and Fission Products
in the Geosphere (Migration '01), Bregenz, A,
September 16-21, 2001
Book of Abstracts S.177   (V50754)

PIERRET, M.C.; RABUNG, T.; BAUER, A.;
GECKEIS, H.; KLENZE, R.; KIM, J.I.;
BRADBURY, M.H.; BAEYENS, B.
Interaction of Cm(III) and Eu(III) with
Ca-montmorillonite: surface complexation

modeling and spectroscopic studies.
8th Internat.Conf.on Chemistry and Migration
Behaviour of Actinides and Fission Products
in the Geosphere (Migration '01), Bregenz, A,
September 16-21, 2001
Book of Abstracts S.64   (V50733)

PLASCHKE, M.; ROTHE, J.; SCHÄFER, T.;
DENECKE, M.A.; DARDENNE, K.; POMPE, S.;
HEISE, K.H.
Combined AFM and STXM in situ study of humic
acid agglomeration by Eu(III) complexation.
8th Internat.Conf.on Chemistry and Migration
Behaviour of Actinides and Fission Products
in the Geosphere (Migration '01), Bregenz, A,
September 16-21, 2001
Book of Abstracts S.72
Jahrestagung der Gesellschaft Deutscher
Chemiker (GDCh), Würzburg, 24.-26.Sept. 2001
Abstracts S.96   (V50737)

PUDEWILLS, A.
Grundwasserströmung und Transportprozesse im
Fernbereich eines Endlagers für radioaktive
Abfälle.
61.Jahrestagung der Deutschen Geo-
physikalischen Gesellschaft, Frankfurt,
19.-23.März 2001   (V50793)

RABUNG, T.; GECKEIS, H.; KIM, J.I.
Solid-water interface reactions of actinides
and lanthanides with mineral surfaces.
8th Internat.Conf.on Chemistry and Migration
Behaviour of Actinides and Fission Products
in the Geosphere (Migration '01), Bregenz, A,
September 16-21, 2001
Book of Abstracts S.185   (V50756)

RABUNG, T.; GECKEIS, H.; MANH, T.N.;
KIM, J.I.; BECK, H.P.
Kinetic aspects of metal ion binding to humic
substances.
Symp.on Refractory Organic Substances in the
Environment (ROSE II), Karlsruhe, August 1-3,
2000
Abstracts of Oral and Poster Papers S.247
                                (V49639)

RABUNG, T.; STUMPF, T.; GECKEIS, H.; KIM, J.I.
Surface complexation of trivalent lanthanides and
actinides onto iron oxides and γ-alumina:
experiment and modelling.
Internat.Workshop on Surface Chemical
Processes in Natural Environments, Ascona,
CH, October 1-6, 2000
Abstracts S.47   (V49638)

RABUNG, TH.; GECKEIS, H.; KIM, J.I.
Grenzflächenreaktionen von Actiniden und
Lanthaniden an Mineralphasen.
GDCh-Jahrestagung Chemie 2001, Würzburg,
23.-29.September 2001   (V50972)

RINEISKI, A.
Intra-nodal reactivity calculations based on
the variational nodal method.
Mathematics and Computations 2001, Salt Lake
City, Utah, September 9-13, 2001   (V50001)

RINEISKI, A.; MASCHEK, W.; RIMPAULT, G.
Performance of neutron kinetics models for
ADS transient analyses.
5th Topical Meeting on Nuclear Applications
of Accelerator Technology (AccApp '01), Reno,
Nev., November 11-15, 2001   (V50267)

ROTHE, J.; DENECKE, M.A.; KIM, J.I.
Actinide speciation with synchrotron
radiation at INE.
Synchrotron Environmental Laboratory (SUL),
1st Users Meeting, Karlsruhe, March 29-30,
2001   (V50944)

ROTHE, J.; DENECKE, M.A.; NECK, V.;
MÜLLER, R.; KIM, J.I.
XAFS investigations of the structure of
aquatic thorium oxide/hydroxide colloids.
HASYLAB Users Meeting 2001, XAFS Satellite
Meeting, DESY, Hamburg, January 25-26, 2001
                    (V50948)

ROYL, P.; TRAVIS, J.R.; BREITUNG, W.
FZK programme on containment integrity:
applications of the 3D code GASFLOW with
emphasis on modeling of catalytic foils.
Hydrogen Workshop, Batelle, Eschborn, March
6-7, 2001   (V49476)

ROYL, P.; TRAVIS, J.R.; BREITUNG, W.
Modeling of catalytic foils and application
in 3D containment analysis using the 3D CFD
code GASFLOW.
IAEA Technical Committee Meeting on
Implementation of Hydrogen Mitigation
Techniques and Filtered Containment Venting,
Köln, June 18-21, 2001   (V50134)

RÖMER, J.; PLASCHKE, M.; BEUCHLE, G.;
KIM, J.I.
Observation of U(IV)-oxide surface
alterations by electrochemical AFM.
Jahrestagung Chemie 2001, Würzburg,
23.-29.September 2001   (V51015)

RÖMER, J.; PLASCHKE, M.; KIM, J.I.
Nanoscopic observation of U(IV)-oxide surface
dissolution and remineralization by
electrochemical AFM.
Actinides-2001 : Internat.Conf., Hayama, J,
November 4-9, 2001
Abstracts S.93   (V50871)

RÖMER, J.; PLASCHKE, M.; KIM, J.I.
Alignment of AFM images using microstructured
reference points and a mathematical procedure.

Workshop NanoScale 2001, Bergisch Gladbach,
14.-16.November 2001   (V51014)

RÖMER, J.; PLASCHKE, M.; KIM, J.I.
Elektrochemische AFM Untersuchung:
Auflösekinetik von Urandioxid.
Jahrestagung der Gesellschaft Deutscher
Chemiker (GDCh), Würzburg, 24.-26.September
2001
Abstracts S.97   (V51102)

SAUTER, H.; HEINZEL, V.
Experimental observation of the behavour of
single, small bubbles in a quiescent fluid and their
wakes.
3rd European Congress of Chemical Engineering
(ECCE), Nürnberg, June 26-28, 2001 (V50485)

SCHMUCK, P.
Assessment of MELCOR 1.8.5: Structural
failure models for severe accidents in a large PWR
without lower head penetrations.
CSARP Meeting (CSARP = Cooperative Severe
Accidents Research Programme), Bethesda, Md.,
May 7-9, 2001   (V49776)

SCHMUCK, P.
Severe accident calculations using MELCOR
with emphasis on results for hydrogen production.
CEA/IPSN/FZK (WG3) Information Exchange
Meeting, Saclay, F, September 21, 2001
                    (V50225)

SCHULENBERG, T.
Kernforschung in Karlsruhe - eine neue Heraus-
forderung.
Vortr.: Forschungszentrum Jülich, 4.September
2001   (V50608)

SCHÄFER, T.; ARTINGER, R.; BAUER, A.;
DARDENNE, K.; KIM, J.I.
Iron oxide/-hydroxide colloid facilitated
americium migration in Gorleben groundwater.
8th Internat.Conf.on Chemistry and Migration
Behaviour of Actinides and Fission Products
in the Geosphere (Migration '01), Bregenz, A,
September 16-21, 2001
Book of Abstracts S.118   (V50743)

SCHÜSSLER, W.
Einfluß von Huminstoffen auf die Actiniden-
migration.
Geowissenschaftliches Kolloquium,
Friedrich-Schiller-Universität, Jena,
4.Dezember 2000   (V49637)

SCHÜSSLER, W.; ARTINGER, R.; KIENZLER, B.;
GECKEIS, H.; RABUNG, T.; KIM, J.I.
Influence of humic colloids on the
contaminant transport: applicability of
laboratory results to natural systems.
2001 Fall Meeting of the Materials Research

Society, Boston, Mass., November 26-30, 2001
Abstracts S.689   (V51022)

SCHÜSSLER, W.; ARTINGER, D.; KIENZLER,
B.; GECKEIS, H.; RABUNG, T.; KIM, J.I.;
KLOTZ, D.
Influence of humic colloids on the
contaminant transport: applicability of
laboratory results to natural systems.
1st Late Summer Workshop 'Interfaces in
Aquatic Systems - Colloids, Biofilms,
Sediment/Water/Air', Maurach, October 1-3,
2001   (V51156)

SCHÜSSLER, W.; ARTINGER, R.; SCHÄFER,
T.; MARQUARDT, C.M.; GECKEIS, H.;
RABUNG, T.; BUCKAU, G.; KIM, J.I.; KLOTZ, D.
Influence of humic colloids on the actinide
migration: applicability of laboratory results to
natural systems.
Vortr.: GRS Braunschweig, 20.Februar 2001
          (V51158)

SCHÜSSLER, W.; KIENZLER, B.; KIM, J.I.;
MEYER, H.; FÖRSTER, B.; STIPPLER, R.
Geochemically based source term for the Asse
salt mine.
Jahrestagung der Gesellschaft Deutscher
Chemiker (GDCh), Würzburg, 24.-26.September
2001
Seminar für Kern- und Radiochemie,
Universität Mainz, 19.Dezember 2001 (V51157)

SCHÜSSLER, W.; KIENZLER, B.; MEYER, H.;
FOERSTER, B.
Geochemically based source term assessment
for the ASSE salt mine.
8th Internat.Conf.on Chemistry and Migration
Behaviour of Actinides and Fission Products
in the Geosphere (Migration '01), Bregenz, A,
September 16-21, 2001
Book of Abstracts S.196   (V50758)

SEIBERT, A.; MARQUARDT, C.M.; KIM, J.I.;
KRATZ, J.V.; TRAUTMANN, N.
Complexation of Np(V) with humic substances:
comparison of natural Aldrich humic acid with
synthetic humic substances.
8th Internat.Conf.on Chemistry and Migration
Behaviour of Actinides and Fission Products
in the Geosphere (Migration '01), Bregenz, A,
September 16-21, 2001
Book of Abstracts S.128   (V50745)

SEIBERT, A.; MARQUARDT, C.M.; KIM, J.I.;
KRATZ, J.V.; TRAUTMANN, N.
Komplexierung von Np(V) mit Huminsäuren:
Vergleich von synthetischen mit natürlichen
Huminsäuren.
Jahrestagung Chemie 2001, Würzburg,
23.-29.September 2001   (V50959)

SEILER, J.M.; SEHGAL, B.R.; ALSMEYER, H.;
KYMÄLÄINEN, O.; TURLAND, B.; GRANGE, J.L.;
FISCHER, M.; AZARIAN, G.; BÜRGER, M.;
CIRAUQUI, C.J.
European group for analysis of corium
recovery concepts (EUROCORE).
FISA-2001 : EU Research in Reactor Safety,
Mid-Term Symp.on Shared-Cost and Concerted
Actions, Luxembourg, L, November 12-14, 2001
          (V51027)

STEINBRÜCK, M.
Hydrogen absorption by zirconium alloys at
high temperatures.
EUROMAT 2001 : 7th European Conf.on
Advanced
Materials and Processes, Rimini, I, June
10-14, 2001   (V50888)

STEINBRÜCK, M.; MEIER, A.; STEGMAIER, U.;
STEINBOCK, L.; STUCKERT, J.; PALAGIN, A.
Separate effects tests within the scope of
the QUENCH program at FZK.
CSARP Meeting (CSARP = Cooperative Severe
Accidents Research Programme), Bethesda, Md.,
May 7-10, 2001   (V50889)

STEINWARZ, W.; KOLLER, W.; HÄFNER, W.;
JOURNEAU, C.; SEILER, J.M.; FROMENT, K.;
COGNET, G.; GOLDSTEIN, S.; FISCHER, M.;
HELLMANN, S.; EDDI, M.; ALSMEYER, H.;
ALLELEIN, H.J.; SPENGLER, C.; BÜRGER, M.;
SEHGAL, B.R.; KOCH, M.K.; ALKAN, Z.;
PETROV, J.B.; GAUNE-ESCARD, M.; WEISS,
F.P.; BANDINI, G.
Ex-vessel core melt stabilization research
(ECOSTAR).
FISA-2001 : EU Research in Reactor Safety,
Mid-Term Symp.on Shared-Cost and Concerted
Actions, Luxembourg, L, November 12-14, 2001
          (V51026)

STUMPF, T.; BAUER, A.; KIM, J.I.; COPPIN, F.
Time-resolved laser fluorescence spectroscopy
(TRLFS) study of the sorption of Cm(III) onto
smectite and kaolinite.
8th Internat.Conf.on Chemistry and Migration
Behaviour of Actinides and Fission Products
in the Geosphere (Migration '01), Bregenz, A,
September 16-21, 2001
Book of Abstracts S.34   (V50729)

STUMPF, T.; FANGHÄNEL, T.; GRENTHE, I.;
KIM, J.I.
Complexation of Cm(III) and Eu(III) by glycolic
acid: TRLFS studies.
Actinides-2001 : Internat.Conf., Hayama, J,
November 4-9, 2001
Abstracts S.132   (V50868)

SZABO, G.; GUCZI, J.; KOBLINGER-BOKORI, E.; GECKEIS, H.; MIYAJIMA, T.; BULMAN, R.A.
Complexation of americium with humic acid studied by sorption-desorption experiment on-from immobilised humic acid silica gel.
8th Internat.Conf.on Chemistry and Migration Behaviour of Actinides and Fission Products in the Geosphere (Migration '01), Bregenz, A, September 16-21, 2001
Book of Abstracts S.131   (V50747)

WALTHER, C.
How to characterize aquatic colloids relevant to radionuclide migration?
8th Internat.Conf.on Chemistry and Migration Behaviour of Actinides and Fission Products in the Geosphere (Migration '01), Bregenz, A, September 16-21, 2001
Book of Abstracts S.182   (V50755)

WALTHER, C.; GEIPEL, G.
Properties of laser induced plasmas for particle detection.
Frühjahrstagung des Arbeitkreises Atome, Moleküle Quantenoptik und Plasmen der DPG, Berlin, 2.-6.April 2001
Verhandlungen der Deutschen Physikalischen Gesellschaft, R.6, Bd.36 (2001) P 7.3
http://bibliothek.fzk.de/zb/veroeff/49132.htm
                    (V49132)

WEIGL, M.; GEIST, A.; MÜLLICH, U.; GOMPPER, K.
Kinetik der hochselektiven Actiniden(III)-Extraktion aus salpetersaurer Lösung mittels n-Propyl-bis(triazinyl)pyridin (n-Pr-BTP).
Deutsche Vereinigung für Chemie und Verfahrenstechnik (DVCV), Gemeinschaftsausschuss Extraktion, Frankfurt, 27.-28.September 2001   (V50590)

WEISENBURGER, S.
New developments in glass immobilization technology for nuclear waste.
221st American Chemical Society Meeting, San Diego, Calif., April 1-5, 2001   (V50915)

WILHELM, D.
Extrapolation of the thermite dispersion experiment SNL/Sup-1 to prototypic conditions.
16th Internat.Conf.on Structural Mechanics in Reactor Technology (SMiRT-16), Post Conf.Seminar 'Containment of Nuclear Reactors', Albuquerque, N.M., August 20-21, 2001   (V50329)

WÖRNER, M.; CACUCI, D.G.; SABISCH, W.; GRÖTZBACH, G.
Derivation of two-phase volume-averaged conservation equations for volume-of-fluid interface tracking.
39th European Two-Phase Flow Group Meeting, Aveiro, P, June 17-20, 2001   (V50469)

YUN, J.I.; KLENZE, R.; KIM, J.I.
Laser-Induzierte Breakdown Spektroskopie zur Qualitätssicherung und Prozesskontrolle der HAW-Verglasung.
Jahrestagung der GDCh-Fachgruppe Nuklearchemie, Würzburg, 23.-29.September 2001   (V50954)

ZHELEZNYAK, M.; HELING, R.; RASKOB, W.
Hydrological dispersion module of the decision support system RODOS.
Internat.Congress on the Radioecology-Ecotoxicology of Continental and Estuarine Environments, Aix-en-Provence, F, September 3-7, 2001   (V50602)

ZIMMER, P.; BOHNERT, E.; KIM, J.I.
Formation of secondary phases after long-term corrosion of simulated HAW glass in brine solutions at 190°C.
8th Internat.Conf.on Chemistry and Migration Behaviour of Actinides and Fission Products in the Geosphere (Migration '01), Bregenz, A, September 16-21, 2001
Book of Abstracts S.122   (V50744)